Spectroscopic studies of adsorbed gases on transition metal exchanged zeolites

Zahrah Abdul Kadir

SPECTROSCOPIC STUDIES OF ADSORBED GASES ON TRANSITION METAL EXCHANGED ZEOLITES

BY

ZAHRAH ABDUL KADIR

(B.Sc. University of Malaya)

A thesis sudmitted for the degree of
Doctor of Philosophy in the Department
of Chemistry University of Durham

1983

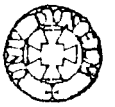

This thesis is dedicated to my parents.

DECLARATION

The work described in this thesis is original except where stated to the contrary. It has not previously been submitted either wholly, or in part, for a degree at this or any other university.

ABSTRACT

Infrared studies of gases, C_2H_4, trans-$C_2D_2H_2$, C_2H_2, C_2D_2, C_3H_6, NH_3, CO and H_2S, adsorbed onto self supporting discs of various transition metal exchanged zeolites are reported (4000-1200cm^{-1}).

C_2H_4 and trans-$C_2D_2H_2$ were adsorbed onto fully silver exchanged type A (AgA) zeolite. AgA samples were subjected to various dehydration treatments prior to adsorption of C_2H_4 and it has been shown that the adsorption behaviour is a function of pretreatment. Under all pretreatment conditions used two adsorption sites were observed. However, whilst AgA samples pretreated at higher temperature held ethylene equally strongly on both sites, those samples pretreated at the lower temperature held ethylene less strongly on one site than the other.

To continue our study on AgA zeolite, we also adsorbed C_2H_2 and C_2D_2 onto AgA samples which had been degassed at temperatures of 543 and 673K for 2 hours. Acetylene was found to be adsorbed on the cations at two different sites, and were easily removed on evacuation. In addition part of the adsorbed acetylene lost hydrogen to form silver acetylide (HC ≡ CAg). The liberated hydrogen formed both hydroxyl and hydronium ions within the framework.

In another study, the adsorption behaviour of C_2H_4 and C_2H_2 on Cu^{II} and $Cu^{I}Y$ zeolites was compared. $Cu^{I}Y$ zeolite was prepared in situ by the reduction of $Cu^{II}Y$ zeolite in an atmosphere of CO with preadsorbed ammonia. It was found that the C_2H_4 adsorbed on $Cu^{II}Y$ was not rotating and that the symmetry of the adsorbed species was apparently preserved (D_{2h}), while, the symmetry of the adsorbed species in $Cu^{I}Y$ zeolite was reduced, probably to C_{2v}. In contrast to the results for C_2H_4 adsorption, the adsorption behaviour of C_2H_2 was found to be

similar on both Cu^{II} and $Cu^{I}Y$ zeolites. Acetylene was found to be adsorbed at two different sites with a 'side-on' interaction, and that one site held acetylene more strongly than the other.

For the $Cu^{I}Y$ sample, following the evacuation of either C_2H_4 or C_2H_2, CO was introduced. It was suggested that C_2H_4 and CO were held with comparable strength by Cu^{+} ions and that the gases were adsorbed on equivalent sites. C_2H_2 and CO, on the other hand, were adsorbed at two different sites.

Partially Zn-, Ni-, and Cu- exchanged NaA zeolites were used to study the isomerization of cyclopropane to propene. ZnNaA samples were subjected to various pretreatment conditions before the adsorption of cyclopropane. Water was found to promote the isomerization in this sample and that isomerization occurred via a protonated cyclopropane intermediate. Bands due to cyclopropane and propene were observed at the same time in samples ZnNaA and NiNaA and it was suggested that the gases were adsorbed at two different sites. Propene was adsorbed on the cations more strongly than cyclopropane since propene could only be removed at 473K while cyclopropane could be removed easily by evacuation.

For CuNaA, however, no interaction between the cations and cyclopropane was observed at room temperature. Upon heating the sample with 100 torr of cyclopropane, isomerization occurred at 473K. It was suggested that isomerization occurred on the external surface of the zeolite and that propene was not adsorbed on the cations within the framework.

Finally, the adsorption of H_2S onto partially Ni-, Cu-, Zn-, Mn-, and Co- exchanged NaA zeolites were studied. No adsorption of H_2S onto the NiNaA and CuNaA samples was observed. On the other hand, two types of adsorption, dissociative and non-dissociative were observed in ZnNaA and MnNaA samples. Water was

also formed. H_2S was found to adsorb weakly and molecularly onto CoNaA.

ACKNOLEDGEMENTS

I wish to thank for his supervision of my thesis Dr. J. Howard of the Chemistry Department at Durham University. I would also like to thank for their help the following technicians; Miss J. Magee, Mrs. E.M. Nevins and Mr. R. Coult.

Finally I would like to thank Tun Ismail Atomic Research Centre (PUSPATI) for sponsoring my research.

CONTENTS PAGE

CHAPTER I

INTRODUCTION

I. Zeolite molecular sieves

Interest in zeolite molecular sieves occurs in both the scientific and industrial worlds. Zeolites can occur naturally or be synthesized in various forms[1,2]. In the natural form, zeolites are crystalline, hydrated aluminosilicates of group I and II elements. Natural or synthetic zeolites consist of SiO_4 and AlO_4 tetrahedra linked to each other by sharing all of the oxygens to form an infinite three-dimensional anionic network . The Si:Al ratio in the zeolites determines the extent of the negative charge on the framework; the higher the aluminium content the greater is the negative charge since each AlO_4 tetrahedron is associated with unit negative charge. This in turn determines the number of exchangeable cations which are required to produce electrical neutrality. The framework contains channels and interconnected voids which are occupied by the cations and water molecules. In the hydrated form, the cations are free to move and can be exchanged to varying degrees for other cations. In many zeolites, the intracrystalline water may be removed reversibly while for others, on dehydration, irreversible changes of the structure occur. It is only to the former, whose structure remain intact on complete dehydration, that the term "molecular sieves" is applied.

Some 40 species of natural zeolite minerals have been identified and over 150 synthetic types were known in 1980[3].

Zeolite molecular sieves are chemically and structurally more complex than some other adsorbents. However, they do possess the advantage of high internal surface area and adsorption sites which are normally well defined. Zeolites typically adsorb molecules with a permanent dipole moment with a selectivity not found in other adsorbents. Their adsorptive and catalytic properties can be modified by ion exchange and they can be synthesized with various Si:Al ratios.

A majority of these applications are in petroleum processing, such as hydrocracking, hydroisomerization and hydrodewaxing, gas and liquid purification processes, removing water from various streams including natural gas for liquefaction, ethane recovery and other purposes[3].

Zeolites have been applied in solving environmental problems, such as weather modification and solar energy[5]. Recently, there is renewed interest in the commercial applications of zeolites as cation exchangers where it was found that zeolite A in the sodium form is suitable for the replacement of triphosphates as a builder in detergents, and, also, their ability to remove isotopes from nuclear power station waste waters[6].

Although only a small number of mineral and synthetic zeolites are being used in industry their potential is obviously immense[3]. Zeolites are currently being utilized to solve or improve the solution of many technological problems.

The chemistry of transition metal complexes has also received considerable attention, because such complexes have potential both in fundamental and applied catalysis. Studies of zeolites modified by transition metals show that

their polyfunctional properties are determined by the structural and chemical properties of the zeolites and the state of the metals in them. The preparative conditions of these zeolites can affect the form of the introduced ions and the thermal stability of the zeolitic structure[7-9]. In some cases, owing to the shielding effect caused by the zeolite network and the electric fields, the transition metal ions may be stabilized in unusual oxidation states. Novel chemical species involving ligands such as C_3H_6 and N_3H_3 rings bonded to transition metal ions[10,11] can also be formed and are stable in the zeolite cages.

II. Spectroscopic studies of zeolites and adsorbed species

Infrared spectroscopy is used extensively in the areas of adsorption and catalysis to identify surface species and to determine their bonding to the surface[12,13]. In the most favourable example, infrared techniques can distinguish directly between physical adsorption and chemisorption. The latter process results in new chemical species, which in general can be distinguished by their vibrational spectra[12].

Infrared spectra of adsorbed species have also been used to study reaction kinetics. The rate of oxidation of adsorbed carbon monoxide on platinum[14] has been studied by monitoring the decrease in the intensity of ν(C=O) band with the addition of oxygen. In a similar way, the hydrogenation and oxidation of ethylene[15,16] over silica supported transition metals have been studied. This work is extremely valuable in the determination of structures of intermediates in catalysed reactions.

The crystal structures and chemical compositions of zeolites make them ideal systems for the spectral investigation of cation movements and their interaction

with adsorbed molecules. Zeolites have such large surface areas that relatively intense bands due to adsorbed species can readily be obtained. Infrared spectroscopy may also provide information on the framework Si:Al composition, the structural changes during thermal decomposition and cation movement during dehydration and dehydroxylation[17-20].

The principal disadvantage in using infrared spectroscopy in surface studies is that, due to strong absorption by the substrate, data can only be confined to limited spectral regions. The unsupported zeolite sample, used to avoid interference from other chemicals, results in the wide regions of complete absorption (below 1200cm^{-1}) by the sample. It is difficult to observe the absorption bands of adsorbed molecules that lie in these regions. Despite this limitation, infrared spectroscopy remains one of the most powerful techniques available to study adsorbed species.

An extension of the spectra to the far infrared region may provide information additional to that obtained by mid-infrared techniques, for instance on the location of the cations and adsorbed molecules, and the structure of the zeolites. Unfortunately, there are few published papers on the far infrared spectra of zeolites and adsorbed species. This is due to the relatively few far infrared spectrometers available with the computation facilities required to give rapid access to the acquired data in a form comparable with that produced by mid-infrared spectrometers[21]. Moreover, the vibrations of the adsorbed molecules with respect to the surface, are strongly masked by the vibrations of the adsorbent and of the adsorbed molecules[22].

Likewise, there are few studies of molecules adsorbed

on zeolites having been made by means of Raman spectroscopy. Zeolites give rise to very weak Raman scattering and their high fluorescence obscure the relatively weak Raman spectra[23,24]. However, by using the picosecond pulsed Raman technique now available[25], these problems will be remedied.

References

1. Breck, D.W., Zeolite Molecular Sieves: Structure, Chemistry and Use, Wiley-Interscience, New York (1974).
2. Barrer, R.M., Zeolites and Clay Minerals as Sorbents and Molecular Sieves, Academic Press, London (1978).
3. Townsend, R.P., Properties and Applications of Zeolites, The Chemical Society, London (1980).
4. Rabo, J.A., Bezman, R.D., and Poutsma, M.L., Acta Phys. Chem., 24(1-2), 39 (1978).
5. Sand, L.B., and Mumpton, F.A., Natural Zeolites, Occurrence, Properties and Use, Pergamon, New York (1978).
6. Campbell, D.O., Advan. Chem. Ser., 121, 281 (1973).
7. Matsumoto, S., Nitta, M., Ogawa, K., and Aumora, K., Bull. Chem. Soc. Jap., 48, 1169 (1975).
8. Schoonheydt, R.A., Vandamma, L.K., Jacobs, P.A., and Uytterhoeven, J.B., J. Catal., 43, 292 (1976).
9. Dyer, A., and Barri, S.A.M., J. Inorg. Nucl. Chem., 39, 1061 (1977).
10. Cruz, W.V., Leung, P.C.W., and Seff, K., J. Am. Chem. Soc., 100 (22), 6997 (1978).
11. Kim, Y., and Seff, K., J. Am. Chem Soc., 99, 7057 (1977).
12. Little, L.H., Infrared Spectra of Adsorbed Species, Academic Press, London (1967).
13. Kiselev, A.V., and Lygin, V.I., Infrared Spectra of Surface Compounds, Wiley, New York (1975).
14. Heyne, H., and Tompkins, F.C., Proc. Roy. Soc., A292, 460 (1965).
15. Hepple, P., Chemisorption and Catalysis, Institute of Petroleum, London (1970).
16. Force, E.L., and Bell, A.T., J. Catal., 38, 440 (1975).
17. Milkey, R.G., Amer. Mineral, 45, 990 (1976).

18. Zhadanov, S.P., Kiselev, A.V., Lygin, R.J., and Titova, I.I., Russ. J. Phys. Chem., 38, 1299 (1964).

19. Flanigen, E.M., Khatami, H., and Szymanski, H.A., Adv. Chem. Ser., 101, 201 (1971).

20. Stubican, V., and Roy, R., Amer. Mineral, 46, 32 (1961).

21. Fripiat, J.J., Dev. Sedimentol, 34, 191 (1982).

22. Yates, D.J.C., J. Chem. Phys., 40, 1157 (1964).

23. Cooney, R.P., Curthoys, G., and Tam, N.T., Adv. Catal., 24, 293 (1975).

24. Tam, N.T., Cooney, R.P., and Curthoys, G., J. Chem. Soc. Trans. Farad, I., 72, 2577 (1976).

25. Howard, J., Personal Communication.

CHAPTER II

ZEOLITES, THEIR CHEMISTRY AND PROPERTIES

1. Zeolite Structure

As mentioned earlier, zeolites are a class of aluminosilicates with a framework consisting of SiO_4 and AlO_4 tetrahedra. A general unit cell composition is given by[1],

$$M_{x/n}\,[(AlO_2)_x\,(SiO_2)_y]\;wH_2O$$

where M is the cation of valence n, w is the number of water molecules, and [ ] represents the framework composition. The ratio y/x usually has the values 1-5, depending upon structure, and the sum (x+y) is the total number of tetrahedra in the unit cell.

Zeolites are classified into groups according to the common features of the aluminosilicate framework structures. The members of a given zeolite group fall into two categories: (i) those which have the same framework topology, but have different chemical compositions (cations or Si:Al ratio); (ii) those members of a group which have frameworks containing one or more structural elements, linked together in different ways, so resulting in different topologies.

If each zeolite framework is assumed to be formed from only one type of building unit, a total of eight such building units have been found[2,3] and these eight building units are shown in figure 2.1(a). These units consist of various arrangements of the primary building unit (i.e. SiO_4 or AlO_4 tetrahedra). In some cases, the larger polyhedral units which occur in these structures are considered. These cagelike units or building 'blocks' (Figure 2.1(b)) are designated by Greek letters[4]: α (a

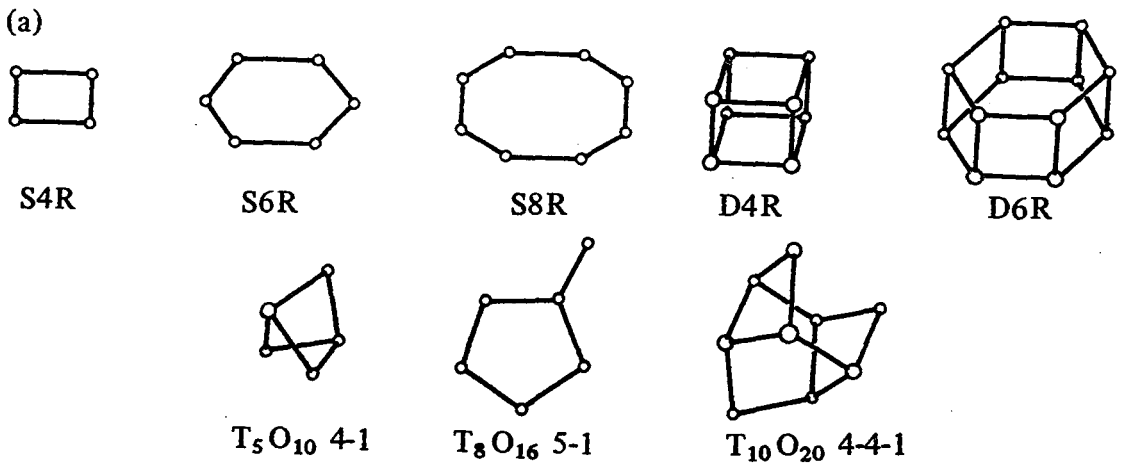

Figure 2.1(a). Secondary building units in zeolite structures. The positions of the Si:Al atoms are shown. Oxygen atoms lie near the middle of the connecting lines[2,3].

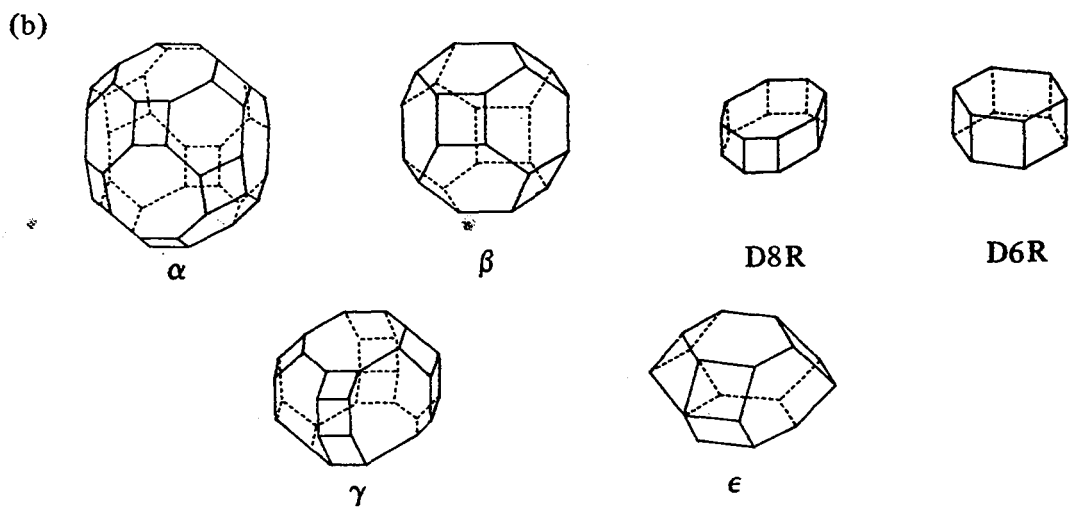

Figure 2.1(b). Some polyhedra in zeolite frameworks: α (a truncated cubooctahedron or 26-hedron); β (a truncated octahedron or 14-hedron); δ or double 8-ring; D6R or double 6-ring(hexagonal prism); γ or 18-hedron; and ϵ or 11-hedron[4].

truncated cubo-octahedron or 26-hedron), β (a truncated octahedron or 14-hedron), γ (an 18-hedron), etc.. The polyhedra then link together to form unit cells. The secondary building unit present in the unit cells may be used to classify a given zeolite into one of the seven general groups[3]. Of particular interest to this work are two large pore synthetic zeolites, types A and Y. Their structures together with their fundamental building block, the sodalite unit, will be described below.

(a) Sodalite

The sodalite unit is a three-dimensional array of SiO_4 and AlO_4 tetrahedra in the form of truncated octahedron (Figure 2.2(a)). The truncated octahedron (or β-cage) is made up of 24 (Si, Al) ions (vertices) interconnected with 36 oxygen anions and contains eight hexagonal and six square faces[1,16].

The free diameter (the distance between diagonally opposite points of the polyhedron which is not impinged upon by the oxygen atom linings[16]) of a 14-hedron (or β-cage) is about 6.6Å and access to the 14-hedral voids is through 6-ring windows of free diameter 2.3Å [1,16].

(b) Zeolite type A

In zeolite type A, each sodalite unit or β-cage is linked to its neighbour by the four bridging oxygen ions across the square faces (Figure 2.2(b))[1,16]. This configuration results in an approximately spherical internal cavity, called an α-cage, which has a free diameter of 11.4Å. The access to the α-cage is through six circular 8-rings of oxygen with a diameter of 4.2Å. The β-cages interconnect with the large cavities by distorted 6-rings of oxygen

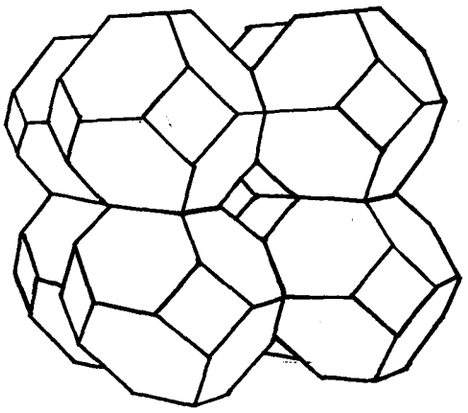

(a) Sodalite

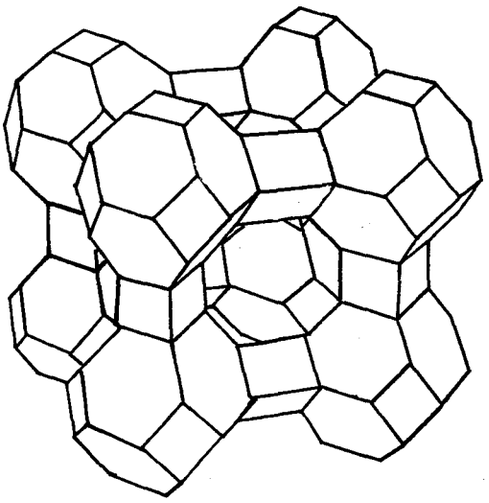

(b) Zeolite
Type A

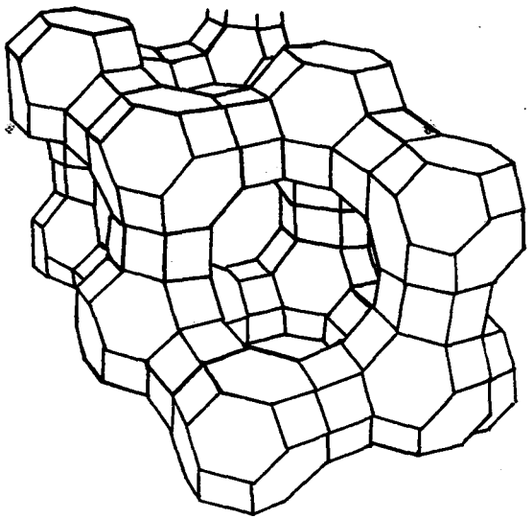

(c) Zeolite
Type 13X

Figure 2.2. Pictorial representations of some alumino-silicate frameworks.

atoms 2.2Å in diameter. There are three distinct oxygen types in zeolite A. The O(1) oxygen ions are the constituents of linkages between sodalite units. Oxygen ions O(2) and O(3) are respectively elements of 6- and 8- membered rings found in this framework. All oxygen ions in the A type lattices are accessible from the large cages (Figure 2.3(a)).

In the sodium form, type A zeolite has the pseudo unit cell of $Na_{12}\ [(AlO_2)_{12}\ (SiO_2)_{12}]\ 27H_2O$ with a cubic unit cell parameter a = 12.3Å . The space group $Pm\bar{3}m$ results if framework aluminium and silicon atoms are not differentiated[5]. Since the Si:Al ratio is 1.0, the electrostatic valence rule presented by Lowenstein[6] requires a rigorous ordering of the AlO_4 and SiO_4 tetrahedra. In order to achieve this, the lattice constant of the true unit cell of zeolite A is 24.6Å and contain eight units of the pseudo cell (192 tetrahedra). This ordering lowers the maximum possible symmetry of $Pm\bar{3}m$ to $Fm\bar{3}c$[7-10].

Recent studies made by Bursill et al[11,12] have shown that the space group of zeolite type A is $R\bar{3}$ (a = 24.6Å) with a 3:1 ordering scheme (where each Si^{4+} is surrounded, via oxygen bridges, to three Al^{3+} and one Si^{4+} and vice versa). With the same 3:1 ordering scheme, the space group Pn3n can also be derived[12].

(c) Zeolite type Y

Zeolite types Y and 13X are synthetic forms of an aluminosilicate framework which has the same topology as that of the natural zeolite, faujasite. The Si:Al content of Y is similar to that of faujasite, while 13X is much more aluminium rich. The value of Si:Al ratio in the unit cell of zeolite 13X vary from 1-1.5 and for Zeolite Y from 1.5-3.0[1].

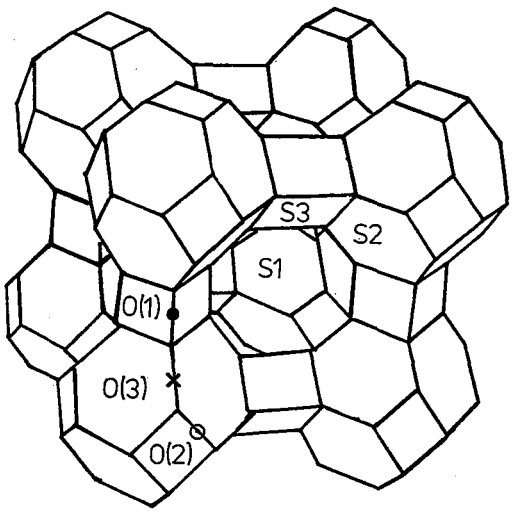

Figure 2.3(a). Cation positions and the positions of the different types of oxygen atoms in zeolite type A.

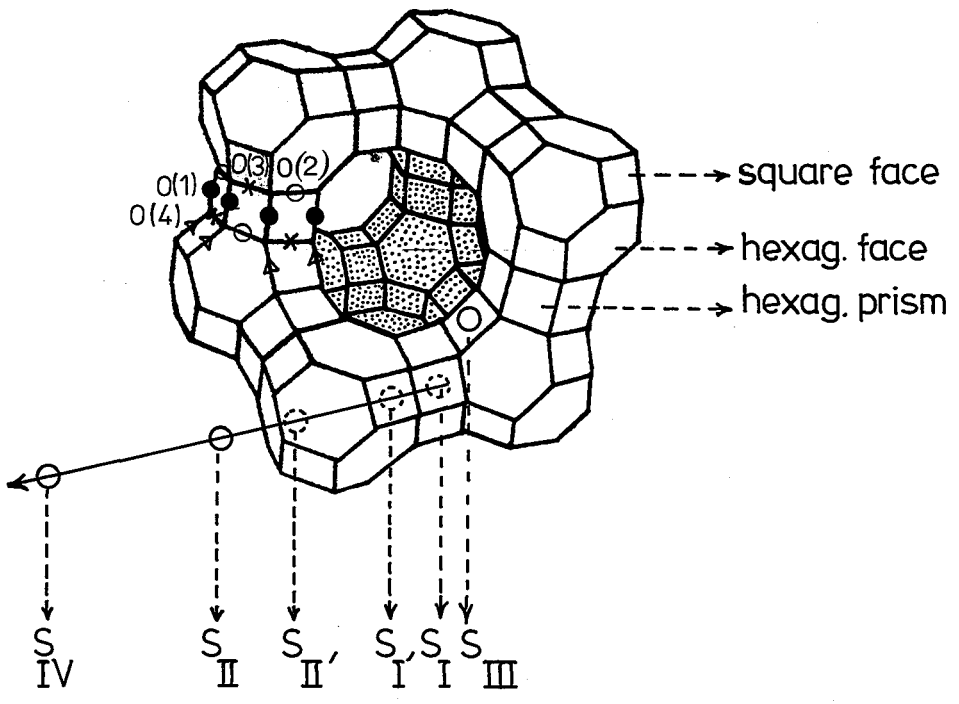

Figure 2.3(b). Cation positions and the positions of the different types of oxygen atoms in zeolite type Y.

The aluminosilicate framework consists of a tetrahedral arrangement of the sodalite units (diamond-like). Each sodalite unit is connected to four other sodalite units across the hexagonal faces by six "bridging" oxygen atoms. This results in a series of wide, nearly spherical cavities usually called the supercages (12Å diameter), which are arranged in the same manner as carbon atoms in diamond[1,16]. The supercage is connected directly to similar supercages by windows of approximately 8-9Å in diameter formed by distorted 12-rings.

There are four distinct oxygen species in types Y and 13X zeolites. These four different types of oxygen atoms are shown in Figure 2.3(b). The O(1) oxygen atoms are bridges making up the hexagonal prisms. The 6-rings of the hexagonal prisms are comprised of alternating O(2) and O(3) oxygen atoms while the 6-ring between the α and β -cages are made up of alternating O(2) and O(4) oxygen atoms. The O(2) oxygen atoms are the oxygen atoms that are in both the hexagonal prism 6-rings and the supercage 6-rings.

The typical unit cell composition[13] of type Y zeolite is $Na_{56}[(AlO_2)_{56}(SiO_2)_{136}] \cdot 236H_2O$ with a cubic symmetry and unit cell parameter, a = 25.028Å[14]. If silicon and aluminium ions occur at random over the zeolite framework, the ideal space group is $Fd3m$[14,15].

II. Cation positions

Charge balancing cations in hydrated zeolites are more often present as hydrated complexes in the larger zeolite cavities. They interact with the lattice only weakly, and are therefore quite mobile. Zeolite framework usually provide more than one kind of site for these cations. The number of cations present may also be less than the total number of

available cation sites of all kinds. Thus when the cations distribute themselves among the sites so as to minimize the free energy of the systems, there may be partial occupancy of some or all of the kinds of sites available.

Dehydration of the zeolites causes the ions to coordinate directly to framework oxide ions. In A and Y zeolites there are many sites available for such coordination and the final distribution of ions represents the best compromise between lattice charge neutralization and the geometric requirements of the cations. Cation resiting due to dehydration is accompanied by small shifts in the positions of the framework atoms. The positions of these sites in relation to the zeolite framework are shown in Figures 2.3(a) and 2.3(b) for zeolites of types A and Y respectively. Tables 2.1 and 2.2 show the possible cation positions and the number of sites available for types A and Y zeolites. In the following discussions of exchange sites, the nomenclature of Barrer[16] will be adopted.

The position and distribution of cations within the zeolite lattice is dependent on the following factors:

(a) the Si:Al ratio

(b) the ionic radius of the cations

(c) the charge of the cations

(d) the concentration of other cations competing for the same sites

(e) the state of hydration/complexation of the cation.

The structure of hydrated zeolite A has been studied by both X-ray powder[5,17,18] and single crystal[7] analyses. From these studies, it was found that of the twelve sodium ions in the hydrated zeolite A, eight are located near the centre

Table 2.1 Cation Positions in Zeolite Type A

Position	Designation	Number
In the 8-ring	S1	3 per pseudo unit cell
Adjacent to an 8-ring but displaced into an α-cage	S1*	
In the 6-ring	S2	8 per pseudo unit cell
Adjacent to a 6-ring but displaced into the β-cage	S2'	
Adjacent to a 6-ring but displaced into the α-cage	S2*	
Against the 4-ring	S3	12 per pseudo unit cell
In the centre of the sodalite (β) cages	SU	1 per pseudo unit cell
In the centre of the α-cage	S4	1 per pseudo unit cell

Table 2.2 Cation Positions in Zeolite Type Y

Position	Designation	Number
In the centre of prisms	I	16 per unit cell
In the β-cages, adjacent to hexagonal prisms	I'	32 per unit cell
In the centre of β-cages	U	8 per unit cell
In the 6-rings linking β-cages and supercages	II	32 per unit cell
Near the 6-rings of sites II but inside the β-cage	II'	
Near the 6-rings of sites II but in the supercages	II*	
Against 4-rings of 'ribs' of supercages	III	48 per unit cell
In the centre of the supercages	IV	8 per unit cell
In the 12-rings of the supercages	V	16 per unit cell

of 6-rings (S2*) on the three-fold axis inside the α-cage. Each was tetrahedrally coordinated to three oxygen atoms of the 6-rings and one water molecule. Three of the remaining sodium ions appear to be located adjacent to the 8-rings (S1*). The twelfth sodium ion , probably entirely hydrated, is situated near the centre of the large cavity (S4).

Single crystal X-ray analyses of dehydrated zeolite A have been published by Seff et al[19,20], and Pluth and Smith[21]. In figure 2.4 is shown a stereoscopic representation of the structure of dehydrated zeolite A[20]. In these studies, again eight sodium ions were located on three-fold axis near the centres of the 6-rings (S2*), but these cations have moved significantly closer to its nearest neighbour, O(3). A further three sodium ions lie in the plane of the 8-rings but off their centres and have moved closer to O(2). The twelfth and final sodium ion was found in the large cavity on a twofold axis opposite a 4-ring (S3). Energetically, site S3 is the least favourable and is occupied only if all other sites are filled or blocked.

There has been no structural study of hydrated zeolite Y reported. However, there are structural studies on hydrated 13X[14,18] and natural faujasite[22]. Early structural studies by X-ray powder diffraction[14] have shown that in hydrated Na13X containing 80 sodium ions per unit cell, 16 were located in the hexagonal prisms (site 1) and 32 were located near the 6-rings linking the sodalite and supercages (site 11). The remainder cannot be located and are believed to be mobile hydrated ions. In a more recent X-ray diffraction analysis of single crystal hydrated NaX[18], 9 sodium ions were found in site 1, 8 in the site 1', and 24 cations in site 11. Little evidence was found for the location of the remaining cations,

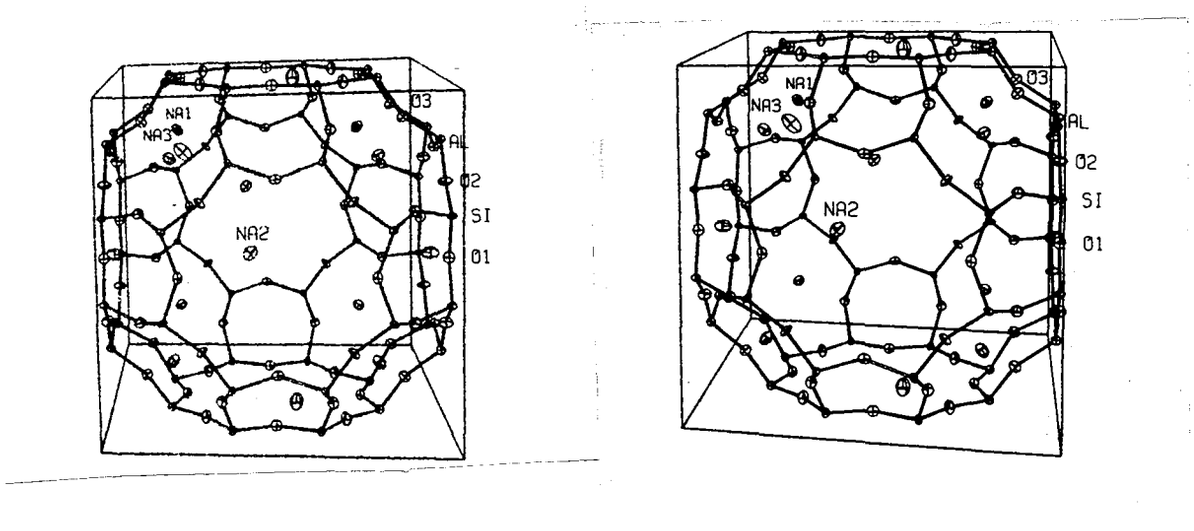

Figure 2.4. Stereoview of dehydrated sodium zeolite type A (after Subramanium and Seff[20]). The cation positions Na1, Na2 and Na3 correspond to sites S2*, S1 and S3 respectively in the text.

and they are presumed to be mobile hydrated ions.

The cation positions in dehydrated zeolite Y were determined by X-ray powder diffraction[23]. 30 cations were found at type II sites and each cation in this position has three nearest oxygen neighbours (O(2)) and three further ones (O(4)). There are an average of 19.5 cations in site 1' position, each coordinated by three O(3) atoms and three O(2) atoms. Finally, there are 7.5 cations in the site 1 position: Each cation at this site is surrounded by six oxygen O(1) atoms forming a slightly distorted octahedron.

III. Ion exchange

One of the most important properties of zeolites is their ability to undergo reversible cation exchange. This property of zeolites was the first attribute of these minerals to be subjected to scientific investigations. Fundamental studies of cation exchange in zeolites have been carried out mainly because of the crystalline and well-defined nature of their anionic framework. Also, because of their three-dimensional framework structure, most zeolites do not undergo any appreciable dimensional change with ion exchange. This ability to be able to exchange cations from solutions is not limited to alkali and alkaline earth cations but extends to all cations of suitable geometry (that is those of small enough dimensions to enter the pores of the crystals in whatever form the cations are present in solution, generally hydrated) and charge.

Ion exchange in zeolites has been extensively studied and many of these systems have been discussed in reviews by Rees[24], Sherry[25], and Breck[1]. The major part of these

studies is with alkali-, alkaline-earth, alkylammonium, and rare-earth cations. In contrast, the ion exchange of transition metals has received relatively little attention. However, there are some studies on the ion exchange of transition metals in mordenites[26], faujasites[27,28], and zeolite type A[29].

While no definitive theory yet exists to predict the equilibrium concentrations of competing cationic species in solution and within the zeolite framework, the factors affecting the cation exchange behaviours in zeolites include[1]:

(a) the nature of the cation species, the cation size (both anhydrous and hydrated) and cation charge;

(b) the temperature at which the exchange procedure is carried out;

(c) the concentration of the cation species in solution;

(d) the anionic species associated with the cation in solution;

(e) the solvent;

(f) the structure and characteristics of the particular zeolite in question, particularly pore diameters and the internal charge density.

Cation selectivities in zeolites do not follow the patterns exhibited by other organic or inorganic ion exchange materials. Zeolite structures have unique features that lead to unusual types of cation selectivity and sieving. Cation exchange in zeolites is accompanied by dramatic alteration of stability, adsorption behaviour and selectivity and catalytic activity.

IV. Adsorption

While many adsorbents do not possess an ordered crystal structure and consequently have a large pore-size distribution, zeolites have pores of uniform size which are uniquely determined by the structure of the crystal. With the extremely uniform pore diameter noted for any given zeolite, the phenomenon of selective adsorption is a well known property of zeolites. One example of this ability to separate molecules with differing dimensions is the ability of a number of zeolites[1,16] to adsorb straight chain hydrocarbon while excluding branching chain hydrocarbon, effecting their complete separation.

The pore sizes of zeolites may vary from 2.6Å in the case of the natural zeolite analcime to 10Å in the case of zeolite omega. This is a particularly convenient size range for molecular separation processes. Table 2.3 shows some zeolites pore diameters and the largest molecules they can adsorb, while figure 2.5 displays the uniformity of zeolite pore sizes in comparison with other common adsorbents.

V. Catalytic activity

The growth of interest in zeolite catalysts in recent years has triggered a large number of reviews on the subject. Much of the earlier work in zeolite catalysis was described by Turkevich[30], and Vernuto and Landis[31]. Recent developments in zeolite catalysts have been reviewed in references 32 to 39.

Zeolite molecular sieves having variable pore sizes are suitable for molecular rearrangements. The intracrystalline volume in zeolites is accessible only to those molecules whose size and shape permits sorption through the entry pores, thus a highly selective form of catalysts, based on sieving effects

Table 2.3 Selected zeolite pore diameters[1,16]

Zeolite	Largest molecules adsorbed	Pore diameter (Å)
Analcime	NH_3	2.6
4A (Na cations)	C_2H_2	3.9
3A (Ca cations)	CF_2-Cl_2	4.6
Faujasite	$(C_2F_5)_3N$	8.0
Omega	$(C_4F_9)_3N$	10.0

Figure 2.5. Distribution of pore sizes in microporous adsorbents.

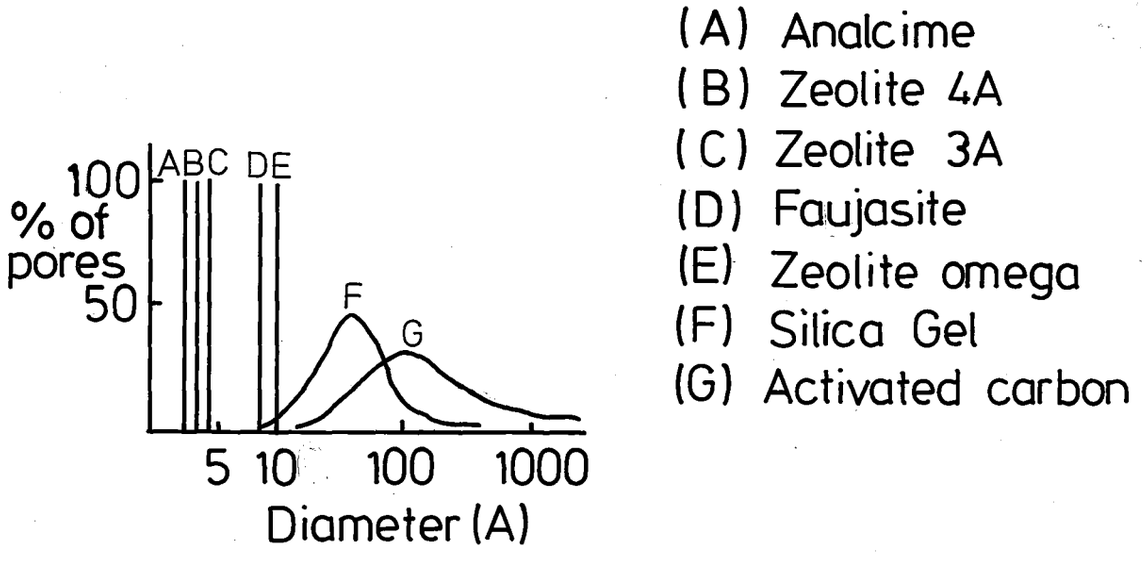

is possible. A review on the molecular shape selective catalysis on zeolites is given by Weisz[40].

The catalytic properties of zeolites can be modified by ion exchange and it has been conclusively shown that catalytic activity in ion-exchanged faujasites is influenced by cation type (including size and charge)[41-47], cation location in the lattice[44] and the presence of proton donors[48,49].

VI. Application

The current applications of the synthetic zeolites are much more diverse and more economically significant than their natural zeolite counterparts. Natural molecular sieve zeolites, however, do find some practical applications and an excellent review article on the subject has been prepared by Mumpton[50], while a detailed review of the applications of natural and synthetic zeolites is given by Breck[51].

Some applications of natural and synthetic zeolites will be detailed here. The most widespread uses of natural zeolites is in fertilizers and soils. The ion exchange capacity of zeolites find application as both a soil conditioner (by stabilizing the pH of the soil) and as a time release mechanism for nitrogen enrichment of the soil (releasing ammonium cations in an exchange process). Another application of natural zeolites of potentially great importance is their use in animal culture. Zeolite minerals in Japan, in particular clinoptilolite and mordenite, have been added to the diets of pigs, chickens, and ruminants[52]. Significant increases in gain of body weight per unit of feed were achieved. Also, the presence of zeolites in their

diet contributed to the well-being of the animals. Sickness and mortality rates were considerably reduced. The functions of the zeolites in dietary and antibiotic behaviour are not understood. Zeolite minerals are also used to control malodour due to animal wastes (by reducing the ammonia and hydrogen sulfide levels).

A small number of mineral zeolite deposits are of sufficient purity to facilitate efficient gas separations. Recently, the zeolite minerals, chabazite and clinoptilolite, were proposed to be used for providing hot water, space heating and cooling (solar energy), and also as flame extinguishers[51].

Synthetic zeolites have been used widely and the largest single user is the petroleum industry. Here, zeolites have been used for hydrocracking, hydroisomerization, and hydrodewaxing. The ion exchange capacity of the zeolites account for the wide application of the modified zeolites to catalytic reactions and the sieving effects of zeolites make selective catalysis possible. Because of the physical properties of zeolites they can be used in the separation of gas mixtures. The known commerical uses of zeolites are summarized in table 2.4[51].

Recently, zeolites have been used as gas storage system, carriers of reactive chemicals, laundry detergents, electrical conductors and for isotopic enrichment, weather modification and beverage carbonation. Most zeolites, by virtue of their structure and composition, exhibit a high affinity for water. It has been shown that this affinity can be reversed by removal of aluminium and, therefore cations, from the structure[53]. Synthetic mordenite was dealuminized by acid treatment, and this zeolite is capable of removing trace

Table 2.4 Summary of Zeolite Applications[51]

(a) Adsorption	
Separations based on sieving	Refrigerants
Separations based on selectivity	Cryosorption
Purification	New adsorbents for sieving
Bulk separations	Hydrophobic adsorbents
Drying	Gas storage systems
	Carriers of chemicals
(b) Ion exchange	
NH_4^+ removal	Artificial kidney dialysate regeneration
Metal separations, removal from waste water	Aquaculture-NH_4^+ removal
Radioisotope removal and storage	Ruminant feeding of non-protein nitrogen
Detergent builder	Ion exchange fertilisers
(c) Catalysis	
Hydrocarbon conversion	Shape selective reforming
Alkylation	Dehydration
Cracking	Methanol to gasoline
Hydrocracking	Organic catalysis
Isomerization	Inorganic reactions
Hydrogenation and dehydrogenation	H_2S oxidation
Hydrodealkylation	NH_3 reduction of NO
Methanation	CO oxidation
(d) Environmental	
Weather modification	Solar energy

(e) Consumer applications	
Beverage carbonation	Flame extinguishers
Laundry detergents	Electrical conductors

organic compounds from water in the same manner as carbon adsorbents, but with the advantage of higher stability to regenerative process.

VII. Infrared analysis of zeolites

(i) Zeolite frameworks

The infrared spectra of some zeolites have been widely studied and the vibrational bands have been empirically interpreted. Most of the infrared spectroscopic studies on aluminosilicate minerals, including tectosilicates, clay minerals and zeolites deal with the behaviour of the main (Si, Al)—O band which is found at $1000cm^{-1}$ [54]. Infrared spectroscopy has also been applied to study zeolites with a variety of crystalline structures, compositions (Si:Al ratios), types of exchange cations and degrees of heat treatment[55].

A systematic investigation of the framework structures of many synthetic zeolites has been carried out in the 1300-$200cm^{-1}$ region by Flanigen et al[56]. Infrared analysis of some natural zeolites have been reported by Burragato et al[57], Joshi et al[58] and Oinuma et al[59].

Each zeolite appears to exhibit a typical infrared pattern and, often, there are general similarities among the spectra of zeolites with the same structural type and in the same structural group. The region 1300-$200cm^{-1}$ can be used to indicate the structural features of zeolite frameworks because this region contains the fundamental vibrations of the framework (Si, Al)O_4 tetrahedra. The infrared spectra of zeolites in the region 1300-$200cm^{-1}$ appear to consist of two classes of vibrations: (i) those due to internal

vibrations of the framework TO_4 tetrahedron, the primary building unit of all zeolite framework which are not sensitive to other structural variations; and (ii) vibrations which may be related to external linkages between tetrahedra which are sensitive to the framework structure and to the presence of some secondary building unit and building block polyhedra, such as double rings and the large pore openings.

Individual assignments to specific tetrahedra are not possible. However, the vibrational frequencies represent the average Si, Al composition and bond characteristics of the central T cation. Typical infrared assignments are shown in table 2.5 and are illustrated with the infrared spectrum of zeolite Y in figure 2.6.

The first class of vibrations common to all zeolites and assigned to internal tetrahedron vibrations results in the two most intense bands in the infrared spectrum, the strongest at 950-1250cm^{-1} and the other, of medium intensity, at 420-500cm^{-1}. The strongest vibration in the 950-1250cm^{-1} region is assigned to a T-O stretch, while the next strongest band, which occurs in the region 420-500cm^{-1}, is assigned to a T-O bending mode. Stretching modes involving mainly the tetrahedral atoms are assigned in the region of 650-820cm^{-1}.

The external linkage frequencies which are sensitive to topology and building units in the zeolite frameworks occur principally in two regions of the spectrum, 500-650cm^{-1} and 300-420cm^{-1}. A medium intensity band in the former is related to the presence of double ring polyhedra in the framework, while the latter, is related to the pore opening motion of the tetrahedra units which form the pore openings in the zeolites. This band at 300-420cm^{-1} is prominent in those structures which have cubic unit cell symmetry, and

Table 2.5 Zeolite Infrared Assignments[56]

(a) Internal tetrahedra	
Antisymmetric stretch	1250-950cm^{-1}
Symmetric stretch	720-650cm^{-1}
T-O bend	420-500cm^{-1}
(b) External linkages	
Double ring	650- 500cm^{-1}
Pore opening	300- 420cm^{-1}
Symmetric stretch	750- 820cm^{-1}
Antisymmetric stretch	1050-1150cm^{-1}

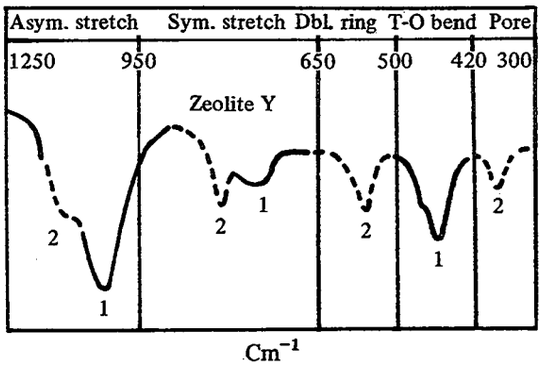

Figure 2.6. Infrared assignments illustrated with the spectrum of zeolite Y (Si:Al = 2.5):

1- Internal tetrahedra - structure insensitive

2- External linkages - structure sensitive.

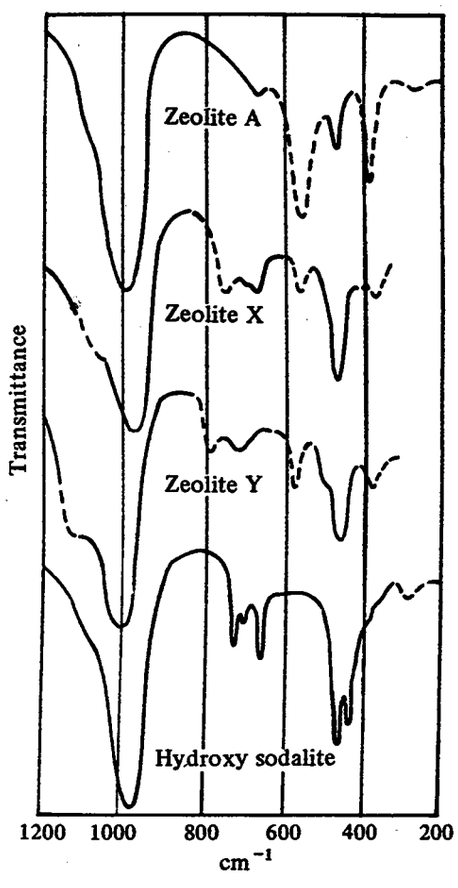

Figure 2.7. Infrared spectra of some zeolites.

decreases in prominence as the symmetry decreases.

Other infrared bands showing characteristics related to framework topology and assigned to external linkage modes occur as a shoulder near 1050-1150cm^{-1} and in the region, 750-820cm^{-1}. Figure 2.7 shows some spectra of zeolites A,X and Y (KBr discs).

(ii) The Si:Al ratio

The frequency shifts of the infrared stretching bands, with substitution of tetrahedral Al for Si in aluminosilicate frameworks, have been reported by many authors[54-56,60-62]. Milkey[54] reported a quantitative linear relationship between the main antisymmetric stretch (1000-1100cm^{-1}) and the atom fraction of Al in the tetrahedral site for a large number of tectosilicate minerals. Flanigen et al[56] also found that a linear relationship was obtained using similar treatment to Milkey[54]. Figure 2.8 shows the frequency variation with the number of aluminium atoms in the framework structure[56].

A shift in frequency with Si:Al content for several other classes of infrared bands was also found for the synthetic zeolites X and Y. Plots of frequency versus fraction of Al in the framework are shown in figure 2.9. A linear decrease in frequency with increase in fraction of Al in the framework was observed for the main antisymmetric stretching band (970-1020cm^{-1}), a symmetric stretching band (670-725cm^{-1}), the double 6-ring band (565-580cm^{-1}), and the 12-ring pore opening band (360-385cm^{-1}). Kiselev et al[55] and Wright et al[63] also showed that similar infrared spectral shifts occur with varying Si:Al ratios for a series of X and Y zeolites.

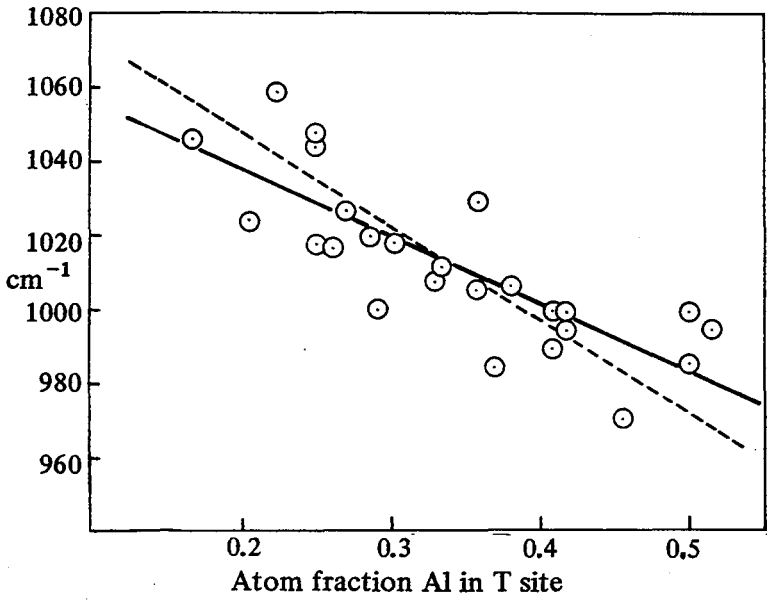

Figure 2.8. Frequency of the main antisymmetric stretch versus the atom fraction of Al in the framework for all synthetic zeolites studied by Flanigen et al[56].

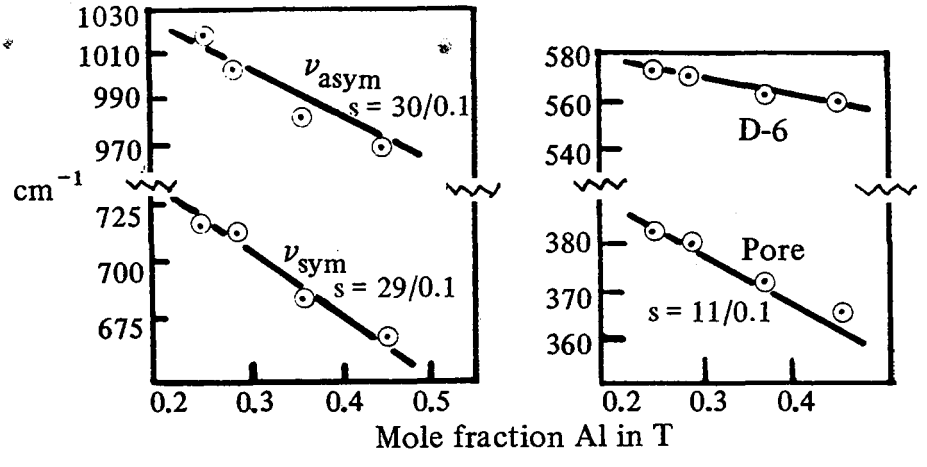

Figure 2.9. Frequency versus atom fraction of Al in the framework for zeolites X and Y for several infrared bands[56].

(iii) Cation types and cation sites

The effect of the compensating cation on the spectrum of the crystalline framework was studied by Zhadanov et al[55]. They found that for the various cationic forms of zeolites studied (Na-, Ca-, Sr-Faujasites), the vibrational spectrum of the crystalline skeleton is sensitive to the charge and radius of the exchanged cation. Figure 2.10 shows the spectra of Na-, Sr- and Ca-faujasites after vacuum treatment at 673 K for four hours. It can be seen that the difference between spectra of the zeolite containing a univalent cation (NaX) and divalent cations (SrX, CaX) is greater than between spectra with different divalent exchange cations (SrX and CaX). The band at 763cm^{-1} is found to be sensitive to the type of exchange cation which implies that this band belongs to the vibrations of the Al-O bond.

For the zeolites A, X, Y, L, and Ω containing alkali metal cations, Flanigen et al[56] found that the framework distortion is mimimal on dehydration. The multivalent cation forms, of many zeolite frameworks, however, cause significant changes in the distortion of the framework elements upon dehydration as is indicated by the infrared spectra of a calcium exchanged zeolite Y (Figure 2.11). Dehydration causes migration of the divalent calcium ions from positions inside the sodalite (β) cage into positions near the centre of the double 6-rings (site I). A change in symmetry of the double 6-ring unit results, as evidenced by a shift in the double 6-ring band (570cm^{-1}) and the band indicative of the pore opening (390cm^{-1}). Changes in the character of the broad symmetric stretching band structure near 710 to 750cm^{-1} are also observed. These changes are reversable on rehydration[56].

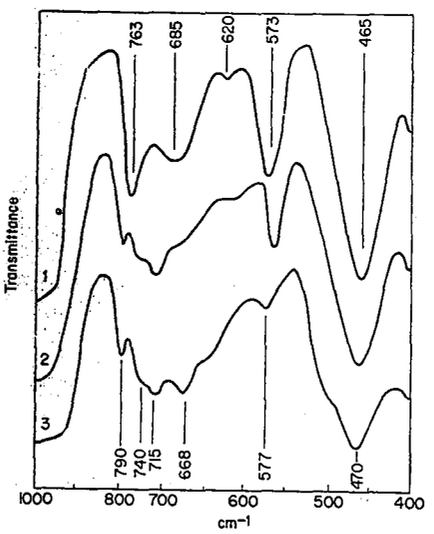

Figure 2.10. Infrared vibrational spectra for the crystalline skeletons of synthetic faujasites with different exchangeable cations after vacuum treatment at 673K for 4 hours: (1) NaX (2) SrX (3) CaX.

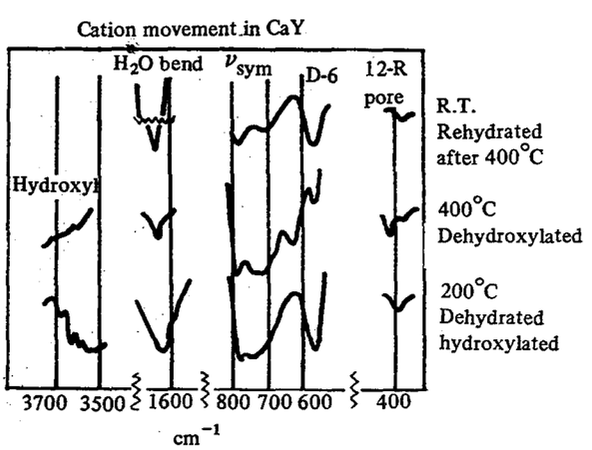

Figure 2.11. Infrared spectra for calcium exchanged zeolite Y (Si:Al = 2.5) after dehydration, dehydroxylation and rehydration[56].

(iv) Structural hydroxyl groups

The infrared spectra of zeolites have been extensively studied in the OH stretching region[64-80] because of their importance in adsorption and catalysis. Some of these bands have been attributed to OH groups associated with the metal ion[65-67]. Others have been assigned to OH groups connected to the aluminosilicate portion of the zeolite[64,65,67-70]. Some of this work has been reviewed in references 81 to 83.

In general, in all of these studies, at least three types of hydroxyl groups were detected. One, at a frequency of about $3750cm^{-1}$ has been found by most workers and is attributable to SiOH groups either on the surface[69] or on silica impurities[70]. Two others at $3650cm^{-1}$ and $3550cm^{-1}$ are attributed to protons bonded to framework oxygen atoms O(1) and O(3) respectively[74]. These absorption bands are at frequencies similar to those observed in hydrogen Y zeolite.

Other bands found in the spectra of the divalent cation zeolites are not found in the spectra of the alkali cation and hydrogen zeolites and must be specific to the presence of divalent cations. A band observed near $3690cm^{-1}$ is assigned either to AlOH groups[70] or to physically adsorbed water[78,84]. Another band occurring between 3600 and $3570cm^{-1}$ is attributed to MOH^+ groups[78,84]. This band varies in frequency with the cation, increasing with decreasing cation size. It is very sensitive to the level of hydration, and it disappears on mild dehydration, possibly with the formation of MO or M^+-O-M^+ groups[84,85].

(v) Surface acidity of zeolites

Basic molecules such as ammonia, pyridine and piperidine were used as probes in most acidity studies. These molecules have the property that their interaction with Brönsted acid

sites, Lewis acid sites, and cations and their hydrogen-bonding interactions give rise to different species detectable by infrared spectroscopy. Absorption bands at 1475, 1545, and 1610cm^{-1}, due to ammonium, pyridinium and piperidinium ions, respectively, is indicative of Brönsted acidity. If the bases are coordinated to trigonal aluminium (Lewis site) or to cations, then the bands are observed near 1630, 1450, and 1450cm^{-1} [83].

Numerous studies of the surface acidity of cation in zeolites have been made[17,63,86-90]. The groups 1A zeolites are found to be nonacidic[77,79,86] while the studies of the alkaline earth zeolites have shown that there are Brönsted and/or Lewis acid sites on the surface depending on calcination conditions[77,79,86,87]. Studies of pyridine adsorbed on NaY by Watanabe and Habgood[88] have shown that there are Brönsted acid sites. After calcination at 773K of the alkaline earth zeolites Ward[77] found no Lewis acid site but a band appeared near 1440-50cm^{-1}, whose frequency depended on the cations and hence was attributed to the cations. On calcination at higher temperatures (923K), the concentration of Brönsted acid sites is less but Lewis sites are detected. Rehydration removes the Lewis acid sites and increases the concentration of Brönsted acid sites. Eberly[79] has also shown that the addition of trace amounts of water increased the concentration of Brönsted acidity and decreased the concentration of Lewis acidity. Christner et al[86] in their studies of pyridine adsorbed on Mg-, Ba- and Zn Y zeolites have observed the Brönsted acidity sites in these studies.

Hattori and Shiba[87] studied the acidity of Mg, Mn, and ZnX zeolites and reported that a small amount of Brönsted acidity and Lewis acidity, which is too weak to be converted into Brönsted acidity, in all 11A zeolites and also on those containing the

transition metal ions Mn, Co, Zn, Ag, Cd, but not on CuX zeolites. In all cases, the concentration of Brönsted acidity was increased by hydration. Similar results were obtained in the studies of the same series of transition metal ion Y zeolites. There appear to be no relationship between the concentration of acid sites and the physical properties of the zeolites. The factors involved in the formation of Brönsted acid sites are far more complicated than for alkaline earth zeolites[77]. It was observed that some of the partially transition metal exchanged Y zeolites have more acid sites than the fully exchanged transition metal Y zeolites.

(vi) Zeolites and adsorbed molecules

There are numerous published papers and reviews available on this subject and another review in this chapter is inappropriate. However, the molecules of relevant interest to this thesis will be discussed briefly. A detailed discussion of the relevant work is given in each chapter.

(a) Water

Infrared studies of water adsorbed on zeolites have been studied by a number of workers[66,70,79,84,91]. Bertsch and Habgood[66] studied the adsorption of small amounts of water on alkali metals exchanged zeolite X. They observed a sharp band between 3720 and 3648cm^{-1}, depending on the cation, together with broad bands near 3400 and 3200cm^{-1}. These bands were considered to represent water directly bonded to the cation via the oxygen and to the oxygen ions of the surface by a hydrogen atom. Ward[78] and Uytterhoeven et al[84] reached similar conclusions.

Zhadanov et al[55] investigated the infrared spectra of water molecules adsorbed by zeolites of various compositions. The

Si:Al ratios in the extreme samples of the zeolite series under consideration differed by more than a factor of two. For zeolites with the lowest Si:Al ratio a sharp band at 3690cm^{-1} and two broad bands at 3390 and 3235cm^{-1} were observed. In contrast, the zeolite with the highest Si:Al ratio showed only a very broad band at 3500cm^{-1}. The deformation band of the hydroxyl group also changed. For the former an intense band at 1658cm^{-1} and a weak one at 1585cm^{-1} were observed, while for the latter, two overlapping bands of low intensity at 1660 and 1600cm^{-1} were seen.

Readsorption of water on rare-earth zeolite did not give rise to a band at 3690cm^{-1} but to bands at 3610 and near 3560-3550cm^{-1}.

(b) Hydrocarbons

Yates et al[92] studied the adsorption of C_2H_4 on a series of type 13X zeolites. In all their spectra, they observed the υ_2(C=C stretch) and υ_3(CH_2 symmetric deformation) bands which are infrared inactive in the gas phase. This clearly indicates that the symmetry of C_2H_4 reduces with adsorption (probably to C_{2v}). For Ag13X zeolite, there were two distinct CH_2 deformation bands in the adsorbed phase, which suggested two discrete sites for the adsorbed C_2H_4. In all of the exchanged forms, except cadmium and silver, C_2H_4 was found to be weakly held since it could be removed by evacuation at room temperature. For Cd13X, however, evacuation at temperature above 473K was required to remove the C_2H_4 and more severe conditions were needed in the case of Ag13X zeolite.

Infrared spectra of C_2H_2 adsorbed onto various transition and alkali metal exchanged types A and 13X zeolites have been reported by Tsitsishvili et al[93]. They found that, regardless of the nature of the cation and the type of zeolite, they did

not observe a band due to $\upsilon(C\equiv C)$. This, together with the observation of the C-H stretching band, caused them to postulate that "end-on" interaction of the C_2H_2 with the framework occurred in their samples. Some of the measurements made by Tsitsishvili et al have been repeated by Tam et al[94,95], who in their data observed a band due to $\upsilon(C\equiv C)$ for C_2H_2 adsorbed on all of the zeolites studied. They deduced that the mode of interaction of the adsorbed C_2H_2 is that of a "side-on" since the $\upsilon(C\equiv C)$ band occurred at a wavenumber value below that of the gas phase. C_2H_2 was weakly held by Ca^{2+} and Mg^{2+} since it could be removed easily by evacuation at room temperature. For th NaA sample, evacuation for 1 hour at room temperature was needed to remove the C_2H_2 and for the KA sample, C_2H_2 was only removed after evacuation at 473K for several hours.

C_2H_2 adsorbed onto Cu and Ni exchanged Y zeolites have also been reported[96,97]. In the CuY + C_2H_2 system studied, Pichat found bands at 3250, 3190(sh), 3170, 1820(sh) and 1810cm^{-1}. Unlike other zeolites, the $\upsilon(C\equiv C)$ band for C_2H_2 adsorbed onto CuY was shifted down in wavenumber by a large amount (164cm^{-1}) relative to the gas phase. The formation of π-acetylenic complexes was suggested; the Cu^+ ion-acetylene resulting mainly from donation from the unsaturated hydrocarbon to the metal ion.

In the NiY + C_2H_2 system, Pichat et al[97] observed the cyclotrimerization of C_2H_2. It was found that the activity of the various samples depended on the number of the dehydrated or the partially dehydrated Ni^{2+} ions inside the supercages. They have also established from the bands they observed that the benzene obtained did not complex with the Ni^{2+} ions and is weakly adsorbed in the framework.

Angell and Schaffer[98], in their work on benzene adsorbed onto Ni and MgY zeolites found that benzene hydrogen bonded to the 3650cm^{-1} OH groups. Similar spectra were found when

benzene and benzene-d_6 were adsorbed on Mg, Ni, Zn, Ag, La, Ce, and CoY zeolites. The CH frequencies were the same as those for liquid benzene. The frequencies due to vibrations in the plane of the ring were unchanged while those due to out-of-plane vibrations were shifted to higher frequencies. The spectra were interpreted in terms of interaction between the surface and the π orbitals of benzene, assuming the molecule adsorbed parallel to the surface.

(c) Sulfur-containing molecules

H_2S adsorption on NaA and CaNaA zeolites has been reported by Forster and Schuldt[99]. In the case of NaA, they found that the new band observed at 2500cm^{-1} shifted to higher wavenumber with increasing coverage while for CaNaA, upon adsorption of H_2S, a band appeared at 2540cm^{-1} which remained constant over a wide range of coverage. They deduced that in the zeolite NaA H_2S was adsorbed at two different sites while in the zeolite CaNaA, all the H_2S occupied equivalent sites and that no significant adsorbate-adsorbate interaction occurred. In both cases, however, the adsorbed H_2S could be removed easily by evacuation at room temperature. Water formation observed in the spectra of the samples studied, was explained by the authors as due to the reaction of the adsorbed H_2S with molecular oxygen from the gas phase.

Karge and Rasko[100] studied the adsorption of H_2S on faujasite type zeolites with systematically varied Si:Al ratios (1.05-3.24). The authors found that with increasing the pressure of H_2S, the 2560cm^{-1} band for NaX became asymmetric, broadened, and shifted to lower frequency, while the same band for NaY remained symmetric and occurred at an almost constant frequency. It was suggested that in NaX sample both chemisorption and physisorption of H_2S had occurred. In the case of NaY, however, only the

non-dissociative adsorption took place. Both adsorption processes were reversible since the OH, SH^- and H_2S bands could be removed by evacuating the samples.

The adsorption of H_2S and SO_2 on Na and HY zeolites was carried out by Deo et al[101]. H_2S was physically adsorbed on NaY zeolite. Water was formed possibly by the oxidation of H_2S by chemisorbed O_2. Their results on HY zeolite showed that no oxidation of H_2S has occurred, and a broad band at $3200cm^{-1}$ was observed. This band was due to H_2S hydrogen bonded to surface hydroxyl. Adsorption of SO_2 on NaY produced a single band at $1330cm^{-1}$ owing to physically adsorbed SO_2. When H_2S was added, a rapid reaction occurred producing water. Adsorption of SO_2 on HY resulted in hydrogen bonding to the $3650cm^{-1}$ OH groups. No chemisorbed species were detected.

References

1. Breck D.W., Zeolite Molecular Sieves, Wiley-Interscience, New York (1974).
2. Rees L.V.C., Solid Electrolytes, 417 (1978).
3. Meier W.M., Molecular Sieves, Society of Chemical Industry, London (1968).
4. Barrer R.M., Chem. Ind., 1203 (1968).
5. Reed T.B., and Breck D.W., J. Amer. Chem. Soc., 78, 5972 (1972)
6. Lowenstein W., Am. Mineral, 39, 92 (1951).
7. Gramlich V., and Meier W.M., Z. Kristallogr., 133, 134 (1971)
8. Thoni W., Z. Kristallogr., 142, 142 (1975).
9. Pluth J.J., and Smith J.V., J. Phys. Chem., 83, 741 (1979).
10. Pluth J.J., and Smith J.V., J. Amer. Chem. Soc.,102, 4704 (1980).
11. Bursill L.A., Lodge E.A., Thomas J.M., and Cheetham A.K., J. Chem. Soc. Chem. Comm. 276 (1981).
12. Bursill L.A., Lodge E.A., Thomas J.M., and Cheetham A.K., J. Phys. Chem., 85, 2409 (1981).
13. Breck D.W., J. Chem. Ed., 41, 678 (1964)
14. Olson D.H., J. Phys. Chem., 74, 2758 (1970).
15. Dempsey E., Kuhl G.H., and Olson D.H., J. Phys. Chem., 73, 387 (1969).
16. Barrer R.M., Zeolites and Clay Minerals as Sorbents and Molecular Sieves, Academic Press, London (1978).
17. Breck D.W., Eversole W.G., Milton R.M., Reed T.B., and Thomas T.L., J. Amer. Chem. Soc., 78, 5963 (1956).
18. Broussard L., and Shoemaker D.P., J. Amer. Chem. Soc.,82, 1041 (1960).
19. Yanagida R.Y., Amaro A.A., and Seff K., J. Phys. Chem., 77, 805 (1973).
20. Subramanian V., and Seff K., J. Phys. Chem., 81, 2249 (1977).

21. Pluth J.J. and Smith J.V., J. Amer. Chem. Soc. 102, 4704 (1980).

22. Baur W.H., Amer. Mineral. 49, 697 (1964).

23. Eulenberger G.R., Shoemaker D.P. and Keil J.G., J. Phys. Chem. 71, 1812 (1967).

24. Rees L.V.C., Annual Reports, Chem. Soc., London (1970).

25. Sherry H.S., Adv. Chem. Ser. 101, 350 (1971)

26. Barrer R.M. and Townsend R.P., J. Chem. Soc. Trans. Faraday I, 72, 661 (1976).

27. Maes A. and Cramers A., Adv. Chem. Ser., 121, 230 (1973).

28. Maes A. and Cramers A., J. Chem. Soc. Trans. Faraday I, 71, 265 (1975).

29. Gal I.J., Jankovic O., Malcic S., Radovanov P. and Todorovic M., Trans. Faraday Soc., 67, 999 (1971).

30. Turkevich J., Catal. Rev., 1,1 (1967)

31. Venuto P.B. and Landis P.S., Adv. Catal., 18, 259 (1968).

32. Rabo J.A., Amer. Chem. Soc. Monograph, 171 (1976).

33. Venuto P.B., Wu E.L. and Cattanach J., Molecular Sieves, Soc. Chem. Ind., London (1968).

34. Venuto P.B, Amer. Chem. Soc. Adv. Chem., 102, 260 (1971)

35. Rabo J.A. and Poutsma M.L., Amer. Chem. Soc. Adv. Chem. 102, 284 (1973).

36. Minachev M. and Isakov Y.I., Amer. Chem. Soc. Adv. Chem., 121, 451 (1973).

37. Barthomeuf D., Amer. Chem. Soc. Symp. Ser., 40, 453 (1977)

38. Lunsford J.H., Amer. Chem. Soc. Symp. Ser., 40, 473 (1977).

39. Magee J.S., Amer. Chem. Soc. Symp. Ser., 40, 650 (1977).

40. Weisz P.B., Pure and Appl. Chem., 52, 2091 (1980).

41. Merrill H.E. and Arey W.F., Amer. Chem. Soc. Div. Pet. Chem. Prepr. 193 (1968).

42. Benesi H.A., J. Catal., 8, 368 (1967).

43. Bertsch L. and Habgood H.W., J. Phys. Chem., 67, 1621 (1967)

44. Lunsford J.H., J. Phys. Chem. 72, 4163 (1968).

45. Muha G.M. and Yates D.J.C., J. Chem. Phys., 49, 5093 (1968).

46. Olson D.H. and Dempsey E.J., J. Catal., 13, 221 (1969).

47. Rabo J.A., Angell C.L., Kasai P.H. and Schoemaker V., Diss. Farad. Soc., 41, 228 (1966).

48. Richardson J.T., J. Catal., 9, 182 (1967).

49. Sherry H.S., J. Phys Chem., 70, 1158 (1966).

50. Lefond S.S, Industrial Rocks and Minerals, Volume 4, Amer. Inst. of Mining, Metallurgical and Pet. Engineers, Inc. New York (1975).

51. Townsend R.P., The Properties and Applications of Zeolites, Chem. Soc., London (1979).

52. Mumpton F.A. and Fishman P.H., J. Anim. Sci., 45, 1188 (1977).

53. Chen N.Y., J. Phys. Chem., 80, 60 (1976).

54. Milkey R.G., Amer. Mineral., 45, 990 (1960).

55. Zhadanov S.P., Kiselev A.V., Lygin R.J. and Titova I.I., Russ. J. Phys. Chem., 38, 1299 (1964).

56. Flanigen E.M., Khatami H. and Szmanski H.A., Adv. Chem. Ser., 101, 201 (1971).

57. Burragato F., Mathias F. and Parodi G., Rend. Soc. Ital. Mineral. Petrol., 34, 27 (1978).

58. Joshi M.S. and Bhoskar B.T., Indian J. Pure and Appl. Phys., 19, 560 (1981).

59. Oinuma K. and Hayashi H., J. Tokyo Univ., 8, 1 (1967).

60. Stubican V. and Roy R., Amer. Mineral., 46, 32 (1961).

61. Stubican V. and Roy R., J. Amer. Ceram. Soc., 44, 625 (1961).

62. Stubican V. and Roy R., Z. Krist., 115, 200 (1961).

63. Wright A.C., Rupert J.P., and Granquist W.T., Amer. Mineral. 53, 1293 (1968).

64. Szymanski H.A., Stamires D.N. and Lynch G.R., J. Opt. Soc. Am., 50, 1323 (1960).

65. Zhadanov S.P., Kiselev A.V., Lygin V.I. and Titova I.I., Dokl. Akad. Nauk. SSSR, 150, 584 (1963).

66. Bertsch L. and Habgood H.W., J. Phys. Chem., 67, 1621 (1963).

67. Carter J.L., Lucchessi P.J. and Yates D.J.C., J. Phys. Chem., 68, 1385 (1964).

68. Habgood H.W., J. Phys. Chem., 69, 1764 (1965).

69. Uytterhoeven J.B., Christner L.G. and Hall W.K., J. Phys. Chem., 69, 2117 (1965).

70. Angell C.L. and Schaffer P.C., J. Phys. Chem., 69, 3463 (1965).

71. Ward J.W., J. Catalysis, 9, 225 (1967).

72. Ward J.W., J. Catalysis, 9, 396 (1967).

73. Eberly P.E., J. Phys. Chem., 71, 1717 (1967).

74. Hughes T.R. and White H.M., J. Phys. Chem., 71, 2192 (1967).

75. Uytterhoeven J.B., Jacobs P., Makay K. and Schoonheydt R.J., J. Phys. Chem., 72, 1768 (1968).

76. Richardson J.T., J. Catalysis, 9, 172 (1967).

77. Ward J.W., J. Catalysis, 10, 34 (1968).

78. Ward J.W., J. Phys. Chem., 72, 4211 (1968).

79. Eberly P.E., J.Phys. Chem., 72, 1042 (1968).

80. Christner L.G., Liengme B.B. and Hall W.K., Trans. Faraday Soc., 64, 1679 (1968).

81. Basila M.L., Appl. Spectry. Rev., 1, 289 (1968)

82. Yates D.J.C., Catalysis Rev., 2, 113 (1968).

83. Ward J.W., Int. Conf. Molecular Sieve Zeolites, 2nd Worcester, Mass., (1970).

84. Uytterhoeven J.B., Christner L.G. and Hall W.K., J. Catalysis, 13, 425 (1969).

85. Olson, D.H., J. Phys. Chem., 72, 1400(1968).

86. Christner, L.G., Liengme, B.V., and Hall, W.K., Trans. Faraday Soc., 64, 1679(1968).

87. Hattori, H., and Shiba, T., J. Catal., 10, 27(1968).

88. Watanabe, Y., and Habgood, H.W., J. Phys. Chem., 72, 3066(1968).

89. Ward, J.W., J. Catal., 14, 365(1969).

90. Ward, J.W., J. Catal., 22, 237(1971).

91. Rabo, J.A., Angell, C.L., and Schoemaker, V., Intern. Congr. Catalysis, 4th., Moscow(1968).

92. Carter, J.L., Yates, D.J.C., Lucchesi, P.J., Elliot, J.J., and Kervokian, V.J., J. Phys. Chem., 70, 1126(1966).

93. Tsitsishvili, G.V., Bagratishivili, G.D., and Oniashvili, N.I., Zh. Fiz. Khim., 43, 950(1969).

94. Tam, N.T., Cooney, R.P., and Curthoys, G., J. Chem. Soc. Farad. Trans. I, 72, 2577(1976).

95. Tam, N.T., Cooney, R.P., and Curthoys, G., J. Chem. Soc. Farad. Trans. I, 72, 2592(1976).

96. Pichat, P., J. Phys. Chem., 79, 2127(1975).

97. Pichat, P., Vedrine, J.C., Gallezot, P., and Imelik, B., 32, 190(1974)

98. Angell, C.L., and Howell, M.V., J. Colloid Interface Sci., 28, 279(1968).

99. Forster, H., and Schuldt, M., J. Colloid Interface Sci., 52, 380(1975).

100. Karge, H.G., and Rasko, J., J. Colloid Interface Sci., 64, 522(1978).

101. Deo, A.V., Dalla Lana, I.G., and Habgood, H.W., J. Catal., 21, 270(1971).

CHAPTER III

EXPERIMENTAL

I. Instrumentation

(i) Infrared spectrophotometer

The Perkin Elmer 580B instrument used is a double beam, ratio recording infrared spectrophotometer[1]. The source of radiant energy is a ceramic tube heated by an internal element to about 1473K which produces a continuous spectrum of electromagnetic radiation in the infrared region.

The following description refers to figures 3.1, the block diagram, and 3.2, the optics diagram of the spectrophotometer[1].

Radiation from the source is focussed on a baffle by the toroid mirror M(T)1, the baffle ensures that radiation from only a limited surface area of the source is admitted to the optical system to minimize sample heating. The baffle image is focussed onto the first chopper mirror M(C)5, which rotates dividing the source energy into sample and reference beams. Each beam passes through a focal point within the sample compartment.

After the sample compartment the alternate pulses of radiation from the two beams are combined by the action of a second chopper mirror M(C)10. During the first and second quadrants, the second chopper receives energy from the sample and reference beams respectively. During the third and fourth quadrants, the first chopper cuts off the source energy so that any energy appearing at the second chopper is due to reradiation effects from the sample compartment.

The recombined beam passes through a pupil image between M(T)11and M(T)12. A second baffle between M(T)12 and M(T)13

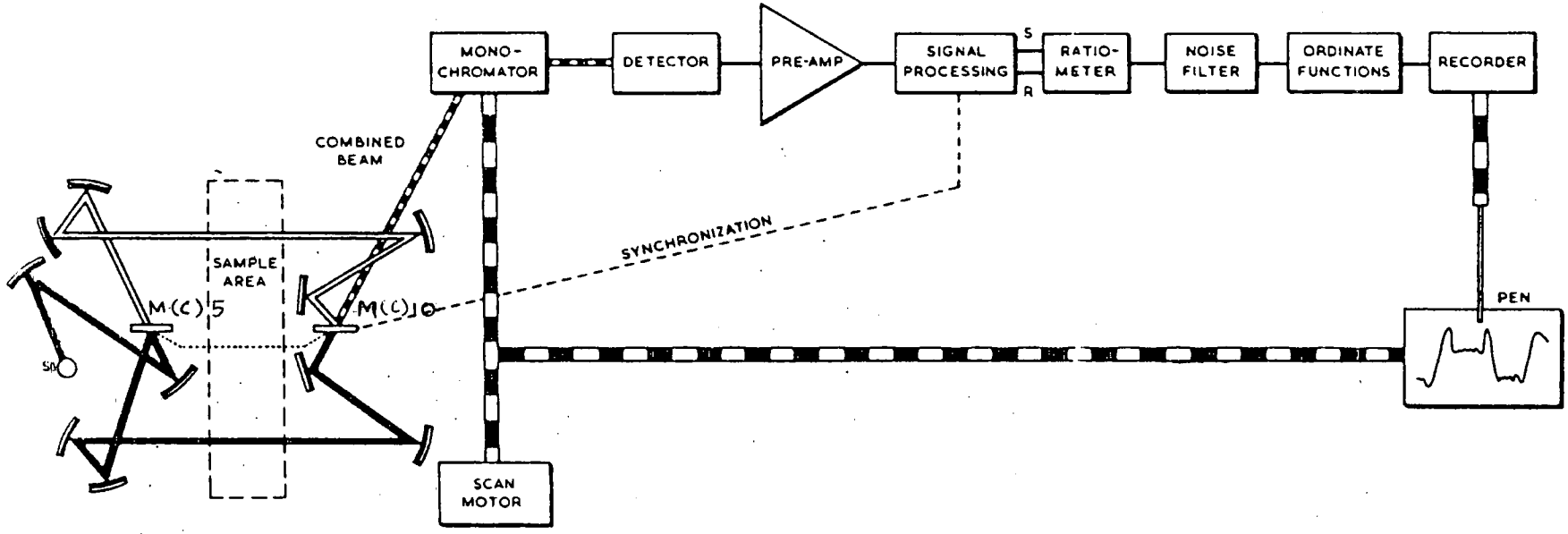

Figure 3.1. A block diagram of PE580 spectrophotometer.

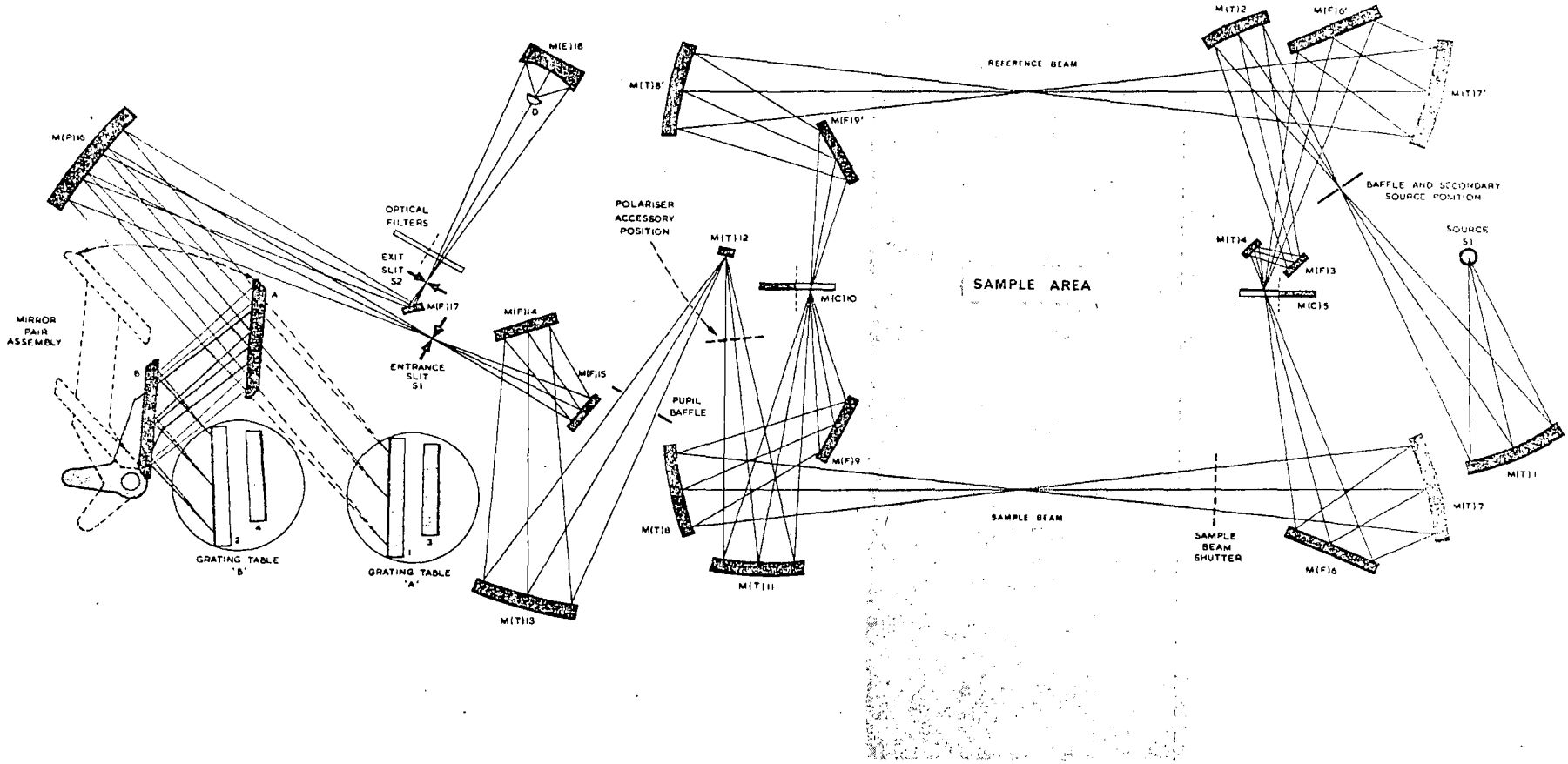

Figure 3.2. An optic diagram of PE580 spectrophotometer. M(C)=chopper mirrors; M(E)=ellipsoid mirrors; M(F)=plane mirrors; M(P)=paraboloid mirrors and M(T)=toroid mirrors.

acts as the limiting pupil aperture in the system, and rejects unwanted radiation from the pre-optics.

M(F)14 and M(F)15 are plane mirrors that direct the beam onto the monochromator entrance slit S1. The beam diverges from S1 until the paraboloid mirror M(P)16 reflects it as a collimated beam into the grating in use. As the grating is rotated, the diffracted radiation is focussed in the plane of the exit slit by M(P)16. This slit restricts the radiation passing through it to a narrow wavenumber band, the mean of which corresponds to the wavenumber at which the measurement is being made. Decreasing the slit width, therefore, decreases the bandwidth and the intensity of the emerging radiation. Finite slit widths are necessary to enable sufficient energy to reach the detector for the efficient operation of the signal processing system. Since the slit width is programmed to maintain approximately constant energy at the detector over most of the wavenumber range the effective bandwidth varies with the wavenumber setting of the instrument.

After leaving the exit slit the radiation passes through one of a set of optical filters; the correct filter is automatically selected for the spectral region being scanned.

The transmitted radiation is then focussed onto a detector. The detector consists of a thermocouple within an evacuated housing at the focus of an on-axis ellipsoid mirror M(E)18. The radiant energy leaving the slit is focussed by the ellipsoid mirror and the image reduction is eight to one. A caesium iodide lens on the thermocouple assembly further reduces the divergence of the slit image falling on the sample.

The alternating signal from the detector is amplified

and before being demodulated by the signal processing electronics to give separate sample and reference beam signals, which are compensated for the effects of thermal reradiation from the sample compartment. The ratiometer produces the ratio of the two signals which corresponds to the transmittance value of the sample. The signal is then filtered to reduce the noise level and subsequently the baseline adjustment, offsetting and scaling operations are performed in the ordinate functions unit. After further amplification this signal is supplied to the recorder.

(ii) Infrared data station

The data station is provided in three modules, namely, the visual display unit, the keyboard and the data processing module.

The visual display unit shows the system condition via the alphanumeric display and graphics facilities are also provided for the display of spectra. The data processing module houses the system electronics and two microfloppy disc drives, one of which is used for the programme disc, while the other is used for data storage.

Figure 3.3 shows a block diagram of the data station. The system contains two kinds of program software: (a) the operating system and (b) the task group. The Perkin-Elmer Terminal Operating System (PETOS) is the general instruction group. PETOS controls all keyboard operations and data organization. The task group includes the PE580 applications program, which is supplied with the system. The program permits acquisition of spectra from the spectrophotometer, enhancement of this data, display of the spectra on the visual display unit and their subsequent storage on a disc.

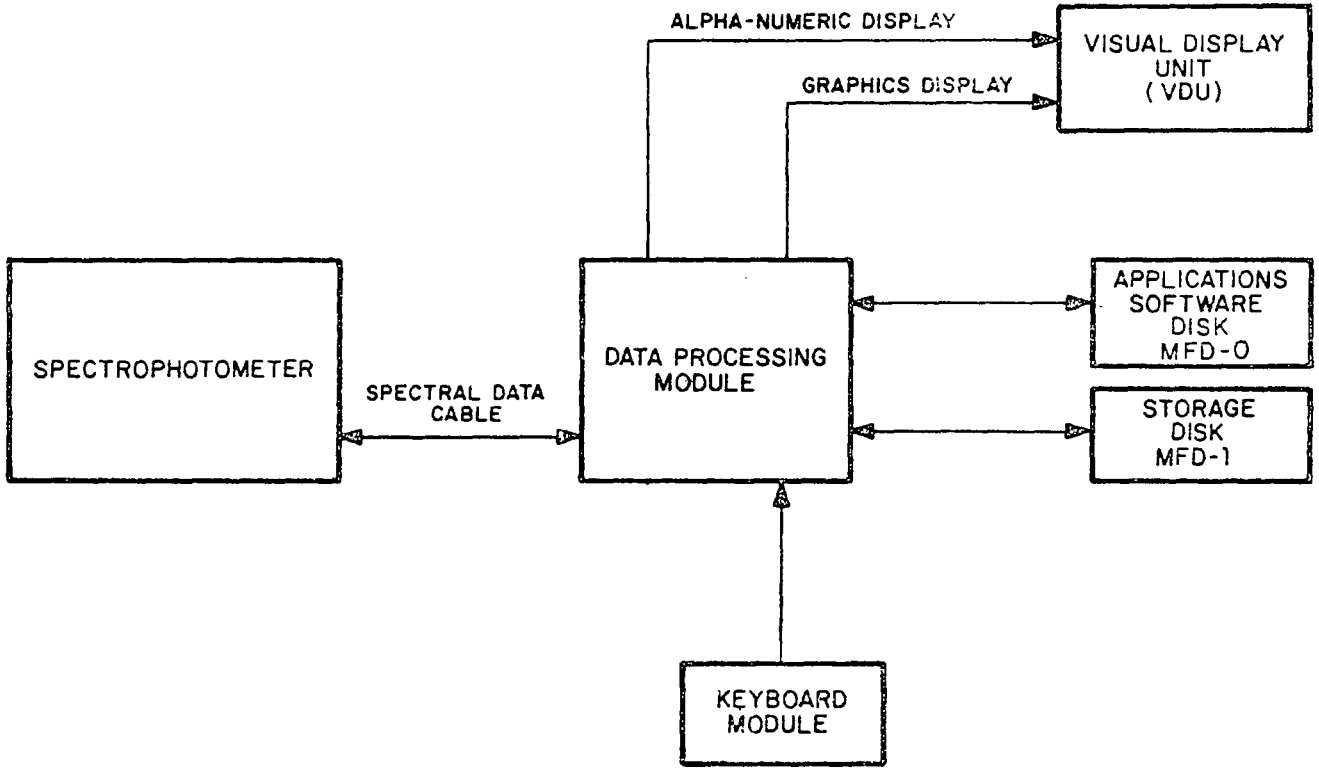

Figure 3.3. A block diagram of the datastation.

For the work described in this thesis, the most important and frequently used data manipulation software is the ABEX command[2]. This command (or function) is equivalent to running a second spectrum with a sample of increased or decreased concentration depending upon the magnitude of the factor used. The expansion (or reduction) results in a spectrum in which the relative intensities of the infrared bands are unchanged. Figure 3.4 shows an example of the spectra of AgA zeolite before and after expansion. The spectrum of AgA before expansion (Figure 3.4(a)) is very poor, with a transmission of less than 10%. With spectra of this quality, it is very difficult to follow the decrease in intensities of the water band ($1640cm^{-1}$) as the zeolite sample is heated. However, after expansion (Figure 3.4(b)) a much clearer spectrum is obtained. With the expanded spectrum, it is easier to follow the decrease in intensity of the water band during dehydration of the sample.

Likewise, during adsorption experiment, those bands due to adsorbed species which occur in the region $2000-1200cm^{-1}$ can be relatively easily observed if the ABEX command is used to expand the spectra. From the example given, it can be seen that it is only possible to study the spectra of adsorbed species on this type of spectrometer if the data station or its equivalent are available.

(iii) Infrared cell

For adsorption studies, any surface impurities on the sample must be removed. This is most commonly done by heating the sample under high vacuum. As part of this study, continuous attention has been paid to the improvement of the cell, especially designed for spectroscopic studies

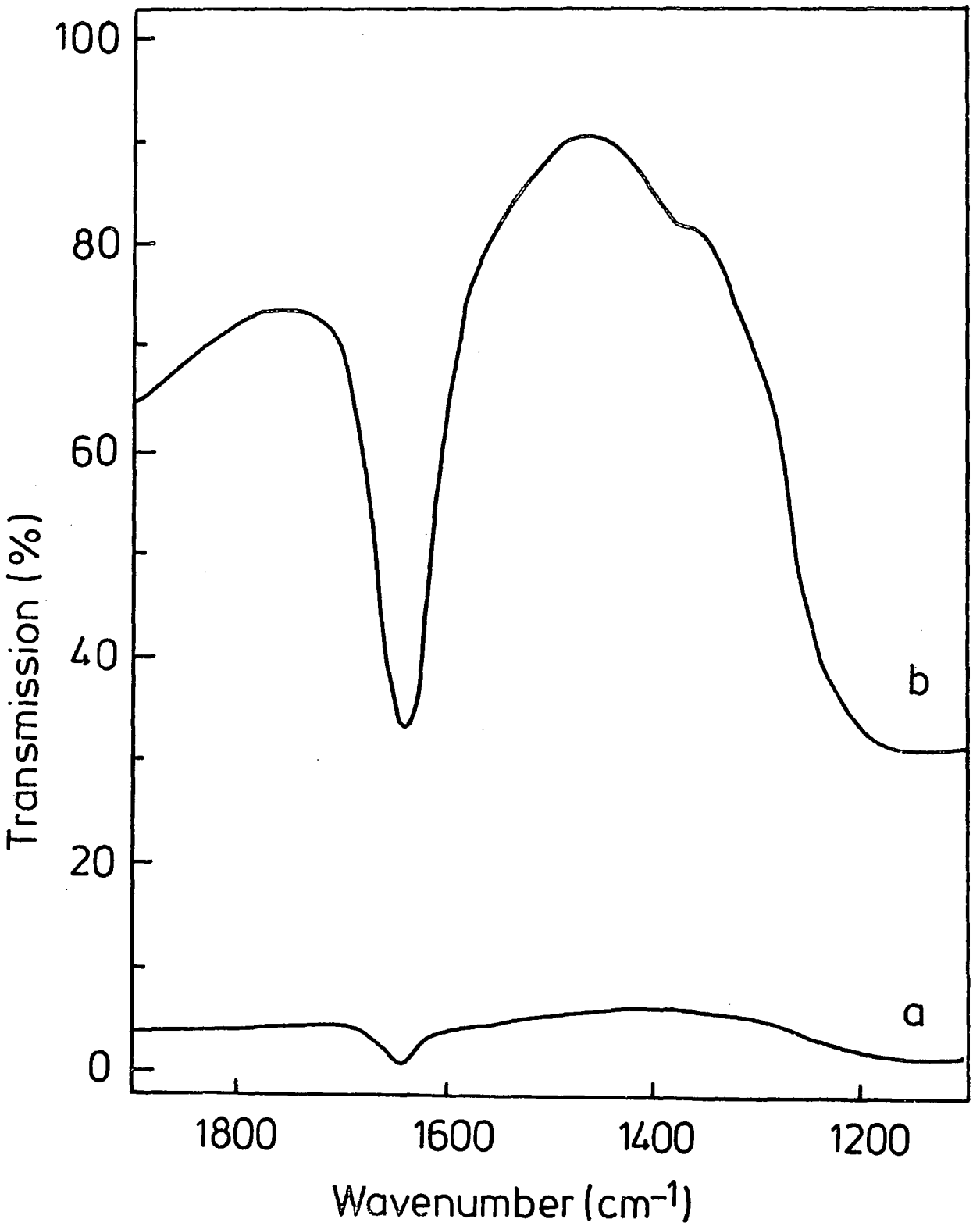

Figure 3.4. Spectra of AgA zeolite (a) before and (b) after expansion.

of adsorbed species. A wide variety of cells has been designed[3-6] for use with pressed discs. Many designs provide for the sample to be moved, either mechanically or by a windlass arrangement, so that heat treatment can be conducted without danger to the infrared cell. In the static designs[7,8] the window joints are often cooled when the sample is heated in order to avoid thermal stresses on the windows.

The infrared cell used for our spectroscopic studies is described below. Plan views of the cell are shown in figures 3.5 and 3.6 and the cell is made entirely of stainless steel. Full details of the dimensions of the cell are shown in figures 3.5 and 3.6. All spectra of the sample during heating, pumping and adsorption experiments were obtained without removing the cell from the sample compartment.

The cell is heated electrically by means of the molybdenum wire (0.5mm diameter) at (A) which is insulated using a sleeving (refrasil) insulator. Extension leads from the electrical feed-through at (B) are connected to a transformer and variac to control the temperature of the sample, which can be heated in situ to temperatures up to 740K. The temperature of the sample is measured with a chromel-alumel thermocouple (C), where the hot junction is imbedded in the sample holder (D).

The optical windows (E) used are made from KRS5 (TlBr-TlI), 5mm thick and 20mm diameter and are placed against packing O-rings of 1mm thickness which are seated at (F). The windows are tightened in position by the knurled rings (G). To keep these windows at an acceptable temperature, a water cooling jacket (H) is used.

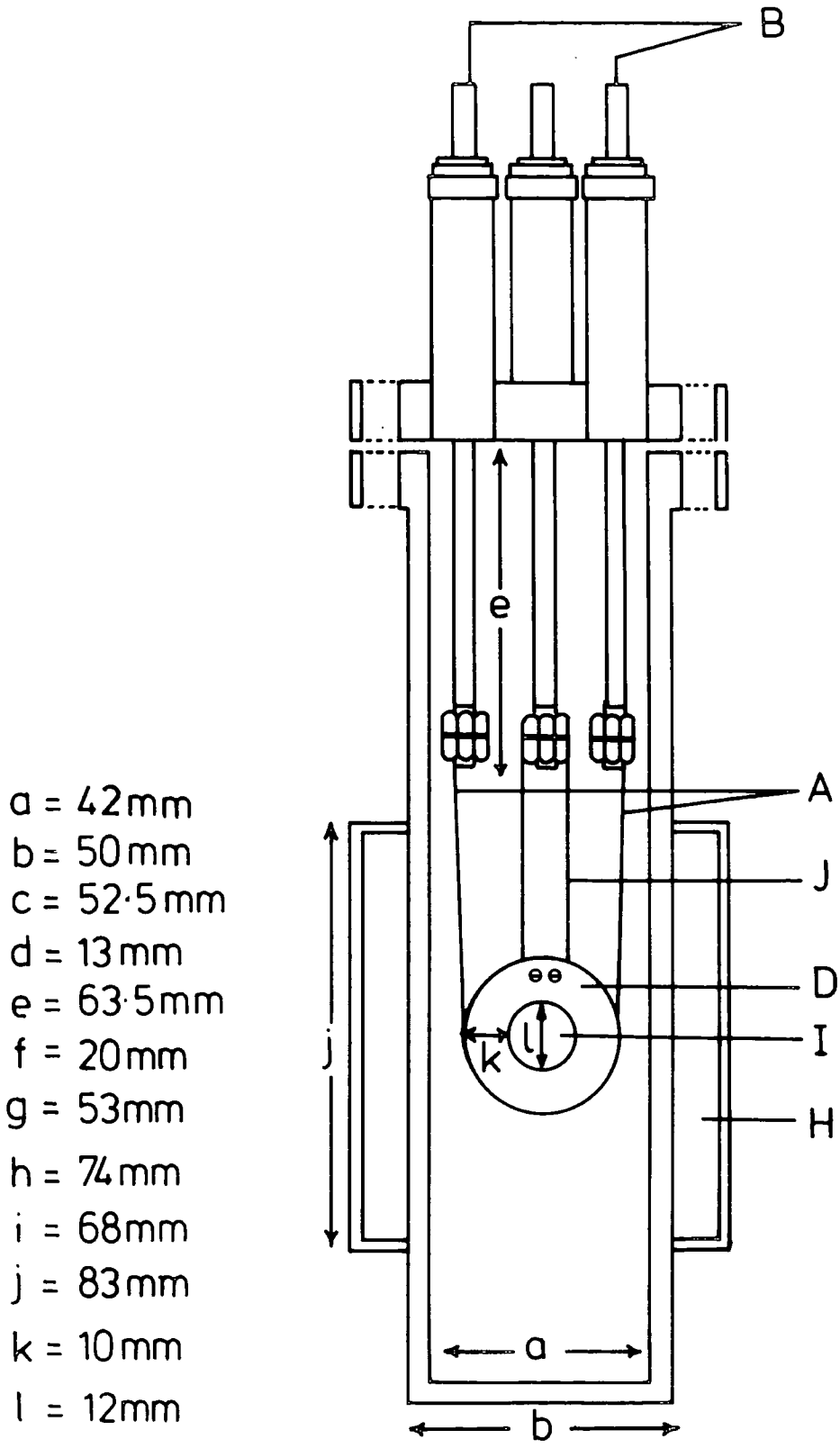

Figure 3.5. A front view of the infrared cell.

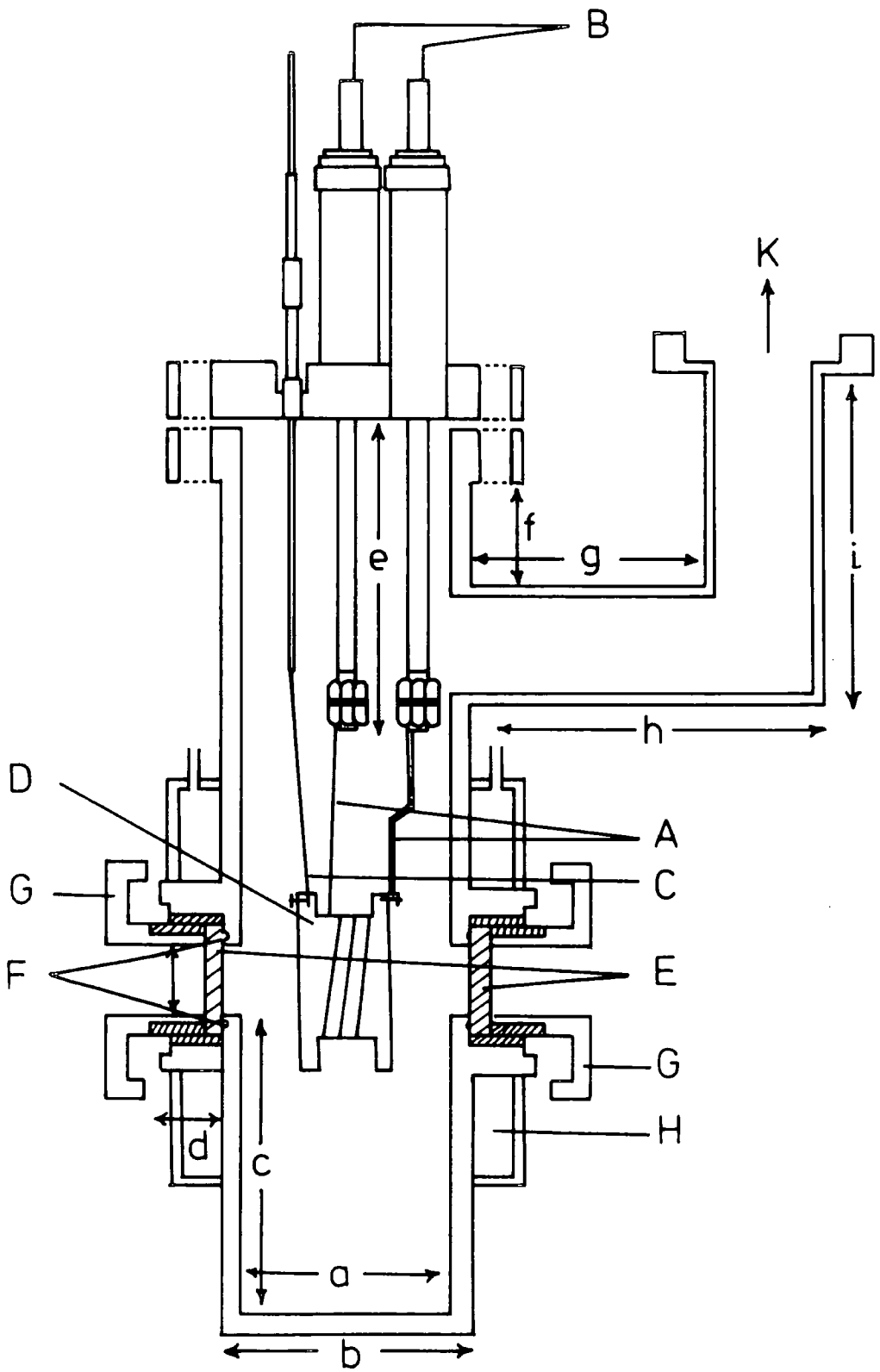

Figure 3.6. A side view of the infrared cell.

The sample (1) is placed between two stainless steel rings and is held intact by another screw-in stainless steel ring. A piece of stainless steel at (J) is used to hold the sample holder in position in the spectrometer.

The cell is connected to the vacuum system at (K).

(iv) Vacuum system

Figure 3.7 shows a block diagram of the vacuum and gas handling system. Apart from the gas handling part, which is made of glass, the whole vacuum line is made from stainless steel.

The cell (A) is connected to the vacuum system by means of the flexible bellows (B). Gases from the glass bulb (C) are admitted into the cell via the valve (D). The pressure of the gas is read from the digital readout of the baratron gauge (E).

A pirani gauge (F) and a hot cathode ionization gauge (G) are used to obtain the pressure in the vacuum system before admitting any gas. The quadrupole mass spectrometer (type QX200 made by Vacuum Generators) at(H) is invaluable in detecting very small leaks and impurities in the system.

The backing pump (1), which is a rotary vane type, is used to pump out the system to a vacuum of 10^{-1} torr or better before the turbomolecular pump (J) is switched on. With the turbomolecular pump, a vacuum of 10^{-6} torr or better is routinely obtained. When necessary, the whole vacuum system is baked out to remove impurities, mainly water vapour, in the system.

(v) Thermogravimetric analysis

The measured variable in thermogravimetric analysis is

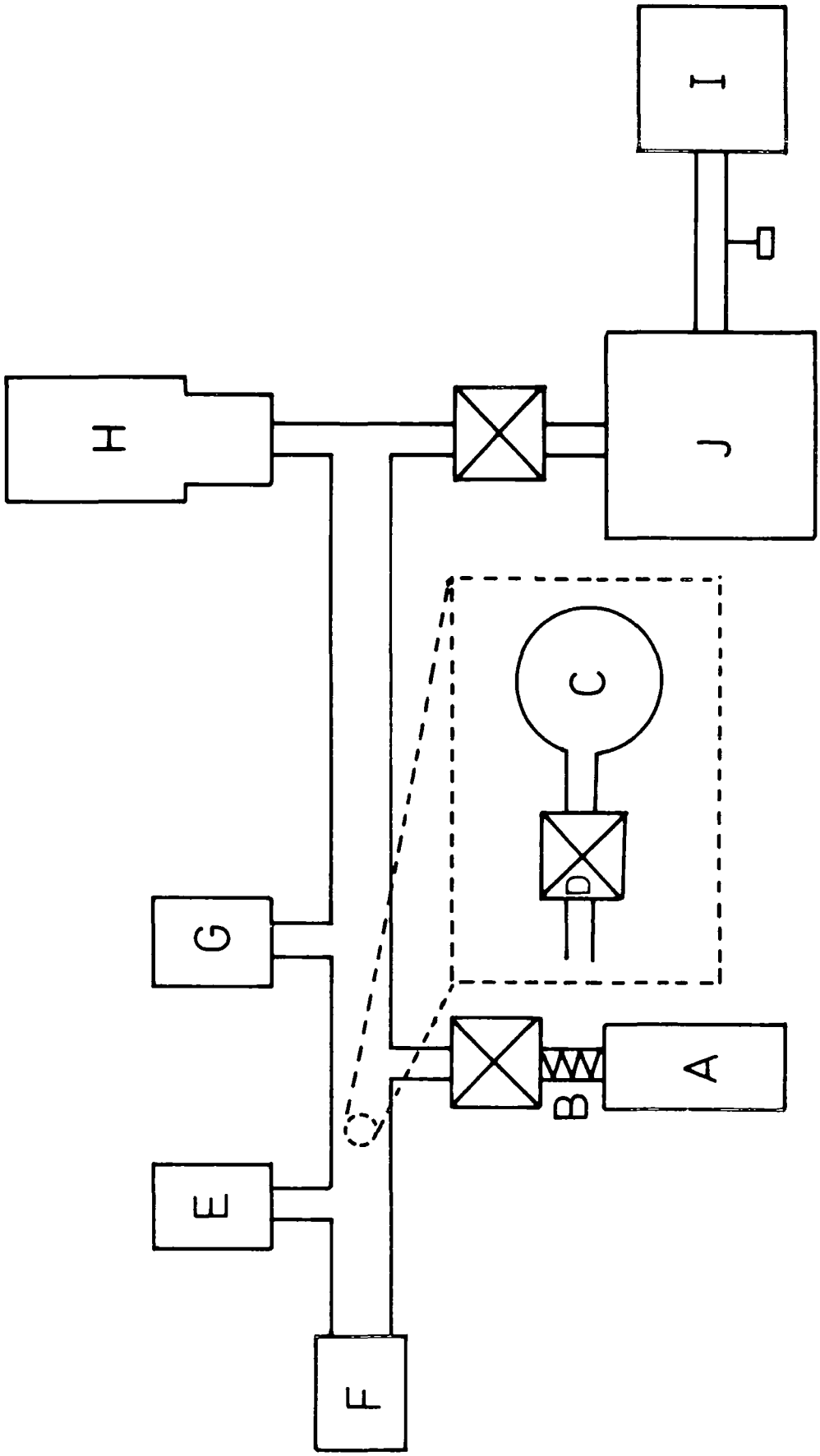

Figure 3.7. A block diagram of the vacuum system.

the change in weight of the sample as it is heated or cooled. The thermogravimetric apparatus used to obtain the thermograms of zeolites is a Stanton Redcroft TG-750 thermobalance. This apparatus is designed to give a direct plot of weight versus temperature for any sample over the range of 300 to 1273K.

These thermograms provide valuable information on the following physical and chemical phenomena: vaporization, sublimation, absorption, adsorption-desorption, decomposition, dehydration, solid-solid reactions involving loss of weight, oxidation, and reduction. The most important aspects, however, in the thermograms of zeolites as far as our work is concerned are dehydration and decomposition.

Plateaus observed in the thermograms of zeolites imply a constant weight representing stable phases over the particular temperature interval. A change in level may imply the formation of an intermediate compound or the removal of water. From the thermograms of the zeolites, the values of percentage water lost at different temperatures can be calculated. We have assumed that at 1273K all the water molecules are removed from the sample. A graph of percentage water loss versus temperature can show to what extent the water molecules are removed from the sample by heating to a particular temperature.

(vi) X-ray powder photograph

X-ray powder photographs have been used to distinguish zeolite structures and to detect any decomposition. The zeolite sample is in powder form and placed in a silica tube before positioning it in the camera. The source of radiation used was CuK_{α}.

II. Sample preparation

Approximately 15mg of the zeolite sample was pressed into a 1.6cm diameter die using a pressure of $2500g/cm^2$. The zeolite disc was then mounted in the infrared cell and evacuated to 10^{-6} torr (1 torr=133.32Pa) using the turbomolecular pump. The zeolite sample was heated to the maximum temperature required, infrared spectra being recorded at various temperatures during heating. It was then left at the maximum bake-out temperature for a specified time and spectra measured at regular intervals during this period before allowing the sample to cool to room temperature, and its spectrum re-recorded. Gases were then admitted into the infrared cell to the required pressure(s). Spectra of the sample and the adsorbate were obtained under the required conditions.

In order to study the low vibrational frequencies of the sample (below $1200cm^{-1}$), a KBr disc of the sample was prepared and the spectrum recorded.

For comparison the spectra of the pure gases at various pressures were obtained by using an infrared cell containing no zeolite disc.

III. Sample analysis

Elemental analyses of the zeolites were performed by using a Perkin Elmer 403 atomic absorption spectrometer.

In the case of zeolite type A, known quantity of the sample was dissolved in dilute nitric acid and measured against the appropriate aqueous standard. For zeolites types 13X and Y, the sample was first digested with hydrogen fluoride and perchloric acid before dissolving in dilute

nitric acid, and measured against the appropriate aqueous standard.

From the percentage of the elements obtained, the amount of the corresponding elements can be calculated. Analysis of Si, Al and the substituted ions were made for all of our samples.

References

1. Model 580B Infrared Spectrophotometer Instructions Manual, Perkin-Elmer Ltd., England (1977)
2. Model 3500 Infrared Data Station, PE580 Application Programme Instructions, Perkin-Elmer Ltd., England (1980)
3. Alpert, N.L., Keiser, W.E., and Szymanski, H.A., Infrared Theory and Practice of Infrared Spectroscopy, Plenum Press, New York (1970).
4. Provotorov, B.I. and Sokolova, N.P., Russ. J. Phys. Chem., 47, 1376 (1973).
5. Ramamoorthy, P. and Gonzalez, R.D., J. Catal., 58, 188 (1979).
6. Ceckiewicz, S. and Galuszka, J., Reaction Kinetics and Catalysis Letters, 5(3), 257 (1976).
7. Dalla Betta, R.A. and Shelef, M., J. Catal., 48, 111 (1977).
8. Gallei, E. and Schadow, E., Rev. Sci. Instrum., 45(12), 1504 (1974).

CHAPTER IV

INFRARED SPECTROSCOPIC STUDIES OF ETHYLENE ADSORBED ON SILVER A ZEOLITE

I. Introduction

The motivation for the work reported here was the discrepancy between the X-ray work of Kim and Seff,[1] in which only one adsorption site for C_2H_4 was located within fully dehydrated Ag_{12}-A zeolite, and recent inelastic neutron scattering (INS) studies, which located two distinct adsorption sites[2]. Although infrared and INS are both vibrational spectroscopic techniques, they differ in selection rules. Furthermore in this particular case, they are complementary in the frequency ranges studied: the INS work was confined to the region below 700cm^{-1} (a region in which it is extremely difficult to obtain infrared spectra of unsupported zeolites), whilst this infrared study is concerned with the region above 1200cm^{-1}.

The structure of Ag_{12}-A and in particular the structural changes which occur on dehydration are the subject of some controversy. Because of its importance to this work the structural information available will be reviewed here.

Almost total replacement of sodium ions, in Linde type 4 A (Na_{12}-A) zeolite, by silver ions may be accomplished[3]. X-ray single crystal determinations of fully hydrated silver type A zeolite (Ag_{12}-A)[4,5] (unit cell = 12.288 Å) have shown the cations to be distributed over three positions within the framework (Table 4.1). Eight silver ions were located on three-fold axes near 6-rings; of these, five were recessed into the large (α) cavity (S2*), each coordinated to at least one water molecule, and the three remaining were displaced into

Table 4.1 Possible cation positions in type A zeolites compared with the site occupancies found for fully hydrated and partially dehydrated zeolite $Ag_{12}A$

Position	Designation	Number of sites (per pseudo unit cell)	Site occupancy in hydrated $Ag_{12}A$ zeolite[5]	Site occupancy in partially dehydrated $Ag_{12}A$ zeolite[5]
In an 8-ring	S1	3	3	1
Adjacent to an 8-ring but displaced into an α-cage	S1*			2
In a 6-ring	S2	8	5	3
Adjacent to a 6-ring but displaced into an α-cage	S2*			
Adjacent to a 6-ring but displaced into a β-cage	S2'		3	2
	S2"#			3
Against a 4-ring	S3	12	1	1
In the centre of a β-cage	SU	1		
In the centre of an α-cage	S4	1		

Position defined in the text.

the sodalite (β) cage (S2') with three water molecules bridging them. A further three silver ions were associated with 8-rings, but off-center (making closest approach to only three oxygen atoms) and displaced into the α cage (S1*). The final cation was found within the large (α) cavity opposite a 4-ring (S3). As a result of the low overall symmetry of the environment in the α cavity many different coordination sites for water exist. These have low occupancies, and hence no definite positions or occupancies could be determined.

Dehydration under vacuum causes Ag_{12}-A zeolite to change colour from pale grey to deep orange. This is a reversible process: Ag_{12}-A becomes bright yellow if allowed to cool in air, and ultimately returns to its initial pale grey state. Matsumoto et al[6] have concluded that Ag_{12}-A is structurally less stable with respect to temperature than Na_{12}-A zeolite.

A single cystal X-ray study has been reported[5] of an Ag_{12}-A zeolite, partially dehydrated by heating at 473K in a stream of oxygen for 12h, and then by evacuating at 623K and 10^{-5} torr for 48h. Eight silver ions were found to be distributed over three-fold axes associated with 6-rings. Of these, three were located in the α cage (S2*), two were situated within the sodalite unit (β cage) 0.44 Å from the ring plane (S2'), and three were within the sodalite unit 1.19 Å from the ring plane (S2"). Three additional silverions were found adjacent to 8-rings, but displaced off-center (as in the case of hydrated Ag_{12}-A zeolite); two of these occupied positions where the cation was recessed into the α cage (S1*), the third lay within the 8-ring plane (S1). The twelfth silver ion was statistically divided among 12 equivalent positions corresponding to a two-fold axis opposite a 4-ring (S3). It was found that even dehydration under vacuum at 623K was insufficient to remove water molecules present within the α cavity, and that

the partially hydrated Ag_{12}-A zeolite studied corresponded to Ag_{12}-A trihydrate.

Additional studies[7,8] have been carried out on more severely dehydrated Ag_{12}-A single crystals from which it appears that the eight 6-ring silver ions (S2* and S2' positions of the fully hydrated zeolite) occupy a relatively stable environment, the effect of heat treatment being only to bring these ions closer to the center of the 6-rings. In contrast, the less energetically favoured 8-ring (S1*) and 4-ring (S3) siver ions are progressively reduced. A maximum of four silver ions may therefore be reduced, and these were found to migrate into the sodalite (β) cavities to form a proposed octahedral Ag_6 molecule[7,8] at position SU. A complex of formula $(Ag^+)_8$ (Ag_6) was suggested with the Ag_6 molecule enclosed by a 'cube', the corners of which corresponded to the stable silver ions within the center of 6-rings (S2*) (Figure 4.1).

Interaction is assumed to occur between the atoms of the Ag_6 clusters and four equivalent framework oxide ions, the silver atoms behaving as weak Lewis acids with respect to the framework, accepting electron density and delocalizing it through coordination interaction onto the silver ions at the 6-rings.

The following scheme has been suggested for silver ion reduction[8] involving initially the residual water molecules found in the sodalite (β) cages of Ag_{12}-A partially dehydrated at ~623K[5]:

$$(Ag^+)_{12}[Si_{12}Al_{12}O_{48}]^{12-}.3H_2O \rightarrow$$
$$(Ag^o)_2(Ag^+)_{10}(H^+)_2[Si_{12}Al_{12}O_{48}]^{12-} + \tfrac{1}{2}O_2 + 2H_2O$$

After depletion of the supply of water molecules, additional silver ions must be reduced by framework oxide ions. Thus, it has been found that evacuation to 10^{-5} torr at 698K for about 10 days leads to all four silver atoms in

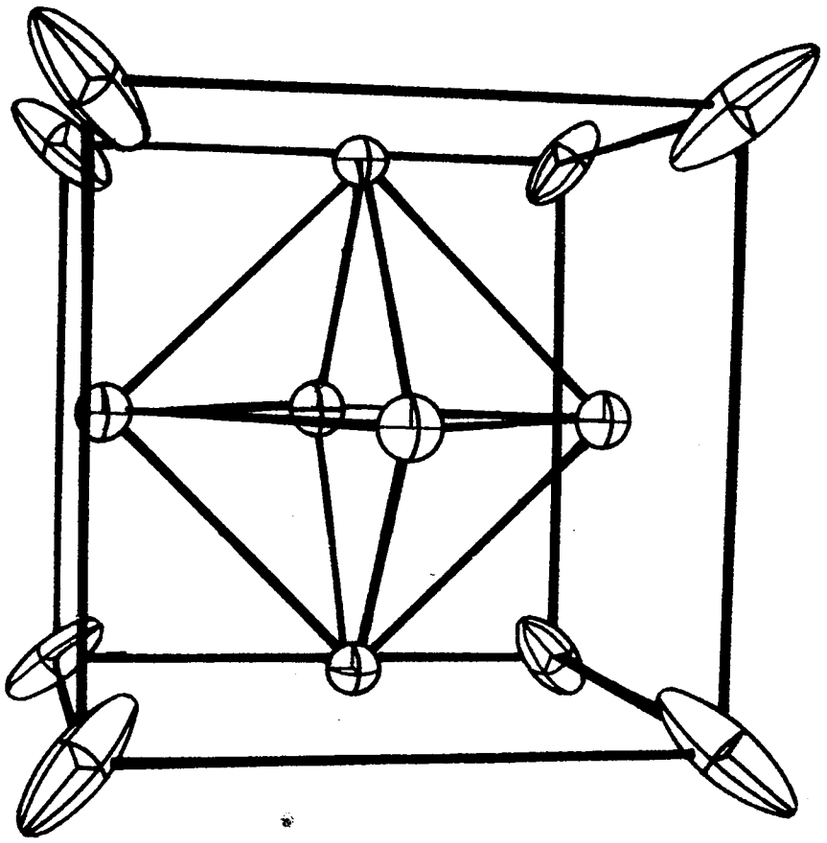

Figure 4.1. The octahedral Ag_6 molecule (SU) stabilized by coordination to eight silver ions at S2* positions[8].

unfavourable sites being reduced:

$$(Ag^{o})_2(Ag^{+})_{10}(H^{+})_2[Si_{12}Al_{12}O_{48}]^{12-} \longrightarrow (Ag^{o})_4(Ag^{+})_8(H^{+})_2[Si_{12}Al_{12}O_{47}]^{10-} + \tfrac{1}{2}O_2$$

The formation of Ag_6 molecules stabilized by eight silver ions requires more silver atoms than are present in the unit cell. There is thus an occupancy of $\frac{2}{3}$ of the sodalite units by Ag_6 molecules, with the remaining cavities empty of all reduced silver ions. Even more severe conditions (heating above 723K) give rise to the appearance of crystallites of silver which result from the reduction process proceeding to include 6-ring silver ions, thereby causing the destablilization of the $(Ag^{+})_8(Ag_6)$ system in some sodalite units.

The almost total reversibility of this dehydration scheme has been demonstrated by X-ray studies carried out on an Ag_{12}-A single crystal[9]. A combination of dehydration and hydrogenation treatments caused complete loss of the zeolite crystalline diffraction pattern and the appearance of lines indicative of silver metal. Oxygen treatment restored the zeolite lattice diffraction pattern, and the silver atoms were re-oxidized to a limit of eleven silver ions per unit cell. The final structure determined showed eight equivalent silver ions on three-fold axes near the centers of 6-rings ($S2^{*}$), and three equivalent cations in the 8-ring planes, but not at their centers (S1). 0.56 silver atoms were located at the neutral silver atom position (SU) where Ag_6 clusters would be expected to have formed (i.e. 9% of the sodalite units held Ag_6 clusters), whilst the remaining 0.44 silver atoms were found to have left the interior of the crystal, presumably as the oxide. Confirmation of the relative stabilities of the cation positions may therefore be seen with the 6-ring and 8-ring sites refilling sequentially, but with the most unfavourable position, the 4-ring, remaining vacant.

Gellens et al[10], disagree with the findings of Kim and Seff[7-9] regarding the formation of Ag_6 clusters in the sodalite (β) cages of Ag_{12}-A zeolite upon heat treatment. Whilst admitting that severe dehydration treatments might lead to the formation of the proposed Ag_6 clusters, these were not found in studies carried out, by X-ray diffraction and U.V. reflectance spectroscopy, on variously exchanged and variously pre-treated $(Ag,Na)_{12}$-A zeolites. Instead, at ~378K Gellens et al suggested the formation of a linear Ag^+-Ag^o-Ag^+ molecule, in which the two Ag^+ ions were present at S2' sites and the Ag^o atom located in the sodalite unit opposite a framework four-ring. Increased severity of treatment (vacuum dehydration at 648K), was found to cause the formation of two such clusters. It was suggested that a probable maximum of four Ag^+-Ag^o-Ag^+ molecules were likely per sodalite (β) cage, with all the Ag^o atoms coplanar. Interaction between clusters was thought possible because the distance between Ag^o atoms of different clusters was similar to that of silver metal. Further X-ray powder studies of partially silver-exchanged type A $(Ag,Na)_{12}$-A zeolites have been reported by Gellens et al[11]. Again, these have been interpreted in terms of the formation of linear Ag^+-Ag^o-Ag^+ ions. It is thus clear that the structural changes which occur on dehydration are unusually complex and imperfectly understood.

The X-ray structure of ethylene adsorbed onto partially decomposed Ag_{12}-A zeolite has been reported[1]. A single crystal was dehydrated at 673K and 5×10^{-6} torr for 4 days and then exposed to 120 torr of C_2H_4 gas at 296K. The dehydration produced approximately 2.76 silver atoms per unit cell, which were believed, by analogy with previous studies[7-9], to result from the reduction of the 4-ring silver ion and 1.76 of the three 8-ring cations. On the assumption that these had formed neutral Ag_6 molecules, it was calculated

that 46% of the unit cells in the crystal contained Ag_6 molecules in sodalite (β) cavities (at site SU).

Sorption of ethylene had little effect on the Ag_6 clusters, their numbers remaining constant and their coordinates scarcely changing. There was, however, a change in the number of coordinated 6-ring (S2*) silver ions, from the anticipated value of eight (for the complex $(Ag^+)_8(Ag_6)$ with the formation of the new complex $(Ag^+)_6(Ag_6)$ (Figure 4.2). The removal of two silver ions from coordination with Ag_6 caused the Ag-Ag bond length (the edge of the Ag_6 octahedron) to decrease, consistent with diminished ability to withdraw electron density from the Ag_6 cluster, and the Ag-Ag^+ distance to shorten indicating stronger interaction. The two remaining silver ions located within this unit cell were associated with 8-rings (S1); these were found not to complex with ethylene.

In the remaining 54% of unit cells whose sodalite (β) cavities did not contain Ag_6 molecules, one out of eight 6-ring silver ions was observed, upon ethylene adsorption, to recede ~1Å into the sodalite unit, thereby taking up an S2' position. No ethylene molecule could be located in coordination with this ion, although this was possibly the result of inadequate experimental resolution. Conversely, each of the remaining seven 6-ring cations, now protruding 1.2 Å into the αcage (S2*), was found to form a π-complex with one ethylene molecules, thus adopting a pseudo tetrahedral configuration.

The carbon atoms of the complexed ethylene molecule were equivalent, each 2.54 Å from a silver ion and, whilst not accurately determined, the C=C bond length did not appear to be significantly different from that of ethylene gas (1.334 Å[12]). No significant approach was made by ethylene to the zeolite framework: at the smallest C-O distance (3.76 Å) the hydrogen

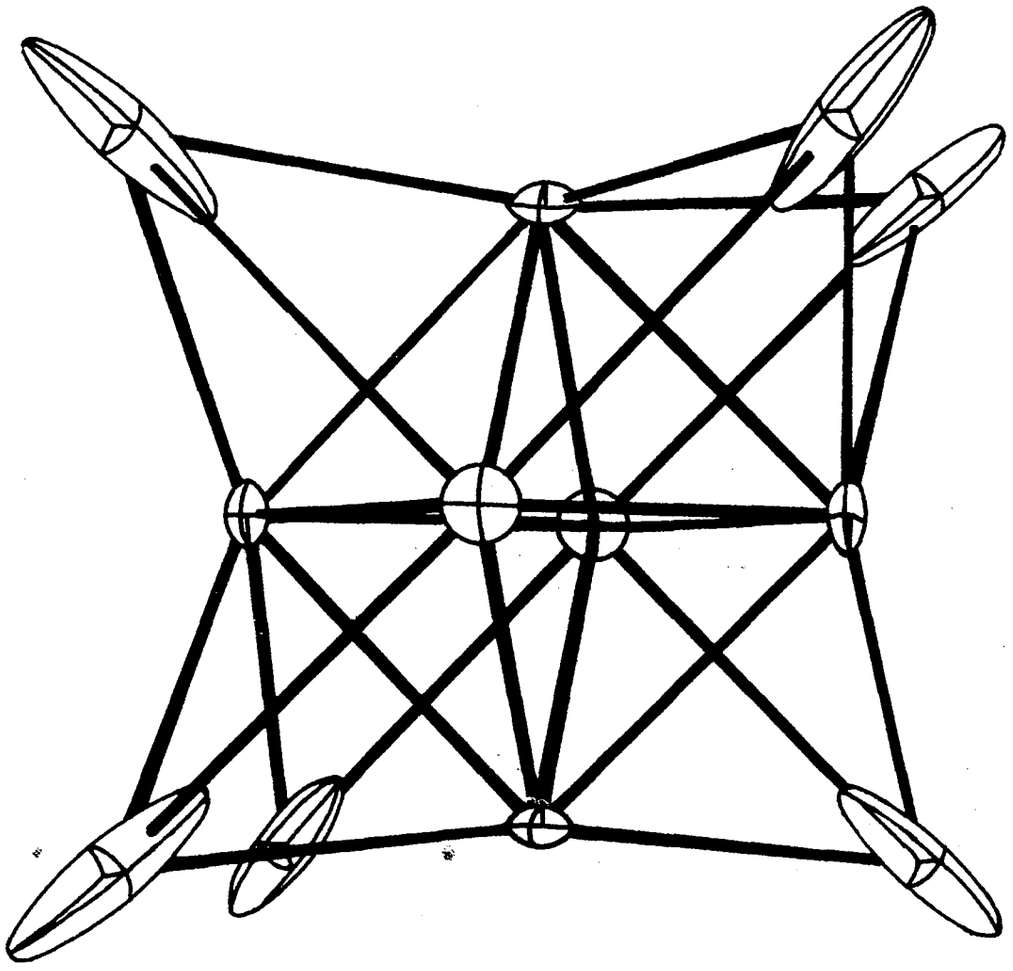

Figure 4.2. The octahedral Ag_6 molecule (SU) stabilized by coordination to six silver ions at S2* positions[1].

atoms were considered too far from the nearest oxygen atoms to interact with them.

In the 46% of unit cells whose sodalite cavities contained Ag_6 molecules, two silver ions were located per unit cell positioned within 8-rings (S1). Again, these appeared not to coordinate to ethylene.

Although no previous infrared or Raman spectroscopic studies have been made of type A zeolite+absorbed ethylene systems, some insight into these systems may be obtained from earlier investigations of ethylene adsorbed onto type 13X zeolites[13-15], and in particular the silver exchanged form. Carter et al[14] have reported infrared spectra in the region 1300-3300cm^{-1} for ethylene adsorbed on Li^+, Na^+, K^+, Ag^+, Ca^{2+}, Ba^{2+} and Cd^{2+} exchanged type 13X zeolites. In all spectra, the formally infrared inactive (in the isolated C_2H_4 molecule) vibrations υ_2 (C=C stretch) and υ_3 (CH_2 symmetric deformation) featured quite strongly, showing that olefin interaction with the surface had taken place[16], and that dissociation had not occurred. Bonding was shown to be weak by the complete removal of adsorbed gas, upon evacuation at room temperature, from all but the silver and cadmium exchanged forms. For the latter two zeolites stronger interaction was indicated, with evacuation at temperatures in excess of 473K necessary to displace ethylene from Cd-13X zeolite, and still more stringent conditions required in the case of Ag-13X zeolite.

A scheme[14,15] was proposed for cation-ethylene interaction in which a bond is formed by overlap of the olefin orbitals with either a 5s or a 5sp orbital of the cation. Additionally in the case of silver, back donation was suggested to occur from filled silver 4d orbitals into the vacant π^* orbitals of ethylene according to the Chatt-Dewar-Duncanson model[17,18].

As the interaction of the silver ion with the framework is partly covalent, a necessary consequence is that its d orbitals are fixed in space and thus olefin rotation about the z axis (Figure 4.3) results in bond-breaking.

II. Experimental

Ag_{12}-A zeolite was prepared[3] from Na_{12}-A (BDH Chemicals Ltd.) by ion-exchange employing a 0.2M solution of $AgNO_3$ (containing the exact equivalence of the sodium ions to be exchanged) and a temperature of 298K . The sample was washed thoroughly and the degree of exchange was determined by chemical analysis.

C_2H_4 gas was obtained from British Industrial Gases Ltd. and its purity checked by mass spectroscopy. Trans-$C_2D_2H_2$ (98 atom % D) was obtained from Merck Sharp and Dohme Ltd.

A self-supporting zeolite disc (~10 mg cm^{-2}) was mounted in an all-metal infrared cell with KRS5 windows (4cm apart). The cell was then evacuated to 10^{-6} torr (1 torr = 133.32 Pa) using a turbomolecular pump, and the zeolite sample heated slowly to the maximum temperature required (543 or 673K), infrared spectra being recorded at various temperatures during heating using a Perkin Elmer 580B spectrophotometer. The sample was left at the maximum bake-out temperature for a specified time (2, 15 or 70 hours) and spectra measured at regular intervals during this period. The sample was then allowed to cool to room temperature and its spectrum re-recorded. Ethylene was then admitted into the infrared cell to a pressure of 100 torr and the spectrum measured. Gaseous ethylene was removed from the cell by evacuation for 5 minutes and the spectrum of the sample re-measured. Following evacuation for a further 25 minutes the spectrum was recorded once more. In some cases (see later) the sample

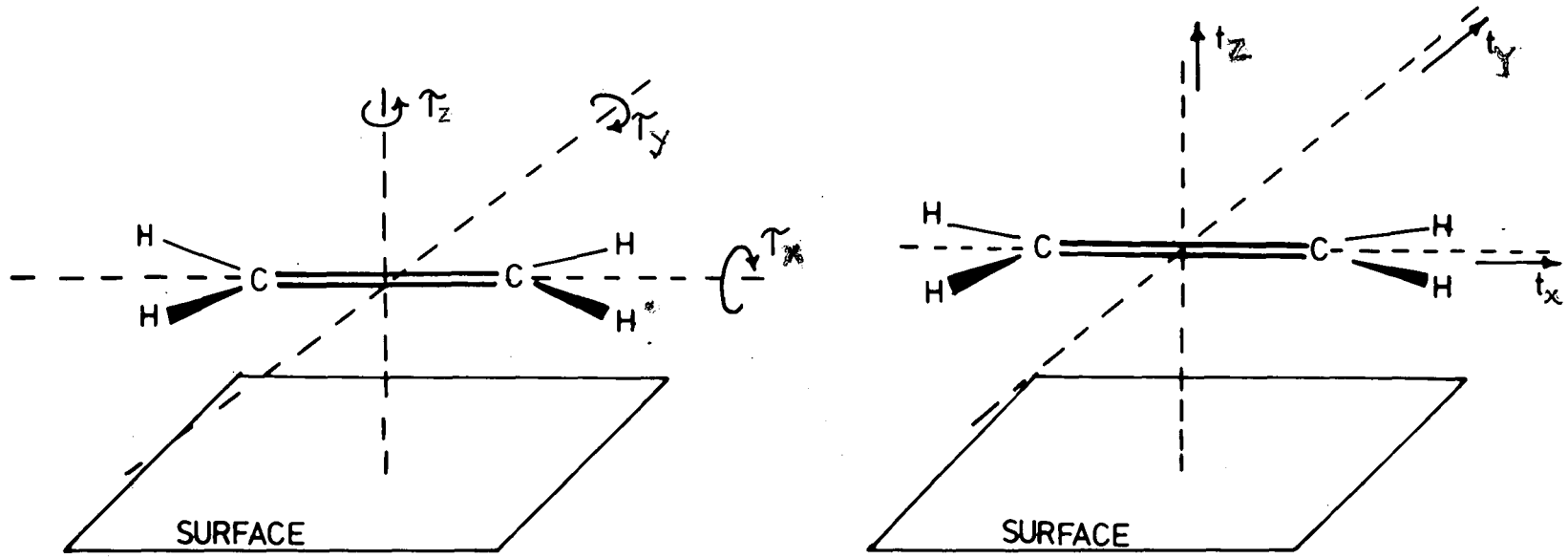

Figure 4.3. The three hindered rotations, τ_x, τ_y (antisymmetric stretch) and τ_z, and the three hindered translations, t_z (symmetric stretch), t_x and t_y, of ethylene relative to the surface.

was then re-heated and its spectrum obtained at the elevated temperature. All sample pre-treatment and gas adsorption/ desorption was carried out without removing the sample from the infrared beam.

A summary of the pre-treatment conditions used on the zeolite sample and the sample reference numbers is given in table 4.2. We will use the representations S(a,b,c) or S(b,c) to describe the different sample pre-treatment conditions employed, where a is the evacuation time (5 or 30 minutes), b is the time (2,15 or 70 hours) the sample was left at the maximum bake-out temperature, c, (543 or 673K).

All spectra measured were stored on microfloppy discs and replotted with expansion (using the ABEX function available on the PE Model 3500 Data Station[19]) from the original recordings. The ABEX function is equivalent to running a second spectrum with a sample of increased or decreased concentration. The expansion results in a spectrum in which the relative intensities of the infrared bands are unchanged. Repetitive scanning was used to reduce noise. All of the spectra reproduced in this chapter are tracings of original data.

III. Results and discussion

Throughout this chapter, we will restrict our attention to the region 1000-2000cm^{-1}, because between 300 and 1000cm^{-1} the sample is totally absorbing, and above 2000cm^{-1} the only feature observed is a broad band (ca. 3600cm^{-1}) due to adsorbed water and hydroxyl groups.

(a) Dehydration of Ag_{12}-A zeolite

Figure 4.4 shows spectra (1100-1900cm^{-1}) of Ag_{12}-A obtained at several temperatures during dehydration. The band

Table 4.2 Summary of the Sample Pretreatment Conditions

Sample number	Temperatures (K)	Duration (hours)
1	543	2
2	543	15
3	543	70
4	673	2
5	673	15
6	673	70

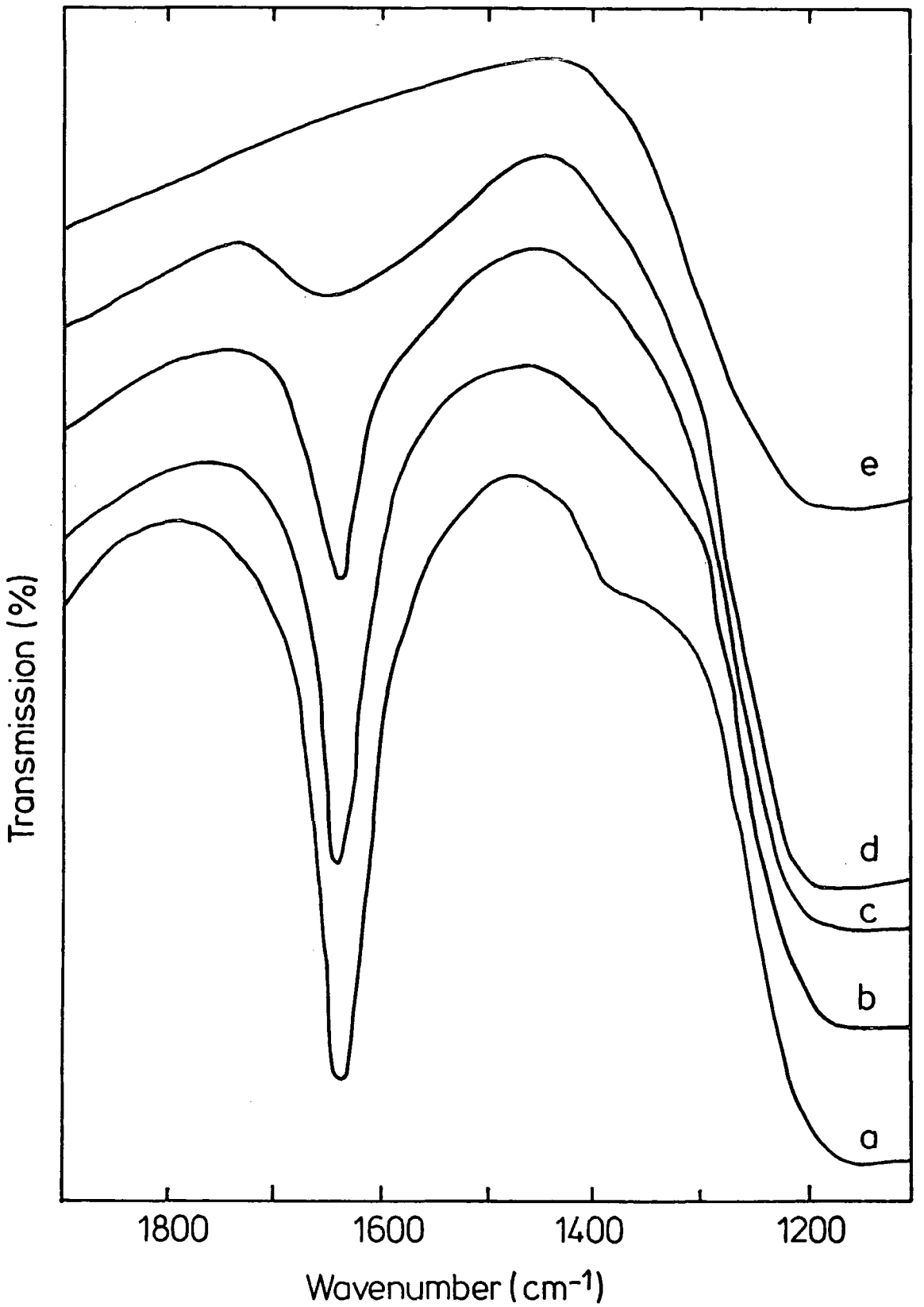

Figure 4.4. Spectra of AgA zeolite obtained at several temperatures during dehydration: (a) 298K, (b) 453K, (c) 543K, (d) 593K and (e) 673K.

at 1640cm^{-1}, corresponding to the deformation mode of adsorbed water, gradually decreases in intensity as the temperature is raised and has completely disappeared at 673K. It is important to note, however, that at ca. 543K (one of the bake-out temperatures used in this work) not all of the adsorbed water is removed. As will be seen later, very little water was re-adsorbed on allowing the sample subjected to the maximum bake-out temperature of 673K to cool to room temperature.

(b) Ag_{12}-A + ethylene

One possible explanation for the discrepancy between the INS and X-ray[1] data for ethylene adsorbed on Ag_{12}-A ($Ag_{12}A$ + C_2H_4) is differences in sample pre-treatment conditions. As Kim and Seff[5-8] and Gellens et al[10] have shown, the position and oxidation state of the cations depend upon the severity of the dehydration conditions. To test this hypothesis, we have studied the Ag_{12}-A + C_2H_4 system using six very different sets of pre-treatment conditions which are intended to span the range used by various authors for their physical measurements. The scheme chosen was to heat different samples either to 543 or 673K and to maintain them at these maximum bake-out temperatures for 2, 15 and 70 hours before allowing them to cool to room temperature and adsorbing ethylene. Data on these six differently prepared samples enables us to observe the effects on ethylene adsorption of both the magnitude of the maximum bake-out temperature, and the duration of heating

In figure 4.5a is shown the spectrum of a sample which had been heated to a maximum bake-out temperature of 543K for 15hours, after being allowed to cool to room temperature. Figure 4.5b shows the spectrum of the same sample after

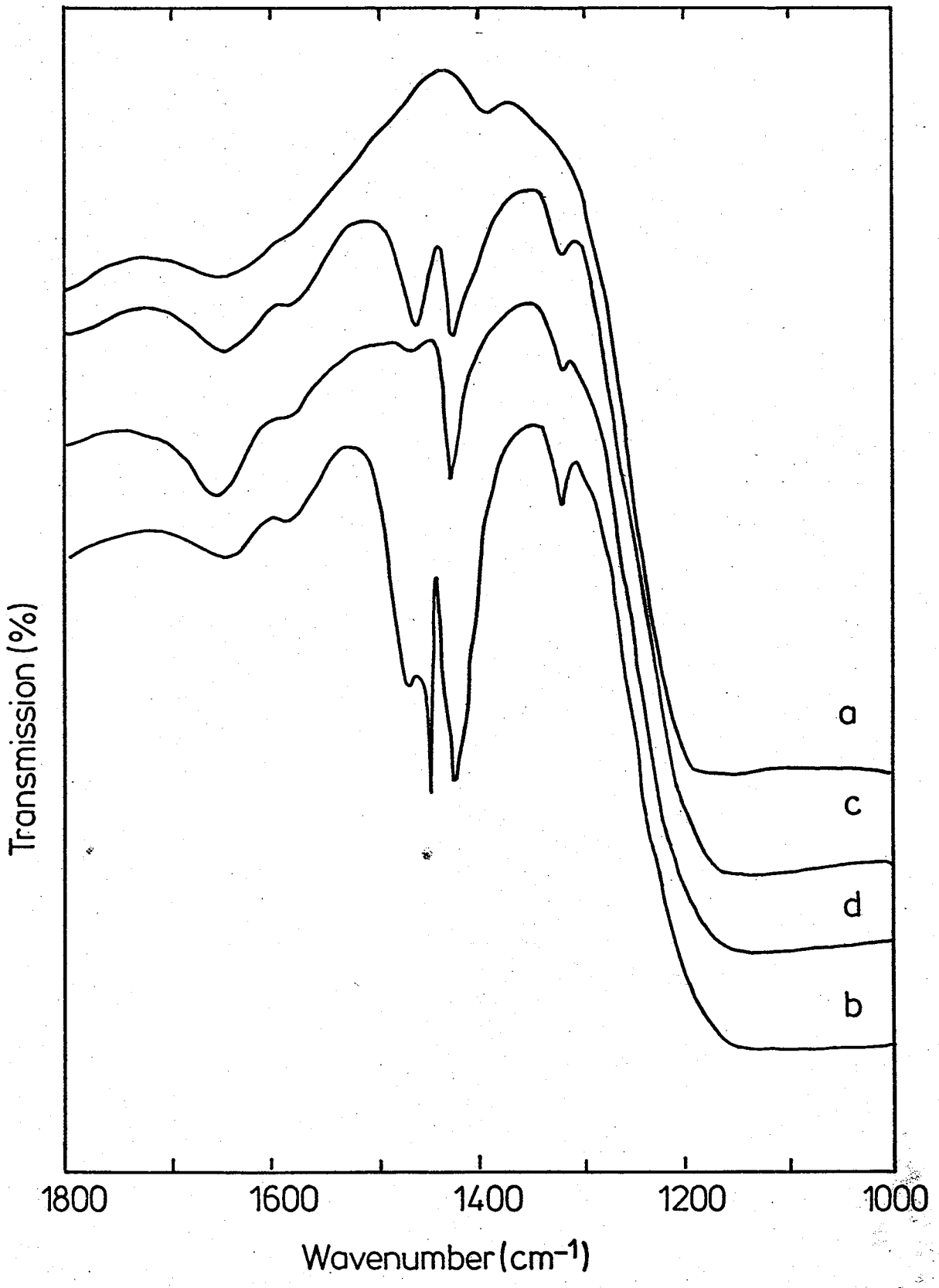

Figure 4.5. AgA zeolite after heating at 543K for 15 hours:
(a) at ambient temperature
(b) sample (a) after admitting 100 torr C_2H_4
(c) sample (b) after evacuation for 5 minutes
(d) sample (c) after evacuation for a further 25 minutes.

admitting C_2H_4 to an overpressure of 100 torr at room temperature. Subsequently, the sample was evacuated ($< 10^{-5}$ torr) at room temperature for 5 minutes, S(5,15,543), (Figure 2c) and then for a further 25 minutes, S(30,15,543), (Figure 4.5d). The apparent variation in the intensity of the band at 1640cm^{-1}, due to adsorbed water, is a consequence of the different expansion (ABEX) factors used in generating these plots.

At high overpressure (100 torr), the spectrum (Figure 4.5b) is dominated, as one would expect, by that of gaseous C_2H_4. On evacuation for five minutes (pressure $< 10^{-5}$ torr), however, two relatively intense bands are clearly visible at 1465 and 1430cm^{-1} due to the absorbed species (Figure 4.5c). We assign these bands to the antisymmetric CH_2 deformation (υ_{12}, following the notation of Herzberg[20]) of C_2H_4 molecules adsorbed on two distinct sites. In the gas phase, υ_{12} occurs as an intense band at 1443cm^{-1} (ref. 20) and is the only observed infrared band in the region 1800 to 1100cm^{-1}. In view of this we would certainly expect to observe this band in the spectra of the adsorbed species. In our spectrum (Figure 4.5c) transitions were observed at 1590 and 1320cm^{-1} which are also due to the adsorbed species. These values compare with those of 1623 and 1342cm^{-1} found for the C=C stretch (υ_2) and CH_2 symmetric deformation (υ_3) respectively in Raman studies[20] of gaseous C_2H_4. In organometallic complexes containing π-bonded C_2H_4, and to a lesser extent in C_2H_4 itself, υ_2 and υ_3 are mixed[21]. This is also very likely to be the case for adsorbed C_2H_4 and so the assignment of observed bands to either υ_3 or υ_2 alone is simplistic. Our results are very similar to those for $Ag(C_2H_4)BF_4$ in which the C_2H_4 is relatively weakly bound[21] and where transitions were

observed at 1579 and 1320cm^{-1}. In this case the higher wavenumber band has been shown to have more C=C (ν_2) than δCH_2 (ν_3) character while the converse is true for the lower wavenumber band. It seems reasonable to propose that the same situation obtains with the bands observed at 1590 and 1320cm^{-1} in our spectra, i.e. they both contain contributions from ν_2 and ν_3 but in the 1590cm^{-1} band ν_2 predominates while in the 1320cm^{-1} band the contribution from ν_3 is greatest. For simplicity therefore we will refer to the 1590 and 1320cm^{-1} bands simply as ν_2 and ν_3 respectively.

ν_2 and ν_3 are infrared inactive in gas-phase C_2H_4 (D_{2h}) but the reduction in symmetry which accompanies adsorption (C_{2v}) results in these modes becoming infrared active. Comparable observations have been reported for C_2H_4 adsorbed on Ag-13X zeolite by Carter et al[14].

Only a single band due to ν_3 is observed in our work. This may arise either because the values for ν_3 on the two distinct sites are similar and the bands unresolved or, more likely, because the lower wavenumber component is obscured by the framework absorption. On evacuation for a further 25 minutes (Figure 4.5d) the 1465cm^{-1} band decreases in intensity while the 1590 and 1320cm^{-1} bands remain very weak.

We have also obtained spectra of trans-$C_2D_2H_2$ adsorbed on Ag_{12}-A discs subjected to pre-treatments analogous to those used for the Ag_{12}-A + C_2H_4 system. Adsorption of trans-$C_2D_2H_2$ (50 torr) at room temperature on Ag_{12}-A, pretreated at maximum bake-out temperatures of 543 and 673K for 2 hours followed by evacuation for 5 minutes S(5,2,543) and S(5,2,673), results in the appearance of a weak band at 1295cm^{-1} due to the adsorbed species. We assign this band to ν_{12} of trans-$C_2D_2H_2$. ν_{12} occurs as an intense band at 1299cm^{-1} in the infrared

spectrum of gas-phase trans-$C_2D_2H_2$[22] and is in fact the only band observed in the region 1800 to 1100cm^{-1}. We do not observe another band due to ν_{12} which might occur at a lower wavenumber than the 1295cm^{-1} band, probably because it is obscured by the framework absorption. Bands due to ν_2 and ν_3 which occur at 1571 and 1286cm^{-1} respectively in gas-phase trans-$C_2D_2H_2$ (ref. 22) are not observed in the Ag_{12}-A + trans-$C_2D_2H_2$ system. These modes are infrared inactive in the gas phase and even if they become active on adsorption, they may not be observed either because they are very weak, or because they occur at a region where the bands are difficult to observe due to framework absorption.

The measured isotopic ratio of the 1465 (Ag_{12}-A + C_2H_4) → 1295 (Ag_{12}-A + trans-$C_2D_2H_2$)cm^{-1} band is 0.89. This compares well with the measured isotopic ratio of ν_{12} in the gas-phase, 0.90.

For the Ag_{12}-A + C_2H_4 sytem it is interesting to note, figure 4.5, that:

(1) Bands due to ν_2(C=Cstretch[20]) and ν_3 (symmetric CH_2 deformation[20]) are observed in the infrared spectrum although these bands are infrared inactive in the gas-phase.

(2) Bands are present which may assigned to ν_{12} of C_2H_4 adsorbed at two different sites. For one of these species ν_{12} occurs at a wavenumber value above that found in the gas-phase, for the other it is below. This is again in agreement with data obtained by Carter et al[14] for C_2H_4 adsorbed on variously exchanged type 13X zeolites.

(3) The species asociated with the higher wavenumber band (1465cm^{-1}) is more easily desorbed than the species associated with the lower wavenumber band (1430cm^{-1}). At

temperatures below 373K, the less strongly bound C_2H_4 may be removed; in contrast heating to in excess of 573K is needed to remove the more strongly bound C_2H_4.

(4) Our results are in agreement with the conclusions reached in the INS study[2] that there are two distinct adsorption sites for ethylene adsorbed on Ag_{12}-A zeolite. They are consequently at variance with the findings of the X-ray diffraction work of Kim and Seff[1].

Rather than consider the remaining spectra individually, we will concentrate on a comparison of the spectra of four of the samples. Spectra of samples subjected to heating at the maximum bake-out temperature for 70 hours will not be discussed. For these samples it was found that their transmission was extremely low ($< 2\%$), and the spectral quality so poor that no definite conclusions could be drawn. On examining the discs they were found to have turned black and it would appear that the silver had migrated from the cages to form crystallites on the surface.

In figure 4.6 are shown four sets of spectra representing Ag_{12}-A samples prepared under various pre-treatment conditions S(b,c) = S(2,543), S(15,543), S(2,673), and S(15,673) which have had C_2H_4 adsorbed on them and which have then been subjected to various evacuation procedures. Each series of spectra is shown together with its relevant background. Table 4.3 displays the frequencies of ν_2, ν_3, and ν_{12} measured for each of the four Ag_{12}-A + C_2H_4 samples after both 5 and 30 minutes evacuation. From these data we note the following:

(1) In the cases of all four Ag_{12}-A + C_2H_4 samples, after 5 and after 30 minutes evacuation, two bands may be observed which can be assigned to ν_{12} of C_2H_4 adsorbed on two different sites.

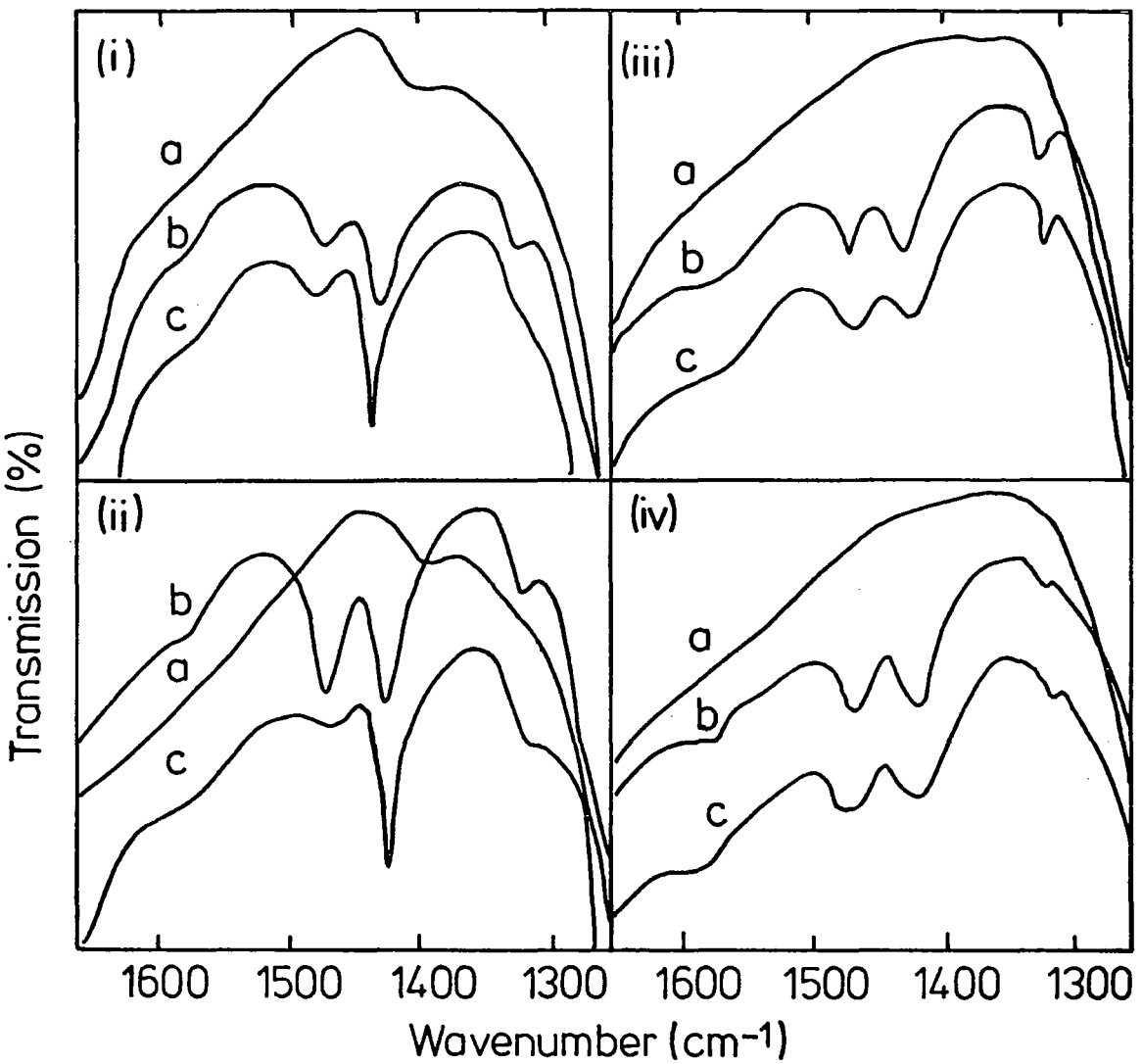

Figure 4.6. (i) AgA pre-treated at 543K for 2 hours
(ii) AgA pre-treated at 543K for 15 hours
(iii) AgA pre-treated at 673K for 2 hours
(iv) AgA pre-treated at 673K for 15 hours

(a) Background
(b) AgA + C_2H_4 after 5 minutes evacuation
(c) AgA + C_2H_4 after 30 minutes evacuation.

Table 4.3 Wavenumbers of ν_2, ν_3 and ν_{12} adsorbed onto AgA zeolite samples subjected to various pretreatments

Samples	AgA + C_2H_4 (a)			
	ν_2	ν_3	ν_{12}'	ν_{12}''
S(5,2,543)	1580	1319	1465	1430
S(30,2,543)	1580	1319	1465	1430
S(5,15,543)	1590	1320	1465	1430
S(30,15,543)	1590	1320	1465	1430
S(5,2,673)	1575	1315	1460	1420
S(30,2,673)	1575	1315	1460	1420
S(5,15,673)	1580	1315	1465	1420
S(30,15. 673)	1580	1315	1465	1420

(a) ν_{12}' and ν_{12}'' are the values of ν_{12} for C_2H_4 on two different sites.

(2) With the exception of sample S(5,2,543), the two bands assigned to ν_{12} are of approximately equal intensity after 5 minutes evacuation. In sample S(5,2,543) the band at 1430cm^{-1} is 2.5 times the intensity of that at 1465cm^{-1}. Making the assumption that the transition dipole does not change in magnitude, it is clear that the site occupancies differ in sample S(5,2,543) from the other samples. This is most probably the result of depletion of one cation site as Ag^{+}-Ag^{o}-Ag^{+} or $(Ag^{+})_8(Ag_6)$ clusters are formed.

(3) After 30 minutes evacuation the band at 1465cm^{-1} is markedly reduced in relative intensity in the case of samples S(30,2,543) and S(30,15,543), but is essentially unchanged in relative intensity in the cases of samples S(30,2,673) and S(30,15,673). These four samples were again heated after the evacuation lasting 30 minutes. It was found that in those samples pretreated at the lower maximum bake-out temperature (543K), one band disappeared after heating to temperatures below 373K, whilst the other band disappeared only after heating to temperatures in excess of 473K. In contrast, the samples pretreated at the higher maximum bake-out temperature (673K) required heating to temperatures in excess of 473K whereupon both bands disappeared together.

It is clear from the above that the strength of the bond between the C_2H_4 and the Ag_{12}-A zeolite is a function of the pre-treatment conditions to which the zeolite is subjected, and that the detailed behaviour is complex. After relatively mild pre-treatment (543K), the strength of bonding at one site is greater than that at the other, whereas after more severe pre-treatment (673K) both species are held almost equally strongly.

Ideally, we would wish to correlate the two adsorbed ethylene species with specific sites within the Ag_{12}-A framework. However, further discussion of this point awaits more detailed information on the cation locations present after the various pre-treatments. Clearly, however, our infrared data are inconsistent with the X-ray diffraction work of Kim and Seff[1], since under all pre-treatment conditions employed we find <u>two</u> adsorption sites.

References

1. Kim, Y. and Seff, K., J. Am. Chem. Soc., 100, 175 (1978)
2. Howard, J., Robson, K., Waddington, T.C. and Kadir, Z.A., Zeolites, 2, 2 (1982)
3. Breck, D.W., Eversole, W.G., Milton, R.M., Reed, T.B. and Thomas, T.L., J. Am. Chem. Soc, 78, 5963 (1956)
4. Thoni, W., Z. Kristallogr., Kristallogeom. Kristallphys., Kristallchem., 142, (1975)
5. Kim, Y. and Seff, K., J. Phys. Chem., 82, 1071 (1978)
6. Matsumoto, S., Nitta, M., Ogawa, K. and Aomura, K., Bull. Chem. Soc. Jpn., 48, 1169 (1975)
7. Kim, Y. and Seff, K., J. Am. Chem. Soc., 99,7055 (1977)
8. Kim, Y. and Seff, K., J. Am, Chem. Soc., 100, 6989 (1978)
9. Kim, Y. and Seff, K., J. Am, Chem. Soc., 82, 921 (1978)
10. Gellens et al., in press
11. Gellens, L.R., Mortier, W.J. and Uytterhoeven, J.B., Zeolites, 1, 11 (1981)
12. Sutton, L.E. Interatomic Distances and Configurations in Molecules and Ions, The Chemical Society, London (1958) M/129
13. Yates, D.J.C., J. Phys. Chem., 70, 3693 (1966)
14. Carter, J.L., Yates, D.J.C., Lucchesi, P.J., Elliott, J.J. and Kevorkian, V.,J. Phys. Chem., 70, 1126 (1966)
15. Yates, D.J.C., Chem. Eng. Progr. Symp. Ser. 63, 73, 56 (1967)
16. Sheppard, N. and Yates, D.J.C., Proc. Roy. Soc. A, 238, 69 (1956).
17. Dewar, M.J.S., Bull. Soc. Chim. France, 18, C71 (1951)
18. Chatt, J. and Duncanson, L.A. J. Chem. Soc., 2939 (1953)
19. Instructions, Perkin Elmer data station 3500 application programme, Perkin Elmer Ltd, (1980)
20. Herzberg, G., Molecular Spectra and Molecular Structure II. Infrared and Raman Spectra of Polyatomic Molecules, Van Nostrand, London, (1945)

21. Powell, D.B., Scott, J.G.V. and Sheppard, N., Spectrochim. Acta, 28A, 327 (1972)

22. Duncan, J.L., McKean, D.C. and Mallinson, P.D., J. Mol. Spectros., 45, 221 (1973)

CHAPTER V

INFRARED SPECTROSCOPIC INVESTIGATION OF C_2H_2 AND C_2D_2 ADSORBED ON AgA AND Ag13X ZEOLITES

I. Introduction

This study of acetylene adsorbed onto fully silver exchanged type A zeolite (AgA) follows naturally from our previous study of ethylene adsorbed onto the same zeolite (Chapter IV). In view of the complexity of AgA zeolite, some differences in adsorption behaviour of C_2H_2 when compared with C_2H_4 were expected because of the more acidic nature of the protons in the former. For comparison , acetylene is also adsorbed onto silver exchanged type 13X zeolite (Ag13X) which is known to be more thermally stable than AgA. The structural changes which occur on dehydrating fully silver exchanged type A zeolite have been studied by both x-ray diffraction[1-3] and u. v. reflectance spectroscopy[4]. While it is clear that some of the Ag^+ cations are reduced on dehydration, there is disagreement over the nature of the metal clusters formed in the sodalite (β) cages. This has been reviewed in detail in Chapter IV. While no structural data are available for the AgA + C_2H_2 system, single crystal x-ray determinations have been published for acetylene adsorbed onto sodium[5,6], partially exchanged manganese[7,8] and cobalt[8] type A zeolites. This will be discussed further in section III.

On adsorption of C_2H_2, four main types of interaction with the zeolite can be envisaged:

(i) 'End-on' interaction; hydrogen bonding between the acidic protons of the acetylene molecule and framework oxygen atoms. For this type of interaction, $\upsilon(C \equiv C)$ occurs at a

frequency higher than the gas phase value ($1974cm^{-1}$). Yates and Lucchesi[9], in their study of acetylene adsorbed onto silica found $\upsilon(C \equiv C)$ at $2005cm^{-1}$ and deduced that the interaction was of the 'end-on' type.

(ii) 'Side-on' interaction; overlap of the π system of acetylene with orbitals of the cation to form a π-complex analogous to those well known in the organometallic complexes of olefines (e.g. $K(PtC_2H_4Cl_3)$). Acetylene has two mutually perpendicular sets of π orbitals and is therefore capable of being bonded to one or two metal atoms[10]. For the 'side-on' interaction, $\upsilon(C \equiv C)$ occurs at a frequency lower than in the gas phase. Table 5.1 shows reported values of $\upsilon(C \equiv C)$ for C_2H_2 adsorbed onto various ion-exchanged forms of types A and 13X zeolites[15,30].

(iii) The acetylene looses one or both of its hydrogen atoms to form acetylides, $RC \equiv CM$ (R=H) or carbides, $MC \equiv CM$ respectively. The resultant hydrogen atom (s) could combine with a lattice oxygen(s) to form an OH group or, alternatively, with water to form hydronium ions. $\upsilon(C \equiv C)$ for this type of complex ($RC \equiv CM$) falls within the range 1850 - $1961cm^{-1}$ [10,11].

(iv) The acetylene looses its identity in the complex, as in for example, the cyclotrimerization of acetylene to form benzene which has been observed , for example, in NiY zeolites[12]. This, obviously, results in the disappearance of the $\upsilon(C \equiv C)$ band.

As we shall see later, the adsorption of C_2H_2 onto AgA zeolite involves the formation of more than one type of adsorbed species. This contrasts with the available data on the more thermally stable alkaline earth or alkali metal exchanged forms of zeolite A.

Table 5.1 The frequencies (cm^{-1}) of $\nu(C\equiv C)$ assigned in the Raman spectra of C_2H_2 adsorbed on some types A and 13X zeolite[15,30]

Cation form	Zeolite type A	Zeolite type 13X
Li^+	1957	1958
Na^+	1953	1954
K^+	1951	1952
Cs^+	-	1951
Mg^{2+}	1956	1956
Ca^{2+}	1957	1958
Ba^{2+}	-	1956

II. Previous spectroscopic studies of zeolite - acetylene system

While there has been no previously published infrared and Raman work of the AgA + C_2H_2 and Ag13X + C_2H_2 systems, there are incoherent inelastic neutron scattering (INS) data available for both of them[13,14]. From the INS study of the Ag13X + C_2H_2 systems, it was shown that acetylene formed a π-bonded complex with the cation[13]. For acetylene adsorbed on AgA zeolite, the authors[14] found that there is only a single type of adsorption site for acetylene in the zeolite framework. In this respect, their observation differs from that of the single crystal x-ray study carried out on NaA + C_2H_2 by Amaro and Seff[5,6], and infrared and Raman spectroscopic studies on several alkali and alkaline earth metal exchanged type A zeolites by Tam et al[15] who found at least two different adsorption sites within the zeolite framework. This contradiction was explained by the authors[14] as an indication of the greater structural complexity of silver exchanged type A zeolite when compared with the more thermally stable alkali and alkaline earth metal exchanged forms. We have also shown (Chapter IV) that for AgA + C_2H_4, the strength of the interaction of the adsorbed C_2H_4 with the zeolite is a function of the pretreatment conditions (e.g. temperature and time) used.

Earlier infrared[16] and electronic[17,18] spectra of C_2H_2 adsorbed onto various transition metal exchanged types A and 13X zeolites had been obtained by Tsitsishvili et al[16] and Klier et al[17,18]. For comparison with their other data, Tsitsishvili et al also obtained infrared spectra of C_2H_2 adsorbed onto some alkali metal exchanged zeolites. They found that[16] regardless of the nature of the cation and the type of zeolite, they did not observe a band due to $\nu(C \equiv C)$

(which occurs at 1974cm^{-1} in the gas phase). This finding, together with the observation of the C-H stretching band, caused them to postulate that 'end-on' interaction of the C_2H_2 with the framework occurred in their samples. However, Klier et al in their study of the electronic spectra of C_2H_2 adsorbed onto Ni- and Co- exchanged type A zeolites found that the acetylene was π bonded to the transition metal ions ('side-on' interaction).

Some of the measurements made by Tsitsishvili et al have been repeated recently by Tam et al[15]. In contrast with earlier authors, Tam et al in their infrared and Raman data, observed a band due to $\nu(C \equiv C)$ for C_2H_2 adsorbed on all of the zeolites studied. On zeolites NaA and CaA, all five fundamental ($2\Sigma g^+ + \Sigma u^+ + \Pi g + \Pi u$) vibrations of acetylene were observed in both the Raman and infrared spectra while on other forms, only the $\nu(C \equiv C)$ band was observed. Acetylene was weakly held by Ca^{2+} and Mg^{2+} since it was easily removed by 5 minutes evacuation at room temperature. Longer time, that is 1 hour evacuation at room temperature, was needed to completely desorb acetylene from NaA. Strongly adsorbed acetylene on KA was only removed after evacuation at 473K for several hours. For NaA + C_2H_2[15], the $\nu(C \equiv C)$ band, observed at 1953cm^{-1}, was distinctly asymmetric and could be resolved by curve fitting into two bands centred at 1949 and 1954cm^{-1}, the former being the less intense. The authors suggested that the less intense band, at 1949cm^{-1} would result from the interaction of the acetylene molecules with the energetically more favourable cations at site SI (refer to Chapter II), whilst the higher frequency band is due to the interaction of the acetylene molecule with the cations at site S2*. This finding agrees with the x-ray data of Amaro and Seff[5,6].

Other infrared work on adsorbed acetylene has been carried out on Cu and Ni exchanged type Y zeolites[12,19]. In the CuY + C_2H_2 system studied, Pichat[19] found bands at 3250, 3190(sh), 3170, 1820(sh) and 1810cm^{-1}. Unlike other zeolites, the υ(C ≡ C) band for acetylene adsorbed onto CuY zeolite was shifted downwards by a large amount (164cm^{-1}) relative to the gas phase. The possibility of the formation of copper acetylides, (HC ≡ CCu) was discussed. However, because the frequency shifts found for the υ(C-H) and υ(C ≡ C) vibrations were larger than those noted for HC ≡ CM acetylides and because no OH bands were observed as one would expect, doubt was cast on the possible formation of HC ≡ CCu. The author[19] favoured the formation of π-acetylenic complexes; the Cu^{2+} ion - acetylene bond resulting mainly from donation from the unsaturated hydrocarbon to the metal ion.

The infrared study of the cyclotrimerization of acetylene on NiY zeolites was carried out by Pichat et al[12]. It was found that the activity of the various samples depended on the number of the dehydrated or partially dehydrated Ni^{2+} ions inside the supercages. They have also established from the bands they observed that the benzene obtained does not form a weak complex with the Ni^{2+} ions and is weakly adsorbed in the framework.

III. Other zeolite + C_2H_2 system studied

Single crystal x-ray structure determinations have been carried out for acetylene adsorbed onto sodium[5,6], partially manganese[7,8] and cobalt[8] exchanged type A zeolites. The structure of dehydrated sodium type A zeolite has been discussed in Chapter II. However, in summary the cation positions are as follows: eight sodium ions occupy the 6-rings posistions (S2*), three sodium ions were located in the

8-ring positions (SI) and the final sodium ion is normal to the 4-ring position (S3).

Six acetylene molecules were found to interact with the cations at two or more sorption sites in the sodium type A zeolite structure. Figure 5.1 shows the stereoview of the unit cell of zeolite NaA . $6C_2H_2$[5,6]. In each of the acetylene-cation interactions, the cation approaches the acetylene equatorially, indicating that the interaction is between the cationic charge and the lateral π electron system of acetylene. No evidence for interaction between the acetylenic hydrogen and framework oxygen atoms was found. Of the six adsorbed acetylene molecules per unit cell, three were found to coordinate laterally and symmetrically with three of the 6-ring sodium ions (S2*), such that, each carbon atom (CI), of each molecule is 2.8Å from the cation (see figure 5.2). The positions of the remaining three adsorbed acetylene molecules could not be determined with certainty, accordingly, two models were put forward. In the first model, the three acetylene molecules were asymmetrically associated with sodium ions in the 8-rings (SI) at distances of 3.0Å for C(2) and 2.6Å for C(3). The second model, considered the more reasonable by the authors proposed that one or two acetylene molecules associated with the 8-rings position (SI) might also be associated with the 4-ring sodium ions (S3) with distances of 2.6Å from C(2) and C(3), whilst the remaining acetylene molecules bonded symmetrically to other 8-ring sodium cations.

Other single crystal studies of zeolite + C_2H_2 system have been carried out on partially manganese ($Mn_{4.5}Na_3A$) and cobalt (Co_4Na_4A) exchanged type A zeolites[7,8]. The structure of dehydrated manganese and cobalt type A zeolites will be discussed in Chapter VIII. Both the manganese and cobalt ions

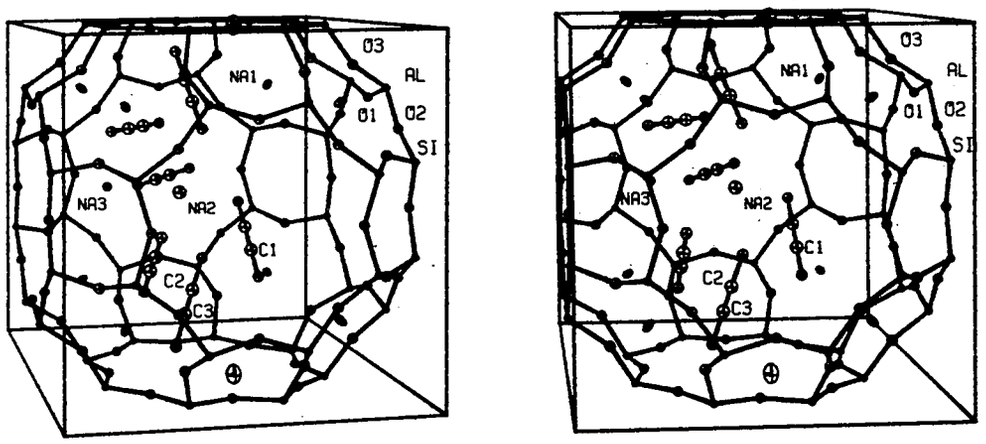

Figure 5.1. A stereoview of the unit cell of zeolite $4A.6C_2H_2$[5,6].

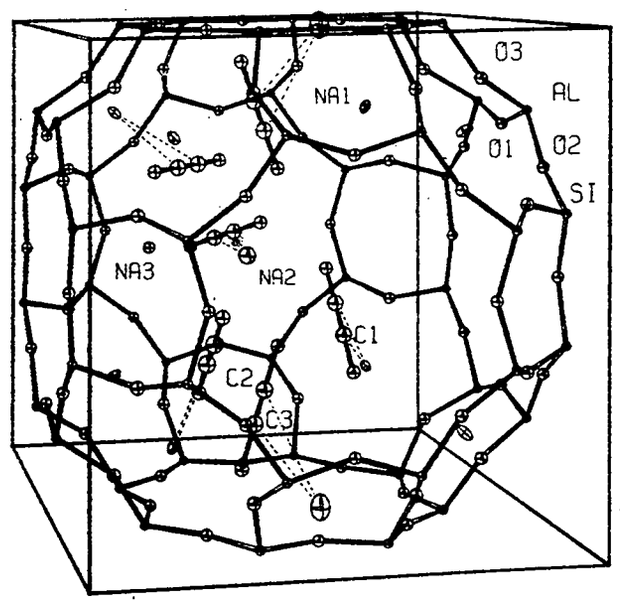

Figure 5.2. Zeolite $4A.6C_2H_2$ (Na(1), Na(2) and Na(3) are equivalent to S2*, S1 and S3 respectively in the text).

occupy 6-ring positions, where they achieve near trigonal-planar coordination with three framework oxygens. Upon addition of acetylene, both the manganese and cobalt ions moved further into the α-cage ($S2^*$). Figures 5.3 and 5.4 show the stereoview of unit cell of zeolite $Mn_{4.5}Na_3A \cdot 4.5C_2H_2$ and $Co_4Na_4A \cdot 4C_2H_2$, respectively. In response to the movement of the transition metal ions, the sodium ions have moved a substantially greater distance into the sodalite cavities (S2'). It was found that acetylene was bonded only to the transition metal ions. In each sorption complex, the interaction was symmetrical to both carbon atoms of an acetylene molecule (see figure 5.5), whereby the Mn^{2+} - C and Co^{2+} - C distances are 2.63Å and 2.54Å, respectively.

IV. Experimental

AgA zeolite was prepared as described in Chapter IV while Ag13X zeolite was prepared as given in reference 14. C_2H_2 was obtained from British Industrial Gases Ltd. and the acetone was removed by passing the gas slowly through a concentrated sulfuric acid trap before use. The purity of the gas was checked by infrared spectroscopy. C_2D_2 (99 atom % D) was obtained from Merck, Sharp and Dohme Ltd. and was used without further purification.

The sample preparation techniques are described in Chapter IV. Two different sample pretreatment conditions were used. The first was to leave the sample for 2 hours at a maximum bake-out temperature of 543K while the second was to leave a different sample for 2 hours at a maximum bake-out temperature of 673K. Once again, the notations S(a,b,c) or S(b,c) will be used to describe the different sample pretreatment conditions employed, where a is the evacuation time (5 or 30 minutes), b is the time sample was left at the maximum bake-out temperature (2 hours) and c is the maximum bake-out

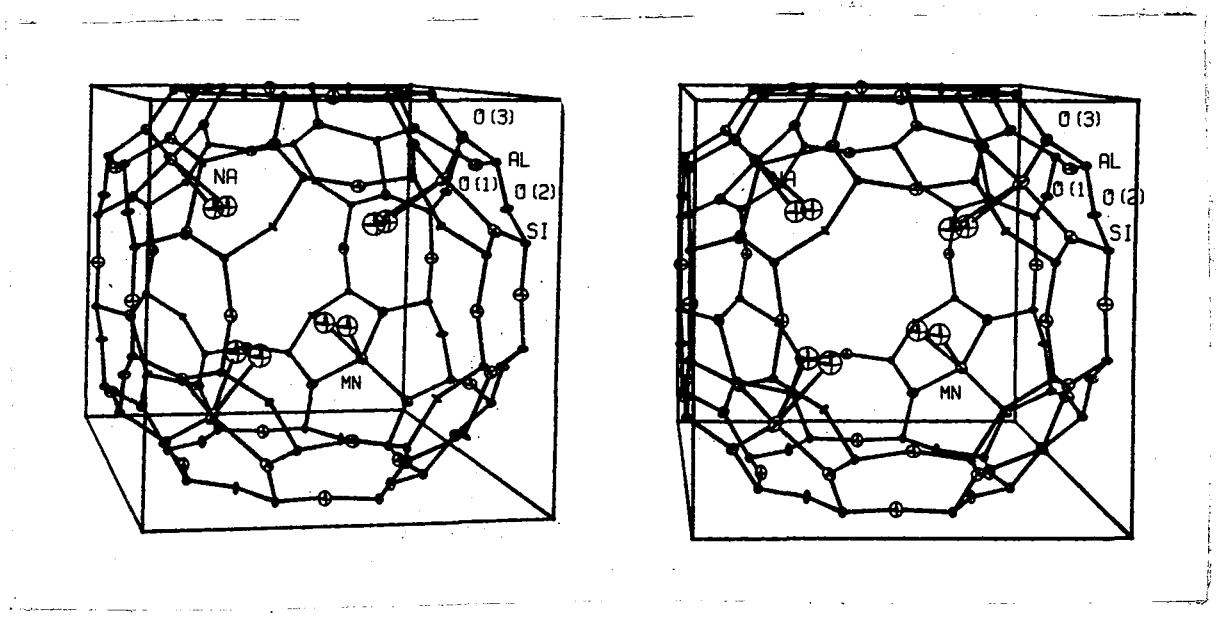

Figure 5.3. A stereoview of the $Mn_{4.5}A.4.5C_2H_2$ unit cell[7,8].

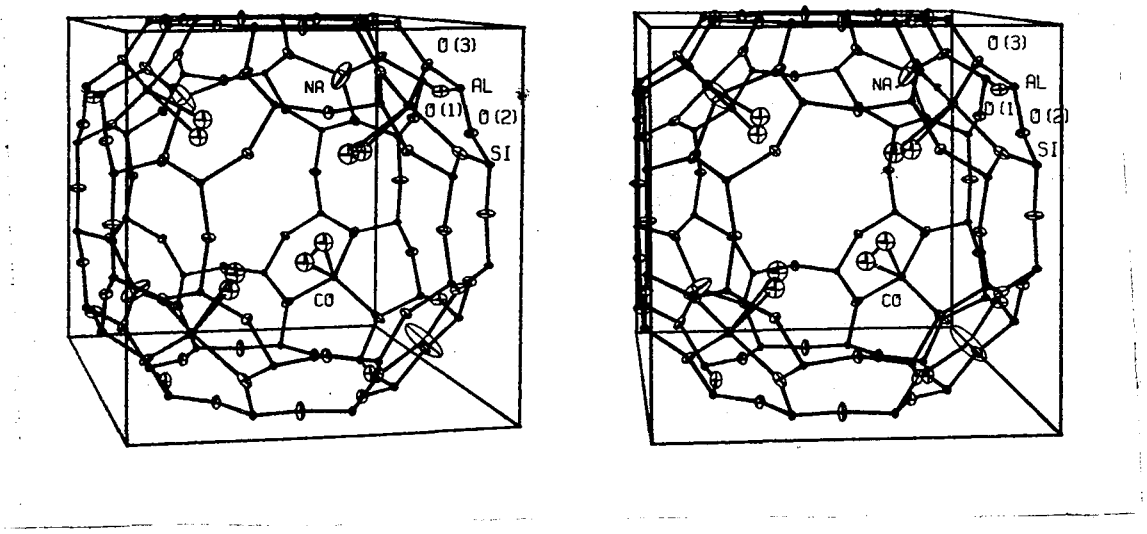

Figure 5.4. A stereoview of the $Co_4A.4C_2H_2$ unit cell[8].

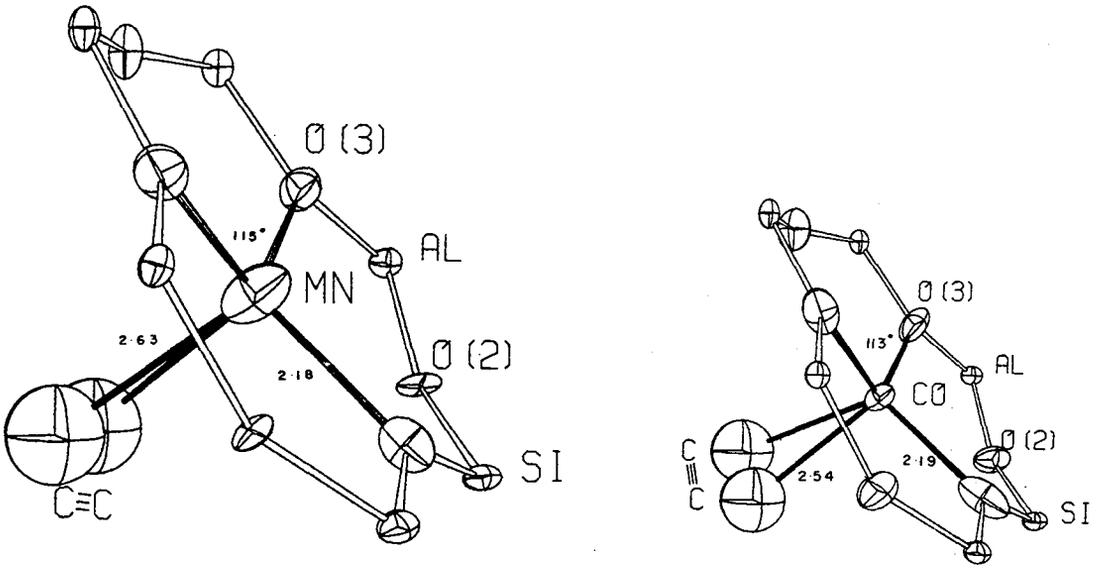

Figure 5.5. The coordination environments of the Mn(II) and Co(II) ions in each structure[8].

temperature (543 or 673K). In order to avoid confusion between experiments in which C_2H_2 and C_2D_2 were used, the notation will be extended to $S(a,b,c)_H$ or $S(b,c)_H$ and $S(a,b,c)_D$, and $S(b,c)_D$, respectively.

V. Results

Of the five fundamental vibrations of acetylene (point group $D_{\infty h}$), only two are infrared active in the gas phase; the C-H stretching (υ_3) and deformation (υ_5) modes. The fundamental frequencies of gaseous C_2H_2 and C_2D_2 are given in table 5.2[25] and the infrared spectra of purified C_2H_2 obtained at different pressures using our infrared cell (windows 4cm apart) are given in figure 5.6. The only strong bands observed in the region above $1200cm^{-1}$, the region of interest in our work on adsorbed species, occur at 3320, 3270 (C-H stretching), and 1355 and $1310cm^{-1}$ (combination bands). The C-D stretching bands in C_2D_2 occur at 2460 and $2420cm^{-1}$ while the combination bands are shifted to below $1200cm^{-1}$.

In figure 5.7 is shown some possible models for the coordinated acetylene molecule, and the symmetry species and spectroscopic activity expected for each is given in table 5.3[31].

The dehydration of AgA zeolite has been discussed already in Chapter IV. It should be noted that at 543K, one of the maximum bake-out temperature used, there are some water molecules present in the zeolite cavities (Figures 5.12a and 5.13a). For the samples that were heated to 673K, little water was readsorbed on allowing these samples to cool to room temperature (Figures 5.14a and 5.15a). We will discuss our infrared data for the AgA + C_2H_2 and AgA + C_2D_2 systems in two spectral regions; (i) 3700 - $2200cm^{-1}$ and (ii) 2000 - $1250cm^{-1}$. The region 1250 - $350cm^{-1}$ will not be discussed

Table 5.2 The frequencies of the fundamental vibrations of gaseous C_2H_2 and C_2D_2 given by reference 25, and compared with our data

C_2H_2		C_2D_2		Vibrational Species	Activity	Assignment
Ref. 25	Our data	Ref. 25	Our data			
3374	-	2700	-	Σg^+	R	υ_1
1974	-	1762	-	Σg^+	R	υ_2
3287*	3320	2427*	2460	Σu^+	IR	υ_3
	3270		2420			
612	-	505	-	Πg	R	υ_4
729	730	539	540	Πu	IR	υ_5

* The average of branches P and R is given.

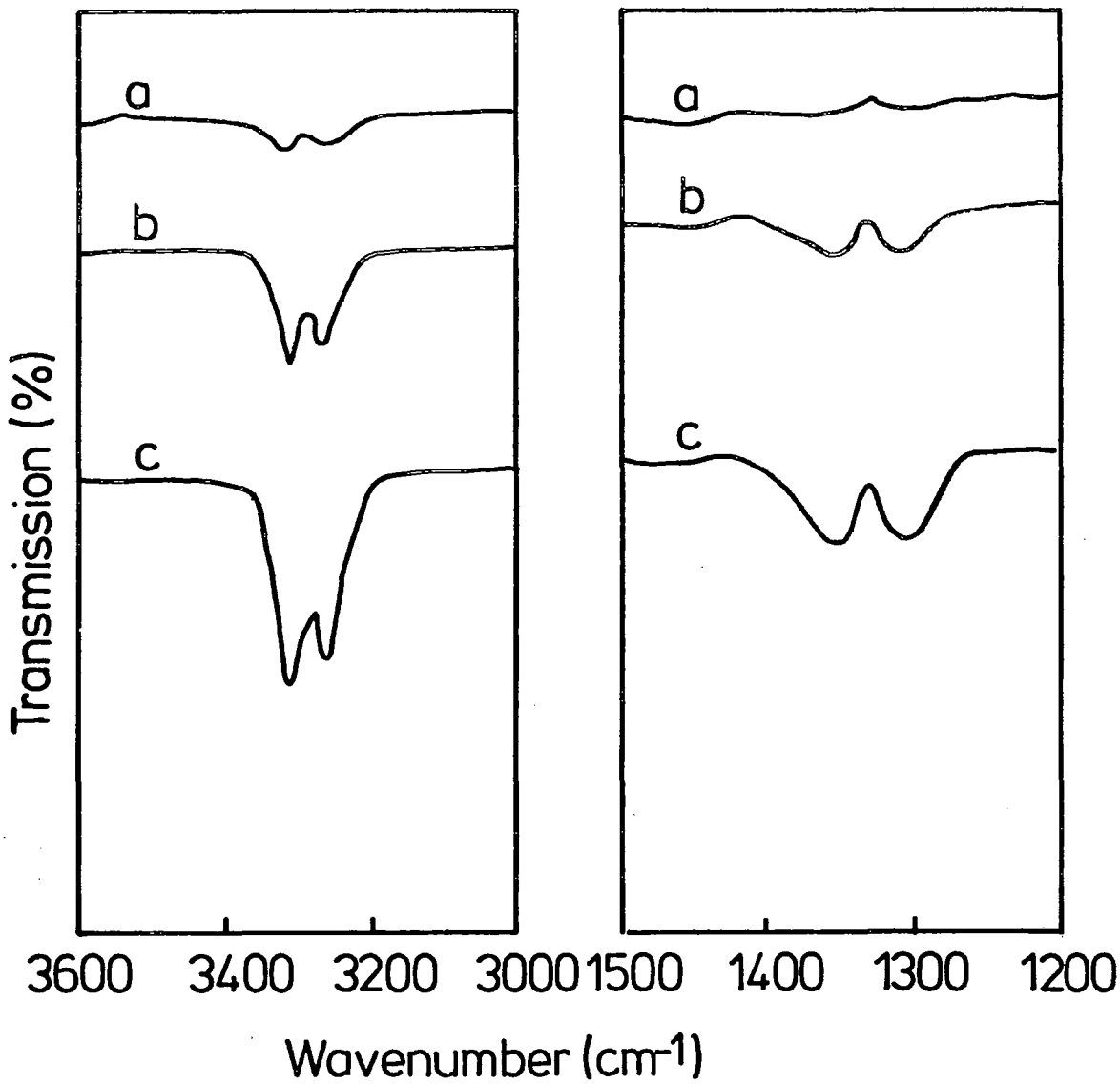

Figure 5.6. Spectra of C_2H_2 obtained at different pressures:
(a) 10 torr
(b) 50 torr
(c) 100 torr.

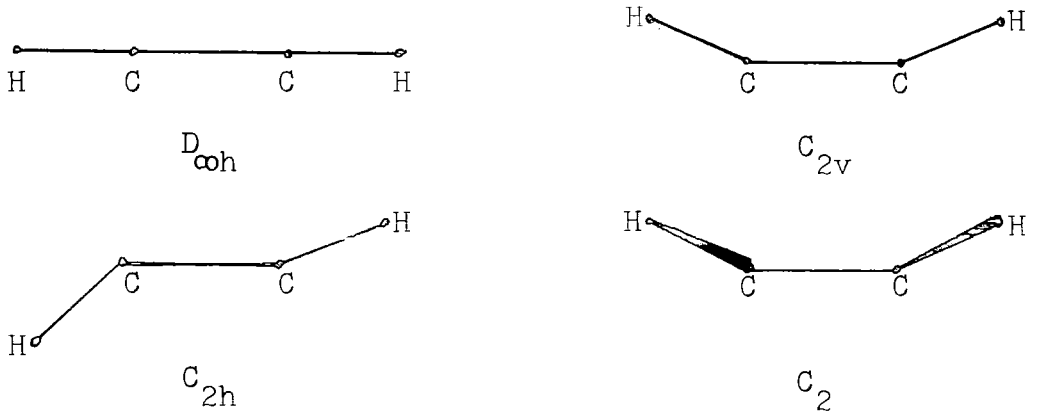

Figure 5.7. Some possible models for the coordinated acetylene molecules[31].

Table 5.3 Correlation of symmetry with infrared and Raman activity for the above models of coordinated acetylene

Symmetry	Vibrational species	Number of modes	Activity
$D_{\infty h}$	Σg^+	2	R
	Σu^+	1	IR
	Πg	2	R
	Πu	2	IR
C_{2v}	A_1	3	IR,R
	A_2	1	R
	B_1	0	IR,R
	B_2	2	IR,R
C_{2h}	A_g	3	R
	A_u	0	IR
	B_g	1	R
	B_u	2	IR
C_2	A	4	IR,R
	B	2	IR,R

since the sample is totally absorbing in this region and the regions 4000 - 3700cm^{-1} and 2200 - 2000cm^{-1} are not discussed because there are no bands observed in these regions.

3700 - 2200cm^{-1} region

Figure 5.8a shows the spectrum of AgA, at room temperature, after heating for 2 hours at 543K ($S(2,543)_H$). The spectrum obtained on admitting C_2H_2 (100 torr) to this sample is shown in figure 5.8b. The corresponding data for the sample used for C_2D_2 adsorption is shown in figures 5.9a and b.

Considering figure 5.8b, three new bands at 3592, 3302 and 3262cm^{-1}, which were not observed in the spectra of the pure zeolite (Figure 5.8a), are observed after admitting 100 torr C_2H_2. After 5 minutes evacuation at room temperature (Figure 5.8c), the band at 3592cm^{-1} and some unresolved and very weak bands in the region 3400 - 3100cm^{-1} remain. A new band in the region ~2500cm^{-1} is also observed after evacuation. The presence of three new bands on admitting C_2H_2 and the observation that only two of them become less intense on evacuation at room temperature indicates that these bands are due to at least two different types of adsorbed species. The band at 3592cm^{-1} is most probably due to υ(OH) indicating that a proportion of the acetylene has lost one or both of its hydrogen atoms per molecule to form an OH group (s) with the framework oxygen. The infrared bands found on adsorption of C_2D_2 (Figure 5.9b) corroborate this assignment of the C_2H_2 (refer table 5.6). There is a band at 2643cm^{-1} which may be assigned to υ(OD). Comparing figures 5.8c ($S(5,2,543)_H$) and 5.9c ($S(5,2,543)_D$), only one strong band at 3592 and 2643cm^{-1} respectively is observed in each. It is reasonable therefore to assume that these bands are due to the same

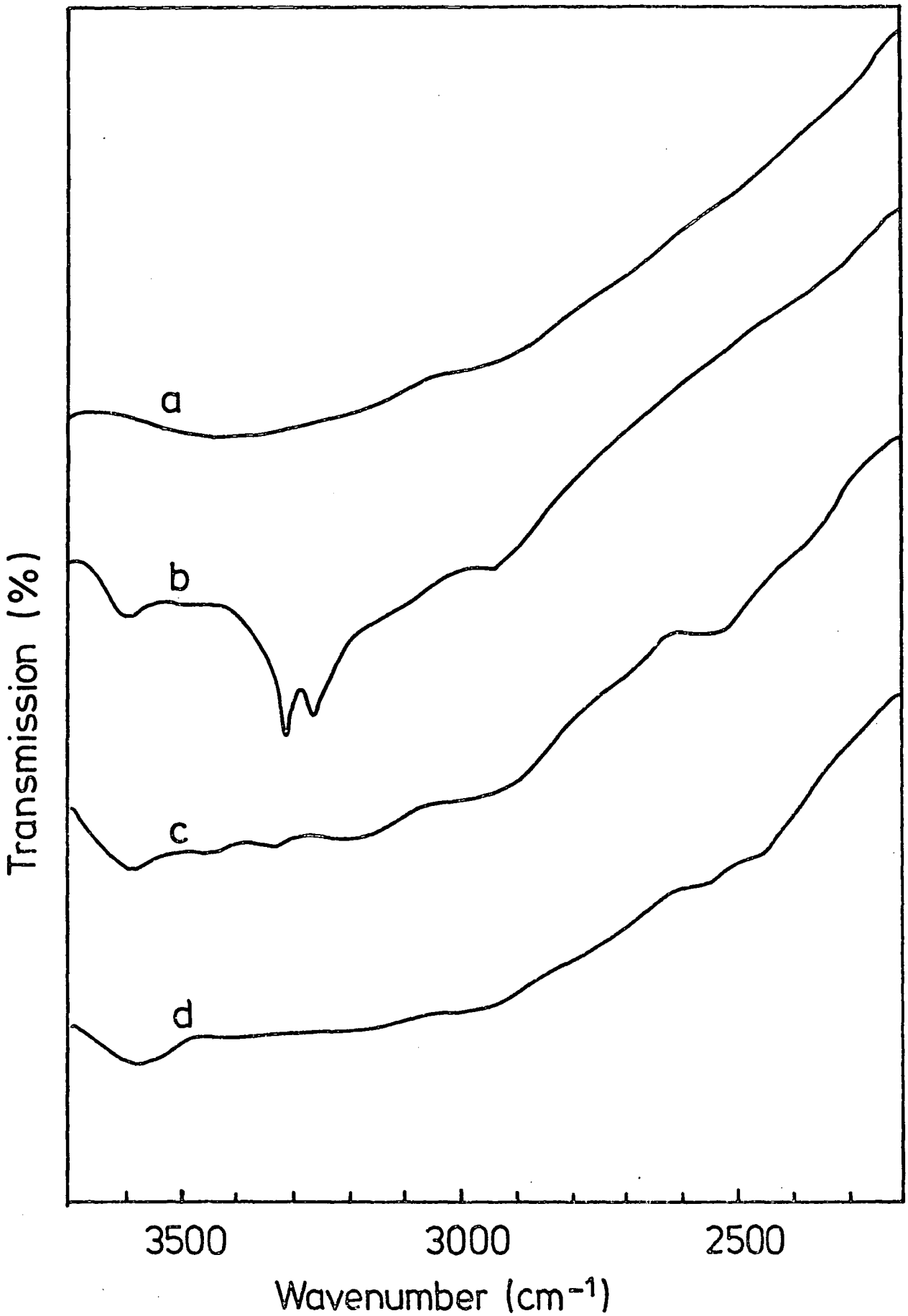

Figure 5.8. AgA zeolite after heating at 543K for 2 hours:
(a) at ambient temperature
(b) sample (a) after admitting 100 torr C_2H_2
(c) sample (b) after evacuation for 5 minutes
(d) sample (c) after evacuation for a further 25 minutes.

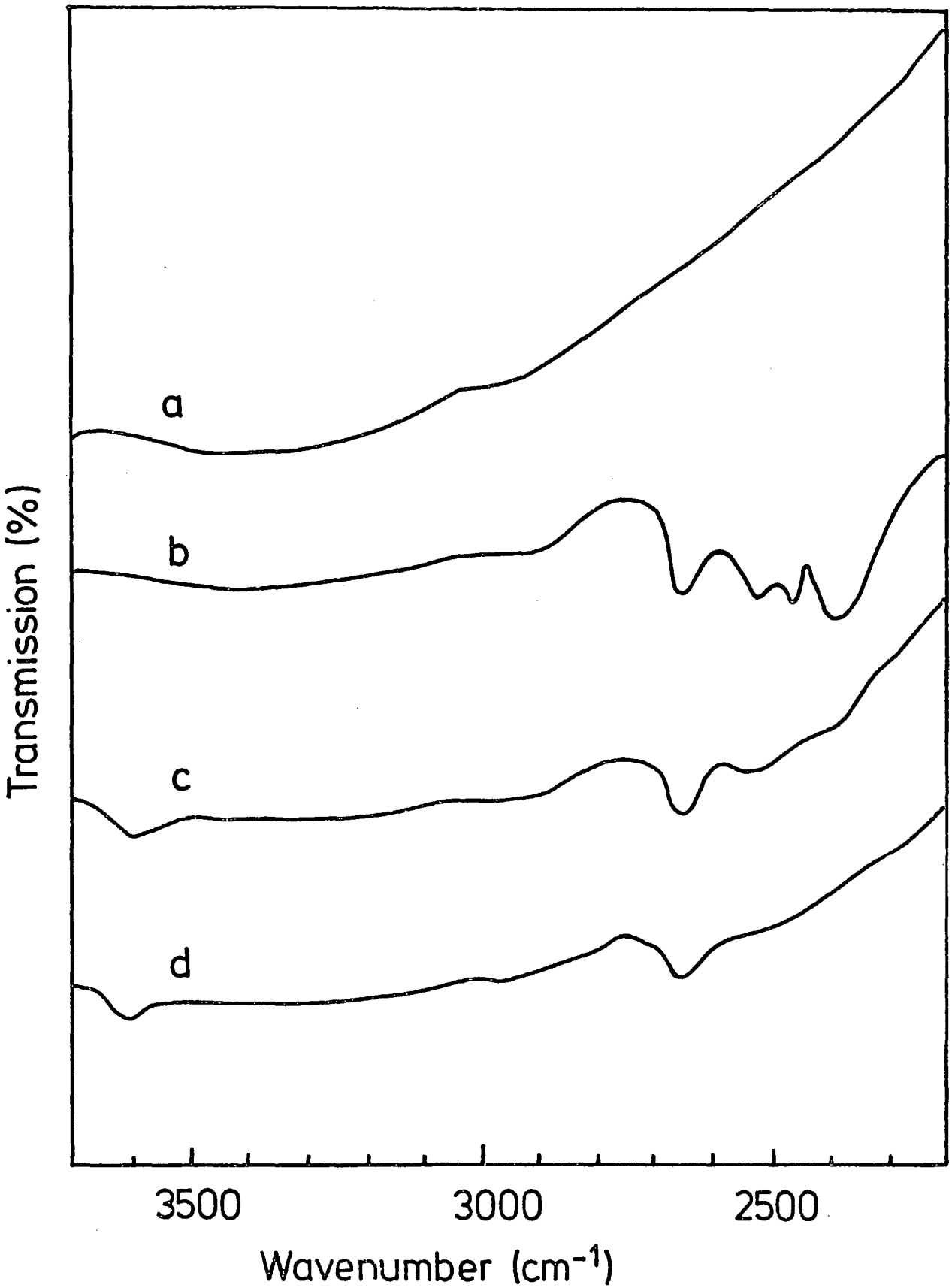

Figure 5.9. AgA zeolite after heating at 543K for 2 hours:
(a) at ambient temperature
(b) sample (a) after admitting 100 torr C_2D_2
(c) sample (b) after evacuation for 5 minutes
(d) sample (c) after evacuation for a further 25 minutes.

vibration. In zeolites, vibrations of the framework hydroxyl groups occur in the region 3550 - 3650cm^{-1} and this has been discussed in detail in Chapter II. From our data ν(OD) / ν(OH) = 0.74, which agrees exactly with the isotopic ratio found with hydroxyl groups in zeolites (0.74)[32].

In sample S(5,2,543)$_H$, some broad bands are observed between 3400 and 3100cm^{-1} (Figure 5.8c) which disappear on further evacuation for 25 minutes at room temperature (Figure 5.8d). We assign these bands to weakly adsorbed acetylene. Here again, the result for C_2D_2 corroborate this assignment. A broad band at 2500cm^{-1} is observed in S(5,2,543)$_D$ (Figure 5.9c) which disappear in S(30,2,543)$_D$ (Figure 5.9d). It can be assumed from the above evidence that the bands at 3302 and 3262cm^{-1} in figure 5.8b and the bands at 2500 and 2450cm^{-1} in figure 5.9b are due to both the gas phase (refer figure 5.6) and the adsorbed species. For sample S(5,2,543)$_D$ (Figure 5.9c), bands are also observed at 3600 and 2376cm^{-1} which we assigned to ν(OH) and ν(OD) of DH_2O^+ (Table 5.6), respectively.

In figures 5.10a and 5.11a are shown the spectra of samples AgA zeolites at room temperature after heating for 2 hours at 673K. Figures 5.10b and 5.11b show the spectra of the samples after admitting C_2H_2 and C_2D_2, respectively, to an overpressure of 100 torr. Although the ν(OH) band is not observed in the spectrum of the sample S(2,673)$_H$ after admitting 100 torr C_2H_2 (Figure 5.10b), a band at 2643cm^{-1} which may be assigned to ν(OD) is observed after admitting 100 torr C_2D_2 (Figure 5.11b). The OH band is not observed in the spectrum of S(2,673)$_H$ because at this temperature, the spectrum of the background is so high that the relatively weak ν(OH) is not observed but only the bands due to the gas phase at 3320 and 3270cm^{-1} are observed (Figure 5.10b). For the

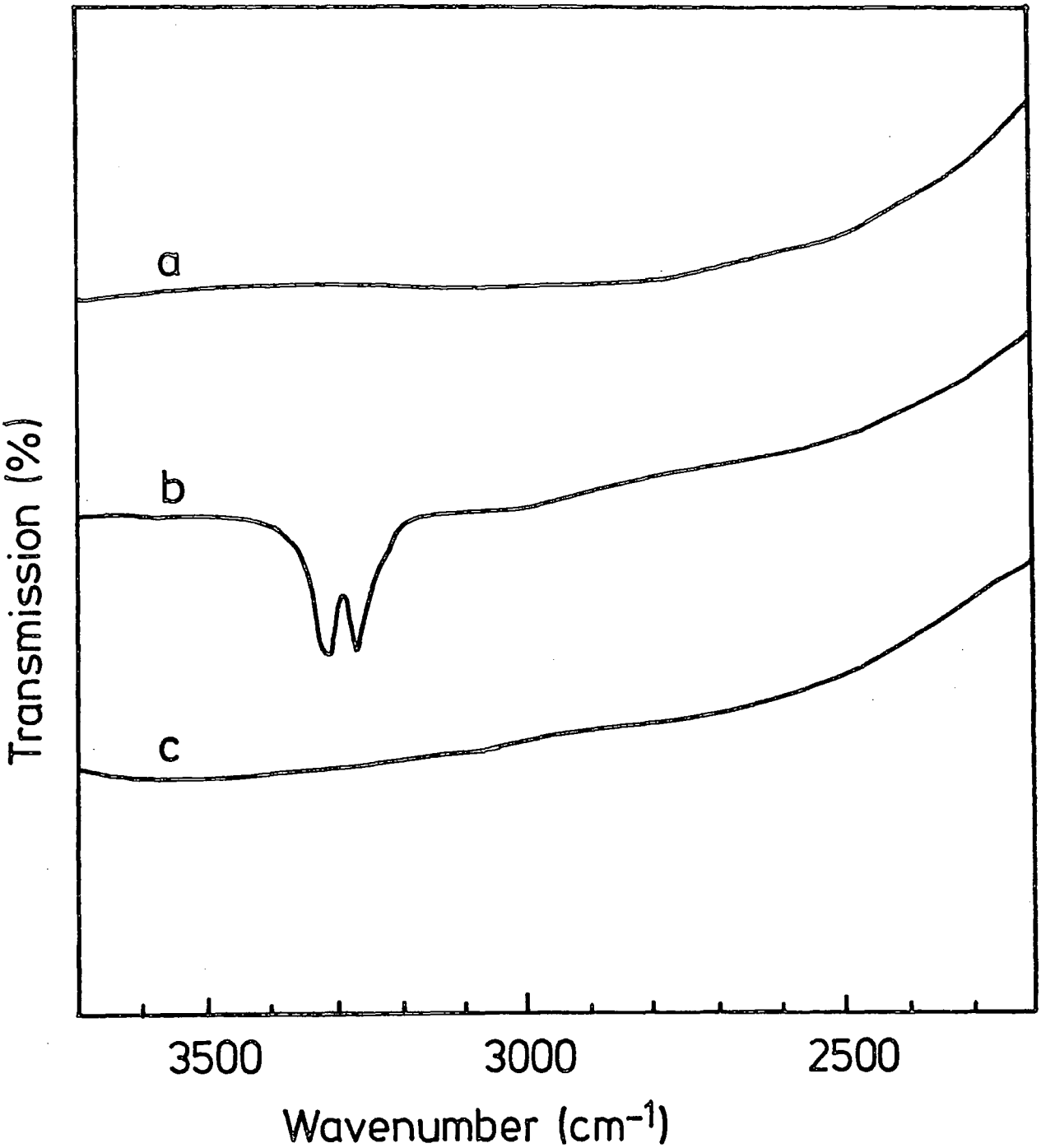

Figure 5.10. AgA zeolite after heating at 673K for 2 hours:
(a) at ambient temperature
(b) sample (a) after admitting 100 torr C_2H_2
(c) sample (b) after evacuation for 5 minutes.

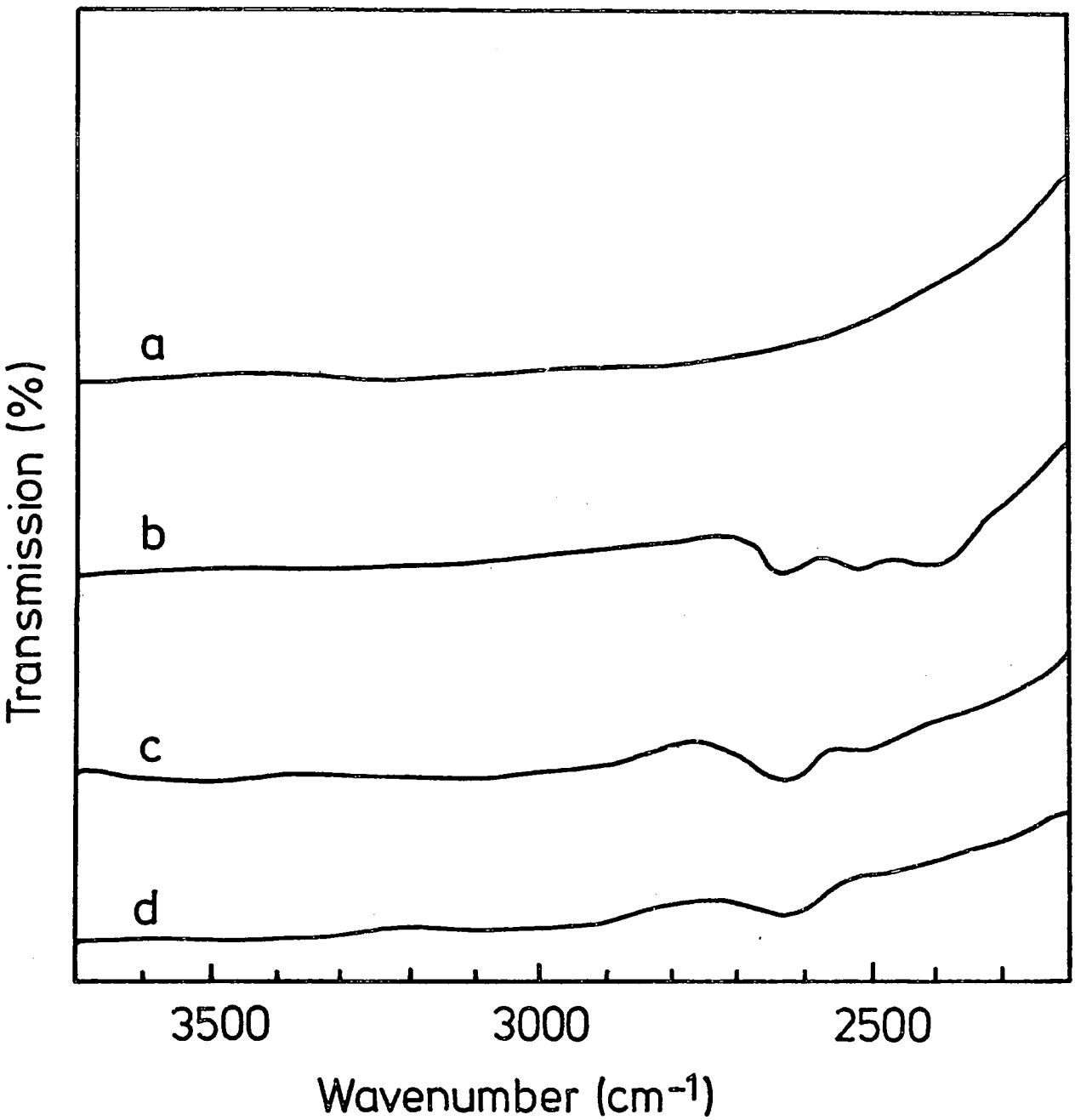

Figure 5.11. AgA zeolite after heating at 673K for 2 hours:
(a) at ambient temperature
(b) sample (a) after admitting 100 torr C_2D_2
(c) sample (b) after evacuation for 5 minutes
(d) sample (c) after evacuation for a further 25 minutes.

AgA + C_2D_2 system, after 5 minutes evacuation at room temperature (Figure 5.11c). the band due to OD still remains. A band at 2500cm^{-1} observed in sample $S(5,2,673)_D$ (Figure 5.11c) which disappear on further evacuation ($S(30,2,673)_D$; figure 5.11d), as in samples $S(5,2,543)_D$ and $S(30,2,543)_D$, is also assigned to weakly adsorbed acetylene.

2000 - 1250cm^{-1} region

In the infrared spectrum of gas phase C_2H_2, there are only two bands observed in this region, at 1355 and 1310cm^{-1}, (due to combination modes[25]) as shown in figure 5.6, while in this region of the infrared spectrum of the gas phase C_2D_2, no bands are observed.

In our data for AgA and Ag13X, regardless of the pretreatment conditions used, bands which can be assigned to the $\upsilon(C \equiv C)$ mode of adsorbed acetylene are observed in all of the spectra of the samples after admitting 100 torr of C_2H_2 (Figures 5.12b, 5.14b for AgA and figures 5.16b, 5.17b for Ag13X) and C_2D_2 (Figures 5.13b and 5.15b). The $\upsilon(C \equiv C)$ values for all the samples are given in table 5.4. It is believed that there are two $\upsilon(C \equiv C)$ values, since the isotopic ratio for the $\upsilon(C \equiv C)$ values in AgA + C_2H_2 (1912 and 1955cm^{-1}) and AgA + C_2D_2 (1710 and 1740cm^{-1}) of 0.89 agrees exactly with the isotopic ratio in the gas phase (0.89).

The bands at 1355 and 1300cm^{-1} observed in both the spectra of $S(2,543)_H$ and $S(2,673)_H$ after admitting 100 torr C_2H_2 (Figures 5.12b and 5.14b) are due to the gas phase bands and disappear after 5 minutes evacuation at room temperature (Figures 5.12c and 5.14c). The disappearance of these bands results in the appearance of a relatively strong band at 1380cm^{-1} in $S(5,2,673)_H$ (Figure 5.12c). This difference

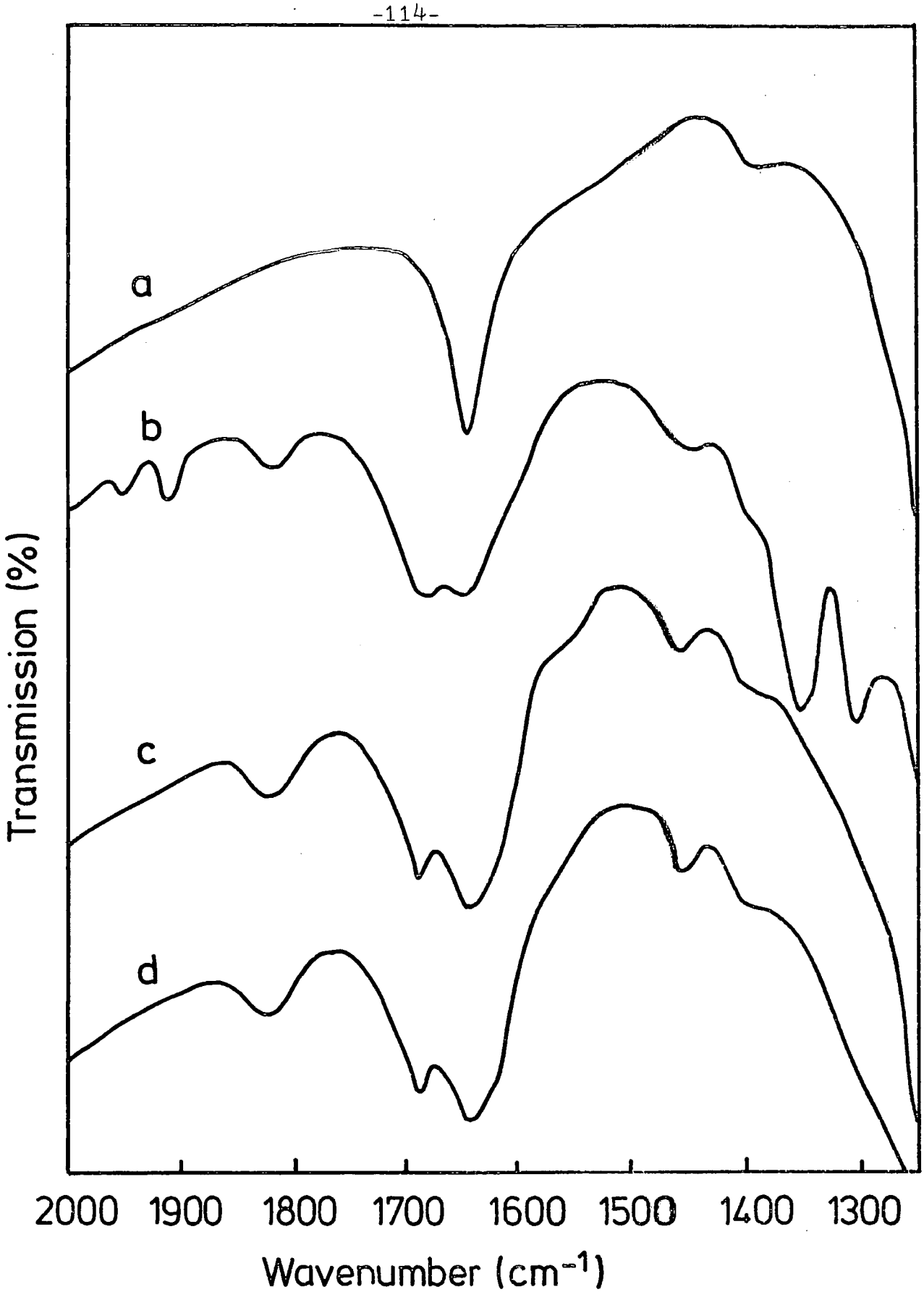

Figure 5.12. AgA zeolite after heating at 543K for 2 hours:
(a) at ambient temperature
(b) sample (a) after admitting 100 torr C_2H_2
(c) sample (b) after evacuation for 5 minutes
(d) sample (c) after evacuation for a further 25 minutes.

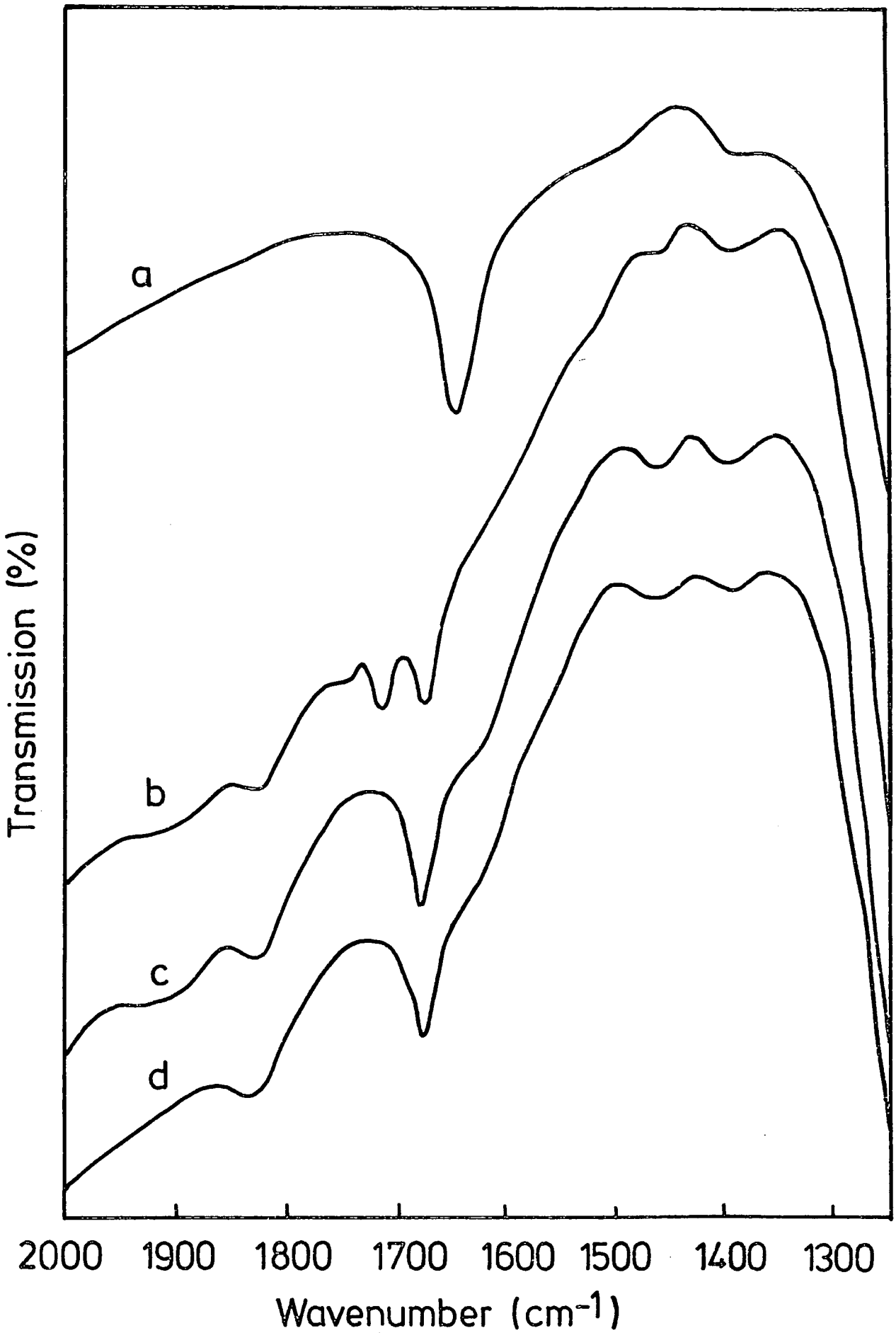

Figure 5.13. AgA zeolite after heating at 543K for 2 hours: (a), (b), (c) and (d) as for Figure 5.11.

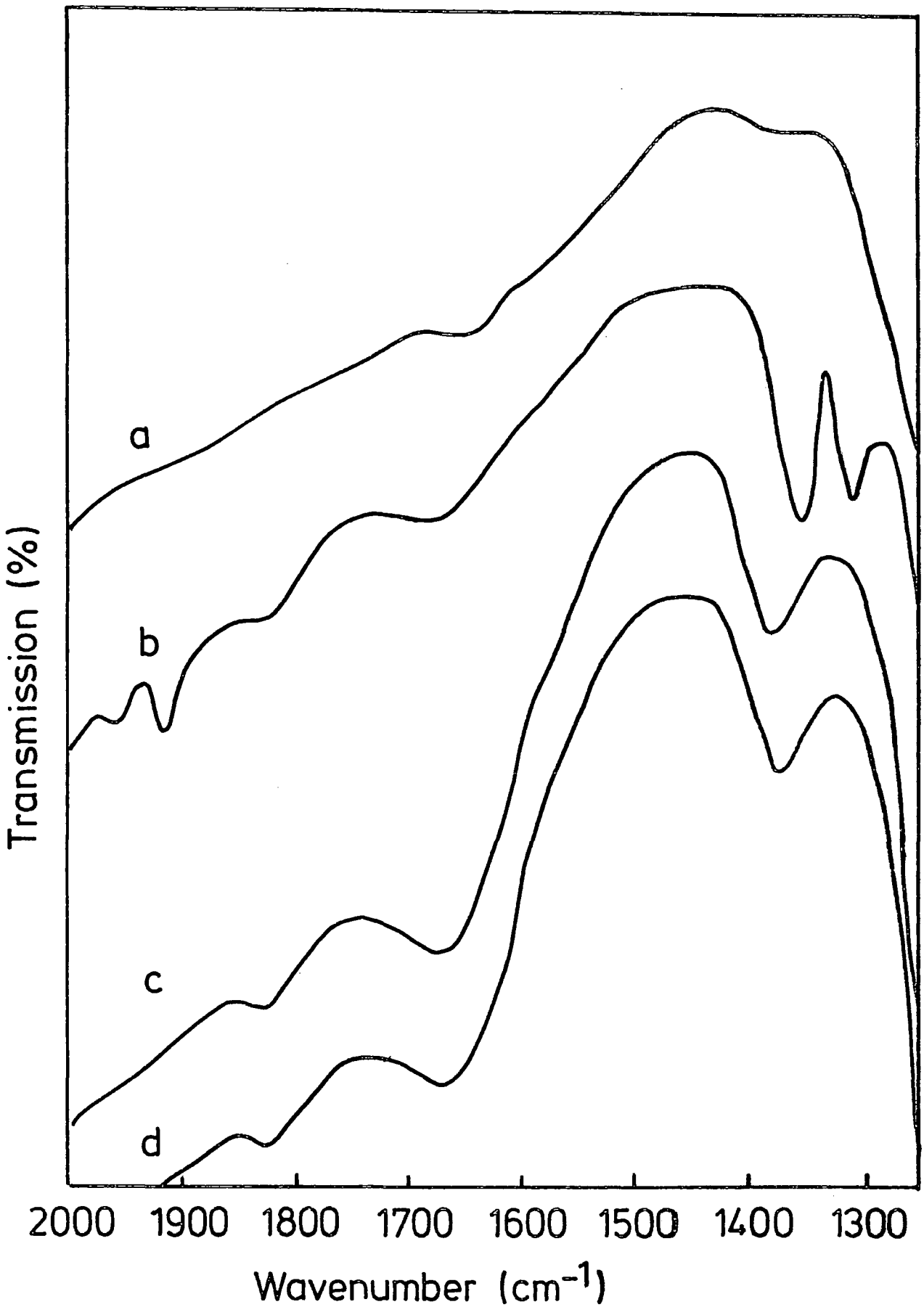

Figure 5.14. AgA zeolite after heating at 673K for 2 hours: (a), (b), (c) and (d) as for Figure 5.12.

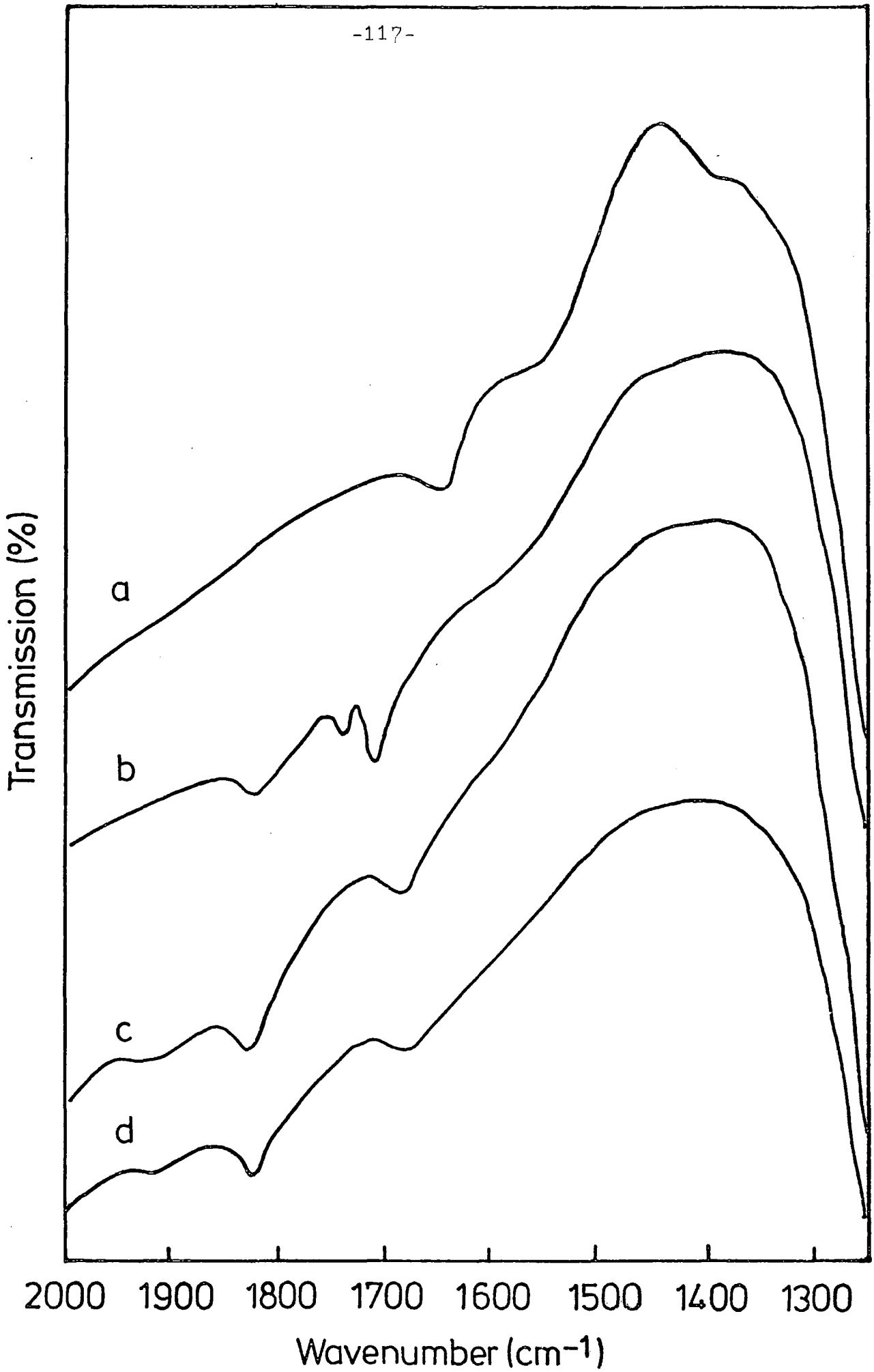

Figure 5.15. AgA zeolite after heating at 673K for 2 hours: (a), (b), (c) and (d) as for Figure 5.11.

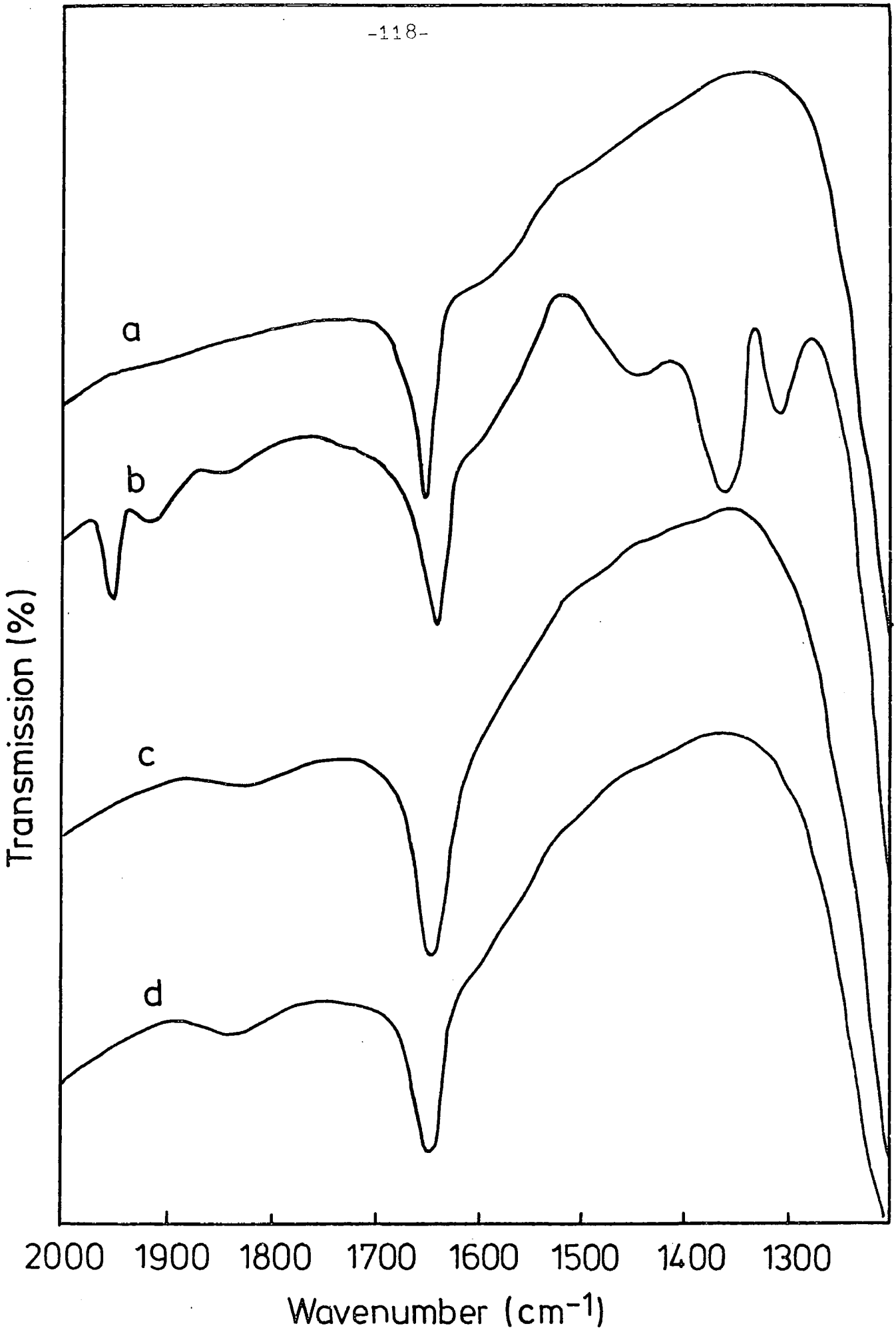

Figure 5.16. Ag13X zeolite after heating at 543K for 2 hours: (a), (b), (c) and (d) as for Figure 5.12.

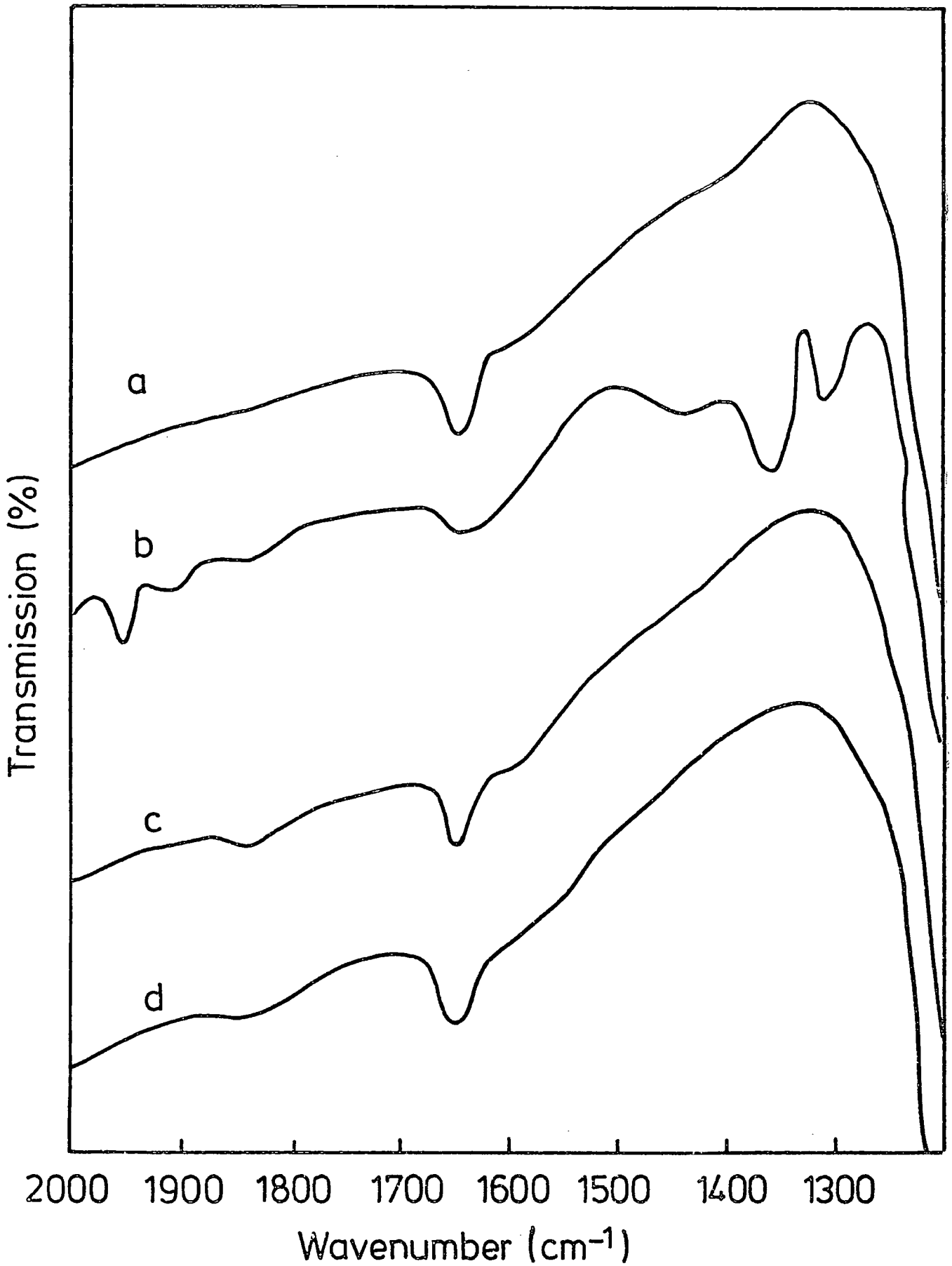

Figure 5.17. Ag13X zeolite after heating at 623K for 2 hours:
(a) at ambient temperature
(b) sample (a) after admitting 100 torr C_2H_2
(c) sample (b) after evacuation for 5 minutes
(d) sample (c) after evacuation for a further 25 minutes.

Table 5.4 Values of $\nu(C\equiv C)$ observed in the infrared spectra of adsorbed C_2H_2 and C_2D_2

Sample AgA	ν_2/cm^{-1}
$S(2,543)_H$	1912
	1955
$S(2,543)_D$	1710
	1740
$S(2,673)_H$	1912
	1955
$S(2,673)_D$	1710
	1740
Sample Ag13X	ν_2/cm^{-1}
$S(2,543)_H$	1915
	1950
$S(2,623)_H$	1915
	1950

could be explained as a consequence of the different pretreatment conditions in each case. As is explained in Chapter IV, the structure and the adsorption behaviour of silver exchanged type A zeolites are a function of pretreatment conditions.

The band observed at 1380cm^{-1} in $S(5,2,673)_H$ is not observed in $S(5,2,673)_D$ (Figures 5.14c and 5.15c) which indicates that this band is not due to cation movements, but is due to an adsorbed species. It is not observed in $S(5,2,673)_D$ because this band could be shifted to a frequency below 1250cm^{-1} and hence is masked by the strong absorption of the zeolite framework. The appearance of the 1380cm^{-1} band in $S(2,673)_H$ which does not disappear even after evacuation for 30 minutes at room temperature (Figure 5.14d), could be due to C_2H_2 complexation with the Ag cation, such that, Ag is bonded to both the carbon atoms. As we shall see later, no other bands observed in the spectra of samples $S(2,673)_H$, $S(5,2,673)_H$ and $S(30,2,673)_H$ (Figures 5.14b - d) can be assigned to this complex.

Comparing $S(5,2,543)_H$ (Figure 5.12c) and $S(5,2,543)_D$ (Figure 5.13c), a new band is observed at 1460cm^{-1} which is not found in the spectrum of the background. This could be due to cation movements during the adsorption of the gases since this band is independent of isotopic substitution.

Apart from the bands due to $\upsilon(C \equiv C)$, a band at 1820cm^{-1} is also observed in all of the spectra of the samples studied after admitting the gases (Figures 5.12b - 5.17b). Unlike the $\upsilon(C \equiv C)$, this band remains after 5 minutes (Figures 5.12c - 5.17c) or even 30 minutes (Figures 5.12d - 5.17d) evacuation at room temperature. The 1820cm^{-1} band appears to be slightly more intense in the spectra of AgA relative to the spectra of Ag13X zeolites. In AgA zeolite, this band may be due to the

$\nu(C\equiv C)$ of acetylide (refer to later section).

As we have shown, at least part of the $C_2H_2(C_2D_2)$ loses hydrogen(deuterium) to form OH(OD) groups. Another possibility for the liberated hydrogen exists; this hydrogen (or deuterium) could combine with residual water molecules in the zeolite cavities to form $H_3O^+(DH_2O^+)$ ions. For the acetylene adsorbed onto AgA samples, bands are observed at ~2500 and 1686cm^{-1} for $S(2,543)_H$ (Figures 5.8 and 5.12) and at 3600, 2376, 1920 and 1694cm^{-1} for $S(2,543)_D$ (Figures 5.9 and 5.13) which may be due to H_3O^+ or DH_2O^+ ions. For the acetylene adsorbed onto Ag13X samples, the band due to the deformation mode (ν_2) of water is shifted to a lower frequency (1640cm^{-1}) compared with the spectrum of the background (1655cm^{-1}). The acetylene could be hydrogen bonded to the water molecules since it has been shown in reference 33 that the deformation mode of water is shifted to lower frequency when it is hydrogen bonded to other molecules. Acetylene was found to weakly hydrogen bonded to the water molecules because this band at 1640cm^{-1} goes back to 1655cm^{-1} after evacuation for 5 minutes at room temperature (Figures 5.16c and 5.17c).

VI. Discussion of results

Hydroxyl and hydronium ions

As we have already shown, the appearance of the OH band at 2592cm^{-1} and OD band at 2643cm^{-1} shows that at least part of the adsorbed C_2H_2 or C_2D_2 loses its hydrogen or deuterium atoms to form OH or OD groups with the framework oxygen. Another possibility is that the hydrogen or deuterium combines with zeolitic water to form H_3O^+ or DH_2O^+ ions.

There is some controversy as to the structure of the

hydronium ion and the bands that occur in its infrared spectrum[20-24]. There are two basic structures proposed for hydronium ions. One is pyramidal (C_{3v} symmetry) and its normal modes are shown in figure 5.18. All four modes ($2A_1$ + 2E) of the hydronium ions are predicted to be infrared active. The second proposed structure is planar (C_{3h} symmetry) would possess only three infrared active fundamentals. Figure 5.18 shows the normal modes of H_3O^+ adopting a C_{3v} symmetry.

In table 5.5 is given the summary of the results of infrared studies of hydronium ions assigned by different authors. From table 5.5, it is obvious that one cannot ascribe fixed stretching frequencies υ_1 and υ_3 of H_3O^+ because, according to Basile et al[20], they are a function of donor-acceptor distances in the hydrogen bonds formed. Basile et al also suggested that is impossible to "fingerprint" H_3O^+ except for the appearance of the $\upsilon_4(E)$ and $\upsilon_2(A_1)$ bands at ~1700 and ~1100cm^{-1}, respectively. In the case of zeolites, it is not easy to observe the band at ~1100cm^{-1} and hence the formation of H_3O^+ is most strongly implied by the presence of the band at ~1700cm^{-1}.

From the spectra of AgA + C_2H_2 (C_2D_2), the bands for the hydronium ions can be assigned as given in table 5.6. At this stage it is clear that at least part of the adsorbed acetylene loses its hydrogen (or deuterium) atoms to form OH (or OD) groups with framework oxygen, and hydronium ions with residual water molecules.

Formation of acetylides, HC ≡ CAg

If acetylene loses one or two of its hydrogen or deuterium atoms then either HC ≡ CAg or AgC ≡ CAg could be formed . The formation of AgC ≡ CAg is unlikely because this complex is explosive in a dry medium[27] and the discussion

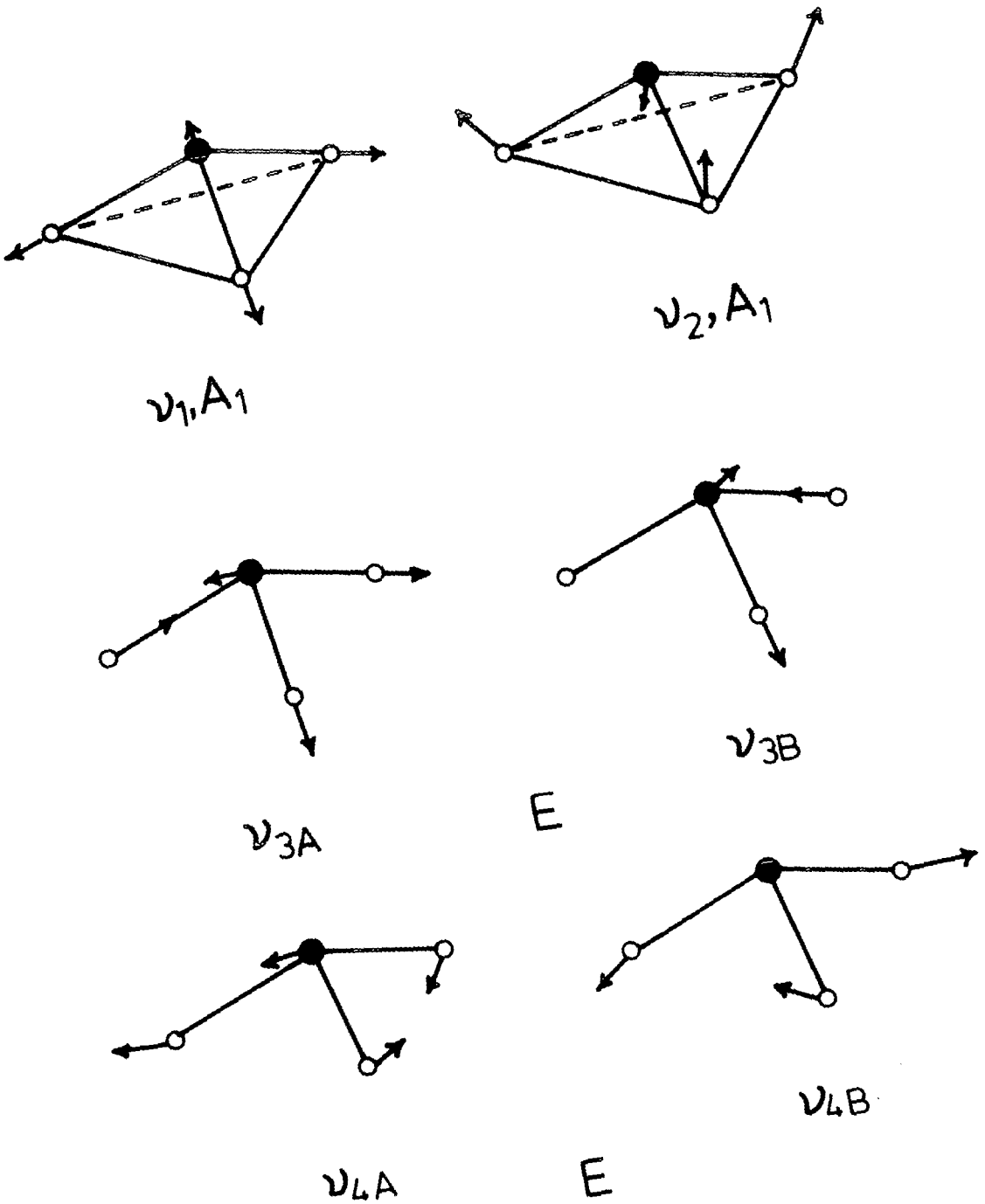

Figure 5.18. Normal modes of H_3O^+: C_{3v} symmetry[25].

Table 5.5 Summary of the frequencies of the normal modes of H_3O^+ ion on various substrates (cm^{-1}, infrared data).

Substrate	$\nu_1(A_1)$	$\nu_3(E)$	$\nu_4(E)$	$\nu_2(A_1)$	Ref.
$(H_3O)_2PtCl_6$	3380-3150	2650-2468	1705-1670	1150-1050	26
$H_3O^+Cl^-$	3020	3800-3400	1600	-	24
$H_3O^+CH_3C_6H_4SO_3^-$	2500 - 3500*		1665	1120	20

* General range of $\nu_1(A_1)$ and $\nu_3(E)$.

Table 5.6 Assignment of bands due to $H_3O^+(DH_2O^+)$ ions in the infrared spectra of AgA + $C_2H_2(C_2D_2)$ (cm^{-1})

Assignment	$H_3O^+(cm^{-1})$	$DH_2O^+(cm^{-1})$
OH stretch (DH_2O^+)	-	3600(vw) (?)
OD stretch (DH_2O^+)	-	2376(vw)
$\nu_1(A_1)$ or $\nu_3(E)$	2500(wb)	1920(wb)
$\nu_4(E)$	1686(s)	-
$2\nu_2(2A_1)$ or $\nu_4(E)$	-	1694(s)

that follows will give more reasons as to why the complex formed is actually HC ≡ CAg.

If HC ≡ CAg were formed, then vibrations are expected for υ(C-H), υ(C ≡ C) and υ(C-Ag) in the infrared spectrum of the sample. In table 5.7 is shown the assignments of υ(C-H) υ(C ≡ C), δ(C-H) and υ(C-M) of some alkali metals[11] and silver[27] acetylides.

The υ(C-Ag) would not be observed in our data because it would occur below 1250cm^{-1} and hence be masked by the strong absorption band of the zeolite. A band due to υ(C ≡ C) of acetylides cannot be assigned with certainty in our spectra. In the spectra of all the AgA + C_2H_2 samples, two bands due υ(C≡C) are observed at 1955(1740) and 1912(1710)cm^{-1}. Both these bands are assigned to the υ(C ≡ C) of the π bonded acetylene complexes. This will be discussed further in the following section. In all of our spectra of AgA + $C_2H_2(D_2)$, there is a band at 1820cm^{-1} which is not removed on evacuation for 30 minutes. We assign this band to υ(C≡C) of acetylide.

As can be seen in table 5.7, the υ(C ≡ C) bands of alkali metal acetylides is indeed very weak in the infrared spectra except for K(Ag$(C_2H_2)_2$). The latter complex has a strong υ(C ≡ C) band because it has two acetylenes per molecule. It has been found that with different number of acetylene molecules in a complex, the υ(C ≡ C) values differ[38]. The υ(C-H) of acetylides are also not observed in the spectra of our samples. Once again, the reason being this band is generally very weak.

The AgA zeolite samples were heated after evacuating for 30 minutes at room temperature. It was found that at elevated temperature, a new band appears at 1585cm^{-1} which could be assigned to the formation of coke. Infrared studies of activated carbon and soot samples by Unger and Gallei[28] show

Table 5.7 Reported infrared frequencies of some acetylides[11,27]

Compounds	Types of vibrations(cm^{-1})			
	ν(C-H(D))	ν(C C)	δ(C-H)	ν(C-M)
CH≡CLi[7]	3270(vw)	1980(w) ?	700(m)	475(vs)
	3220(m)	1895(w)		
CH≡CLi[6]	3270(m)	1980(w)	695(m)	495(vs)
	3225(m)	1890(w)		
CH≡CNa	3215(m)	1865(w)	640(s)	-
CH≡CK	3295(vw)	1850(m)	625(s)	-
	3225(m)			
CD≡CLi[7]	2450(w)	1975(s) ?	-	475(vs)
$K(Ag(C_2H)_2)$	3205(m)	1934(s)	-	-

that a band at 1585cm^{-1} is due to the C=C stretching vibration of microcrystalline graphatic carbon structures, which are present in polycyclic aromatic compounds. The band at 1585cm^{-1} relating to coke formation is also found by Eisenbach and Gallei[29] in their studies of hexene - 1 and n - hexane adsorbed at elevated temperatures onto calcium and ammonium exchanged type Y zeolites.

Formation of π-bonded acetylene complexes

In all of the spectra of AgA + C_2H_2 (C_2D_2) and Ag13X + C_2H_2 systems (Figures 5.12b-5.17b), two bands which are due to $\upsilon(C \equiv C)$ are observed and these data are shown in table 5.4. The measured isotopic ratios of the $\upsilon(C \equiv C)$ in AgA + C_2H_2 (1912,1955) $\longrightarrow$ AgA + C_2D_2 (1710,1740) cm^{-1} is 0.89, which agrees well with the isotopic ratio of the $\upsilon(C \equiv C)$ in the gas phase (0.89). The appearance of υ(C≡C) in the spectra of the adsorbed species indicates a lowering in symmetry of the molecule since $\upsilon(C \equiv C)$ is forbidden in the infrared spectrum of the gas phase. All the $\upsilon(C \equiv C)$ values in our measurement decrease on adsorption compared to the gas phase (1974cm^{-1}). This clearly favours a 'side-on' interaction, that is, the acetylene is π-bonded to the cation. Our conclusion is in agreement with the data of x-ray structure determination of Seff et al[5-8] and the infrared studies of Tam et al[15,30].

Since we observe two υ(C≡C) bands in our AgA + C_2H_2 and Ag13X + C_2H_2 spectra, we assign the υ(C≡C) bands to acetylene adsorbed at two different sites. Yates et al[34] in their studies of ethylene adsorbed onto Ag13X zeolites also found two different sites for the adsorbed ethylene. In our previous work of ethylene adsorbed onto AgA zeolites (Chapter IV), we also observed that ethylene was adsorbed at two different sites

The υ(C-H) of this π-bonded acetylene complex can be

observed in samples $S(5,2,543)_H$ and $S(5,2,543)_D$ (Figures 5.8c and 5.9c). In sample $S(5,2,543)_H$, these bands which occur in the region 3400-3100cm^{-1} are very weak and cannot be resolved whilst in sample $S(5,2,543)_D$, there is a band at 2540cm^{-1} which can be assigned to υ(C-D) of the π-bonded acetylene complex. These bands can be removed after evacuating for 30 minutes at room temperature, ($S(30,2,543)_H$ and $S(30,2,543)_D$ in figures 5.12d and 5.13d), indicating that acetylene is weakly held.

No bands due to υ(C-H) are observed in samples $S(5,2,673)_H$ and Ag13X because the samples are highly absorbing in this region. For Ag13X + C_2H_2, acetylene is believed to be weakly hydrogen bonded to the residual water since the deformation mode of water at 1655cm^{-1} is shifted to a lower frequency, 1640cm^{-1} on admitting acetylene (Figure 5.16b and 5.17b). On evacuating these samples for 5 minutes, however, the deformation mode of water returns to its original position at 1655cm^{-1} (Figures 5.16c and 5.17c).

In table 5.8 is given a summary of the result together with the assignment for C_2H_2 and C_2D_2 adsorbed on AgA zeolite.

VII Conclusion

Unlike other zeolite + C_2H_2 systems previously studied, two types of acetylene complexes were found in the present studies of AgA + C_2H_2. The two complexes formed were the acetylides, HC $\equiv$ CAg and the cation - acetylene π bonded complex. The former finding is corroborated with the finding of OH and H_3O^+ groups which did not disappear on evacuation at room temperature.

On heating the sample after evacuation, coke was formed

Table 5.8 Summary of the vibrational bands (cm^{-1}) and their assignments for acetylene adsorbed on AgA zeolite

AgA + C_2H_2	AgA + C_2D_2	Assignment
3592		ν(O-H)
	2643	ν(O-D)
3400-3100		ν(C-H) of π-bonded
	2500	ν(C-D) acetylene species
	3600	stretching modes of
	2376	DH_2O^+
1955	1740	ν(C≡C) of π-bonded
1912	1710	acetylene on two different sites
1820	1820	ν(C≡C) of acetylide
	1694	$2\nu_2$ or ν_4 of DH_2O^+
1686		ν_4 of H_2O^+
1460	1460	framework vibration associated with the cation

indicating that the acetylides had decomposed. The finding of the cation-acetylene π bonded complex is in agreement with those of other authors on a range of zeolites[5-8, 13,15]. In Ag13X + C_2H_2, the acetylene was found to be weakly hydrogen bonded to the residual water.

We also observed that, like ethylene, acetylene was adsorbed at two different sites in both the Ag13X and AgA zeolites. This finding is in agreement with the conclusion reached by Yates et al[34] in their infrared studies of ethylene adsorbed onto Ag13X zeolite, and the conclusion reached by us in the infrared studies of ethylene adsorbed onto AgA zeolite (Chapter IV). Our conclusion, however, is not in agreement with the conclusions reached by inelastic neutron data of acetylene adsorbed onto AgA zeolite[13]. These authors found only one site for the acetylene adsorbed onto AgA zeolite.

References

1. Kim, Y and Seff, K., J. Phys. Chem., 82, 1071 (1978)
2. Kim, Y and Seff, K., J. Amer. Chem. Soc., 99, 7055 (1977)
3. Kim, Y and Seff, K., J. Amer. Chem. Soc., 100, 6989 (1978)
4. Gallens, L.R., Mortier, W.J., Schoonheydt, R.A. and Uytterhoeven, J.B., J. Phys. Chem., 85, 2783 (1981)
5. Amaro, A.A. and Seff, K., J. Chem. Soc. Chem. Comun., 1201 (1972).
6. Amaro, A.A. and Seff, K., J. Phys. Chem., 77, 906 (1973)
7. Riley, P.E. and Seff, K., J. Amer. Chem. Soc., 95, 8180 (1973)
8. Riley, P.E. and Seff, K., Inorg. Chem., 14, 714 (1975)
9. Yates, D.J.C. and Lucchesi, P.J., J. Phys. Chem., 35, 243 (1961).
10. Adams, D.M., Metal - Ligand and Related Vibrations, Edward Arnold Ltd., London (1967)
11. Rodinov, A.N., Timofeyuk, G.V., Talakeva, T.V., Shigorin, D.N. and Kocheshkov, K.A., Isz. Akad. Nauk. SSSR, Ser Khim., 42 (1965).
12. Pichat, P., Vedrine, J.C., Gallezot, P. and Imelik, B., J. Catal., 32, 190 (1974)
13. Howard, J., Robson, R. and Waddington, T.C., Zeolites, 1, 175 (1981)
14. Howard, J. and Waddington, T.C., Surface Science, 68, 86 (1977)
15. Tam, N.T., Cooney, R.P. and Curthoys, G., J. Chem. Soc. Faraday Trans. I, 72, 2577 (1976)
16. Tsitsishivili, G.V., Bagratishivili, G.D. and Oniashvili, N.I., Zh Fiz Khim., 43, 950 (1969)
17. Klier, K. and Ralek, M. J. Phys. Chem. Solids, 29, 951 (1968)

18. Klier, K., Kellerman, R. and Hutta, P.J., J. Phys. Chem., 61, 4224 (1964)

19. Pichat, P., J. Phys. Chem., 79, 2127 (1975)

20. Basile, L.J., La Bonville, P. Ferraro, J.R. and Williams, J.M., J. Chem. Phys., 60, 1981 (1974)

21. Ferriso, C.C and Hornig, D.F., J. Chem. Phys., 23, 1464 (1955)

22. Fournier, M and Roziere, J., C.R. Acad. Sci. C., 270, 729 1955

23. Fournier, M., Mascherpa, G., Rousselet, D. and Potier, J., C.R. Acad. Sci. C, 269, 279 (1969)

24. Ault, B.S. and Pimentel, G.C., J. Phys. Chem., 77, 57 (1973)

25. Herzberg, G. Molecular spectra and Molecular Structure II Infrared and Raman Spectra of Polyatomic Molecules, Van Nostrand, London (1945)

26. Gillard, R.D. and Wilkinson, G., J. Chem. Soc., 1640 (1964)

27. Nast, V.R. and Schindel, H., Z. Anorg. Allg. Chem., 326, 201 (1963)

28. Unger, K., and Gallei, E., Erdel Kohle Erdgas Petrochem., 29, 409 (1976).

29. Eisenbach, D. and Gallei, E., J. Catal., 56, 377 (1979)

30. Tam, N.T., Cooney, R.P. and Curthoys, G., J. Chem. Soc. Faraday Trans. I, 72, 2592 (1976)

31. Iwashita, Y., Tamura, F. Nakamura, A., Inorg. Chem., 8, 1179 (1969)

32. Angell, C.L. and Schaffer, P.C., J. Phys. Chem., 69, 3463 (1965)

33. Nakamoto, K., Infrared and Raman Spectra of Inorganic and Coordination Compounds, 3rd Edition, Wiley-Interscience (1978)

34. Carter, J.L., Yates, D.J.C., Lucchesi, P.J., Elliot, J.J. and Kevorkian, V.J., J. Phys. chem., 70, 1126 (1966).

CHAPTER VI

ADSORPTION OF SMALL MOLECULES ONTO Cu^{II} AND $Cu^{I}Y$ ZEOLITES

I. Introduction

Numerous studies have been carried out on Cu^{II} exchanged zeolite type Y ($Cu^{II}Y$) over the past few years and it has already been shown that $Cu^{II}Y$ exhibits catalytic activity in oxidation[1-5], cracking[6] and isomerization reactions[7]. This interest in reactions catalysed by $Cu^{II}Y$ zeolite has provided the motivation for our work. Since few infrared studies on $Cu^{I}Y$ zeolite, in the absence and presence of adsorbates, have been reported, we considered it natural to extend our work to this zeolite.

We have prepared samples of $Cu^{II}Y$ with different degrees of exchange to observe the following: (a) the difference in infrared spectra (KBr disc) of $Cu^{II}Y$ zeolite with increasing Cu^{II} loadings, (as will be discussed in Section V(i)), and (b) the effect of increasing Cu^{II} content on the adsorption behaviour of ethylene.

$Cu^{I}Y$ zeolite was prepared as described by Huang[8]. This process involves the reduction of $Cu^{II}Y$ zeolite in a carbon monoxide (CO) atmosphere with pre-adsorbed ammonia. The preparation of $Cu^{I}Y$ zeolite will be discussed in detail in the experimental section and the infrared spectra discussed in section V(iii).

We have adsorbed hydrocarbons onto Cu^{II} and $Cu^{I}Y$ zeolites and compared their adsorption behaviour. As a consequence of the study of the reduction process ($Cu^{II}Y \longrightarrow Cu^{I}Y$), ammonia and CO were also adsorbed onto $Cu^{II}Y$ zeolite individually.

Previous studies of adsorbed C_2H_4 and C_2H_2 will not be discussed here since full discussions have been given in chapters IV and V.

II. Structure of $Cu^{II}Y$ zeolite

(a) Hydrated $Cu^{II}NaY$ zeolite

An x-ray diffraction study of hydrated $Cu^{II}NaY$ zeolite has been carried out by Marti et al[9]. Three samples of the following compositions were used; (sample 1) $Cu_7^{II}Na_{29}H_{13}Y$, (sample 2) $Cu_{12}^{II}Na_{21}H_{11}Y$ and (sample 3) $Cu_{15}^{II}Na_{16}H_{10}Y$. Table 6.1 summarizes the locations of the cations and water molecules in the three samples. From this table, it can be seen that all the Na^+ and Cu^{2+} cations were located in sample 1 but some cations, mainly copper, were not located in the supercage for samples 2 and 3. It was suggested that this was due to their higher tendency towards hydration and greater mobility.

While there is no published single crystal x-ray analysis on hydrated $Cu^{II}NaY$, there is an x-ray study of the Cu^{II} exchanged faujasite[10]. In this study, the sample used was close to 100% exchanged. Copper cations were found to be rather mobile and mainly bound to water molecules. Only 6.3 Cu^{2+} cations per unit cell could be located (at site I') and they were found to be weakly bonded to the zeolite framework.

Other work on hydrated $Cu^{II}NaY$ zeolite has been carried out by Soria et al[11,12] using electron spin resonance (ESR). A number of samples ranging from a minimum of 0.01 Cu^{2+} per unit cell (0.2% exchanged) to a maximum of 19.5Cu^{2+} per unit cell (70% exchanged) were used. Two different types of copper cations were observed in their samples; one, a distorted octahedral complex of $(Cu(H_2O)_6)^{2+}$, was moving freely in the large cavity while the other, Cu^{2+} cations, were localized on the walls of the cavity.

Table 6.1 Summary of the locations of Na^+, Cu^{2+}, and H_2O molecules in hydrated CuNaY zeolite[9]

Samples / Sites	1 $Cu_7^{II}Na_{29}H_{13}Y$	2 $Cu_{12}^{II}Na_{21}H_{11}Y$	3 $Cu_{15}^{II}Na_{16}H_{10}Y$
I	4.5 Na^+	3.6 Na^+	0.8 Na^+
I'	14.9 Na^+	13.5 Na^+	15.5 Na^+
II	1.9 Cu^{2+}	1.5 Cu^{2+}	3.0 Cu^{2+}
II'	15.5 H_2O	15.6 H_2O	14.9 H_2O
III	9.7 Na^+ 5.4 Cu^{2+}	2.4 Na^+ 8.7 Cu^{2+}	- 6.5 Cu^{2+}

(b) Dehydrated $Cu^{II}NaY$ zeolite

Gallezot et al[13,14] have carried out x-ray diffraction studies of dehydrated $Cu^{II}NaY$ zeolite. Two samples, $Cu^{II}_{16}Na_{24}Y$ and $Cu^{II}_{12}Na_5H_{27}Y$ were studied by them. Sample $Cu^{II}_{16}Na_{24}Y$ was first heated in oxygen at 773K and then evacuated at the same temperature under vacuum (10^{-5} torr) for 12 hours while the sample $Cu^{II}_{12}Na_5H_{27}Y$ was also heated in oxygen and treated under vacuum for 12 hours at 573K. Maxwell and De Boer[10,15], on the other hand, have reported the results of a single crystal x-ray analysis of the dehydrated Cu^{II} exchanged faujasite, $Cu^{II}_{28}(AlO_2)_{56}(SiO_2)_{136}$. The sample was heated to 423K for 20 hours. The cation distributions in all the three samples studied are summarize in table 6.2.

In sample $Cu^{II}_{16}Na_{24}Y$, the Cu^{2+} ions at site I were coordinated to six framework oxygen atoms with a Cu^{II}-O distance of 2.535Å. The site I' Cu^{2+} ions were coordinated to three framework oxygens (Cu^{II}-O = 1.991Å) and one non-framework oxygen (Cu^{II}-O = 2.55Å). Cation distribution and cation coordination are quite similar in the two dehydrated samples $Cu^{II}_{16}Na_{24}Y$ and $Cu^{II}_{12}Na_5H_{27}Y$, with the cupric ions exhibiting a greater affinity for site I'; in this position they can be bonded to three framework oxygens.

In sample $Cu^{II}_{28}(AlO_2)_{56}(SiO_2)_{136}$, however, most of the cations at site I' were strongly bound to the framework oxygen and a smaller number of cations were less firmly bound, presumably interacting with residual water (Figure 6.1). The cation-framework coordination geometries at sites of type II and II' are similar to those of sites I and I'. Copper ions at site II' and IIA are strongly bound to the zeolite framework and a smaller number of cations at site IIB are less firmly bound.

Table 6.2 Summary of the locations of Na^+ and Cu^{2+} in dehydrated zeolite samples[10,13-15]

Sites \ Samples	1 $Cu^{II}_{16}Na_{24}Y$	2 $Cu^{II}_{12}Na_5H_{27}Y$	3 $Cu^{II}_{28}(AlO_2)_{56}\cdot(SiO_2)_{136}$
I	3.2 Cu^{2+}	1.7 Cu^{2+}	1.5 Cu^{2+}
I'	11.1 Cu^{2+}	9.9 Cu^{2+}	14.2 Cu^{2+}
II	20.5 Na^+	8.0 Na^+	5.3 Cu^{2+}
II'	-	-	0.8 Cu^{2+}
III	-	-	3.3 Cu^{2+}

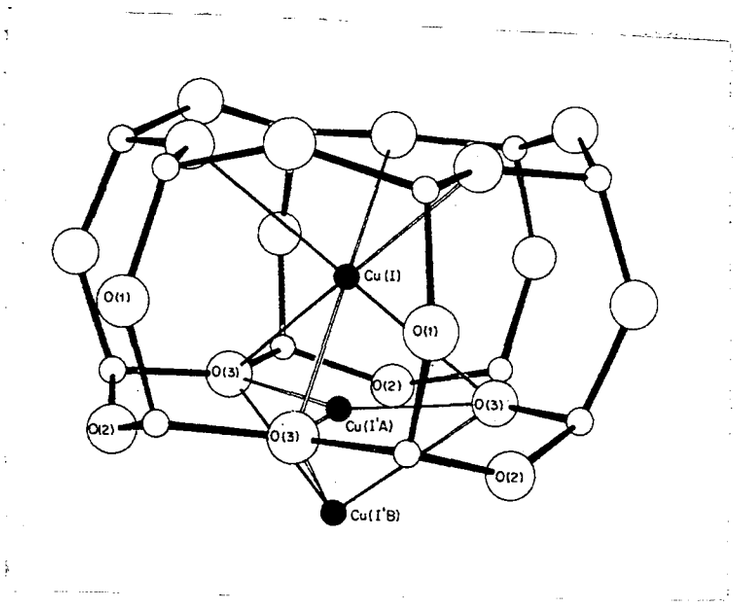

Figure 6.1. Perspective view showing the coordination of $Cu^{II}(I)$, $Cu^{II}(I'A)$ and $Cu^{II}(I'B)$ cations to the hexagonal prism in dehydrated copper(II) exchanged faujasite[10].

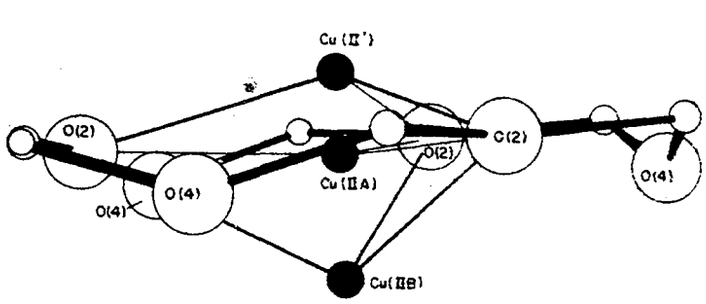

Figure 6.2. Perspective view showing the coordination of $Cu^{II}(II')$, $Cu^{II}(IIA)$ and $Cu^{II}(IIB)$ cations to the single 6-membered ring in dehydrated copper(II) exchanged faujasite[10].

Electron paramagnetic resonance (EPR) studies on copper exchanged type Y zeolite have been carried out by several workers[16-18]. Morke et al[18] used two samples, $Cu^{II}_{4.5}Na_{44.5}Y$ and $Cu^{II}_{18.5}Na_{16.5}Y$, in their studies both of which were dehydrated at 873K. The copper cations were distributed among three different locations, sites I', II and a cluster in the supercage. In sample $Cu^{II}_{4.5}Na_{44.5}Y$, 1.6, 0.9 and 2.0 copper cations per unit cell were found in sites I', II and the cluster, respectively. For sample $Cu^{II}_{18.5}Na_{16.5}Y$, 8.2, 4.8 and 5.5 copper cations per unit cell were located at the three different locations, sites I', II and cluster, respectively.

Schoonheydt and Velghe[19] have calculated the distribution of Cu^{II} ions from studies of electrical conductivity and they found that for samples, $Cu^{II}_{3.4}Y$ and $Cu^{II}_{11.6}Y$, all the copper cations were located in the small cages. However, for sample $Cu^{II}_{20}Y$, they found that approximately 11-14 copper cations were located in the small cages and approximately 7-10 copper cations per unit cell were found to be in the supercages.

Soria et al[11,12] studied the dehydration of copper exchanged Y zeolites with several copper contents using the ESR technique. The samples were evacuated and heated at various temperatures up to 873K and their ESR spectra recorded at different temperatures during dehydration. In general, they found that the copper cations had distorted octahedral (site II), square-pyramidal (site II') and possibly distorted trigonal (site I') environments.

In the samples evacuated at low temperatures only one Cu^{II} species, in a moderately distorted octahedral environment, was located. These cations at site II were coordinated to three water molecules and three framework oxygens. On further heating the samples, the cations at site II lose water gradually, and some of them enter the sodalite cage. It was suggested that

these cations could occupy sites II' or I' with square-pyramidal coordination. In the final dehydrated state the copper remained mainly near sites I and II, and some water was still retained rigidly inside the sodalite units. On increasing the copper concentration, coupling of the copper ions was observed between one cation in the supercage and another in site I', with H_2O, OH^- or O^{2-} as the bridging ligand. The authors[12] suggested that if the coupling was between two copper ions at sites I' in the same sodalite unit, linked by an O^{2-} bridge, then the environment of the cations must be of distorted trigonal symmetry.

III. Previous studies of ammonia and carbon monoxide adsorbed onto zeolites

(a) Ammonia

Single crystal x-ray analyses of ammonia adsorbed onto NaA and AgA have been carried out by Seff et al[20-22]. The structures of NaA and AgA have been discussed in chapters II and IV, respectively. The NaA sample was dehydrated at 623K and 10^{-5} torr for 24 hours and allowed to sorb 32 molecules per unit cell of dry ammonia at 604 torr.

In figures 6.3 and 6.4 are shown stereoviews of the structure of NaA + NH_3 and the NH_3 is located in both the sodalite unit and the large cavity. Of the thirty-two ammonia molecules per unit cell, twelve were found in the sodalite unit and twenty in the large cavity. Eight of the twelve ammonia molecules in the sodalite unit were located at N(1) (Figure 6.3) and hence coordinate with the cations at S2' (N(1) - Na(S2') = 2.5Å). Four more ammonia molecules (at N(2)) hydrogen bond to these eight ammonia molecules and to framework oxygens (N(1) - N(2) = 1.8Å; N(2) - O(3) = 3.1Å).

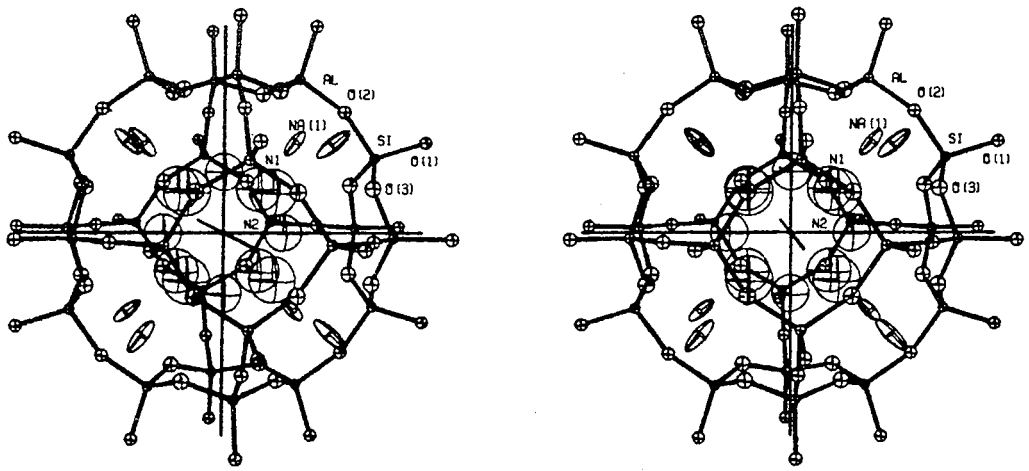

Figure 6.3. A stereodrawing of the sodalite unit in zeolite A containing twelve ammonia molecules[20]. Na(1) refers to site S2' in the text.

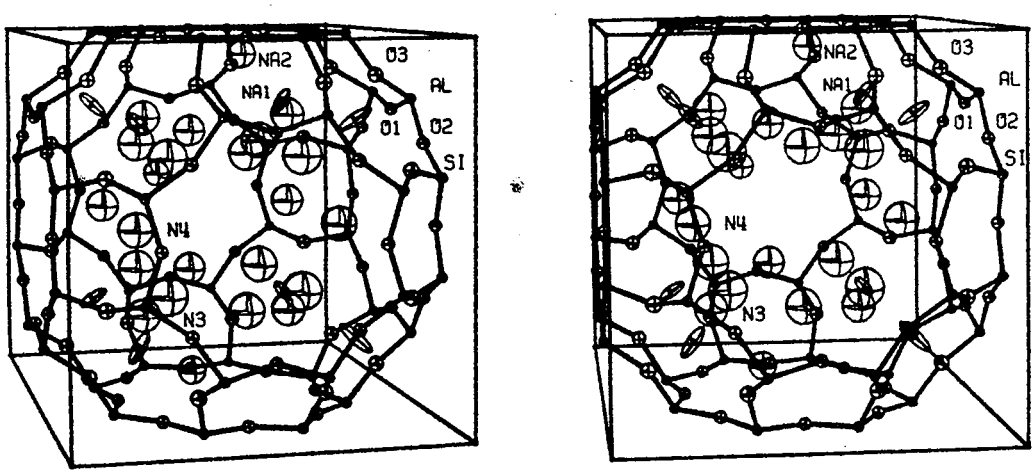

Figure 6.4. A stereodrawing of the large cavity in zeolite A containing twenty ammonia molecules[20]. Na(1) and Na(2) refer to sites S2* and S1 in the text respectively.

Of the twenty ammonia molecules in the large cavity, eight ammonia molecules (at N(3)) were found to coordinate with the eight sodium ions at S2* (N(3) - Na(S2*) = 2.2Å; N(3) - N(4) = 2.5Å; N(3) - O(3) = 3.6Å). The remaining twelve ammonia molecules hydrogen-bond to these eight ammonia and to other framework oxygens and may loosely coordinate to the cations at sites SI (N(A) - Na(SI) = 2.9Å) (Figure 6.4).

Seff et al[21] carried out another structure determination with fewer adsorbed ammonia molecules per unit cell by exposing the dehydrated NaA zeolite to only 12 torr of ammonia, as opposed to the 604 torr used in the earlier experiment. It was found that even at a loading of as few as eight ammonia molecules per unit cell, the sorbed molecules were not predominantly found at a single type of sorption site. The authors suggested that this is perhaps because all three kinds of Na^+ compete favourably at room temperature for ammonia association, all at sites where further hydrogen bonding could occur to framework oxygens.

A single crystal x-ray study of ammonia adsorbed onto vacuum-dehydrated partially decomposed fully Ag^+-exchanged zeolite A[22] demonstrated the formation of the inorganic complexes triazane and cyclotriazane with the Ag^+ cations in the cavities (Figures 6.5 and 6.6). The AgA crystal was first dehydrated for 60 hours at 673K before being treated with a continuous flow of dry ammonia at 765 torr and 296K for 36 hours.

Three triazane (N_3H_5) molecules per sodalite cage and four cyclotriazane (N_3H_3) molecules per supercage were found to complex with Ag^+ cations. The three triazane molecules complexed with two Ag^+ cations in the sodalite unit (S2') as shown in figure 6.5 and were stabilized further in the sodalite

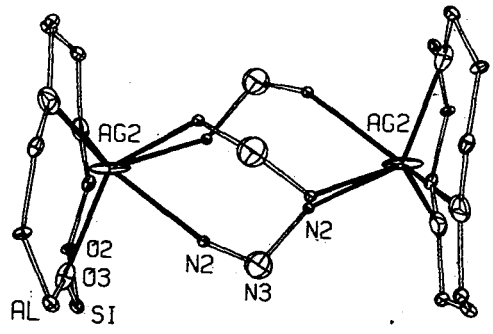

$Ag_2(N_3H_5)_3^{2+}$ COMPLEX

Figure 6.5. The $Ag_2(N_3H_5)_3^{2+}$ cation in the sodalite unit[22]. Selected bond lengths are: Ag(2)-O(3) = 2.39(3), Ag(2)-N(2) = 2.45(2), and N(2)-N(3) = 1.6(1)Å. Some bond angles are: O(3)-Ag(2)-O(3) = 107(1), N(2)-Ag(2)-N(2) = 65(1), Ag(2)-N(2)-N(3) = 1.34(5), and N(2)-N(3)-N(2) = 107(8)°. Ag(2) refers to site S2' in the text.

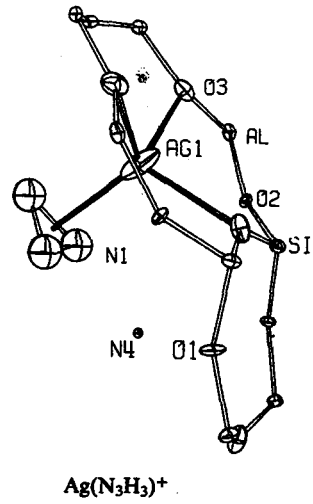

$Ag(N_3H_3)^+$

Figure 6.6. One of the four $Ag(N_3H_3)^+$ complexes in the large cavity[22]. Selected bond lengths are: Ag(1)-O(3) = 2.46(2), Ag(1)-N(1) = 2.59(5), N(1)-N(1) = 1.49(8), N(1)-N(4) = 2.53(12), and N(4)-O(1) = 2.86(5)Å. Ag(1) refers to site S2* in the text.

unit by the hydrogen bonding of all five hydrogen atoms to framework oxygens.

One of the four equivalent cyclotriazane molecules that complex with the Ag^+ cations in the large cavity (S2*) is shown in figure 6.6. Further stabilization of the cyclotriazane molecule was achieved by hydrogen bonding to an ammonia molecule at N(4), which in turn hydrogen bonds to the zeolite framework.

The formation of these two novel species was further confirmed by mass spectroscopic analysis of the vapour phase above the zeolite from 298 to 363K.

The EPR spectra of cupric-ammonia complexes in zeolites X and Y have been obtained by Vansant et al[23,24] while the adsorption-desorption isotherms of ammonia in copper (II) Y zeolite has been measured by Huang and Vansant[25].

In the EPR measurements, two samples, $Cu^{II}_{3.5}Na_{48}(AlO_2)_{55}(SiO_2)_{39}$ and $Cu^{II}_4 Na_{77}(AlO_2)_{85}(SiO_2)_{107}$ were used. Each of these was dehydrated to 673K at 10^{-5} torr before admitting ammonia. The authors[23,24] concluded from their EPR spectra, that all the Cu^{2+} ions were available for complexation. This indicates that a migration of all Cu^{2+} ions into the large cavities has occurred. In contrast with zeolite Y, it was found that upon adsorption of ammonia onto zeolite X, some of the original Cu^{2+} ions remained in the small cavities (probably at sites I) and were inaccessible to ammonia.

Comparing the spectra of the dehydrated and the ammoniated X and Y zeolites, the authors[23,24] concluded that the symmetry of the Cu^{II}-ammonia complex was square-planar. Both the ammoniated samples were evacuated at various temperatures. Upon partial desorption at 373K, it was found that the symmetry of the complex changed to a distorted tetrahedron. This complex was formed by Cu^{2+} ion coordinated to three lattice

oxygens and one ammonia molecule. Increasing the desorption temperature to 523-573K caused most of the Cu^{2+} ions to be reduced to Cu^{+} ions.

Huang and Vansant[25] used 13, 48 and 75% exchanged copper (II) Y zeolites in their gravimetric measurements. The samples were heated to 673K before being exposed to 70 torr ammonia at room temperature. Their findings agree with the conclusion reached from EPR measurements that the ammonia complexes were mainly $(Cu(NH_3)_4)^{2+}$ and that migration of the Cu^{2+} ions from the sodalite cages to the supercages did take place on adsorption of ammonia.

(b) Carbon monoxide

Infrared studies of CO adsorbed on X and Y type zeolites have been reported by Angell and Schaffer[26] and Huang[27]. Angell and Schaffer measured the infrared spectra of CO adsorbed onto various univalent (Na^{+} and Li^{+}) and bivalent (Mg^{2+}, Ca^{2+}, Sr^{2+}, Ba^{2+}, Mn^{2+}, Fe^{2+}, Co^{2+}, Ni^{2+}, Zn^{2+}, and Cd^{2+}) cation exchanged zeolites X and Y, while Huang made his measurements using AgX and AgY zeolites. Their data is summarised in table 6.3.

All of the samples used by Angell and Schaffer were "flash activated" that is they were evacuated briefly at $\sim 10^{-3}$ torr, heated to 773K in less than 10 minutes, left at this temperature for 3 hours at a pressure of $\sim 5 \times 10^{-6}$ torr, and then allowed to cool to room temperature under vacuum. Each of the samples was then exposed to 200 torr CO at room temperature. Huang, on the other hand, heated his samples to a temperature of 623K for AgX and 673K for AgY zeolites, before admitting 50 torr CO at room temperature.

Angell and Schaffer showed that the high wavenumber band at $\sim 2200 cm^{-1}$ was found only in zeolites containing

Table 6.3 Infrared adsorption frequencies of carbon monoxide adsorbed on zeolites[26,27]

Cation	Frequencies on Y zeolites / cm^{-1}			Frequencies on X zeolites / cm^{-1}		
Na^+		2172	2122		2164	2121
Li^+		2172				
Mg^{2+}	2213	2170		2205	2173	
Ca^{2+}	2197	2172		2192		2104
Sr^{2+}	2186		2098			
Ba^{2+}	2178		2105	2172		2112
Mn^{2+}	2208	2173	2119	2203		
Fe^{2+}	2198	2172				
Co^{2+}	2208	2172	2119	2204	2170	
Ni^{2+}	2217	2172	2120	2211		
Zn^{2+}	2214	2170	2118			
Cd^{2+}	2209	2170	2120			
Ag^+		2195			2195	

divalent cations and that the actual frequency depended on the nature of the cation and could be correlated with the strength of the electric field near it. Bands at ~2170 and ~2120cm^{-1} found in all zeolites were due to CO adsorbed at two different adsorption sites. All of these bands disappeared on pumping at room temperature indicating that they resulted from relatively weakly adsorbed CO. In contrast, Huang[27] found that CO adsorbed very strongly on AgX and AgY zeolites.

Huang[8,28] also studied the adsorption of CO on $Cu^{I}Y$ zeolite spectroscopically and gravimetrically. Table 6.4 summarises the C=O stretching frequencies in $Cu^{I}Y$ zeolite and various coordination compounds[29-32]. From the adsorption measurements[8], it was shown that CO was adsorbed on specific sites on $Cu^{I}Y$ zeolite, the uptake being approximately one CO per Cu^{+} ion below 373K and at 100 torr. The infrared study[28] confirmed the adsorption measurements concerning the formation of Cu^{+} - CO complexes in zeolites. From table 6.3, it can be seen that the carbonyl complexes in $Cu^{I}Y$ zeolite resemble those observed in solution and in coordination compounds. The author[28] suggested that the σ complex due to the carbon lone-pair electrons could be responsible for the high ν(C=O) stretching frequency in the $Cu^{I}Y$ zeolite.

Calorimetric measurements of CO on $Cu^{II}Y$ (14.3, 50.3 and 80.7% exchanged) zeolites have been carried out by Miwa et al[33-36]. They observed that the cupric ions were found to migrate from the inaccessible sites for CO to accessible ones. The migration probably takes place from sites II' to II, and is dependent on the quantities of Cu^{2+} ions in the zeolites and of CO adsorbed as well as the pretreatment conditions.

As the degree of copper exchange increases, the rate of desorption of CO was observed to decrease while the rate of adsorption increased.

Table 6.4 Infrared frequencies of ν(C=O) in copper(I) carbonyls

Compound or medium	ν(C=O) cm^{-1}	Ref.
Copper(I) trifluoroacetate carbonyl-trifluoroacetic acid	2155	29
Cu(CO)Cl in water	2112	30
Cu(CO)Cl in pyridine	2069	30
Cu(CO)Cl in methanol	2090	31
(Cu(en)(CO))Cl	2080	31
$((en)Cu(CO)_2Cu(en))Cl_2$	1905	31
$(Cu(CO)Cl(Me_2N{=}CH_2))Br$	2080	32
Cu(I)Y (75%) zeolite	2160	28

With the assumption that the number of CO molecules adsorbed on specific sites could be considered as a measure of accessible cupric ions, it was determined that, irrespective of the degree of exchange, approximately 17-19% of the exchanged cupric ions occupy the accessible sites. From the heats of adsorption curves, the authors suggested that the cupric ions prefer sites I' and/or sites II'.

IV. Experimental

$Cu^{II}Y$ zeolites were prepared by ion exchanging 5g of NaY zeolite (Union Carbide Corporation) with portions of the copper (II) chloride solutions (Fisons Scientific) at different concentrations for the stated number of days (1,2,3 or 21) For some of the samples, the temperature used was varied (293 or 333K). Table 6.5 summarises the experimental conditions used for the preparation of our samples. After the exchange, the samples were thoroughly washed with distilled water and dried in an oven (333K) before being analysed by atomic absorption spectroscopy. The number of Cu^{2+} and Na^{+} ion per unit cell were calculated and the results are also shown in table 6.5.

X-ray powder photographs of six of the samples were obtained to ensure that no breakdown of structure had taken place. A thermogram of one of the samples was also obtained to observe the removal of water from the zeolite cavities.

For the reduction and adsorption experiments, sample 5 (73.2% exchanged) was used except in the study of C_2H_4 adsorbed onto $Cu^{II}Y$ zeolite, wherein two samples, 3 and 10 (70.4 and 92.9% exchanged) were used. The flow chart in figure 6.7 summarises the adsorption experiments carried out on Cu^{II} and $Cu^{I}Y$ samples.

The copper (II) Y sample was pressed into a self supporting

Table 6.5 Conditions of the ion exchange and the number of Cu^{2+} and Na^{+} ions per unit cell.

Samples	Concentration of $CuCl_2.2H_2O$	Volume of $CuCl_2.2H_2O$ used	Time taken for the exchange	Temperature K	No. of Na^{+} per unit cell	No. of Cu^{2+} per unit cell	Percentage exchanged
1	0.1N	162.2ml	1 day	293	20.9±0.2	17.5±0.2	62.5%
2	0.1N	Excess	1 day	293	16.2±0.2	19.9±0.1	70.4%
3	0.1N	Excess	2 days	333	16.7±0.2	19.7±0.1	70.4%
4	0.4N	40.55ml	2 days	293	21.8±0.3	17.1±0.2	61.1%
5	0.4N	Excess	1 day	293	15.1±0.2	20.5±0.3	73.2%
6	0.4N	Excess	2 days	333	15.2±0.2	20.4±0.2	73.2%
7	2.0N	Excess	3 days	293	9.4±0.4	23.3±0.3	83.2%
8	2.0N	Excess	3 days	333	8.4±0.3	23.8±0.2	85.0%
9	4.0N	Excess	21 days	293	4.6±0.4	25.7±0.3	91.8%
10	6.6N	Excess	3 days	293	4.0±0.2	26.0±0.2	92.9%
11	6.6N	Excess	3 days	333	4.6±0.2	25.7±0.2	91.8%
12	6.6N	Excess	21 days	293	2.0±0.2	27.0±0.1	96.4%

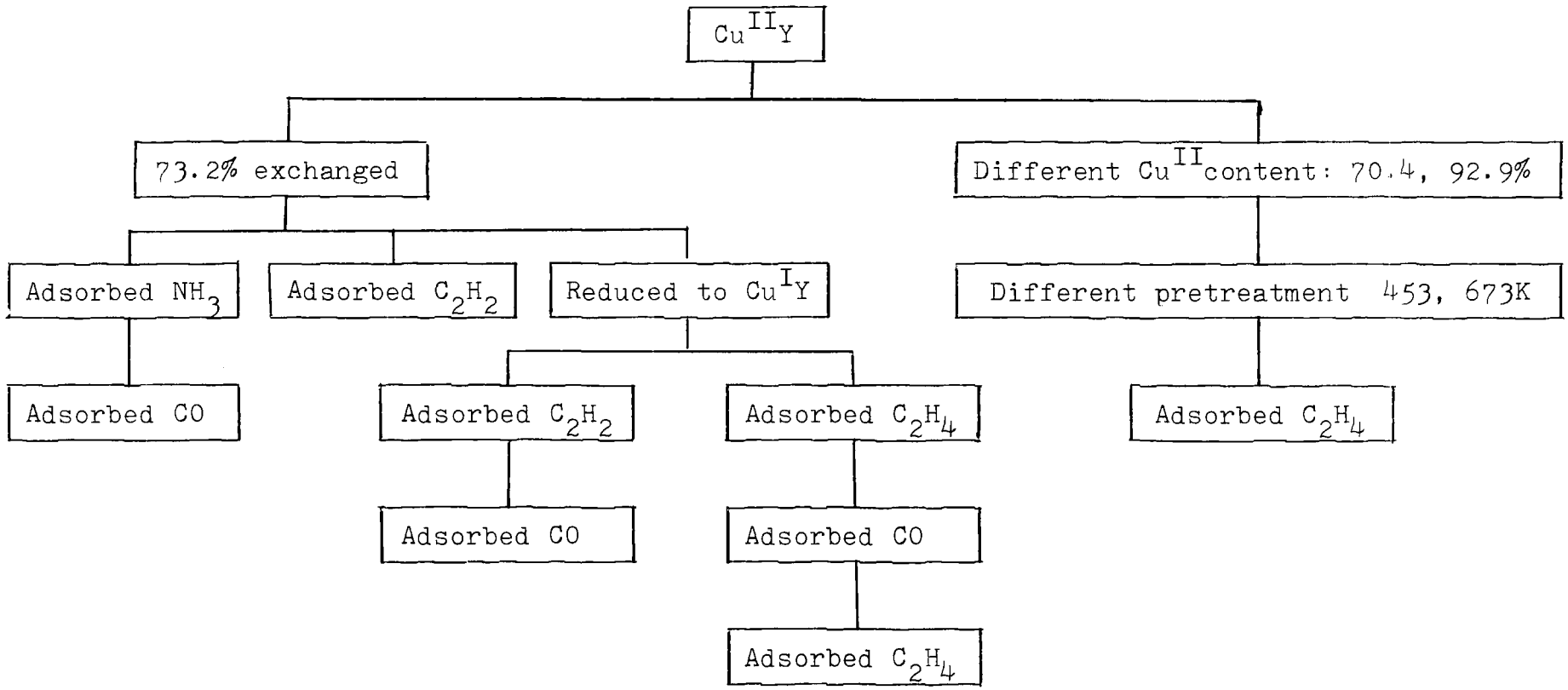

Figure 6.7 Summary of adsorption experiments on Cu^{II} and Cu^{I} Y zeolites

disc and placed in the infrared cell. Dehydration was carried out by evacuating the sample to a pressure of 1×10^{-6} torr (or better) and then heating the sample to a temperature of 673K. Spectra of the sample at room temperature and at various temperatures during dehydration were obtained. The sample was allowed to cool to room temperature and the spectrum recorded before admitting 50 torr of ammonia (BOC special gases; 99.98% purity). After obtaining the spectrum of the sample with 50 torr ammonia, the gas phase was then removed from the cell by evacuating for 5 minutes, and a further 25 minutes at room temperature. Each spectrum of the sample during both processes was recorded.

The sample was then evacuated and heated to elevated temperatures; spectra of the sample at different temperatures were again obtained. The sample was again allowed to cool to room temperature and the spectrum recorded. This same sample was used to adsorb CO. CO (99.5% purity) obtained from Air Products Limited was passed slowly through a cold trap (77K) before being used. The procedure described for the adsorption of ammonia was repeated for CO adsorption.

In order to observe the adsorption behaviour of $Cu^{II}Y$ zeolite, ethylene (British Industrial Gases Limited) was adsorbed onto two different samples (70.4 and 92.9% exchanged), each prepared at two maximum bake-out temperatures (453 and 673K). Acetylene, obtained from British Industrial Gases Limited and purified before use (by passing through concentrated sulphuric acid to remove the acetone), was also adsorbed onto pretreated dehydrated $Cu^{II}Y$. The adsorption procedure for both the ethylene and acetylene gases was similar to that used for ammonia.

$Cu^{I}Y$ zeolite was prepared[8] in situ in the infrared cell before the adsorption measurements by the reduction of $Cu^{II}Y$

zeolite using CO with preadsorbed ammonia. Approxiamately 14 torr of ammonia was first adsorbed onto a dehydrated $Cu^{II}Y$ zeolite. CO at a pressure of 155 torr was then introduced to the sample. The whole system ($Cu^{II}Y + NH_3 + CO$) was heated to 583K. The reduced sample was then evacuated overnight at 603K before being cooled to room temperature. Spectra of the sample during each of the above processes were recorded.

50 torr of acetylene was admitted into the cell containing the freshly prepared $Cu^{I}Y$ zeolite and the spectrum measured. Gaseous acetylene was removed from the cell by evacuation for 5 minutes at room temperature and the spectrum of the sample re-measured. Following evacuation for a further 25 and 55 minutes, the spectra of the sample were recorded each time.

After the removal of gaseous acetylene by evacuating for 60 minutes at room temperature, CO at a pressure of 40 torr was then admitted into the cell and the spectrum of the sample recorded. The sample was evacuated for 5 and a further 25 minutes at room temperature, to remove the gaseous CO, before the sample was evacuated and heated to elevated temperatures. Spectra of the sample after each evacuation processes and at various temperatures during heating were obtained.

Another freshly prepared $Cu^{I}Y$ zeolite was used for the adsorption of ethylene and the procedure described for the adsorption of acetylene was repeated. In summary, the ethylene gas was first adsorbed and then removed before the adsorption of CO. After removing the CO gas by evacuating the cell at room temperature, ethylene was re-admitted into the cell. Following this, the sample was evacuated and heated to elevated temperature.

V. Results and discussion

(i) Ion exchange

It was not the major purpose of our work to study the detailed ion exchange behaviour of Cu^{2+}. The project was first undertaken to prepare different degrees of exchange of Cu^{2+} in zeolite Y to be used later for adsorption experiments.

From the data for Cu^{2+} ions exchanged with NaY, obtained by varying the experimental conditions (concentration, volume, time and temperature) as shown in table 6.5, it can be concluded that the ion exchange of Cu^{2+} ions in Y zeolite behaves as one normally expects (Chapter II).

X-ray powder photographs of six of the samples were taken and compared with literature data to ensure that there was no breakdown in structure. Thermogravimetric analysis of one of the samples was carried out using a 5^{o}/min rate of heating. From the thermogram obtained, a graph of W (where W=100 x Weight lost at temperature T/Total weight lost at 1273K) against temperature was drawn (Figure 6.8). The graph in figure 6.8 shows that there is a substantial weight loss on heating the sample from 273 to 573K. This is most possibly due to the removal of water from the zeolite cavities. On heating the sample further to 1273K, the weight lost is very slight and could indicate structural decomposition.

Infrared spectra of the KBr discs of some of the hydrated samples were obtained. It should be noted that all the samples were prepared in the same way (refer to Section IV and Table 6.5). The region of interest in this case is the hydroxyl region only, and this will be discussed here. The spectra of samples 2,5,7 and 12 with 19.9 (70.4% exchanged),

Figure 6.8. Graph of W (Weight lost at temperature T x 100/ Total weight lost at 1273K) against temperature.

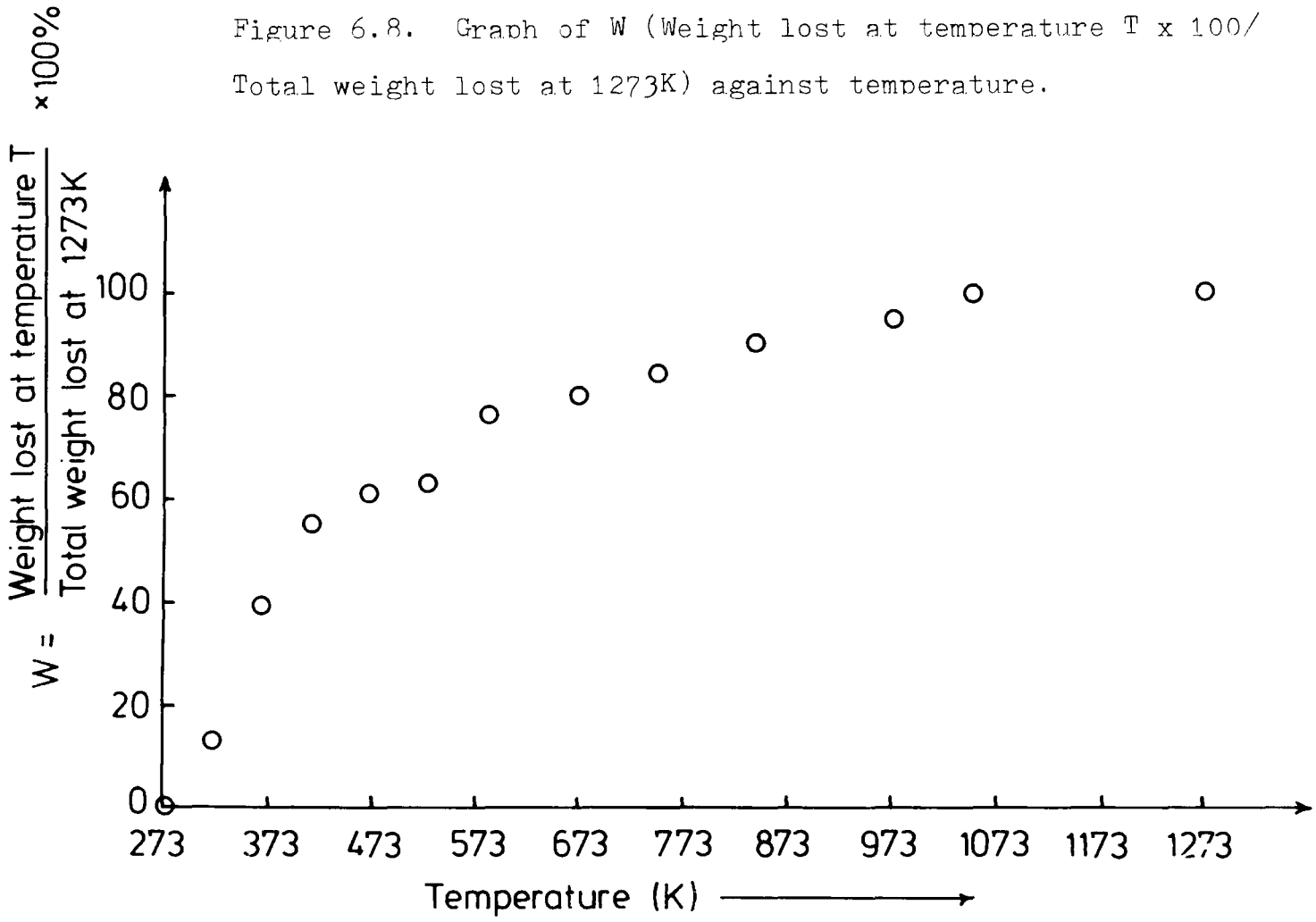

20.4 (73.2% exchanged), 23.3 (83.2% exchanged) and 27.0 (96.4% exchanged) Cu^{2+} per unit cell are shown in figure 6.9 (4000-2700cm^{-1}).

In the infrared spectrum of the sample with 19.9 Cu^{2+} per unit cell (Figure 6.9a), a broad band at approximately 3550cm^{-1} is observed, which could be due to the stretching mode of water. The deformation mode of water is observed at 1630cm^{-1}. As the amount of Cu^{2+} per unit cell increases, three sharp bands at 3450, 3360 and 3320cm^{-1} appear (Figures 6.9c and d). In these spectra, the band at 3550cm^{-1}, which was a broad intense band in the spectrum of sample 2, is observed as a shoulder. The decrease in intensity of the 3550cm^{-1} band is also accompanied by the decrease in intensity of the 1630 cm^{-1} band, which is the deformation mode of water. This could indicate that the number of water molecules in the zeolite cavities decreases with increasing Cu^{2+} content.
The decrease in the amount of water molecules in the zeolite cavities could only be due to the formation of copper hydroxides or/and bridging hydroxyl copper complexes. This is clearly indicated by the increase in intensities of the 3450, 3360 and 3320cm^{-1} bands in the spectra of $Cu^{II}Y$ zeolite with increasing Cu^{2+} content (Figure 6.9), which we will discuss presently.

The band at 3450cm^{-1} is assigned to the ν(O-H) of the bridging hydroxyl copper complexes, while the bands at 3360 and 3320cm^{-1} could be due to ν(O-H) of copper hydroxide. Table 6.6 summarizes the ν(O-H) of a series of bridging copper complexes studied by Ferraro and Walker[39]. If we examine table 6.6 carefully, we can see that all except two (when X = Phen; Yn = Br_2, $(ClO_4)_2$), of the ν(O-H) of the bridging copper complexes studied by Ferraro and Walker occur at a frequency below 3400cm^{-1}. Note that the complex

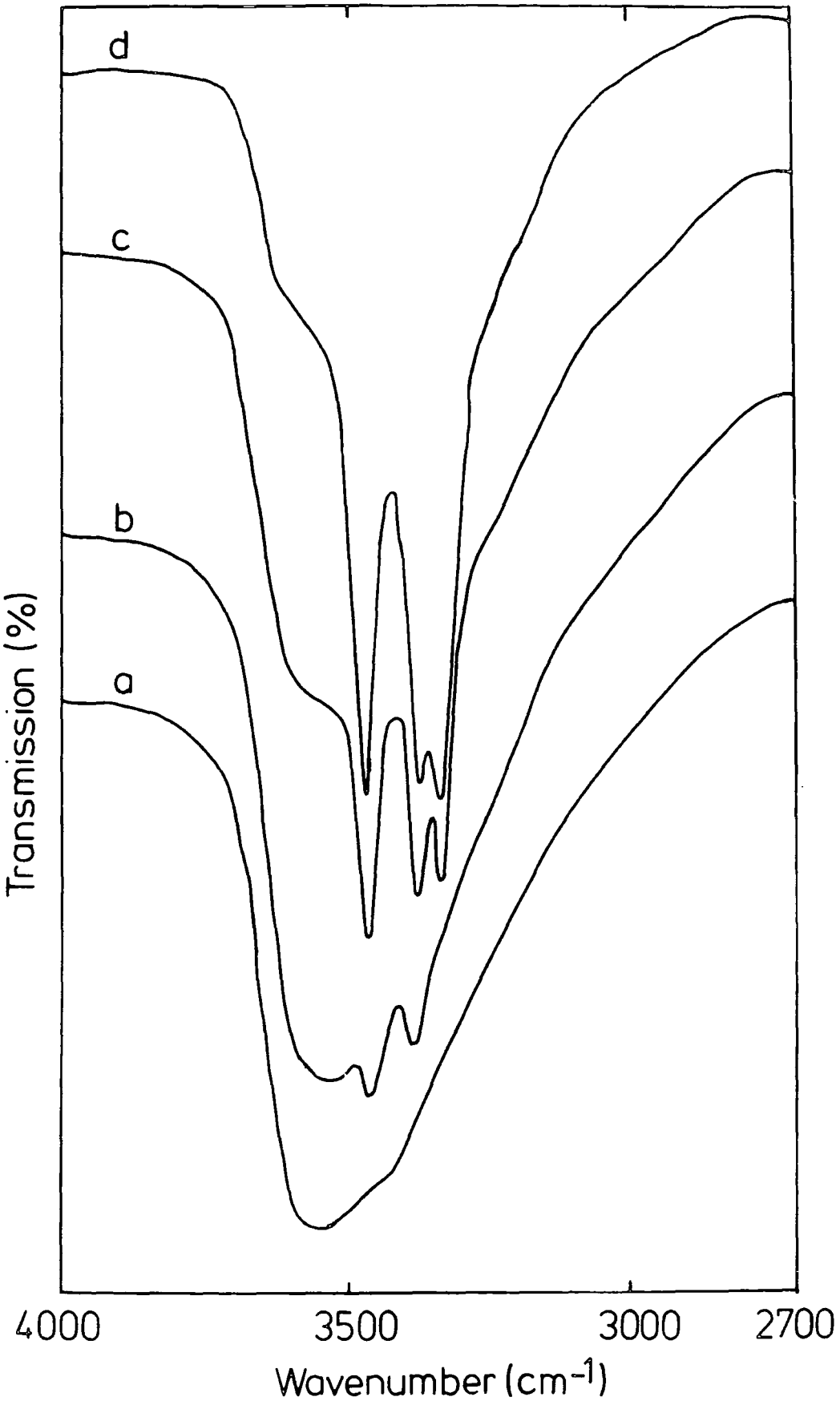

Figure 6.9. Spectra (KBr discs) of samples:
(a) 2 (70.4% exchanged), (b) 5 (73.2% exchanged),
(c) 7 (83.2% exchanged) and (d) 12 (96.4% exchanged).

Table 6.6 The infrared absorption frequencies of ν(O-H) in copper complexes, (XCu(OH)(OH)CuX)Yn.ZH_2O[39]

X	Yn	ν(O-H) cm^{-1}
Bipy	SO_4	3400
Bipy	I_2	3430
Bipy	Br_2	3440
Bipy	$(ClO_4)_2$	3440
Bipy	$PtCl_4$	3550
Bipy	Cl_2	3430
Bipy	$(SCN)_2$	3515
Bipy	$(PF_6)_2$	3601
Phen	SO_4	3400
Phen	I_2	3480
Phen	Br_2	3350
Phen	$(ClO_4)_2$	3400,3340
Phen	Cl_2	3400
Phen	$(SCN)_2$	3525

$((Phen)Cu(OH)ClO_4)_2$ is the only anhydrous complex studied, hence, the bridge OH stretching vibration is a doublet at 3400 and 3340cm^{-1} (Table 6.6). Our assignment of the ν(O-H) of bridging hydroxyl copper complexes is thus in accord with the assignment given by Ferraro and Walker[39]. Support for the assignment of ν(O-H) in copper hydroxide is given by Tarte[40], who found ν(O-H) for $CuSO_4.3Cu(OH)_2$ at 3390 and 3270cm^{-1}.

Further evidence for our assignments is provided by the observation of three bands at 925, 865 and 830cm^{-1} in the spectra of samples 7 and 12, which could be due to δ(O-H) of bridging hydroxyl copper complex or copper hydroxide. Ferraro and Walker[39] found that the δ(O-H) of the complex $((Bipy)Cu(OH))_2SO_4.5H_2O$ occurs at 955cm^{-1}. In addition, the δ(O-H) in basic copper compounds are reported by Tarte[40] to be in the region 1000-677cm^{-1}.

(ii) Dehydration of $Cu^{II}Y$ zeolite

Spectra of $Cu^{II}Y$ zeolite (73.2% exchanged) obtained at various temperatures during dehydration are shown in figure 6.10. In the spectrum of the sample at room temperature (Figure 6.10a), we observe two sharp bands at 3450 and 3360cm^{-1} which we may assign to the ν(O-H) of bridging hydroxyl and copper hydroxide. The evidence for these assignments has already been given in part (i). An intense band observed at 1650cm^{-1} is due to the deformation mode of water. Another band observed at 1465cm^{-1} is correlated with cation movements, as we shall show later.

As the sample was heated to 493K (Figure 6.10b), the 3450 and 3360cm^{-1} bands become slightly more intense compared with the spectrum of the sample at 293K and three new sharp bands appear in the hydroxyl region, at 3740, 3640 and3550cm^{-1}.

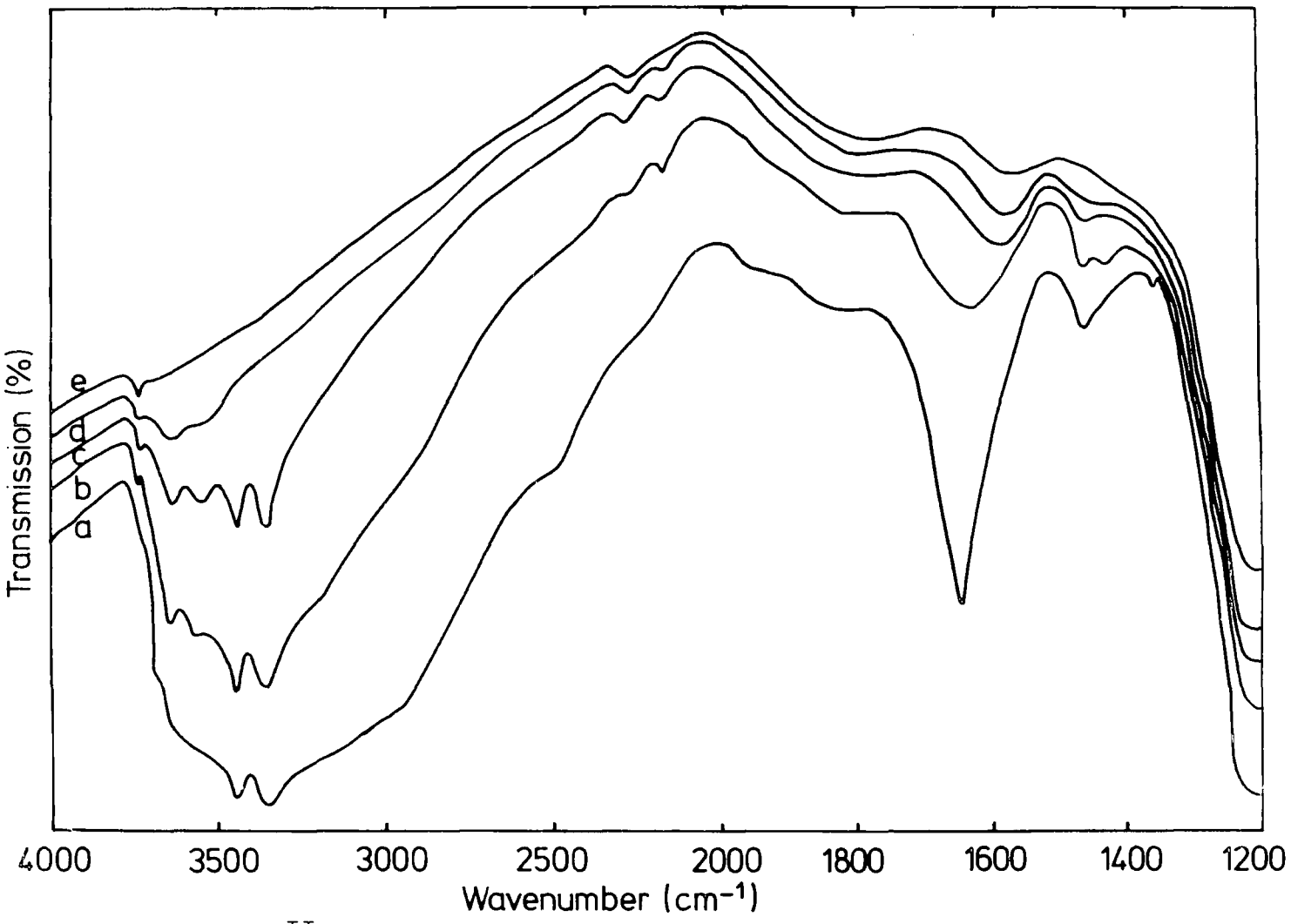

Figure 6.10. $Cu^{II}NaY$ zeolite at various temperatures during dehydration: (a) 293K, (b) 493K, (c) 553K, (d) 633K and (e) 673K.

These three new sharp bands are more prominent in the spectrum of the sample at 553K (Figure 6.10c). A detailed discussion of the infrared spectra of zeolites in the hydroxyl region is given in chapter II. The 3740cm^{-1} band may be due to Si-OH while the 3640 and 3550cm^{-1} bands are due to surface hydroxyl groups. The band which is due to the deformation mode of water reduces markedly in intensity on increasing the temperature showing that some of the water has been removed from the cavities. Two very weak bands appear at 2200 and 2100cm^{-1} which must be due to framework vibrations.

As the sample was heated further to 633K (Figure 6.10d) bands, which are due to ν(O-H) of bridging hydroxyl and copper hydroxide, disappear and most of the water has been removed from the cavities as shown by the low intensity of the 1650cm^{-1} band. A band observed at 1580cm^{-1} could be due to a framework vibration. It was not observed in the spectra of the sample at room temperature and 493K, perhaps, because it was masked by the broad band of water. When the sample was heated to 673K (Figure 6.10e), most of the bands in the hydroxyl region are removed except the 3740cm^{-1} band which has been assigned to Si-OH.

(iii) Study of the reduction of Cu^{II} to $Cu^{I}Y$ zeolite

$Cu^{II}Y$ zeolite (73.2% exchanged) was reduced by CO with preadsorbed ammonia. Figures 6.13 and 6.14 show the spectra of dehydrated $Cu^{II}Y$ zeolite, in the presence of both the gases, at different temperatures during the reduction process. In trying to understand these complicated spectra we performed experiments on dehydrated $Cu^{II}Y$ zeolite in which ammonia was adsorbed and then removed before the adsorption of CO i.e. the interaction between each of the gases and the zeolite was studied separately.

In figure 6.11a is shown the spectrum of $Cu^{II}Y$ zeolite at room temperature after heating to 673K for 2 hours while in figure 6.11b is shown the spectrum of the same sample after admitting 50 torr ammonia at room temperature. Upon adsorption of ammonia, we observed new bands at 3600 (sh), 3250 (very broad and intense), 1625, 1450 and some very weak bands around 2100cm^{-1}. The band at 3600cm^{-1} could be due to ν(O-H) of ammonia hydrogen bonded to the framework oxygens. As explained in section III, in the single crystal study of ammonia adsorbed onto NaA[20,21], ammonia was found to be hydrogen bonded to another ammonia and also the framework oxygens.

The strong bands at 3250 and 1625cm^{-1} are due to the stretching and deformation modes of NH_3. However, the 3250cm^{-1} band is very broad, indicating either that hydrogen bonding has occurred or that there might be some unresolved bands present. We found that this band was better resolved in the spectra of the sample (Figures 6.11e and f) after the gaseous ammonia was removed by evacuating and the sample heated to elevated temperatures. We observed four bands at 3350, 3280, 3220 and 3180cm^{-1} in the spectra of the sample at 373 and 483K (Figures 6.11e and f). On further heating the sample to 583K (Figure 6.11g), two bands at 3280 and 3220cm^{-1} disappeared. In this spectrum, we also observed that the 1620 and 1450cm^{-1} bands disappear at the same time.

Since the bands at 3280 and 3180cm^{-1} disappeared together with the band at 1620cm^{-1}, we correlate them as due to the same adsorbed molecule, which is ammonia. Schmidt and Muller[41], in infrared spectrum of $Cu(NH_3)_4SO_4 \cdot H_2O$ found bands at 3330*(s) and 3260*(sh)cm^{-1} due to ν_{as}(NH), 3178(m)cm^{-1} due to ν_s(NH), 1640*(m) and 1670*(vw)cm^{-1} due to δ_{as}(HNH) (Lattice water vibrations are also expected in the

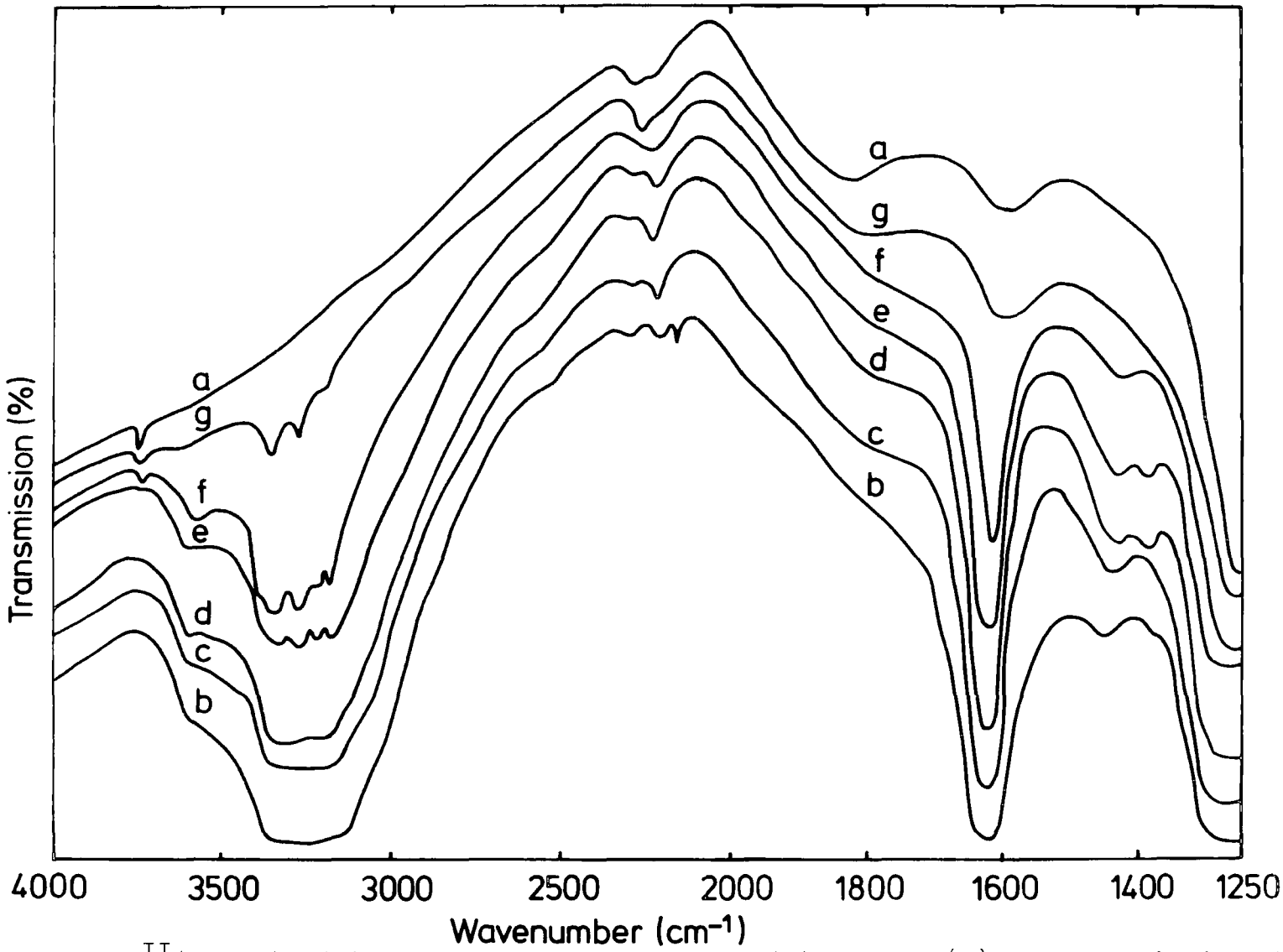

Figure 6.11. $Cu^{II}(2,673)$: (a) at ambient temperature, (b) sample (a) after admitting 50 torr NH_3, (c) sample (b) after evacuation for 5 minutes, (d) sample (b) after evacuation for 30 minutes, (e) sample (d) at 373K, (f) sample (d) at 483K and (g) sample (d) at 673K.

region marked by *). We can thus assign our data for adsorbed ammonia as follows: 3280cm^{-1} to ν_{as}(NH), 3220 cm^{-1} to ν_{s}(NH) and 1620cm^{-1} to δ_{as}(HNH).

By analogy with the spectra of $Cu^{II}Y$ obtained at various temperatures during dehydration (Figure 6.10), the band observed at 1450cm^{-1} could be due to a framework vibration associated with cation movements. It was explained in section II that the copper ions are very mobile. On dehydrating the sample, the Cu^{2+} ions tend to move to the small cavities. Upon adsorption of ammonia, the Cu^{2+} ions moved out of the small cavities to form copper-ammine complexes[23,24]. This explains why we observe the 1450cm^{-1} band in the hydrated and ammoniated samples and why this band disappeared when either water or ammonia was removed.

The bands at 3350 and 3220cm^{-1}, which remain after the sample was heated to 583K (Figure 6.11g) may be due to ν(O-H) of $Cu(OH)_2$ and Cu(OH), respectively. We assigned the 3280cm^{-1} band as due to ν(O-H) of Cu(OH) because we do not observe this band in the spectra of dehydrated $Cu^{II}Y$ and also because from EPR studies of ammonia adsorbed onto $Cu^{II}Y$ zeolite, it was concluded that some of the Cu^{2+} ions had been reduced to Cu^{+} ions. Further proof of this reduction was obtained when CO was adsorbed onto the sample used for the adsorption of ammonia.

After the removal of ammonia at 673K, the sample was allowed to cool to room temperature. CO at a pressure of 40 torr was admitted to the cell. The spectrum of the sample upon adsorption of CO is shown in figure 6.12b. A very strong band at 2140cm^{-1} is observed which is due to a Cu^{+}-CO complex, in agreement with several authors[8,28]. This confirms the presence of Cu^{+} in the sample.

Upon adsorption of 40 torr CO another very strong band is observed at 2180cm^{-1}. Judging by this spectrum alone, we

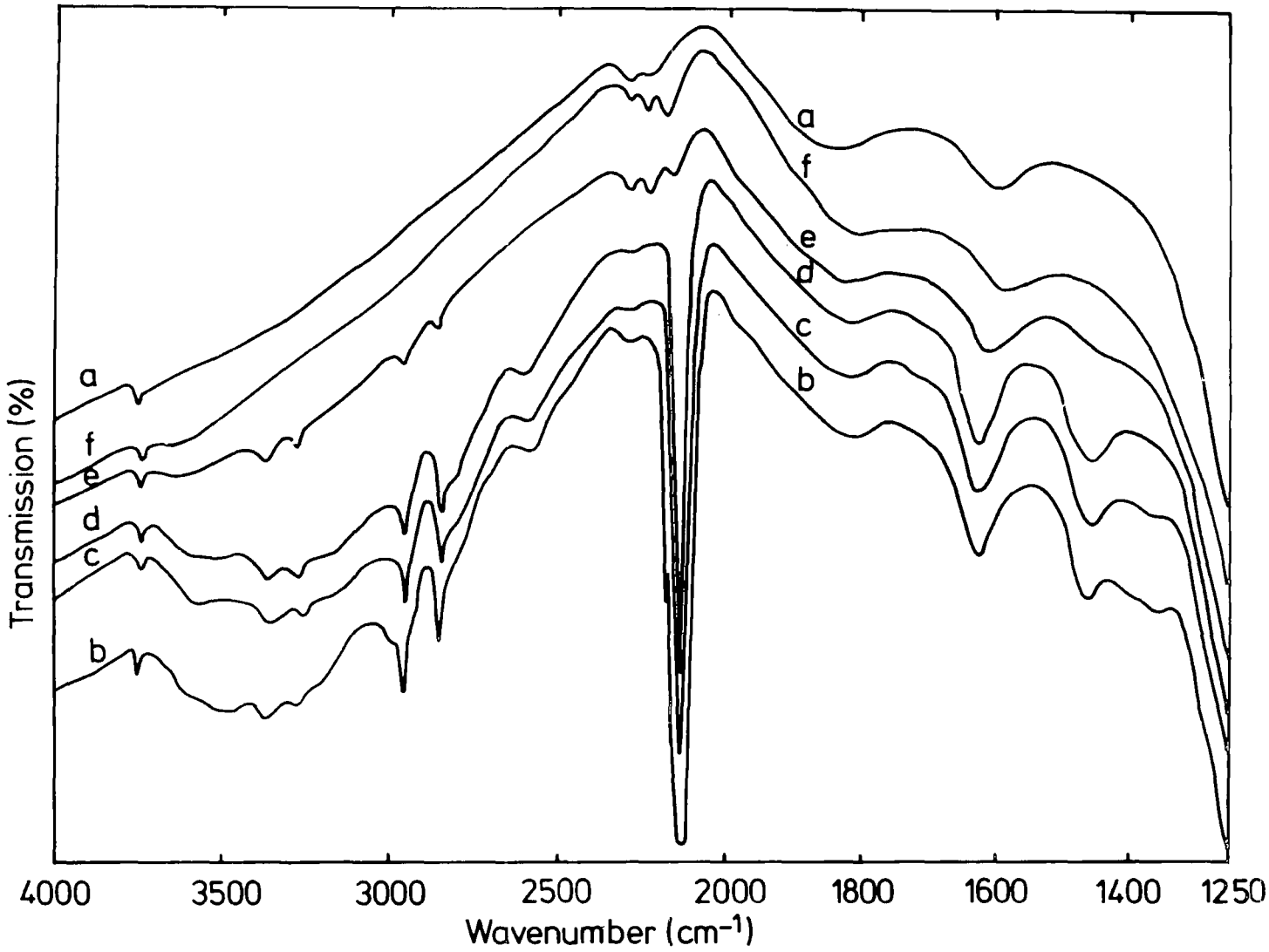

Figure 6.12. (a) sample 6.11(g) at ambient temperature, (b) sample (a) after admitting 40 torr CO, (c) sample (b) after evacuation for 5 minutes, (d) sample (b) after evacuation for 30 minutes, (e) sample (d) at 473K and (f) sample (d) at 673K.

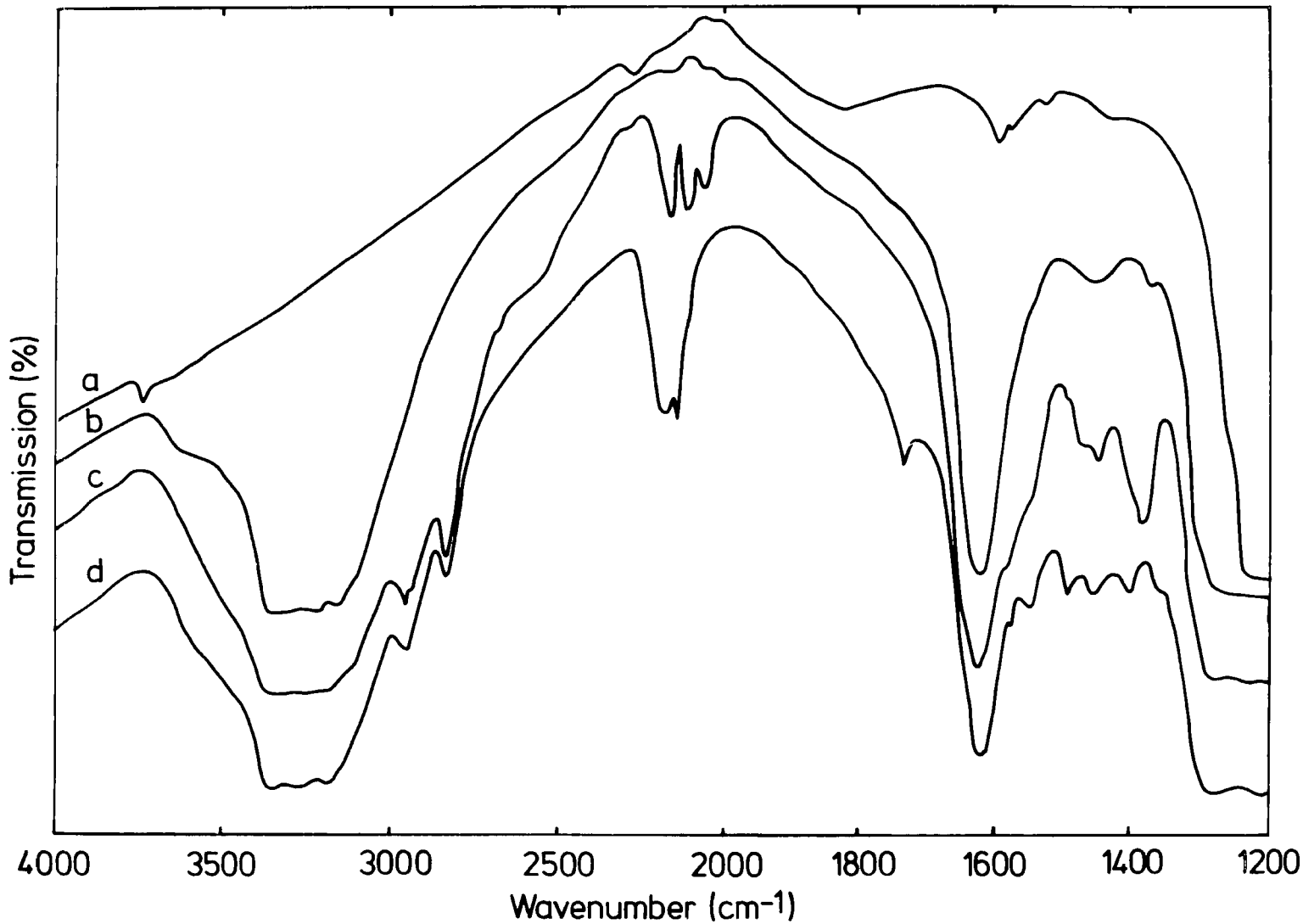

Figure 6.13. $Cu^{II}NaY$ zeolite after heating at 673K for 2 hours:
(a) at ambient temperature, (b) sample (a) after admitting 14 torr NH_3,
(c) sample (b) after admitting 155 torr CO and (d) sample (c) at 383K.

would be inclined to assign this band as due to CO bonded to Cu^{2+}. However, this band is also observed in the spectrum of CO adsorbed onto a fully reduced copper zeolite sample as shown in figure 6.20a. We prefer to assign the 2180cm^{-1} band to CO adsorbed at a second site. This is in agreement with the finding of Angell and Schaffer[26] in their studies of CO adsorbed onto various cations (Table 6.2), who found that the CO was adsorbed at two different sites for all of the cations studied. The CO adsorbed onto the site related to the 2180cm^{-1} band is weakly adsorbed since it can be pumped off easily (after 5 minutes evacuation; Figure 6.12c).

The bands at 3360 and 3280cm^{-1} may be assigned to ν(O-H) of Cu^{2+} and Cu^{+} hydroxides, respectively. Bands observed at 3500 and 1630cm^{-1} are due to water while bands at 2960, 2860 (hydrocarbons) and 2580cm^{-1} (CO_2) may be due to impurities in the CO gas. The impurities expected from the CO purchased (99.5% purity) are nitrogen (0.32 v/v), oxygen (800 ppm), CO_2 (500 ppm) hydrocarbons (50 ppm) and water (5 ppm).

Another band observed at 1460cm^{-1}, like the ammonia adsorption, may be due to a framework vibration associated with cation movements. CO adsorbed onto the site related to the 2140cm^{-1} band is strongly adsorbed since it cannot be removed until the sample is heated to a temperature of 673K (Figure 6.12f).

Figure 6.13a shows the spectrum of the $Cu^{II}Y$ sample (73.2% exchanged) at room temperature after heating to 673K for 2 hours. In figures 6.13b and c are shown the spectra of the same sample after admitting 14 torr of ammonia followed by 155 torr of CO, respectively. Ammonia and CO adsorbed individually onto $Cu^{II}Y$ zeolite have already been discussed. The $Cu^{II}Y$ sample in the presence of both the ammonia and CO was heated to 583K and the spectra of the sample at various

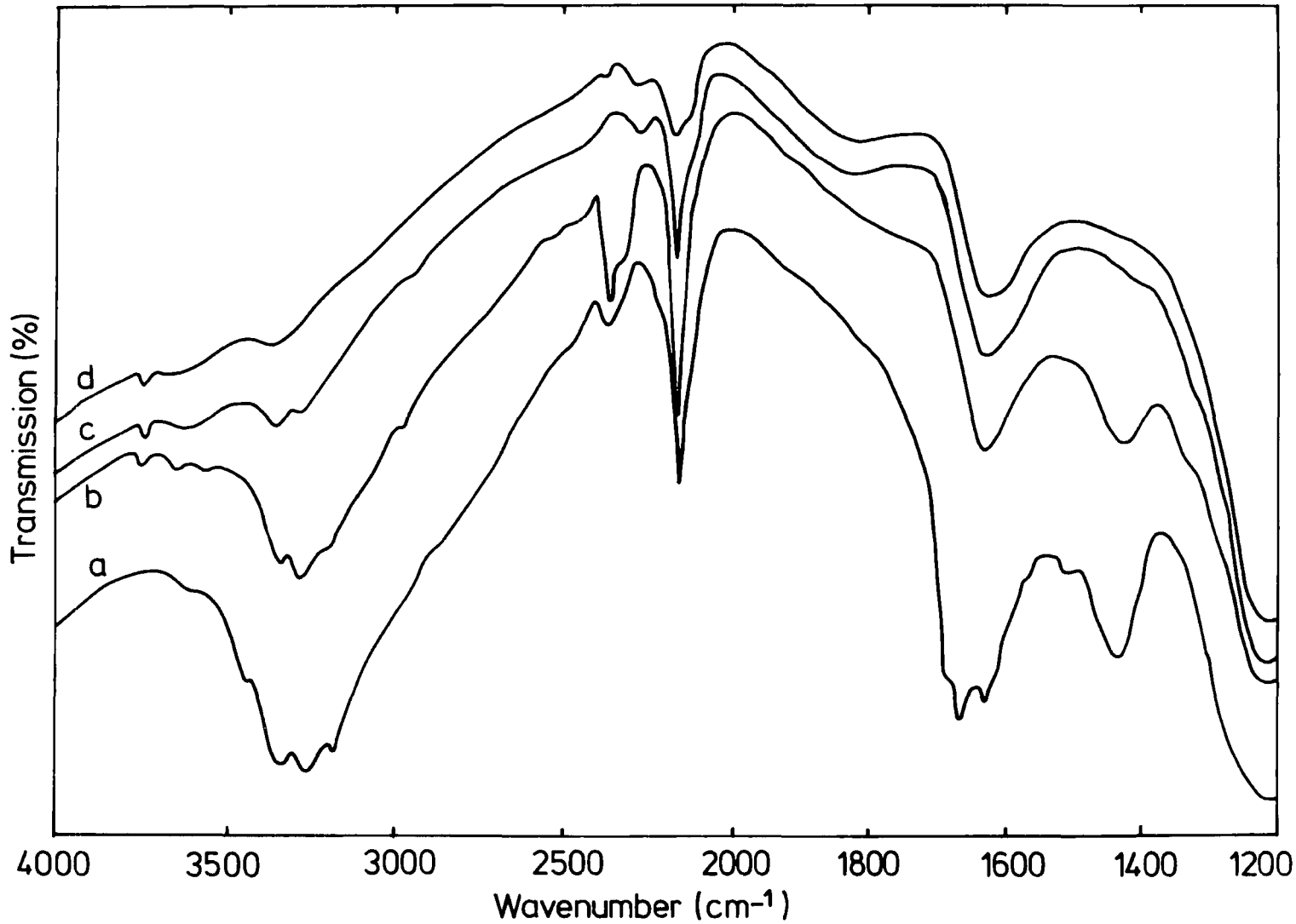

Figure 6.14. (a) sample 6.13(c) at 503K, (b) sample 6.13(c) at 583K, (c) sample (b) after evacuation for 40 minutes at 603K and (d) sample (c) after evacuation for a further 1 night at 603K.

temperatures are shown in figures 6.13d, 6.14a and b. As can be seen, the spectra are rather complicated, however, with reference to the spectra of the gases adsorbed onto $Cu^{II}Y$ sample individually, we will try to assign some of the bands observed. It should be noted that the region of importance is 2100-2200cm^{-1}, whence proof of the presence of Cu^{+} will be obtained.

In the spectrum of the sample plus both the gases at room temperature (Figure 6.13c), we observed a broad band at around 3250cm^{-1} and another intense band at 1625cm^{-1} which we may assign to the stretching and deformation modes of ammonia. We have already discussed this in detail earlier. We are not able to explain the presence of the bands at ca. 1350-1550cm^{-1}. The bands in the region 2000-2200cm^{-1} are due to gas phase CO.

The sample in the presence of both ammonia and CO was heated to 383K and the spectrum is shown in figure 6.13d. Two strong bands are observed at 2150 and 2190cm^{-1} which may be due to CO adsorbed onto Cu^{+} ions. Additional bands are observed in the region 1350-1550cm^{-1} which we could not explain. However, as the sample was heated further to 503K (Figure 6.14a), most of the bands in this region disappear and we observed a strong broad band at 1430cm^{-1}. This could be attributed to ammonium ions, indicating that Bronsted acid sites are being formed. Eischens and Pliskin[46], observed a band at 1450cm^{-1} on rehydrated silica-alumina which was assigned to the formation of ammonium ions.

The sample was heated further to 583K (Figure 6.14b) and we can see that the band at 2160cm^{-1} becomes more intense. This band, which is due to a Cu^{+}-CO complex, confirms the reduction of Cu^{2+} to Cu^{+} ions. Complete reduction of Cu^{2+} to Cu^{+} was achieved after the sample was left standing for 1

hour at 583K in the presence of the gases, since the 2160cm^{-1} band did not increase further in intensity. Huang[27], in his study of the reduction of Cu^{2+} to Cu^{+} using the same procedure as described above found that most of the Cu^{2+} ions could be reduced in a few hours at temperature as low as 373K.

After complete reduction of Cu^{2+} to Cu^{+} was obtained, the cell was evacuated overnight at 603K. The sample was then cooled to room temperature before the adsorption experiments were begun.

(iv) Adsorption of hydrocarbons onto Cu^{II} and $Cu^{I}Y$ zeolites

(a) Ethylene

Ethylene was adsorbed onto two $Cu^{II}Y$ samples, the 70.4 and 92.9% exchanged. Samples of each of these were subjected to two different pretreatment conditions (453 and 673K) before the adsorption of ethylene. In figure 6.15a is shown the spectrum of $Cu^{II}Y$ sample (70.4% exchanged) at room temperature after heating to 673K for 15 hours, while in figures 6.15b and c are shown the spectra of the same sample upon adsorption of 50 torr C_2H_4 and evacuation for 5 minutes and 2 hours at room temperature, respectively.

After removal of the gaseous C_2H_4 by evacuation for 5 minutes at room temperature, we observe only one strong and sharp band, at 1428cm^{-1}, which is due to the adsorbed species. This is true for all of the samples used and at different pretreatment conditions. We assign this band to the anti-symmetric CH_2 deformation (ν_{12}, following the notation of Herzberg[42]) of adsorbed C_2H_4. In the infrared spectrum of the gas phase, ν_{12} occurs at 1443cm^{-1} [42]. The sharpness of the ν_{12} band could indicate that the C_2H_4 molecule is not rotating. This is in agreement with Yates et al[43], in their infrared

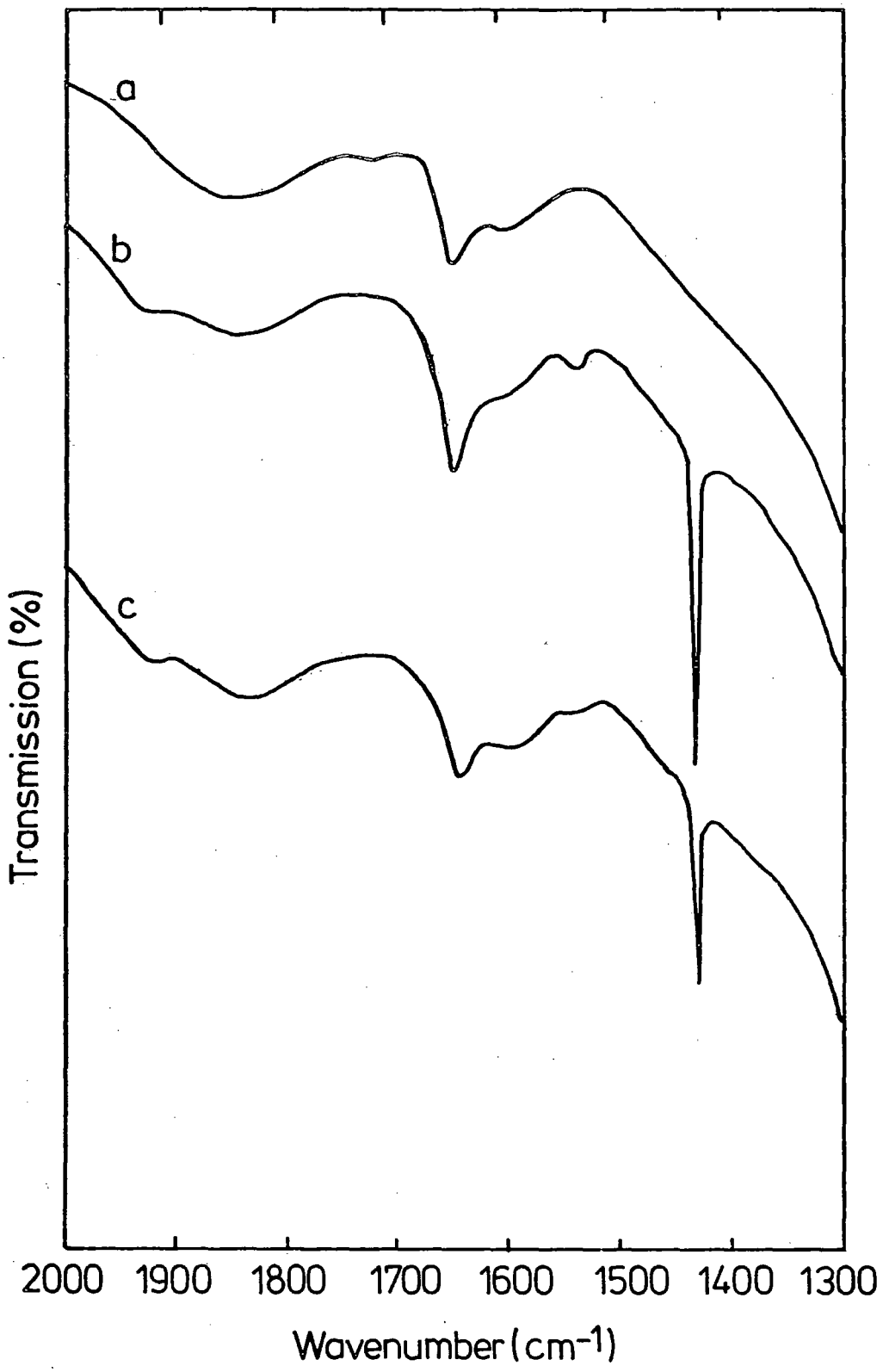

Figure 5.15. $Cu^{II}NaY$ zeolite after heating at 673K for 2 hours:
(a) at ambient temperature
(b) sample (a) after admitting 50 torr C_2H_4 and evacuated for 5 minutes
(c) sample (b) after evacuation for 2 hours.

studies of C_2H_4 adsorbed onto Ag13X zeolite, who also found that the ν_{12}band was sharp and concluded that the adsorbed C_2H_4 is not rotating in their sample.

Unlike the C_2H_4 adsorbed onto AgA zeolite (Chapter IV), we do not observe any bands which we can assign to the C=C stretch (ν_2) or CH_2 symmetric deformation (ν_3) which occur at 1623 and 1342cm^{-1}, respectively, in the Raman spectrum of the gas phase[42]. The non-appearance of the ν_2 and ν_3 bands in the spectrum of C_2H_4 adsorbed onto $Cu^{II}Y$ zeolite indicates that the symmetry of the C_2H_4 is preserved in the adsorbed species (D_{2h}). This is only possible if two Cu^{2+} ions are coordinated to one C_2H_4 molecule. Huang et al[44] studied the adsorption of C_2H_4 onto Cu^{II} and $Cu^{I}Y$ zeolites spectroscopically and gravimetrically. However, they did not assign the bands due to the adsorbed species or analyse their spectra in detail but simply stated that the spectra were different. In their gravimetric measurements of the adsorption of C_2H_4 in both zeolites, they found that more C_2H_4 was adsorbed onto $Cu^{I}Y$ zeolite (approximately twice as much at 100 torr) than $Cu^{II}Y$ zeolite. This could arise because two Cu^{2+} ions are coordinated to one C_2H_4 molecule. In our experiments, we found that C_2H_4 was strongly adsorbed onto $Cu^{II}Y$ zeolite since it could not be removed until after the sample was heated to 473K. This is in contrast to the conclusion reached by Huang et al[44], who found that the C_2H_4 could be pumped off easily (room temperature).

In figure 6.16a is shown the spectrum of $Cu^{I}Y$ at room temperature while in figure 6.16b is shown the spectrum of the same sample upon admitting 30 torr C_2H_4. Subsequently, the sample was evacuated for 5 minutes (Figure 6.16c) and a further 55 minutes (Figure 6.16d) at room temperature.

After 5 minutes evacuation of the sample at room temperature, unlike the C_2H_4 adsorbed onto $Cu^{II}Y$ zeolite, we

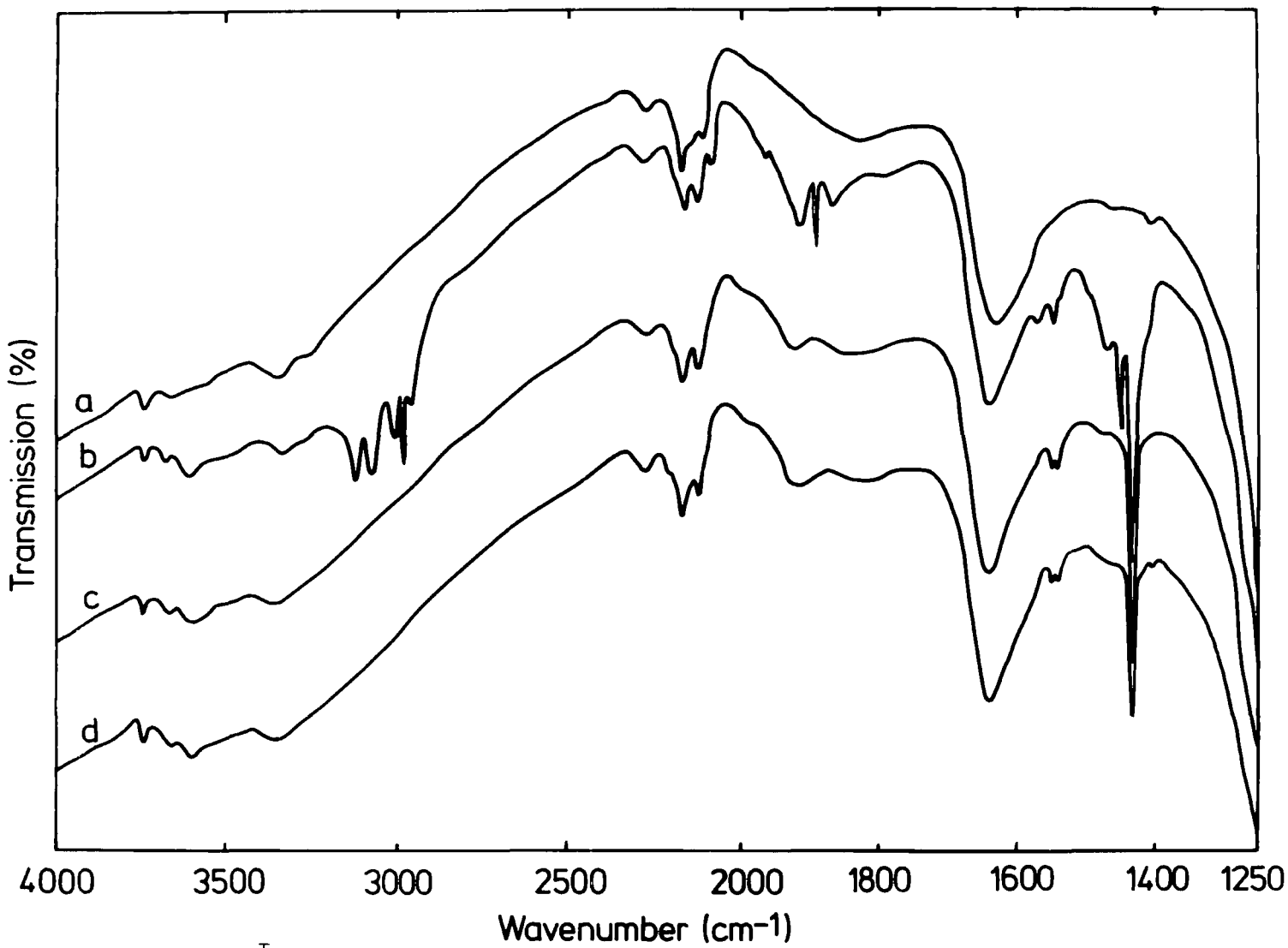

Figure 6.16. $Cu^{I}NaY$ zeolite: (a) at ambient temperature, (b) sample (a) after admitting 50 torr C_2H_4, (c) sample (b) after evacuation for 5 minutes and (d) sample (c) after evacuation for a further 55 minutes.

observed three bands at 1920, 1535 and 14 28cm^{-1}. We assign the 1920cm^{-1} band to a combination band ($\nu_7 + \nu_8$), 1535cm^{-1} band to the C=C stretch (ν_2) and the 1428cm^{-1} to the CH_2 anti-symmetric deformation (ν_{12}). In the spectrum of the gas phase[42], ($\nu_7 + \nu_8$), ν_2 and ν_{12} occur at 1889, 1623 and 1443 cm^{-1}, respectively.

In the spectrum of the adsorbed species, we could not observe the band due to ν_3 which occurs at 1342cm^{-1} in the Raman spectrum of the gas phase[42]. This could be because ν_3 is rather weak and is masked by the strong framework vibration. Clearly here, since ν_2 is observed, which is infrared inactive in the gas phase, this indicates that the adsorption of C_2H_4 causes a reduction in symmetry (probably to C_{2v}).

The combination band ($\nu_7 + \nu_8$) was not observed in our i.r. study of C_2H_4 adsorbed onto AgA zeolite (Chapter IV) or by Yates et al[43] in their infrared studies of C_2H_4 adsorbed onto various cation exchanged 13X zeolites. As explained by Yates et a the observation or otherwise of combination bands is difficult to predict in the gas phase, let alone in the adsorbed phase.

In the $Cu^IY + C_2H_4$ experiment, after 60 minutes evacuation at room temperature (Figure 6.16d) and with some C_2H_4 still adsorbed, CO (40 torr) was introduced to the sample. Upon adsorption of CO (Figure 6.17a), we observed a very strong band at 2130cm^{-1} and a shoulder at 2180cm^{-1}, and those bands which were due to adsorbed C_2H_4 are removed. As explained in part (iii), the 2130cm^{-1} band, which shifted to 2140cm^{-1} on evacuation (Figure 6.17b), is due to a Cu^+-CO complex while the shoulder at 2180cm^{-1}, which was removed after 5 minutes evacuation at room temperature (Figure 6.17b), is due to CO weakly adsorbed to Cu^+ ions at a different site.

When 30 torr of C_2H_4 was readmitted to the evacuated sample, the Cu^I-C_2H_4 complex with characteristic bands at

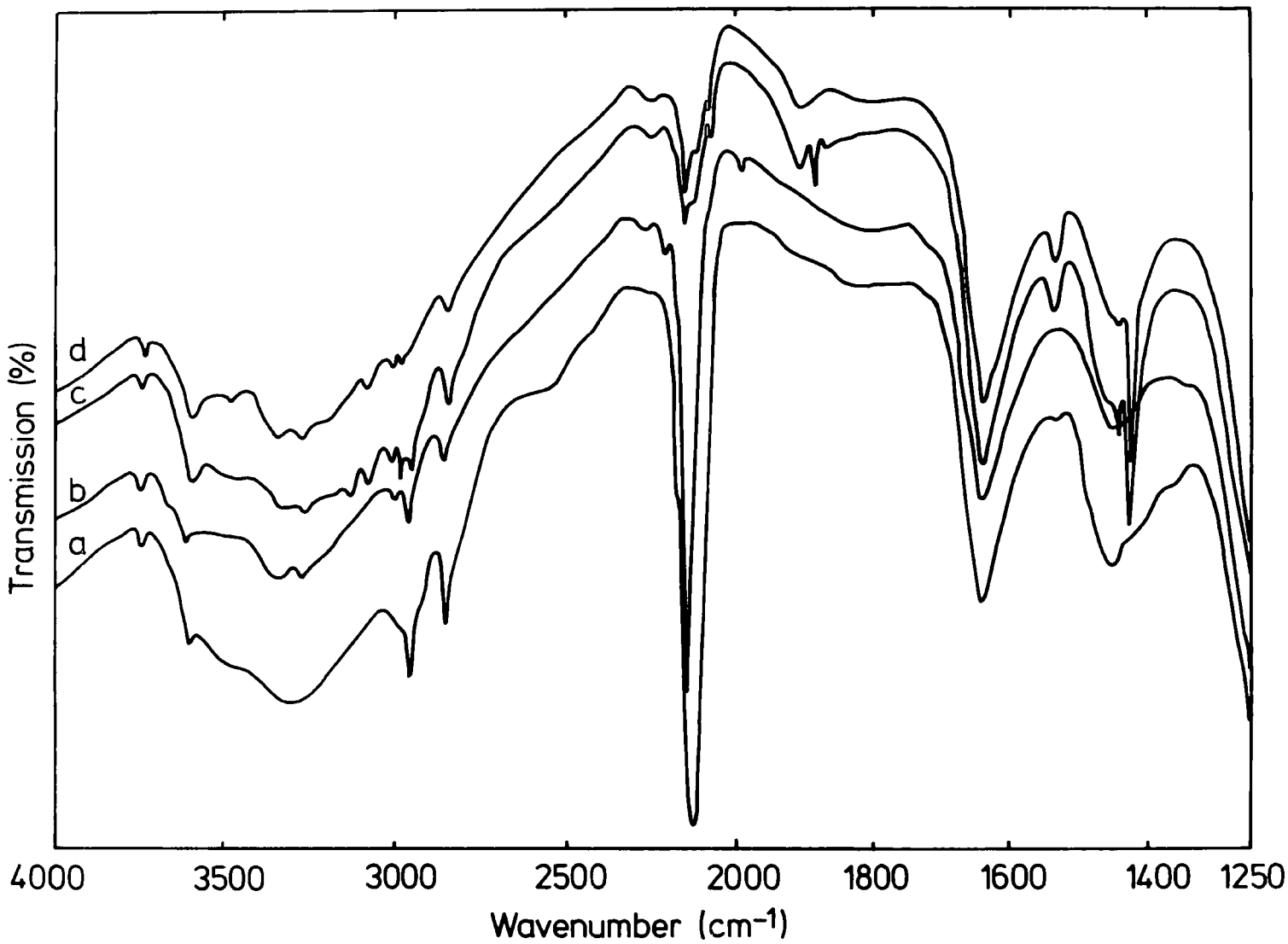

Figure 6.17. (a) sample 6.16(d) after admitting 40 torr CO, (b) sample (a) after evacuation for 5 minutes, (c) sample (b) after admitting 30 torr C_2H_4 and (d) sample (c) after evacuation for 5 minutes.

1920, 1535, and 1428cm^{-1} (Figures 6.17c and d) is formed again and the adsorbed CO removed. The observation that C_2H_4 was removed upon adsorption of CO and vice versa, indicates that both of the adsorbed species are held with comparable strength by Cu^+ions. It also indicates that both C_2H_4 and CO are adsorbed at the same site. Depending on the concentration of either of the gases, as revealed by the spectra of the adsorbed species, one or the other will be observed.

The Cu^IY zeolite sample, after the readsorption of C_2H_4, was evacuated and heated (Figures 6.18b, c and d). It was found that C_2H_4 was removed after heating the sample to 423K (Figure 6.18b).

(b) Acetylene

Acetylene was adsorbed onto Cu^{II} and Cu^IY zeolites and their adsorption behaviour compared. Figures 6.19b and 6.20b show the spectra of Cu^{II} and Cu^IY zeolites, respectively, upon adsorption of 50 torr C_2H_2. Gaseous C_2H_2 was removed from the samples by evacuating for 5 minutes (Figures 6.19c and 6.20c) and a further 25 minutes (Figures 6.19d and 6.20d) at room temperature.

In both the samples, upon adsorption of C_2H_2, we observe some bands at ca. 3200cm^{-1} (Figures 6.19b and 6.20b) which are due to the adsorbed species and the gas phase. We also observe bands at 1960, 1830(sh) and 1810cm^{-1} which are due to the adsorbed species. In the spectra of the samples after 5 minutes evacuation at room temperature (Figures 6.19c and 6.20c), the band at 1960cm^{-1} disappears while the bands at 3250, 3200(sh), 3170, 1820(sh) and 1810cm^{-1} remain. Subsequently, little change was observed after 30 and 60 minutes evacuation (Figures 6.19d, 6.20d and e).

We assign the 1960cm^{-1} band to $\nu(C\equiv C)$, which occurs at

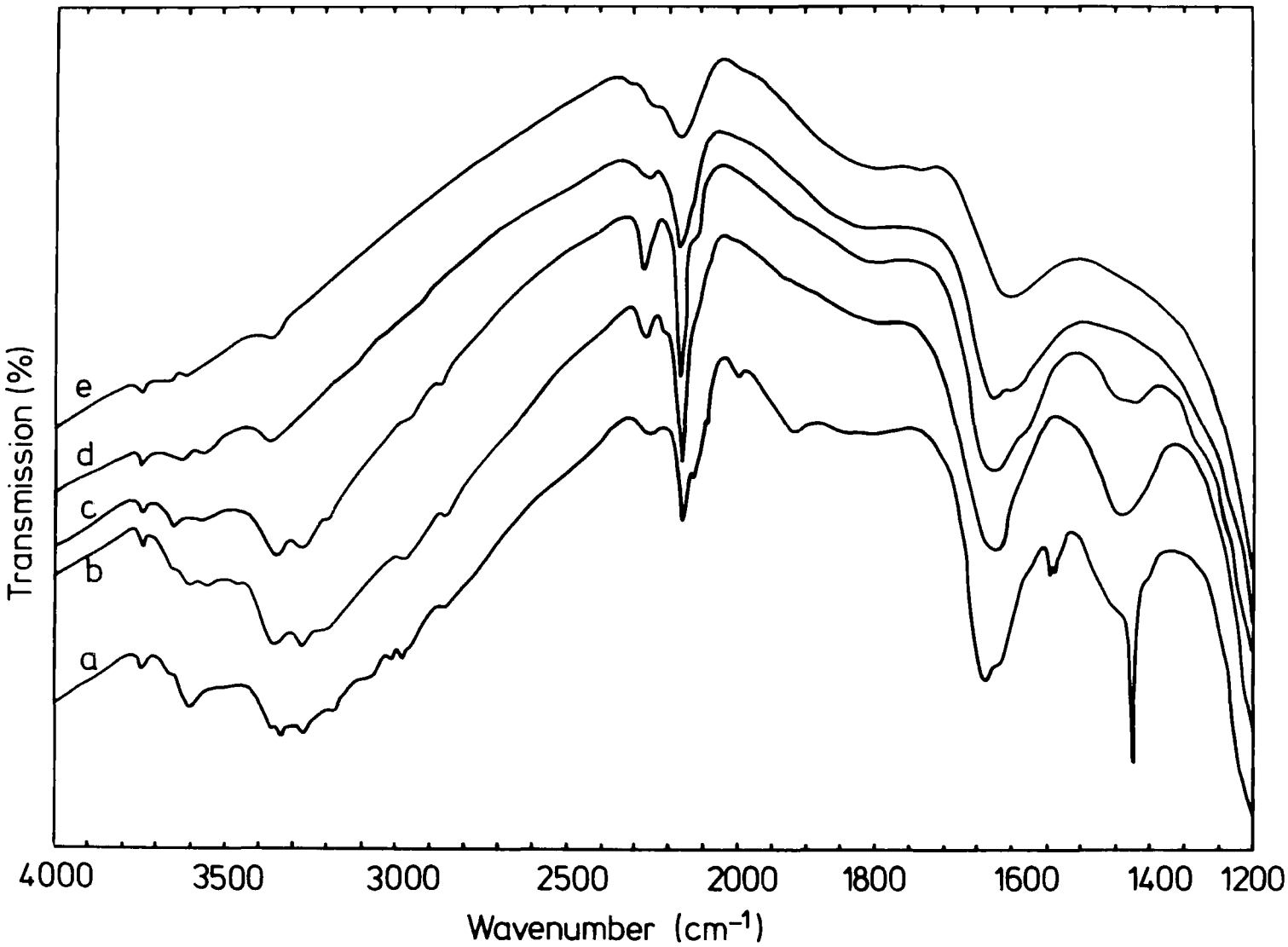

Figure 6.18. (a) sample 6.17(d) after evacuation for a further 25 minutes, (b) sample (a) at 423K, (c) sample (a) at 513K, (d) sample (a) at 613K and (d) sample (a) at 693K.

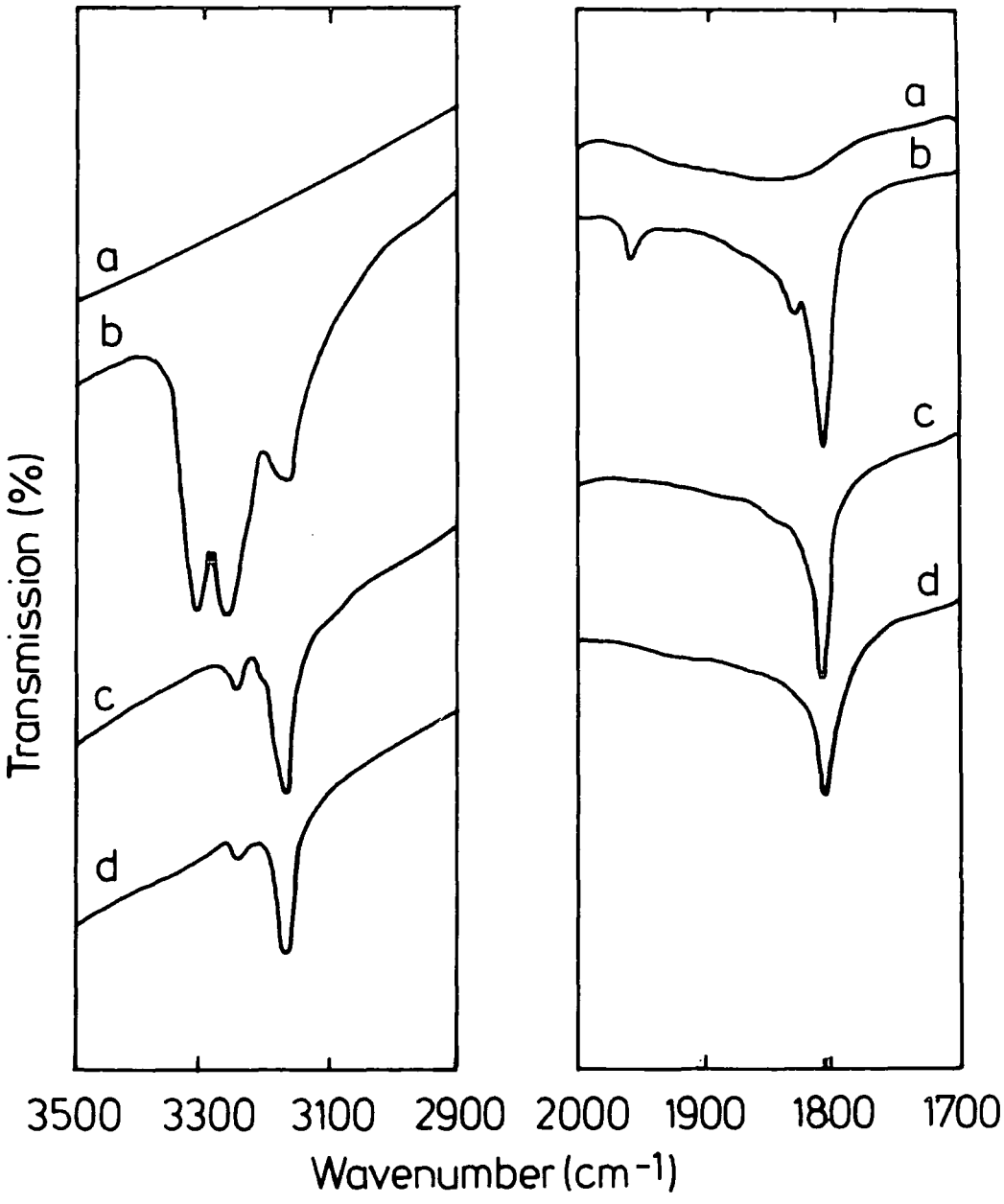

Figure 6.19. $Cu^{II}NaY$ zeolite after heating at 673K for 14 hours:

(a) at ambient temperature

(b) sample (a) after admitting 50 torr C_2H_2

(c) sample (b) after evacuation for 5 minutes

(d) sample (c) after evacuation for a further 25 minutes.

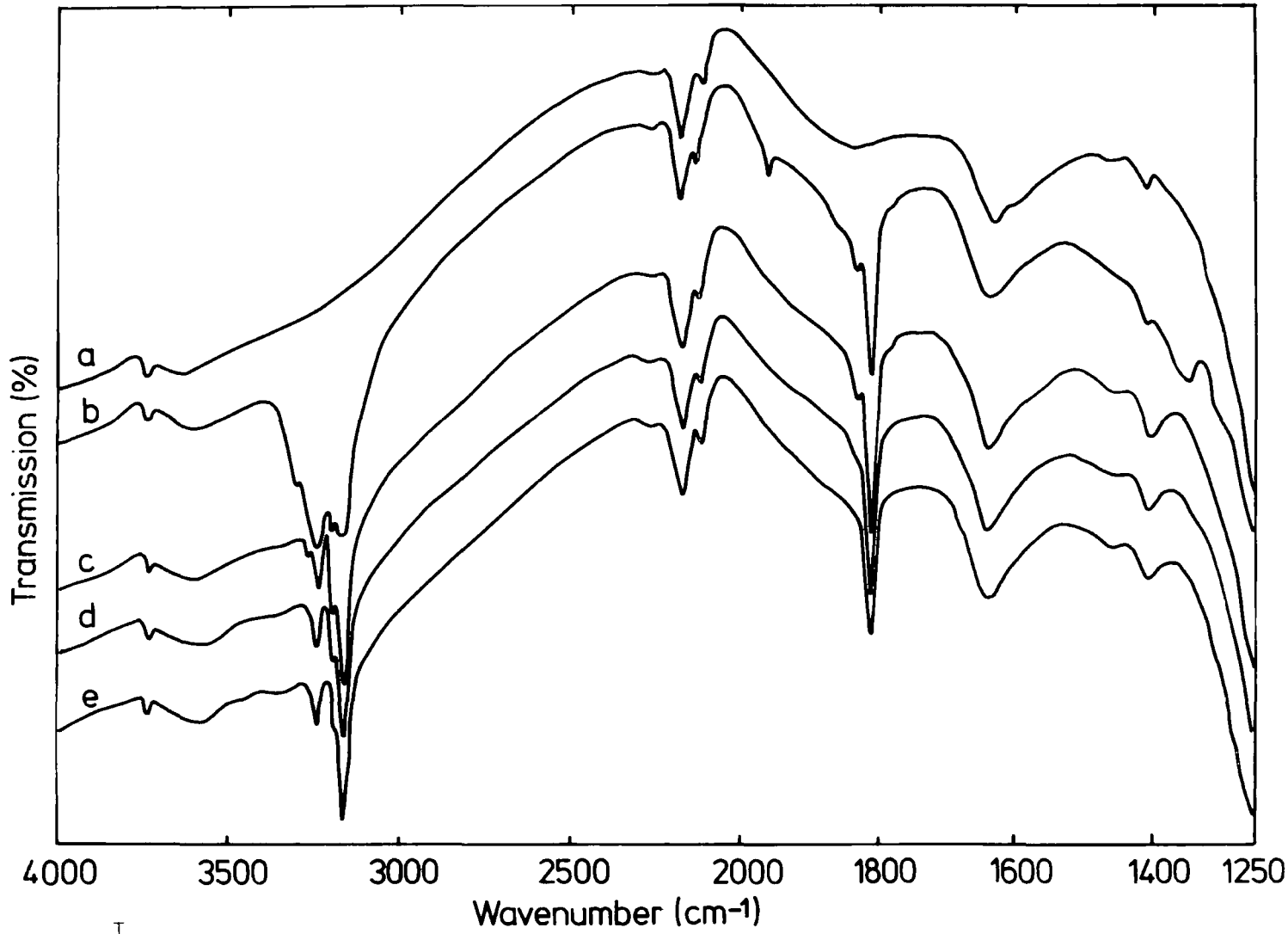

Figure 6.20. $Cu^{I}NaY$ zeolite: (a) at ambient temperature, (b) sample (a) after admitting 50 torr C_2H_2, (c) sample (b) after evacuation for 5 minutes, (d) sample (c) after evacuation for a further 25 minutes and (e) sample (d) after evacuation for a further 30 minutes.

1974cm^{-1} in the Raman spectrum of the gas phase[42]. The appearance of this band, which is inactive in the infrared spectrum of the gas phase, indicates a lowering in symmetry of the adsorbed C_2H_2. Since ν(C≡C) for the adsorbed species occurs at a value lower than the gas phase then the mode of interaction of this adsorbed C_2H_2 must be 'side-on' (Chapter V). Acetylene adsorption at this site must be weak since the 1960cm^{-1} band disappears after 5 minutes evacuation at room temperature.

The bands observe at 3250, 3200(sh), 3170, 1830(sh) and 1810cm^{-1} must be due to C_2H_2 adsorbed at a different site. In $Cu^{II}Y$, these bands can only be removed on heating the sample to 503K indicating that the C_2H_2 is very strongly adsorbed. We assign the 3250, 3200(sh) and 3170cm^{-1} bands to ν(C-H) while the 1830(sh) and 1810cm^{-1} are assign to ν(C≡C).

After the $Cu^{I}Y$ zeolite had been evacuated at room temperature for 60 minutes (Figure 6.20e), CO at a pressure of 40 torr was introduced to the sample. Upon adsorption of the CO, the bands which are due to C_2H_2 adsorption still remain although they are reduced in intensity and new bands due to the adsorbed CO are observed at 2180 and 2140cm^{-1} (Figure 6.21a). These bands as have already been explained (Part (iii)) are due to CO adsorbed at two sites, one weakly and the other strongly. The weakly adsorbed CO was removed after 5 minutes evacuation at room temperature (Figure 6.21b).

The observation of the bands due to adsorbed C_2H_2 and CO at the same time indicates that the gases were adsorbed at different sites. Both gases are strongly adsorbed since they could only be removed after the sample was heated to 483K (Figure 6.21e).

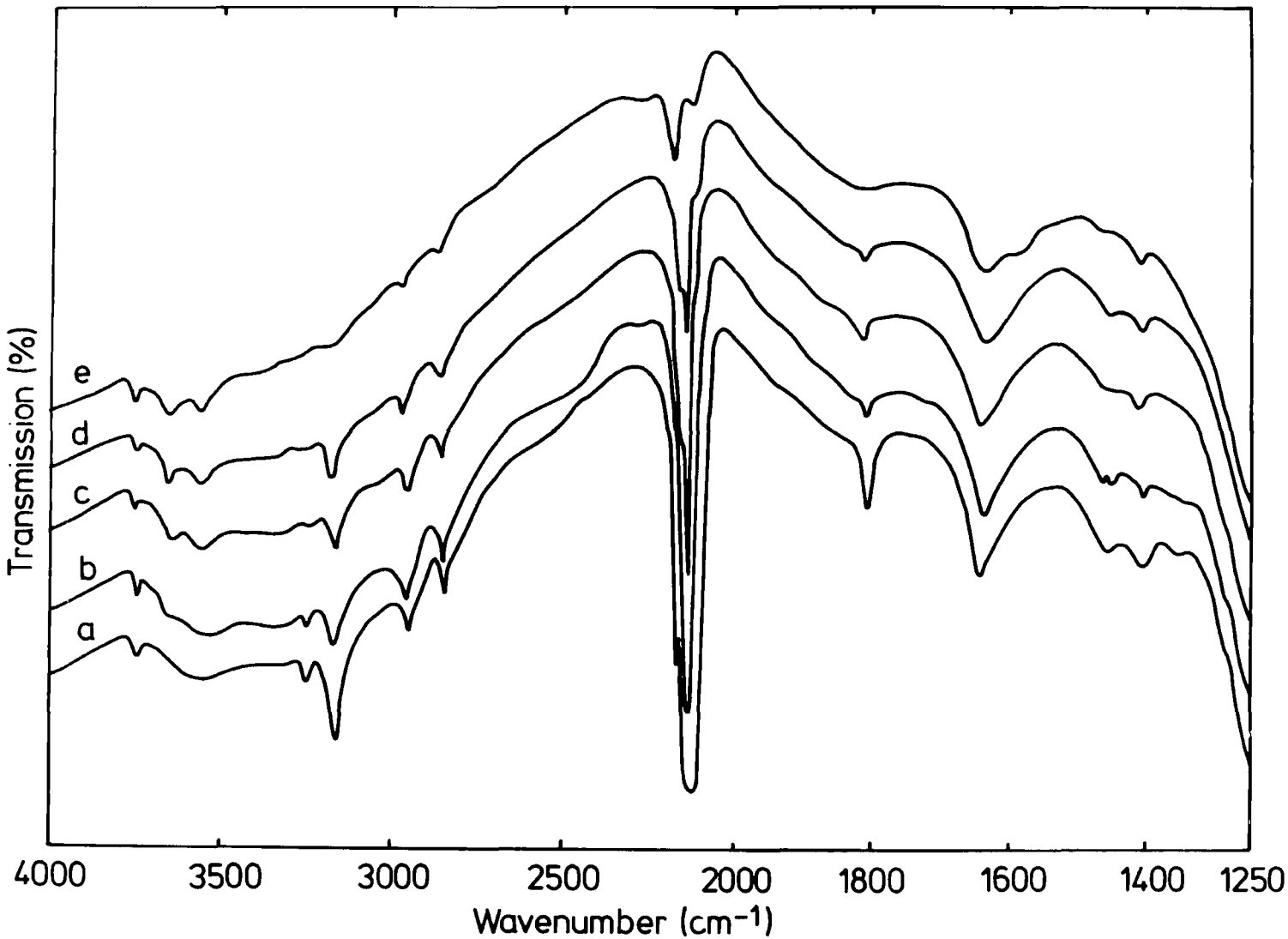

Figure 6.21. (a) sample 6.20(e) after admitting 40 torr CO, (b) sample (a) after evacuation for 5 minutes, (c) sample (b) after a further evacuation for 25 minutes, (d) sample (c) at 373K and (e) sample (c) at 483K.

VI. Conclusion

Infrared spectra of $Cu^{II}Y$ zeolites with different degrees of exchange reveal that increasing the copper content gives rise to three sharp bands above $3000cm^{-1}$ which are due to ν(O-H) of bridging hydroxyls and copper hydroxides.

Adsorption of ammonia onto dehydrated $Cu^{II}Y$ zeolite (73.2% exchanged) shows that most of the Cu^{2+} ions are reduced to Cu^{+} cations. Proof of this was obtained when CO was adsorbed after ammonia. A band at $2140cm^{-1}$, which is due to a Cu^{+}-CO complex, confirms the presence of Cu^{+} cations. It was found that CO was adsorbed at two different sites, one was weakly adsorbed and the other more strongly adsorbed.

In another experiment, the complete reduction of Cu^{2+} to Cu^{+} cations was carried out on a $Cu^{II}Y$ sample in the presence of a CO atmosphere with pre-adsorbed ammonia. Ammonia was used to remove the Cu^{2+} cations from the small cavities so that they can be reduced by CO[27].

Hydrocarbons (C_2H_4 and C_2H_2) were adsorbed onto the freshly prepared $Cu^{I}Y$ zeolite and their adsorption behaviour compared with $Cu^{II}Y$ zeolite. Regardless of the copper contents in the $Cu^{II}Y$ samples and the pretreatment conditions used, after 5 minutes evacuation of the gaseous C_2H_4, only one sharp band at $1428cm^{-1}$ was observed. This band was assigned to the CH_2 antisymmetric deformation (ν_{12}) of the adsorbed species. No other bands observed could be assigned as due to the adsorbed species indicating that the symmetry

of the adsorbed species is the same as the gas phase (D_{2h}), which can only be achieved if two Cu^{2+} cations coordinate to one C_2H_4 molecule.

Unlike the C_2H_4 adsorbed onto $Cu^{II}Y$ zeolite, C_2H_4 adsorbed onto $Cu^{I}Y$ zeolite gives rise to three bands, at 1920, 1535, and

1428cm^{-1}, which are assigned to the combination bands ($\nu_7 + \nu_8$), C=C stretch (ν_2) and CH_2 antisymmetric deformation (ν_{12}), respectively. The appearance of the ν_2, which is infrared inactive in the gas phase, indicates that there is a reduction in symmetry (C_{2v}) with adsorption.

Following the evacuation of C_2H_4 for 60 minutes at room temperature, 40 torr of CO was introduced to the sample. After 5 minutes evacuation at room temperature, C_2H_4 was reintroduced to the sample. It was suggested from the above process that C_2H_4 and CO are held with comparable strength by Cu^+ ions and that the gases are adsorbed at the same site. It was also suggested that it was the relative concentration of the gases that determine which gas was to be predominently adsorbed.

The adsorption behaviour of C_2H_2 on Cu^{II} and $Cu^{I}Y$ zeolites were found to be similar. From the bands observed, it can be concluded that C_2H_2 is adsorbed at two different sites and that the mode of interaction is 'side-on' since $\nu(C\equiv C)$ for the adsorbed species occured at a wavenumber lower than that of the gas phase (1974cm^{-1}). C_2H_2 was weakly bonded to the cation at one site and strongly at the other. The weakly bonded C_2H_2 could be removed by 5 minutes evacuation at room temperature while the strongly bonded C_2H_2 could only be removed after the sample was heated to 503K.

For sample $Cu^{I}Y$ zeolite, following 60 minutes evacuation of C_2H_2 at room temperature, CO (40 torr) was introduced to the sample. Bands due to C_2H_2 adsorption were observed to decrease in intensity even upon adsorption of CO. It was deduced that CO and C_2H_2 were adsorbed at two different sites.

References

1. Mochida, I., Hayata, S., Kato, A., and Seiyama, T., J. Catal., 15, 314(1969).
2. Mochida, I., Hayata, S., Kato, A., and Seiyama, T., J. Catal., 23, 31(1971).
3. Mochida, I., Jitsumatsu, T., Kato, A., and Seiyama, T., Bull. Chem. Soc. Jpn., 44, 2595(1971).
4. Naccache, C., and Ben Taarit, Y., J. Catal., 23, 171(1971).
5. Mochida, I., Hayata, S., Kato, A., and Seiyama, T., Bull. Chem. Soc. Jpn., 44, 2282(1971).
6. Tsutsumi, K., Fuji, S., and Takahashi, H., J. Catal., 24, 146(1972).
7. Dimitrov, C., and Leach, H.F., J. Catal., 14, 336(1969).
8. Huang, Y.Y., J. Catal., 30, 187(1973).
9. Marti, J., Soria, J., and Cano, F.H., J. Phys. Chem., 80, 1776(1976).
10. Maxwell, I.E., and de Boer, J.J., J. Phys. Chem., 79, 1874(1975).
11. Soria, J., and Turkevich, J., and Ono, Y., J. Catal., 25, 44(1972).
12. Soria, J., and Conesa, J.C., J. Chem. Soc. Trans. Farad. I, 75, 406(1979).
13. Gallezot, P., Ben Taarit, Y., and Imelik, B., J. Catal., 26, 295(1972).
14. Gallezot, P., Ben Taarit, Y., and Imelik, B., Compt. Rend., C272, 261(1971).
15. Maxwell, I.E., and de Boer, J.J., J. Chem. Soc. Chem. Comm., 814(1974).
16. Chao, C.C., and Lunsford, J.H., J. Chem. Phys., 57, 2890(1972).
17. Herman, R.G., and Flentge, D.R., J. Phys. Chem., 82, 720 (1978).

18. Morke, W., Vogt, F., and Bremer, H.Z., Anorg. Allg. Chem., 422, 273(1974).

19. Shoonheydt, R.A., and Velghe, F., J. Chem. Soc. Trans. Farad. I, 72, 172(1976).

20. Yanagida, R.Y., and Seff, K., J. Phys. Chem., 76, 2597 (1972).

21. Yanagida, R.Y., and Seff, K., J. Phys. Chem., 77, 138 (1973).

22. Kim, Y., and Seff, K., J. Amer. Chem. Soc., 99, 7057(1977).

23. Vansant, E.F., Recueil, 92, 1152(1973).

24. Vansant, E.F., and Lunsford, J.H., J. Phys. Chem., 78, 2860(1972).

25. Huang, Y.Y., and Vansant, E.F., J. Phys. Chem., 77, 663 (1973).

26. Angell, C.L., and Schaffer, P.C., J. Phys. Chem., 70, 1413(1966).

27. Huang, Y.Y., J. Catal., 32, 482(1974).

28. Huang, Y.Y., J. Amer. Chem. Soc., 95, 6636(1973).

29. Larson, A.T., and Teitsworth, C.S., J. Amer. Chem. Soc., 44, 2878(1922).

30. Stewart, R., and Evans, D.G., Anal. Chem., 35, 1315(1963).

31. Scott, A.F., Wilkening, L.L., and Rubin, B., Inorg. Chem., 8, 2533(1969).

32. Alben, J.O., Yen, L., and Farrier, N.J., J. Amer. Chem. Soc., 92, 4475(9170).

33. Miwa, Y., Tsutsumi, K., and Takahashi, H., Seisan-Kenkyu, 30, 181(1978).

34. Miwa, Y, Tsutsumi, K., and Takahashi, H., Seisan-Kenkyu, 30, 221(1978).

35. Miwa, Y., Tsutsumi, K., and Takahashi, H., Zeolites, 1, 3(1981).

36. Miwa, Y., Tsutsumi, K., and Takahashi, H., Zeolites, 1,

98(1981).

37. Maes, A., and Cremers, A., J. Chem. Soc. Trans. Farad. I, 71, 265(1975).

38. Breck, D.W., and Flanigen, E.M., Molecular Sieves, Soc. Chem. Ind., London(1968).

39. Ferraro, J.R., and Walker, W.R., Inorg. Chem., 4, 1382(1965).

40. Tarte, P., Spectrochim. Acta, 13, 107(1958).

41. Schmidt, K.H., and Muller, D., J. Molecular Structure, 22, 343(1974).

42. Herzberg, G., Molecular Spectra and Molecular Structure II. Infrared and Raman Spectra of Polyatomic Molecules, Van Nostrand, London(1945).

43. Carter, J.L., Yates, D.J.C., Lucchesi, P.J., Elliott, J.J., and Kervorkian, V., J. Phys. Chem., 70, 1126(1966).

44. Huang, Y.Y., and Mainwaring, D.E., J. Chem. Soc. Chem. Comm., 584(1974).

45. Pichat, P., J. Phys. Chem., 79, 2127(1975).

46. Eichens, R.P., and Pliskin, W.A., Advan. Catal. Relat. Subj., 1(1958).

CHAPTER VII

INFRARED STUDIES OF THE ISOMERIZATION OF CYCLOPROPANE OVER ZINC, NICKEL AND COPPER EXCHANGED TYPE A ZEOLITES

I. Introduction

The skeletal isomerization of cyclopropane to propene is a widely used test reaction in studying the catalytic activity of oxides[1-7] and zeolites[8-14]. Most authors have reported that the isomerization of cyclopropane proceeds via a nonclassical protonated cyclic carbonium ion intermediate. Hall et al[2,7] and Larson et al[6], however, in their studies of the isomerization over silica-alumina catalysts have raised some questions as to whether the carbonium ion intermediate was formed by addition of a proton from a Bronsted site or by an abstraction of a hydride ion at a Lewis site. Flockhart et al[11] have shown that in addition to the Bronsted acid mechanism, a second mechanism, possibly involving a Lewis acid site, may be operative depending on the activation of the zeolite. George and Habgood[10] in their studies of the isomerization of cyclopropane over zeolite Y using a chromatographic pulse technique suggested the following mechanism:

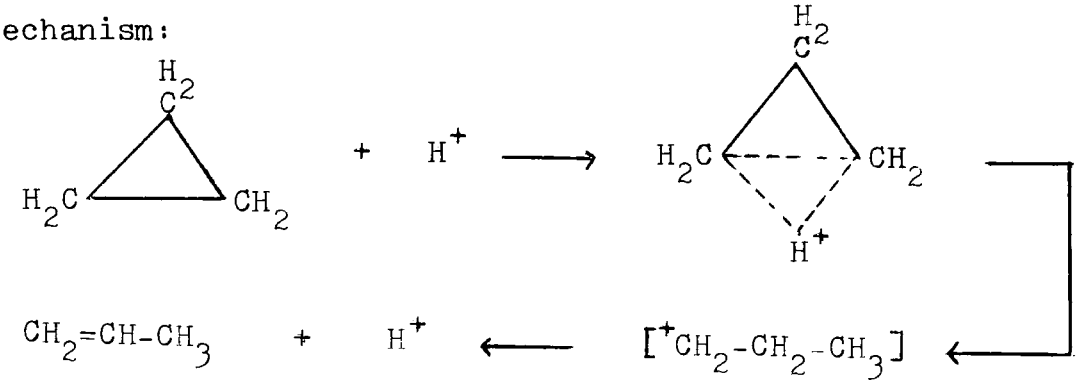

In these experiments slugs of cyclopropane were passed over NaY zeolite catalyst that was maintained in deuterated form by a low constant partial pressure of D_2O.

Tam et al[12], on the other hand, in their infrared studies

of chemisorption and reactions of cyclopropane in HY zeolite found that isobutane was the major product and suggested the following mechanism (Mechanism I):

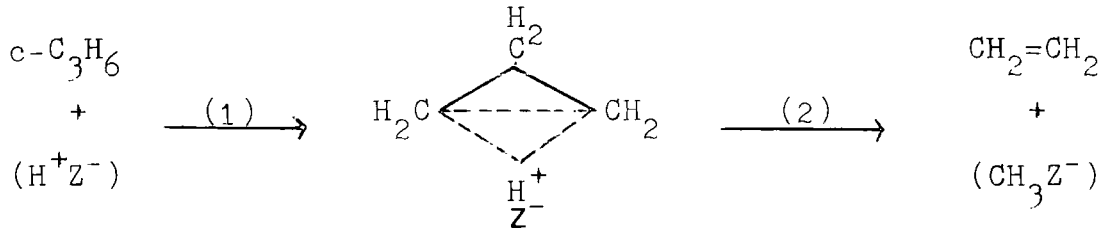

(1) cyclopropane chemisorption on acid centres

edge-protonated cyclopropane

(2) splitting (cracking) reaction

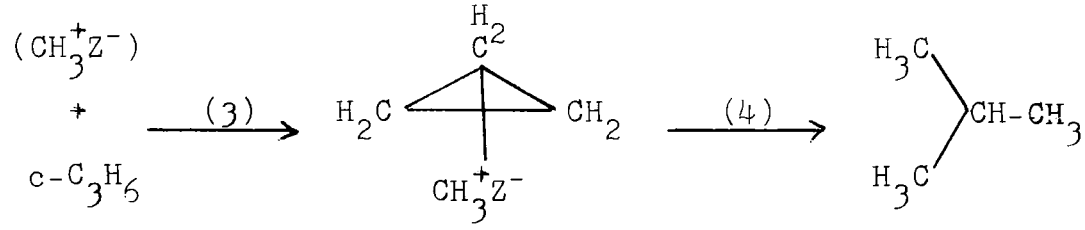

(3) reaction of the methyl cation with cyclopropane

chemisorbed methyl cyclopropane cation

(4) Formation of isobutane with regeneration of the acid centre

According to Tam et al[12], edge-protonated cyclopropane could be produced from propene by the following reaction sequence (Mechanism II):

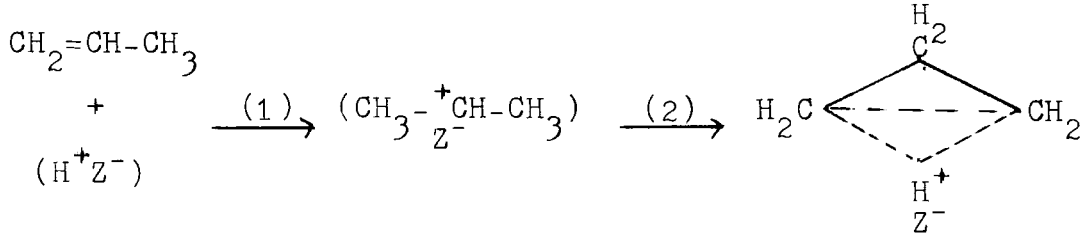

(1) propylene chemisorption

classical propyl cation

(2) Formation of edge-protonated cyclopropane

and following this the protonated cyclopropane reacts as indicated in Mechanism I.

On the basis of the above mechanism it was expected that the ν(C-H) of ethylene should have been observed but the authors[12] explained that the ethylene formed may well

have been removed during the evacuation of the excess cyclopropane in the gas phase.

Kiricsi et al[13] have carried out experiments on the skeletal isomerization of cyclopropane in a static reactor over NaY, CaNaY and HNaY. They disagree with the findings of Tam et al[12] that the production of isobutane from cyclopropane over acidic zeolite catalyst, follows mechanism I. Kiricsi et al agree that isobutane is only one, though major, representative of a more complex reaction mixture formed from propene as an intermediate of cyclopropane isomerization, and suggested that the isomerization occurs by the oligomerization-isomerization-cracking process.

Recently, Forster and Seebode[15] applied infrared spectroscopy to a study of the sorption and isomerization of cyclopropane in type A zeolites. They deduced that the cyclopropane was sorbed 'face-on'; that is the cation is bonded to the centre of the cyclopropane ring. The absence of reaction by-products and of Bronsted sites in type A zeolites led them to propose the following: the cations act as Lewis acids polarizing the electron density of cyclopropane thus activating the sorbed molecules for isomerization. This concept is called carboniogenesis and the Linde group[16,17] has proposed it to be one of the factors for catalytic activity where the cation themselves are carboniogenic centres.

The isomerization of cyclopropane to propene[8] is also a water promoted reaction. Bassett and Habgood[8] have demonstrated that water promotes the isomerization of cyclopropane over NaX zeolite. Other water promoting reactions have been observed by Gourisetti et al[18,19] in the

dehydration of tert-butanol over CaX zeolite. Maximum activity was observed when the number of water molecules equaled the number of zeolitic calcium cations. A promoting role for water has been observed in numerous reactions over silica-alumina[20].

Although water is a promoter, it can effectively screen cation fields (i.e. by solvation), and thus modify the magnitude of the fields accessible to reactants. In an extreme case, a catalytically inactive, fully hydrated zeolite would result[18,19].

In the present work we report studies of the isomerization of cyclopropane over partially exchanged zinc, nickel and copper type A zeolites. The purpose of this work was to observe the effect of the degree of hydration and the presence of different cations on the rate of isomerization. It was also hoped that insight to the mechanism of isomerization would be obtained and that the controversy as to the mechanism of cyclopropane isomerization in zeolites would be resolved.

II. Structure of zinc, nickel and copper exchanged type A zeolites

(a) Hydrated zinc exchanged type A zeolite.

Single crystal x-ray diffraction measurements of hydrated partially (Zn_5Na_2A) and fully (Zn_6A) zinc exchanged type A zeolites have been made by Seff et al[21,22]. In the structure of hydrated Zn_5Na_2A, the five zinc(II) ions were located at three distinct crystallographic sites (see figures 7.1 and 7.2). One zinc(II) ion was located at the centre of the sodalite unit (SU) and was octahedrally coordinated by six water molecules, at distances 2.11Å. Three zinc(II) ions lie on three fold axes just inside the large cavity (S2*) and are distributed among the eight equivalent positions in this equipoint. Each of these ions was tetrahedrally coordinated to three framework oxygens (Zn - O = 2.25(1)Å) and one hydroxide ion (probably not a water molecule; Zn - O = 2.19(6)Å). The fifth zinc(II) ion liy deep within the large cavity (S4) and was octahedrally coordinated by six water molecules. Finally, each of the two sodium ions were associated with 8-ring oxide ions (S1) and with two water molecules.

The zinc(II) ions in the structure of hydrated Zn_6A, like Zn_5Na_2A, were also found at three different crystallographic sites (Figure 7.3). One zinc(II) ion was found in the centre of the sodalite unit but unlike Zn_5Na_2A, the zinc(II) ion here was tetrahedrally coordinated at 1.95(5)Å to four nonframework oxygens (water molecules, some of which might have dissociated; Figure 7.4). The difference in the coordination of the zinc(II) ions at position SU for the partially (Zn_5Na_2A) and fully (Zn_6A) exchanged A zeolite was explained as being due to the tendency

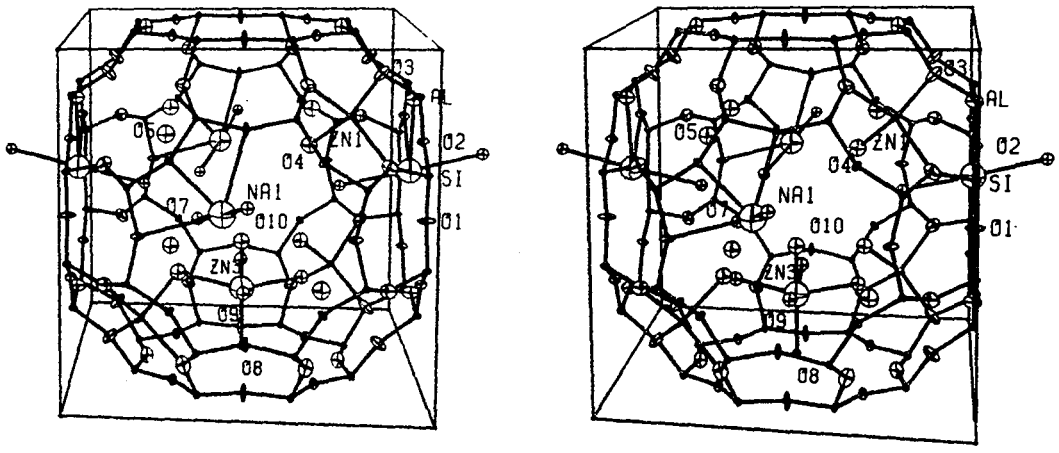

Figure 7.1. A stereoview of hydrated Zn_5Na_2A after Seff et al[21]. Ellipsoids of 20% probability are shown.

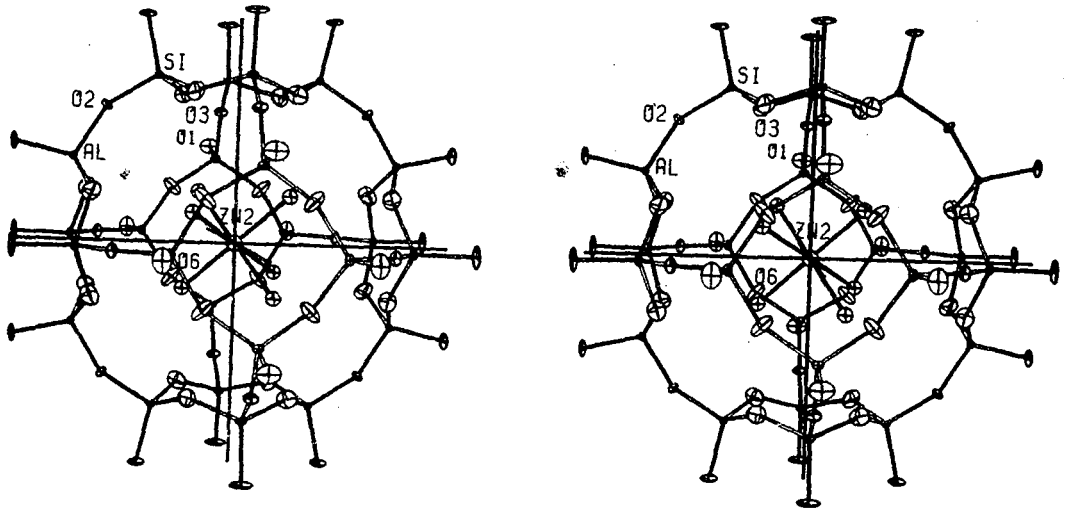

Figure 7.2. A stereoview of the octahedral coordination about the ion Zn(2) in the sodalite cavity. Ellipsoids of 20% probability are shown[21]. Zn(1), Zn(2) and Zn(3) refer to sites S2*, SU and S4 respectively in the text.

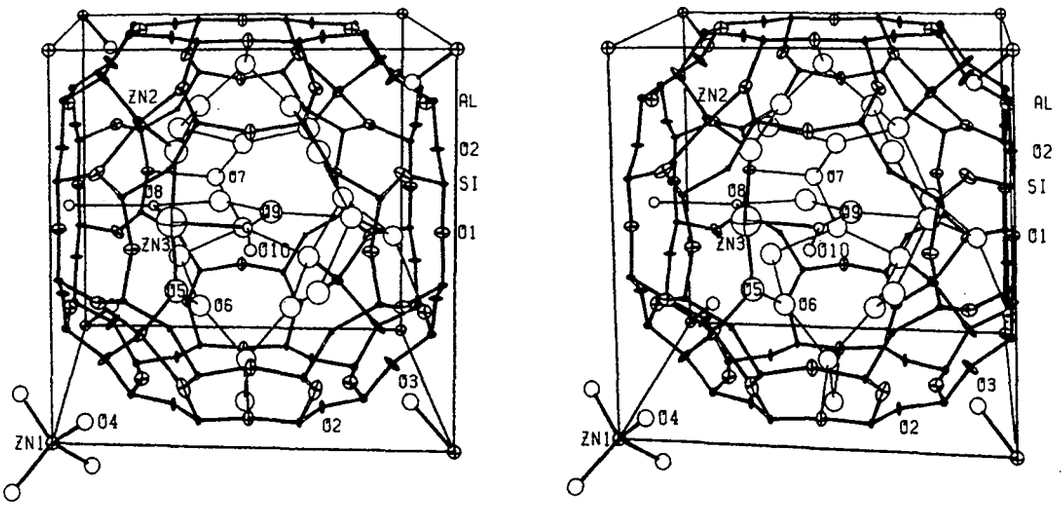

Figure 7.3. Stereoview of the large cavity of hydrated Zn_6A after Seff et al[22]. Ellipsoids of 20% probability are shown.

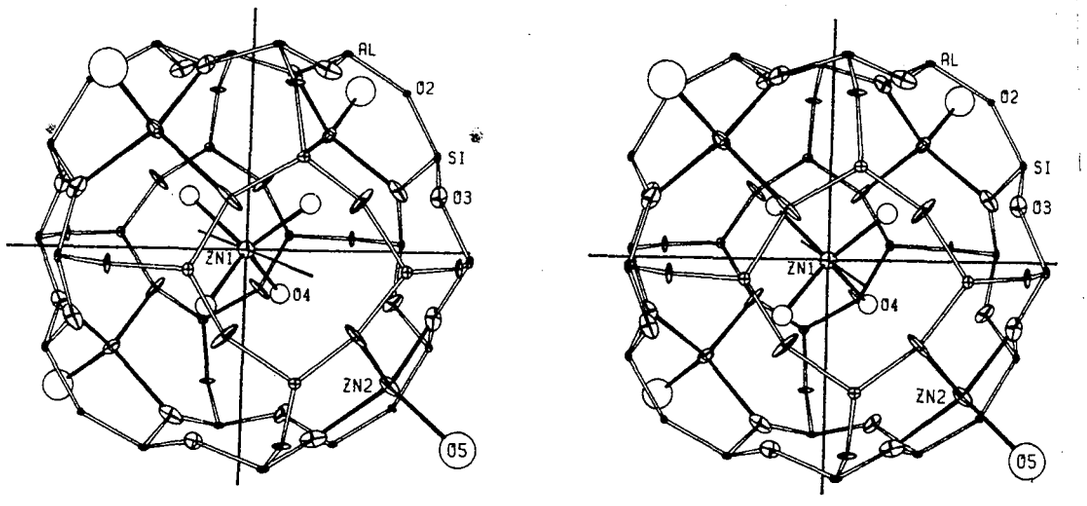

Figure 7.4. Stereoview of the sodalite unit of hydrated Zn_6A. Ellipsoids of 20% probability are used[22]. Zn(1), Zn(2) and Zn(3) refer to sites SU, S2* and S3 respectively in the text.

of zinc(II) ions to hydrolyse coordinated water molecules, to produce $ZnOH^+$ and H^+ ions. This tendency being enhanced in the fully exchanged zinc(II) A zeolite. The combination of an unfavourable environment in the sodalite unit for a hexaquo zinc ion and the increasedlikelihood that hydrolysis will occur (perhaps to form a neutral $Zn(OH)_2(H_2O)_2$ species in the sodalite unit) may cause the coordination number of the zinc(II) ion at position SU to decrease as the number of zinc(II) ions increased.

Four more zinc(II) ions were located on three-fold axes and entend into the large cavity (S2*), where each is coordinated to three oxygens of a 6-ring and to one non-framework oxygen deeper in the large cavity in a tetrahedral manner. The sixth and final zinc(II) ion was located also in the large cavity but opposite a 4-ring of the zeolite framework (S3) and was a long distance (3.8Å) from the nearest framework oxygens. If the distant framework oxygens were considered to be a single weak ligand, this cation (at site S3) has approximate trigonal bipyramidal geometry. The axial oxygen ligands were probably OH^- of hydrolyzed water molecules bridging between this cation (at site S3) and the 6-ring zinc(II) ions (S2*) and the two equatorial ligands were water molecules which hydrogen bond to the non-framework oxygens. Here again, the coordination of the cation was different from the partially exchanged zinc (Zn_5Na_2A) type A zeolite which was octahedrally coordinated. The authors[22] suggested that the two nonframework oxygens bridging between the two 6-ring zinc(II) ions (S2*) and this two-fold axis zinc(II) ion (S3) were hydroxyls of dissociated water molecules and that a zinc(II) ion would prefer a site where it could coordinated to two bridging hydroxyls over

one where it could coordinated to water molecules only.

(b) Dehydrated zinc exchanged type A zeolite.

The partially and fully exchanged zinc(II) ions in type A zeolites were dehydrated, under vacuum, for 48 hours at 623K[21] and 873K[22], respectively. In the dehydrated Zn_5Na_2A zeolite, zinc(II) ions were found at two sites on three-fold axes, one on each side of the 6-rings. Three zinc(II) ions were located inside the large cavity (S2*) and were tetrahedrally coordinated by three framework oxide ions and one water molecule. The remaining two zinc(II) ions were bridged by a single water molecule within the sodalite unit (S2').

An additional x-ray study has been carried out on Zn_5K_2A, dehydrated for 44 hours at 673K[23]. Here the five zinc(II) ions occupy three kinds of sites, all on the unit cell three-fold axes, near the centres of 6-rings. Of these ions, one lies in the sodalite unit (S2') and the Zn^{2+} is coordinated to an oxygen atom of a water molecule or an OH^- ion (Zn - O = 2.2(1)Å). This cation assumed an approximately tetrahedral coordination sphere as shown in figures 7.5 and 7.6. 1.5 zinc(II) ions lie very close to the 6-ring planes (S2) and achieved a near trigonal-planar coordination (Figure 7.5). The remaining 2.5 zinc(II) ions were located near the 6-rings but recessed into the large cavity (S2*). Each of these zinc(II) ions was associated with an oxygen atom of a water molecule or an hydroxyl ion, which was located farther into the large cavity and assumed an approximately tetrahedral coordination (see figures 7.5 and 7.6).

Zinc(II) ions exchanged in zeolite A tend to hold coordinated water oxygen atoms (presumably as H_2O or OH^-) more tenaciously than do manganese(II)[24,25] or cobalt(II)[26].

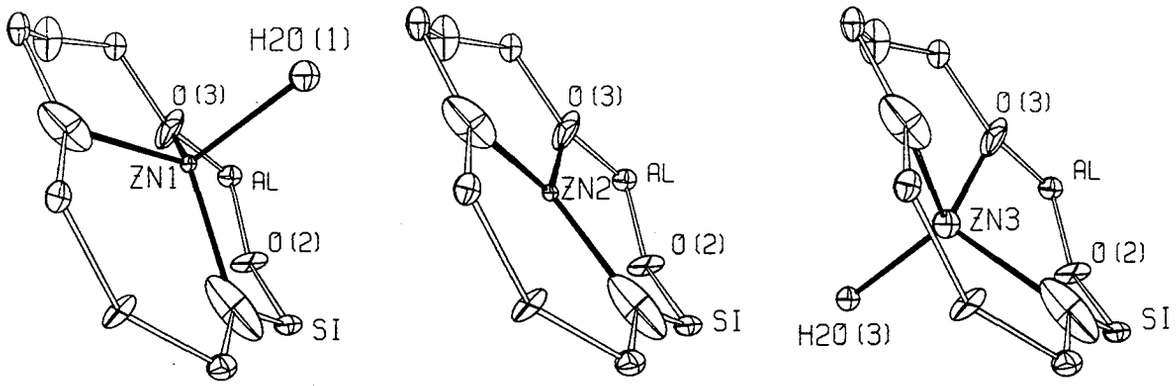

Figure 7.5. The sitings of the three non-equivalent zinc(II) ions, each in its respective 6-ring, are shown[23]. Ellipsoids of 50% probability are used. Zn(1), Zn(2) and Zn(3) refer to sites S2', S2 and S2* respectively in the text.

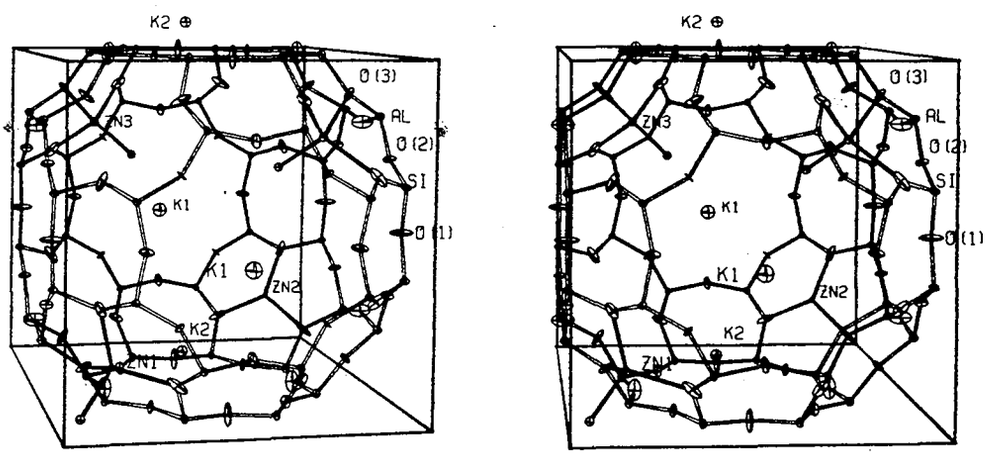

Figure 7.6. A stereoview of the unit cell is shown. Ellipsoids of 20% probability are used[23]. K1 and K2 refer to sites S1 and S1* respectively in the text.

Zeolite A partially exchanged with manganese(II) or cobalt(II) ions has been found by the same authors to be fully dehydrated after evacuation at 623K (Chapter VIII). This difference in behaviour was explained by the authors[21,23] as being due to the ability of the cation to dissociate H_2O to give OH^- ions coordinated to Zn^{2+}, and H^+ ions coordinated to the zeolite framework.

In the dehydration of fully exchanged zinc(II) A zeolite[22], all of the cations were located on three-fold axes and were distributed over two sites. A stereoview of the sodalite unit of Zn_6A is shown in figure 7.7. Two zinc(II) ions were located in the sodalite cage (S2'), each associated with three framework oxygens and one nonframework oxygen deeper in the sodalite cage in a distorted tetrahedral arrangement. The remaining four zinc(II) ions were almost in the planes of the 6-rings (S2) where each was coordinated in a trigonal-planar manner to three framework oxygens.

There were no major differences in the dehydrated Zn_5Na_2A and Zn_6A structures. In both cases, the zinc(II) ions were located on three-fold axes and have either trigonal planar or tetrahedral geometries. Zn_5Na_2A contained 3.5 water molecules per unit cell while Zn_6A, only 2 after dehydration.

(c) Hydrated nickel exchanged type A zeolite.

A single crystal x-ray analysis of the structure of hydrated partially exchanged nickel(II) A zeolite (Ni_3Na_6A) has been carried out by Seff et al[27]. The u.v. reflectance spectrum of hydrated $Ni_{1.7}Na_{8.6}A$ was obtained by Klier et al[28] and the magnetic properties of hydrated $Ni_{3.7}Na_{4.6}A$ studied by Egerton and Vickerman[29].

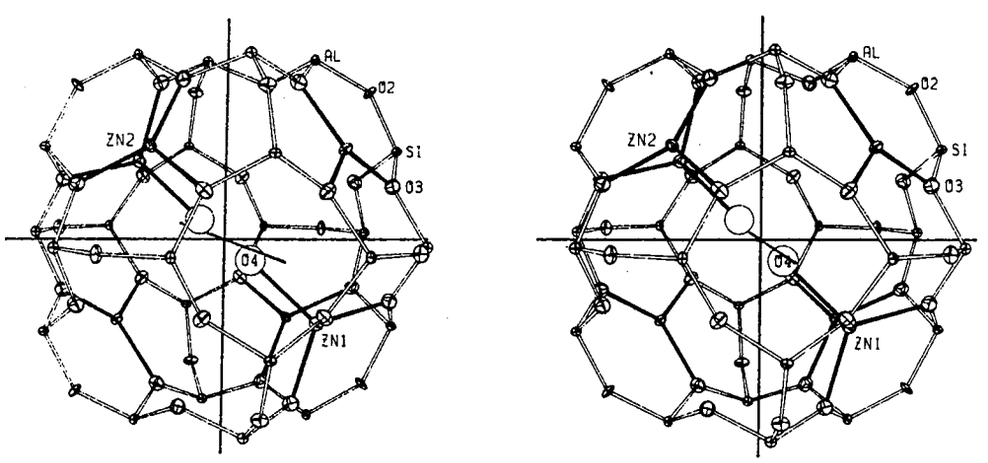

Figure 7.7. A stereoview of the sodalite unit of Zn_6A evacuated at 873K and 10^{-6} torr[22]. Ellipsoids of 20% probability are shown. Zn(1) and Zn(2) refer to sites S2' and S2 respectively in the text.

From the single crystal analysis of the structure of hydrated Ni_3Na_6A [27], the three nickel(II) ions were located in threefold axes deep within the large cavity (S2*). Each of these nickel(II) ions was six coordinate; having three water molecules, at 2.29(7)Å which extended further into the large cavity, and three oxide ions (probably OH^- groups) which bridged between nickel(II) and (Si,Al). As a result, the equivalent number of (Si,Al) ions, probably Al^{3+}, have increased their coordination number to five.

Only four of the six sodium ions were located, and they were along threefold axes near the planes of 6-rings (S2). Each Na^+ has coordinated to it one water molecule deep in the large cavity and one in the sodalite unit. The water in the sodalite unit also hydrogen bonds to framework oxygens.

The u.v. reflectance spectrum of hydrated $Ni_{1.7}Na_{8.6}A$ taken by Klier and Ralek[28] matched the spectrum of $Ni(H_2O)_6$ complex indicating that nickel(II) ions was octahedrally coordinated by zeolitic water. Egerton and Vickerman's findings from their magnetic susceptibility measurements of hydrated $Ni_{3.7}Na_{4.6}A$ [29], also agrees with the findings of Seff et al[27] and Klier and Ralek[28].

(d) Dehydrated nickel exchanged type A zeolite

It was found that, depending upon the number of the nickel(II) ions in the zeolite, dehydrating nickel exchanged type A zeolite leads to breakdown of the structure[29-32]. Gal et al[31] has reported that dehydration of partially nickel(II) exchanged type A zeolite of composition $Ni_{4.9}Na_{2.2}A$ resulted in the destruction of the zeolite structure at temperatures just above 343K, as evidenced by x-ray diffraction and differential thermal analysis. A similar instability was observed by

Egerton and Vickerman[29] for $Ni_{3.7}Na_{4.6}A$ during an investigation of the magnetic properties of nickel(II) exchanged A, Y, and X zeolites. For $Ni_{1.3}Na_{9.4}A$[32], $Ni_{1.7}Na_{8.6}A$[28] and Ni_2Na_8A [30], dehydration for 10 hours at 703, 603 and 623K resulted in no loss in crystallinity. It will be shown later (in section VII(a)) that the structure of the $Ni_{2.2}Na_{7.6}A$ used in our work is not destroyed even after dehydration for 40 hours at 723K.

Klier and Ralek[28], from their studies of the u.v. reflectance spectrum of $Ni_{1.7}Na_{8.6}A$ showed that after partial dehydration and with only one water molecule per nickel(II) ion, a stable complex was formed in which the nickel(II) ion was partially coordinated to the aluminosilicate skeleton. The colour of the zeolite at this stage was pink (The colour of hydrated nickel exchanged A zeolite was light green). On further dehydration, this complex was destroyed and the zeolite turned yellow. Since the water content of this yellow zeolite was zero, the spectrum was attributed to fully dehydrated $Ni_{1.7}Na_{8.4}A$ zeolite in which the nickel(II) ions were fully coordinated to the aluminosilicate skeleton. Further, these nickel(II) ions were easily accessible to adsorbing molecules, which suggested that they were located in the planar coordinated hexagonal sites. Their actual geometry D_{3h} (or D_{6h}) is shown in figure 7.8.

(e) Hydrated copper exchanged type A zeolite

There are no single crystal x-ray data on the structure of hydrated copper exchanged type A zeolite. Ichikawa and Kevan[33] in their electron spin modulation study of hydrated CuNaA (less than 0.28% exchanged) zeolite located the copper(II) io at site S2 where it was coordinated to two water molecules, one located in the α-cage and the other in the β-cage (Figure

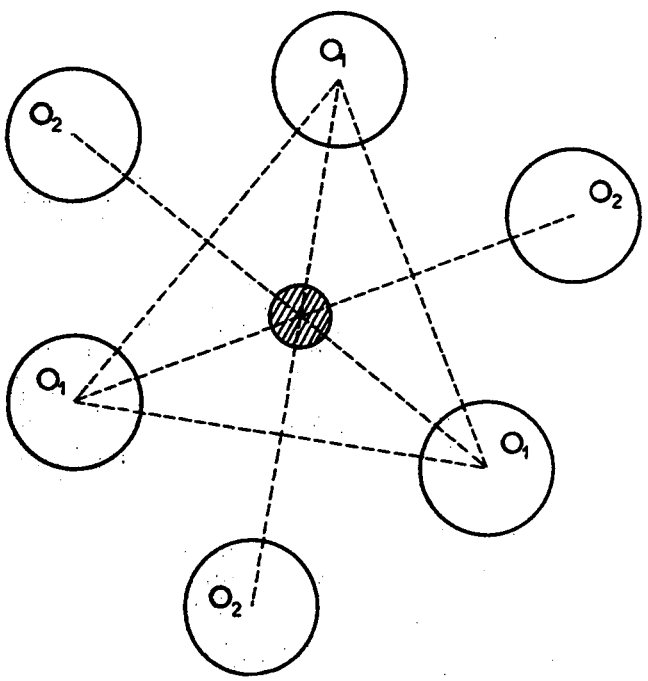

Figure 7.8. Geometry of nickel at the hexagonal site $(S2)^{28}$.

7.9 (a)). In this position the copper(II) ion interacted with three oxygen atoms in the 6-ring.

In another electron spin echo modulation study of copper(II) ions in Cs_7Na_5A, Narayana and Kevan[34] found that two caesium ions at SI left on entry of each copper(II) ion, which then displaced a sodium ion from S2 to one of the two newly emptied sites. Figure 7.9(c) shows the possible location of the copper(II) ion relative to a hexagonal window. The copper (II) ion was located on a threefold axis (S2') presumably, coordinated to a water molecule inside the β-cage.

(f) Dehydrated copper exchanged type A zeolite

On dehydrating CuNaA at 673K, Ichikawa and Kevan[33] found that the copper(II) ion at S2 in the hydrated sample migrated along the axis of a hexagonal face in the β-cage (S2') as shown in figure 7.9(b). At this position the cupric ion interacted more weakly with the aluminium atoms in the 6-ring. In contrast to this result, Narayana and Kevan[34] found on dehydration at 323 or 373K, that the water molecule inside the -cage was removed and the copper(II) ion moved along the threefold axis into the α-cage($S2^*$) as shown in figure 7.9(d).

Lee and Seff[35] have investigated the structures of four desolvated fully copper exchanged type A zeolite crystals by using x-ray diffraction. The crystals were each evacuated at 5×10^{-6} torr and desolvated as follows: crystal 1, 623K for 48 hours; crystal 2, 623K for 48 hours and then exposed to 300 torr of O_2 at 623K for 2 hours, followed by evacuation at 623K for 2 hours; crystal 3 723K for 48 hours; and crystal 4, 773K for 120 hours.

In crystal 1, five Cu^{2+} ions, one Cu^+ ion, and a Cu^+-OH^--Cu^+ group were located in a unit cell of approximate composition

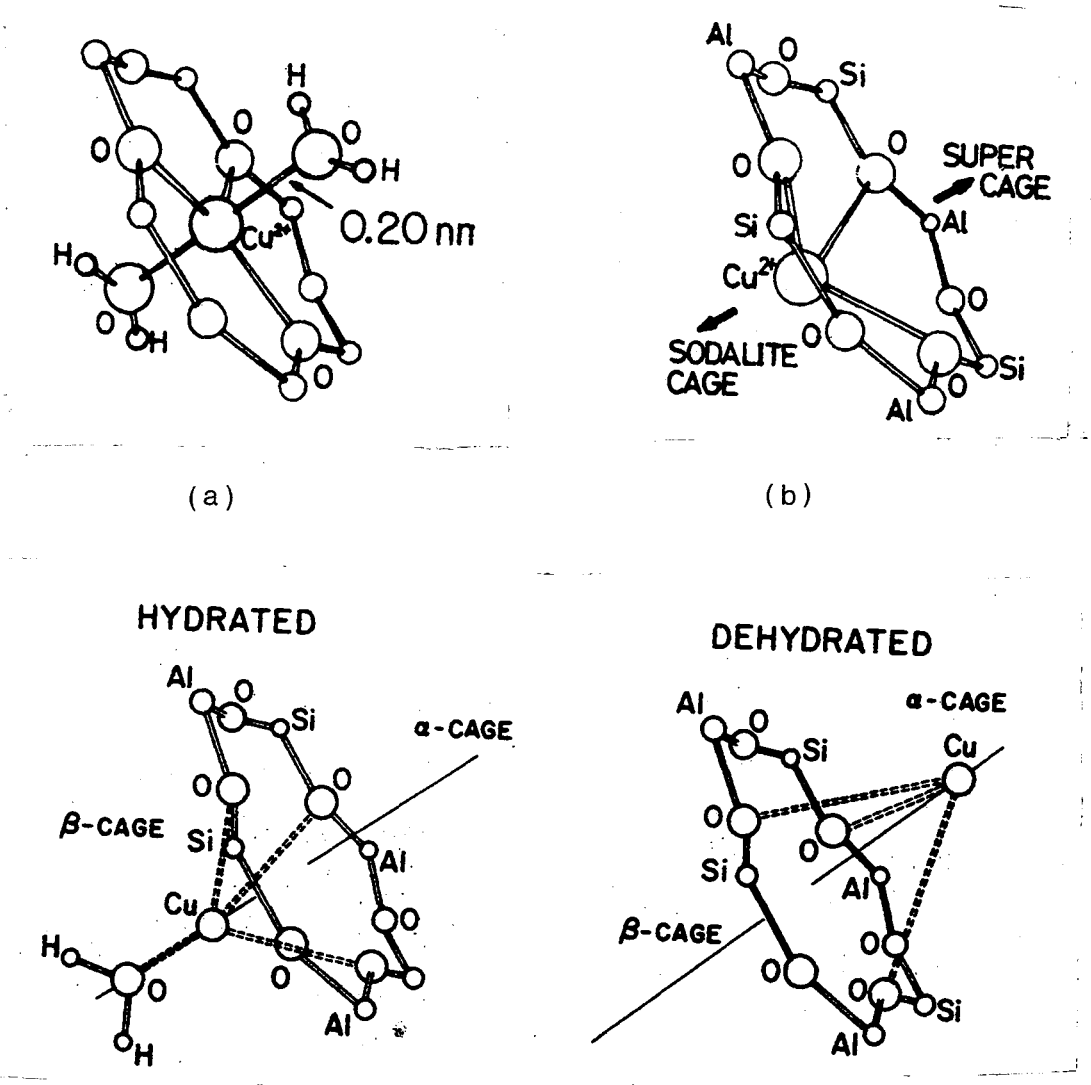

Figure 7.9. (a) Hydrated copper(II) ion in CuNaA[33];
(b) Dehydrated copper(II) ion in CuNaA[33];
(c) The location of copper(II) ions with respect to the hexagonal window between the α- and β-cages of type A zeolite in hydrated Cs_7Na_5A[34] and,
(d) in dehydrated Cs_7Na_5A[34].

$(Cu^{2+})_5 (Cu^{+})_3 OH^{-} Si_{12} Al_{12} O_{48}.XH_2O$ (refer Figure 7.10). The five Cu^{2+} ions were located in the threefold axes in the planes of the 6-rings (S2) where each of these Cu^{2+} ions was coordinated to three framework oxygens (Cu^{2+}-O=2.11(1)Å). Four of these Cu^{2+} ions have trigonal coordination while the remaining one appeared to have trigonal pyramidal or even trigonal bipyramidal coordination. Another ligand (unlocated) occurs on the threefold axis in the large cavity.

One Cu^{+} ion was located on the threefold axis but recessed 1.27Å into the large cavity ($S2^{*}$). This ion was coordinated to three framework oxygens and to an OH in a near tetrahedral manner.

Two Cu^{+} ions were located in the large cavity of the zeolite, on twofold axes and opposite 4-rings (S3). These two Cu^{+} ions were bridged by an OH oxygen to form Cu^{+}-OH^{-}-Cu^{+} or Cu^{+}-O^{2-}-Cu^{+} group with its angle (Cu-O-Cu) calculated to be 89(8)°.

It was not clear how Cu^{+} came to be in crystal 1. The authors[35] suggested that the Cu^{+} ions may arise from the reduction of Cu^{2+} in solution by excess ammonia at 373K, or may have resulted from the reduction of over-exchanged Cu^{2+} ions by residual solvent molecules upon evacuation.

Dramatic changes were observed in the positions of copper ions in crystal 2 compared with crystal 1. Here again eight copper ions were located and all of them were Cu^{2+} ions indicating that the three Cu^{+} in crystal 1 have been oxidized to Cu^{2+} in crystal 2. Of these, five Cu^{2+} ions were found to occupy nearly the same position as in crystal 1 (S2). Each of these Cu^{2+} ions was coordinated to three framework oxygens (Cu^{2+}-O=2.146(5)Å) and two of them coordinated further at 2.6(1)Å to OH in the

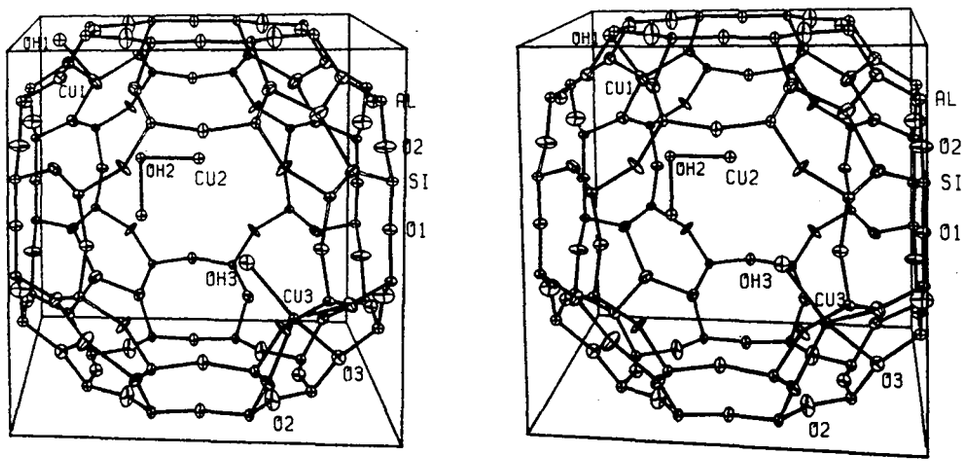

Figure 7.10. Stereoview of the large cavity of $(Cu^{2+})_5(Cu^{+})_3OH^{-}A$ desolvated at 623K[35]. Ellipsoids of 20% probability are shown. Cu(1), Cu(2) and Cu(3) refer to sites S2, S3 and S2* respectively in the text.

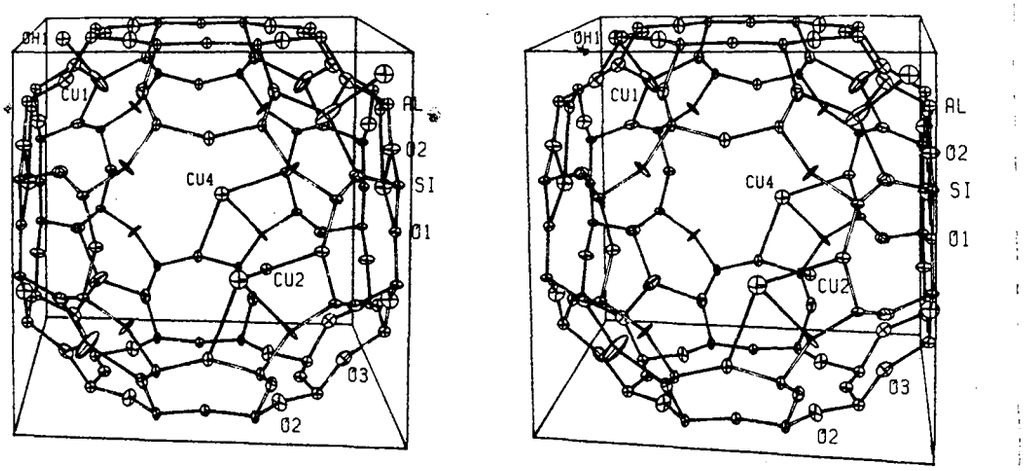

Figure 7.11. Stereoview of the large cavity of $(Cu^{2+})_8(OH^{-})_4A$ desolvated at 723K and then exposed to O_2[35]. Ellipsoids of 20% probability are shown. Cu(1), Cu(2) and Cu(4) refer to sites S2, S3 and S1 respectively in the text.

sodalite unit.

One Cu^{2+} ion was located on a twofold axis opposite a 4-ring (S3) with Cu^{2+}-O distance of 4.0Å. This Cu^{2+} ion would be the bridged species Cu^{2+}-OH-Cu^{2+} or Cu^{2+}-O^{2-}-Cu^{2+}, and since there was only one Cu^{2+} ion located at this position per unit cell, this pair of Cu^{2+} ions can exist only in alternate unit cells.

Two other Cu^{2+} ions were located in the planes of the 8-rings but off their centres (S1). Figure 7.11 shows the stereoview of the large cavity of crystal 2^{35}.

On desolvating at higher temperatures (723 and 773K), the copper species rearrange further (Crystals 3 and 4). Approximately eight copper ions per unit cell were located in crystal 3 while only six were found in crystal 4.

The copper ions occupied five crystallographic sites in crystal 3, and of these five positions, three were identical to crystal 1(S2, S2* and S3). Five Cu^{2+} ions were located on a threefold axis (S2) and coordinated to three framework oxygens (Cu^{2+}-O=2.15(1)Å). One of these five Cu^{2+} ions was found to coordinate to a residual solvent anion, OH^- at 2.3(1)Å. One Cu^+ ion was located at site S2* and two Cu^+ ions at sites S3. These Cu^+ ions at sites S3 could either be Cu^+-OH^--Cu^+ or Cu^+-O^{2-}-Cu^+ as in crystal 1.

It was found that there were fewer of the Cu^+ ions in crystal 3 than in crystal 1. The depopulation of the copper ions at sites S3 and the appearance of two copper ions at sites SU (in the sodalite unit) indicate that small reduced copper clusters were produced by desolvation at elevated temperature (see Figure 7.12). The distance between these copper ions was found to be 2.49(11)Å, a distance similar to the Cu^o-Cu^o distance of 2.56Å in copper metal. It was suggested

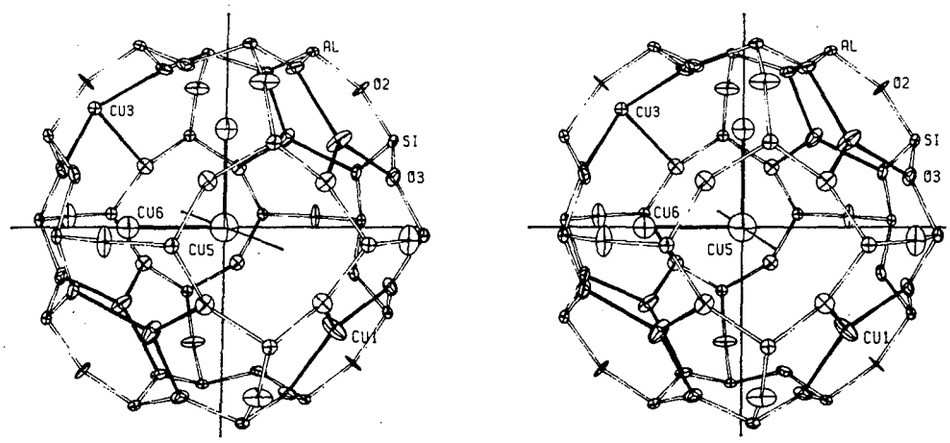

Figure 7.12. Stereoview of the sodalite unit of $(Cu^{2+})_5(Cu^{+})_{2.5}(Cu^{o})_{0.5}(OH^{-})_{0.5}A$ desolvated at 723K[35]. Ellipsoids of 20% probability are shown. Cu(1), Cu(3), Cu(5) and Cu(6) refer to sites S2, S2* and SU in the text.

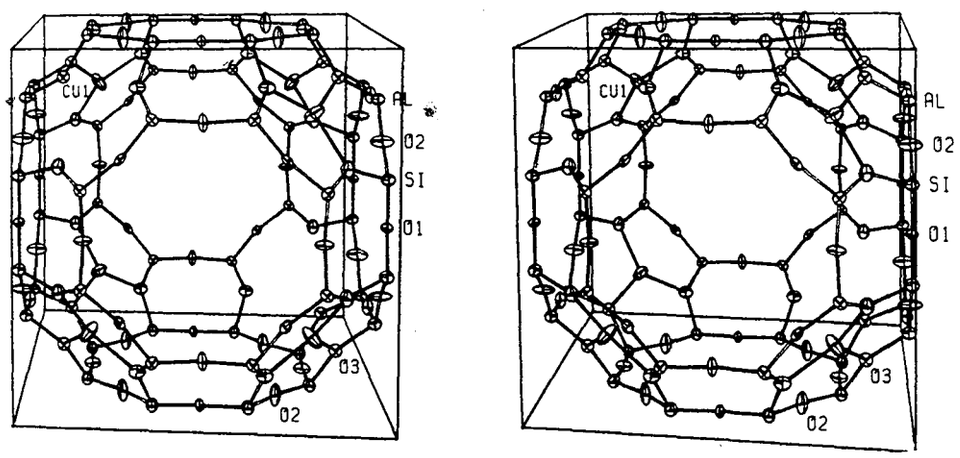

Figure 7.13. Stereoview of the large cavity of Cu_6A desolvated at 773K[35]. Ellipsoids of 20% probability are shown. Cu(1) refers to site S2 in the text.

that triatomic copper clusters have formed in a fraction (one out of four) of the sodalite units. By comparison with H_3^+, the cluster was thought to be bent with an acute angle.

The six Cu^{2+} ions found in crystal 4 were located on threefold axes very near 6-ring planes (S2) and each of these ions was coordinated to three framework oxygens as shown in figure 7.13 (Cu^{2+}-O=2.14(4)Å). Approximately two copper ions per unit cell had migrated to the surface of the crystal. The framework was unusually strained because the six Cu^{2+} ions were strongly bonded to framework oxygens.

III. Single crystal x-ray determinations of cyclopropane adsorbed onto partially Co(II) and Mn(II) exchanged A zeolites

The single crystal x-ray structures of cyclopropane sorption complexes of partially Co(II) (Co_4Na_4A) and Mn(II) (Mn_4Na_4A) exchanged zeolite A have been determined by Seff et al[36]. The positions of the Co(II) and Mn(II) ions in zeolite A will be discussed in Chapter VIII.

Upon addition of cyclopropane to Co_4Na_4A zeolite, the Co(II) ions change their positions compared with their positions in the dehydrated zeolite. The Co(II) ions move deeper into the large cavity with a Co(II)-O distance of 2.174Å (In the dehydrated state, Co(II)-O=2.08Å). Also, the O-Co(II)-O bond angle changes from a near trigonal planar value of $117.5(1)^\circ$ in the dehydrated Co_4Na_4A, to $112.5(4)^\circ$ in the cyclopropane complex, a value closer to tetrahedral.

For packing reasons, the author[36] explained that the four cyclopropane molecules in a unit cell must be arranged tetrahedrally, close to alternate 6-ring oxygens. Since it was found that each Co(II) ion was associated with a cyclopropane

molecule, these four Co(II) ions must also be arranged tetrahedrally as shown in figure 7.14. The Co(II) to cyclopropane distance was 2.74Å indicating that the interaction was not very strong. The coordination environment of the Co(II) ion is shown in figure 7.15. Recent work involving the calculation of non-bonded atom-atom potentials, however, indicate that the minimum separation between adsorbed cyclopropane molecules in the same cage is such that the reported metal-C distances are too large[40].

The Mn(II) ions, like the Co(II) ions, also move to new positions upon complexation with cyclopropane molecules. In the dehydrated structure, the Mn(II) ions were located in the 6-rings but displaced into the sodalite cage (S2') and on complexation these Mn(II) ions move to positions S2* (Chapter II). Also, the bond angle O-Mn(II)-O changed from a near trigonal planar value of 119.6(1)° to a more tetrahedral value of 115.7(6)°. Consequently, the cyclopropane molecules, each associated with a Mn(II) ion, were therefore arranged tetrahedrally in the unit cell. A stereoview of the $Mn_4Na_4A \cdot 4C_3H_6$ is shown in figure 7.16[36].

Each Mn(II) ion retained a strong interaction with the 6-ring oxygens since there was no significant change in the Mn(II) to O distance between the complex and the dehydrated structure. As in Co_4Na_4A, each carbon atom of a cyclopropane molecule approached a Mn(II) ion equivalently (see Figure 7.17). The observed Mn(II)-C distance of 3.09(6)Å indicated that the cyclopropane interaction must be weaker than Co(II).

In neither complex was any interaction between Na^+ ions and cyclopropane molecules observed.

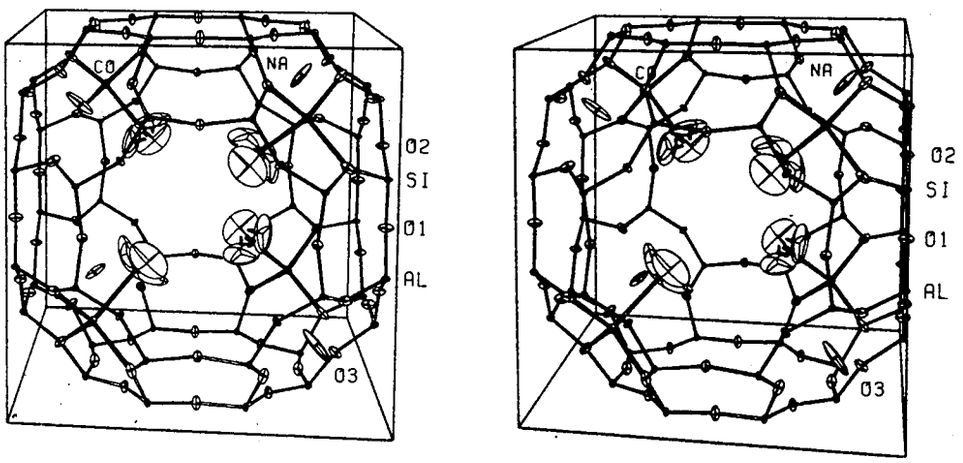

Figure 7.14. A stereoview of the $Co_4Na_4A.4C_3H_6$ unit cell. Heavy bonds indicate the approximate tetrahedral coordination about Co(II)[36]. Ellipsoids of 20% probability are shown.

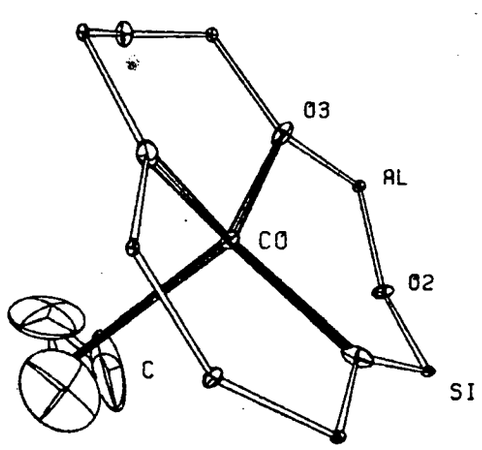

Figure 7.15. The coordination environment of the Co(II) ion[36]. Ellipsoids of 10% probability are shown.

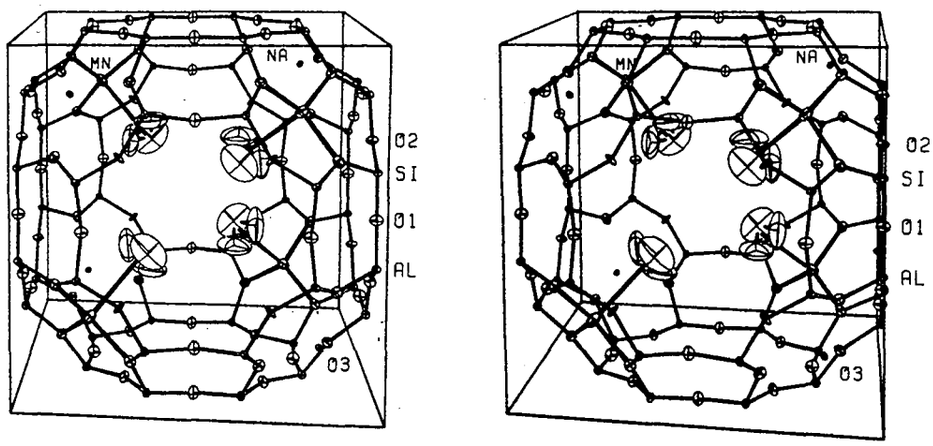

Figure 7.16. A stereoview of the $Mn_4Na_4A.4C_3H_6$ unit cell. Heavy bonds indicate the approximate tetrahedral coordination about Mn(II)[36]. Ellipsoids of 20% probability are shown.

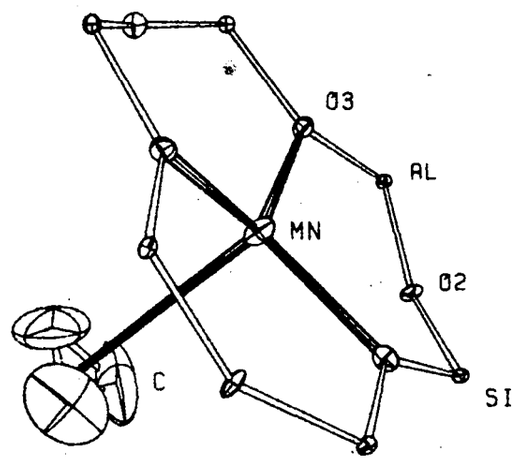

Figure 7.17. The coordination environment of the Mn(II) ion[36]. Ellipsoids of 10% probability are shown.

VI. Experimental

All the zeolites used were prepared by ion-exchanging Linde 4A (BDH) in 0.1M of MCl_2 solution (M = Zn, Ni or Cu) at room temperature for three days. After washing thoroughly with distilled water and drying in the oven (333K) overnight, the zeolites were analysed. The compositions of the zeolites were determined to be:

$$Zn_{4.8}\ Na_{2.4}\ Al_{12}\ Si_{12}\ O_{48} \cdot xH_2O$$
$$Ni_{2.2}\ Na_{7.6}\ Al_{12}\ Si_{12}\ O_{48} \cdot yH_2O$$
$$Cu_{4.6}\ Na_{2.8}\ Al_{12}\ Si_{12}\ O_{48} \cdot zH_2O$$

In the discussion that follow the above zeolites will be designated, ZnNaA, NiNaA and CuNaA respectively.

Cyclopropane (99.8%) was obtained from Matheson Limited, U.S.A., and was purified by freeze-pump-thaw technique before use. The purity was checked by infrared spectroscopy.

Sample preparation techniques were the same as described in Chapter IV. Table 7.1 summarizes the maximum bake-out temperature used, the time the samples were left at these maximum bake-out temperatures and the overpressures of cyclopropane used.

V. Results and discussion

Throughout this chapter, the region 1300-300cm^{-1} will not be considered since the samples are totally absorbing in this range.

(i) Dehydration of the samples

Figures 7.18, 7.19 and 7.20 show the spectra (1900-1300cm^{-1}) of ZnNaA, NiNaA and CuNaA zeolites, respectively, obtained at different temperatures during dehydration. The band due to the deformation mode of water (ν_2), which occurs at 1655cm^{-1}

Table 7.1 Summary of the sample pretreatment conditions and the pressure of cyclopropane used

Samples	Temperature K	Duration Hours	Pressure of $c\text{-}C_3H_6$/torr
ZnNaA	523	18	5
	653	2	10,30
	623	16	5
	623	36	5,10,50,100
	723	38	5,10
NiNaA	673	2	10,30
	723	40	5,10
CuNaA	673	2	100

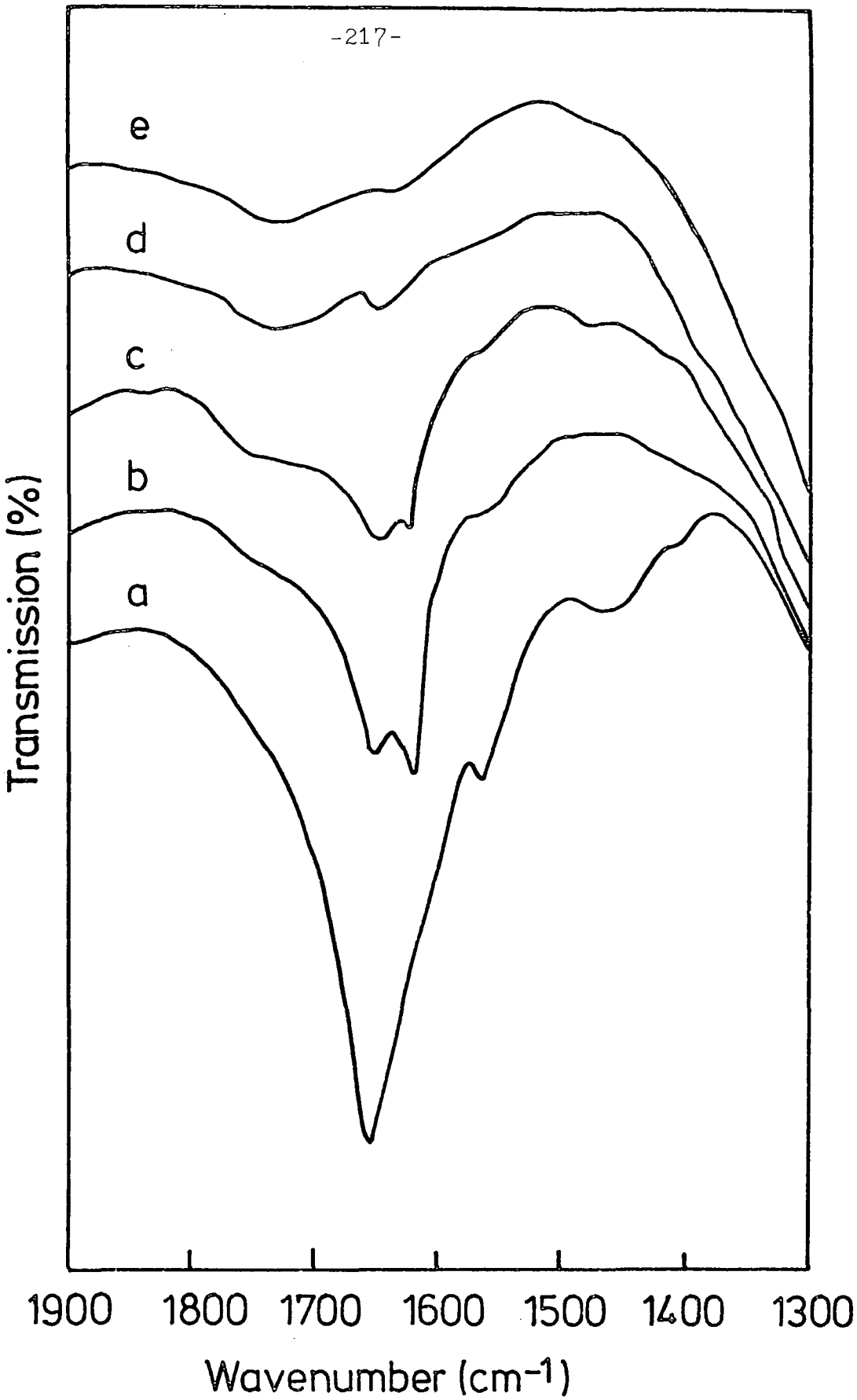

Figure 7.18. Spectra of ZnNaA zeolite obtained at various temperatures during dehydration: (a) 298K, (b) 323K, (c) 473K, (d) 523K and (e) 723K.

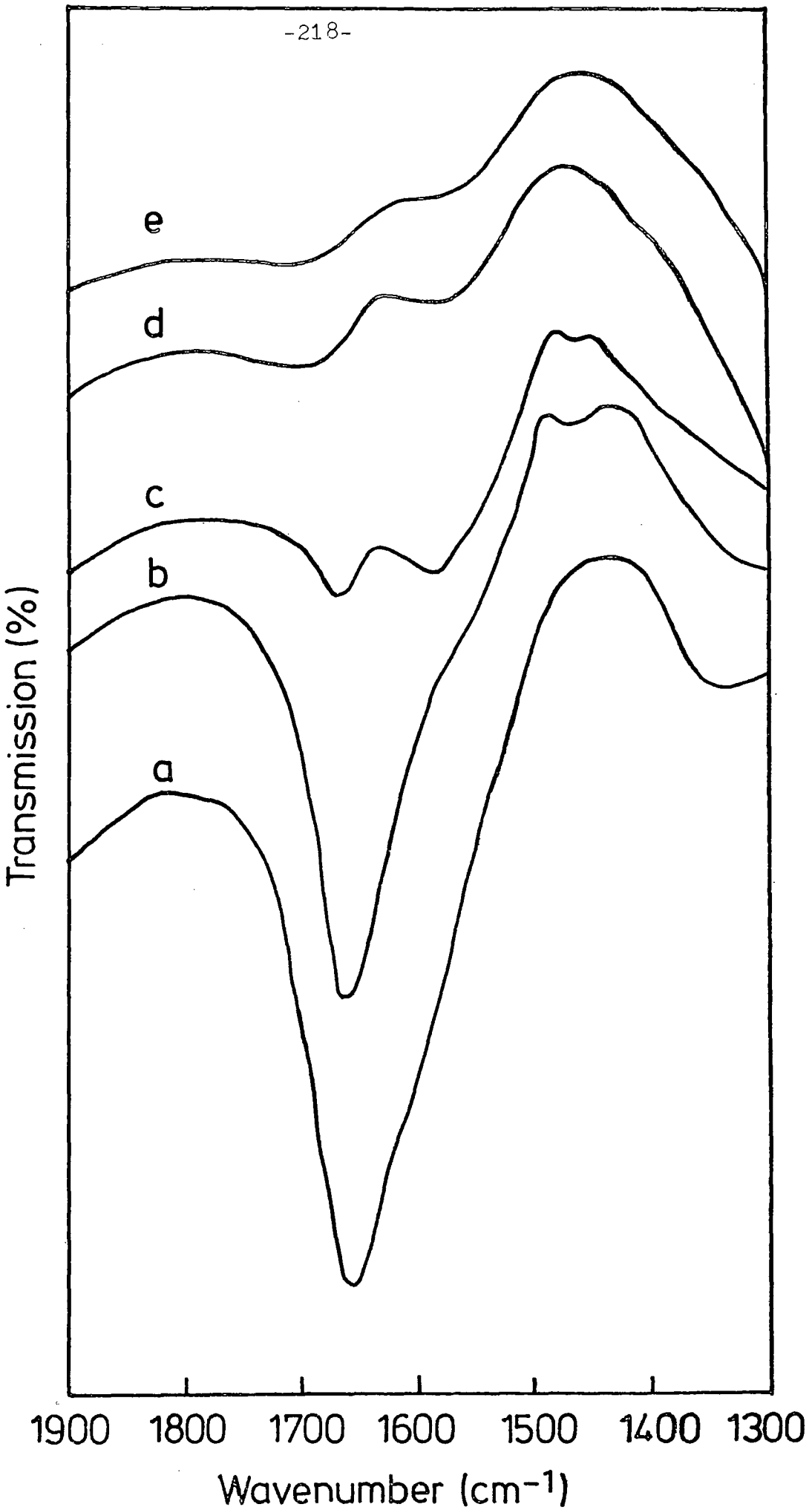

Figure 7.19. Spectra of NiNaA zeolite at: (a) 298K, (b)423K, (c) 523K, (d) 623K and (e) 723K.

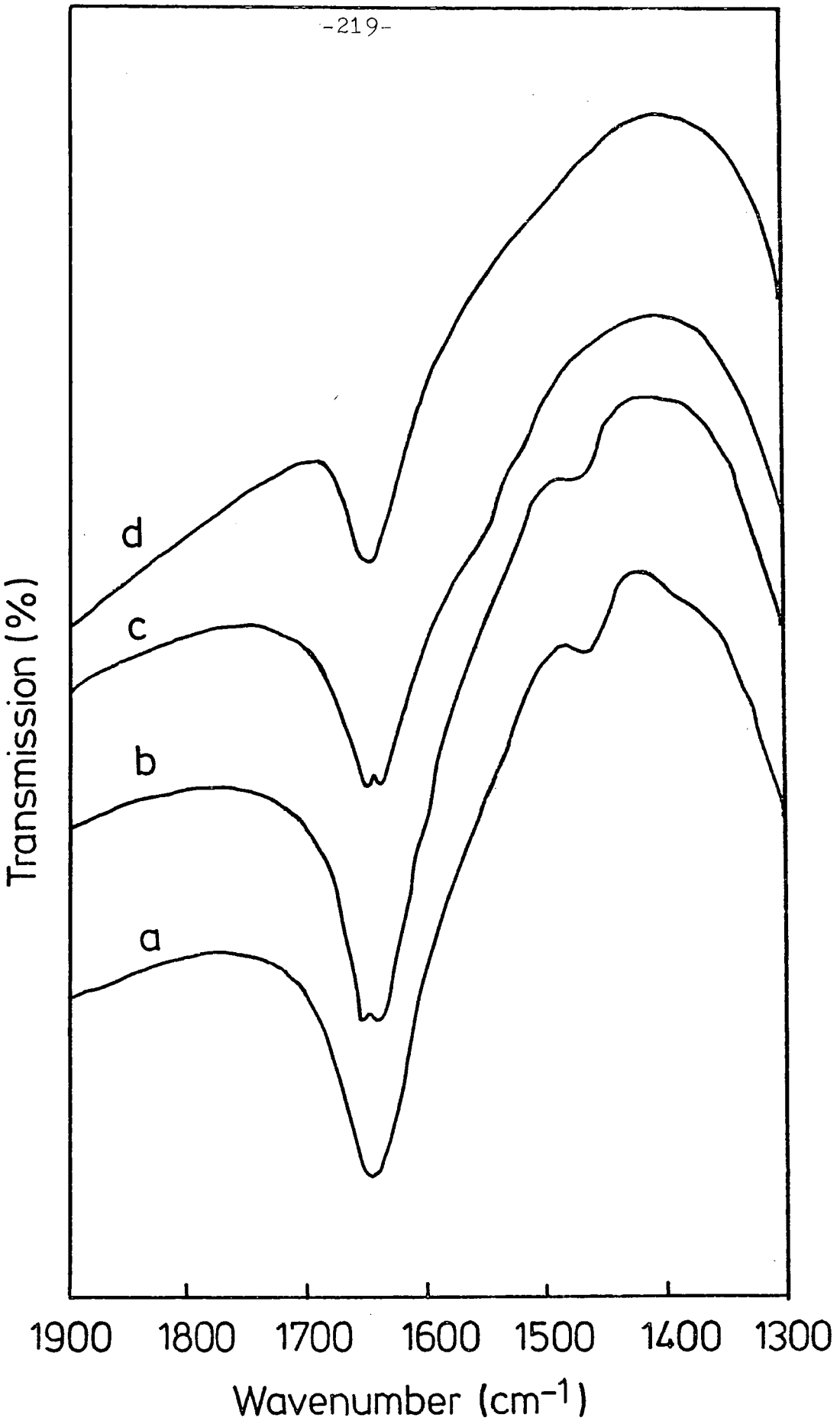

Figure 7.20. Spectra of CuNaA zeolite obtained at various temperatures during dehydration: (a) 298K, (b) 473K, (c) 573K and (d) 673K.

for ZnNaA, 1665cm^{-1} for NiNaA and 1645cm^{-1} for CuNaA decreases in intensity as the temperature is raised. In all cases, the water band reappears on allowing the sample to cool to room temperature. This band is very weak in ZnNaA and CuNaA (Figures 7.22a-7.25a and 7.36a) and very strong in NiNaA (Figures 7.33a and 7.35a). The appearance of the ν_2 band on cooling indicates either: (a) that the water has been readsorbed from the surrounding of the cell (since zeolites are sensitive to water, but this does not normally occur in our work, indicating that water was readsorbed because of the nature of the zeolite itself) or (b) that the water has been dissociated at high temperature and on cooling the sample to room temperature, water is formed again. The latter reasoning is the more probable since it is not unknown that the transition metal exchanged zeolites have a very high tendency for dissociating water molecules to OH^- and H^+ at high temperatures (Section II), forming metal hydroxides and Bronsted acids.

A band is observed at 1620cm^{-1} in the spectra of ZnNaA (Figure 7.18b and c) which could be due to the deformation mode of water coordinated to zinc[37,38]. The existence of two ν_2 of water indicates that water is present at two different sites. As was explained in section II(a), from the x-ray diffraction studies of hydrated zinc exchanged type A zeolite, aquozinc-complexes were located at two different sites, S4 and SU. We could not observe a band at 1620cm^{-1} in the spectrum of fully hydrated ZnNaA (Figure 7.18a) because the broad band of water at 1655cm^{-1} would mask it. However, at temperatures of 323 and 473K (Figures 7.18b and c), when some of the water molecules have been

removed from the zeolite cavities, the band due to another aquozinc-complexes ($1620cm^{-1}$) could be observed. As the sample was heated further, this band at $1620cm^{-1}$ disappears (Figures 7.18d and e) indicating that most of the water from the zeolite cavities has been removed.

The band observed at $1745cm^{-1}$, which becomes clearer at high temperatures (Figures 7.18d and e) after most of the water molecules in the zeolite cavities have been removed, is due either to the movement of the Zn^{2+} as the sample was heated, or; at lower temperatures (Figures 7.18a and b), this band is obscured by the broad water band at $1655cm^{-1}$.

For NiNaA, it is observed that at high temperatures (Figures 7.19d and e), there are two broad bands at 1700 and $1550cm^{-1}$ which may be due to a framework vibration associated with the cations. The band at $1550cm^{-1}$, however, could be present in the spectra of the sample at lower temperatures (Figures 7.19a, b and c) but is obscure by the broad water band at $1665cm^{-1}$.

In the spectra shown for CuNaA (Figure 7.20), the water band at $1645cm^{-1}$ (Figure 7.20a) observed at room temperature is split into two bands, at 1650 and $1635cm^{-1}$, at 473 and 573K (Figures 7.20b and c), and reverts back to a single band ($1645cm^{-1}$) at 673K (Figure 7.20d). Here again, like the ZnNaA, the presence of two ν_2 bands indicates that at temperatures 473 and 573K, water was located at two different sites. On further heating the sample to a temperature of 673K (Figure 7.20d), the water at one of the sites was removed and hence only one ν_2 is observed.

(ii) Isomerization of cyclopropane

In this section, the three different zeolites, ZnNaA, NiNaA and CuNaA will be discussed separately. The following

notations will be used in the discussion; M(a,b,c) or M(b,c) where M = Zn, Ni or Cu; a = the evacuation time (5 or 30 minutes); b = the time at which the sample was left at the maximum bake-out temperature (hours) and c = the maximum bake-out temperature (K).

In tables 7.2 and 7.3 are given literature infrared data, Raman data and assignments for cyclopropane and propene, respectively[39], while in figure 7.21 (1900-1300cm^{-1}) are shown the infrared spectra of cyclopropane (gas phase) taken at various pressures in our infrared cell (4cm path length).

Two different modes of interaction of cyclopropane with surfaces have been discussed (Table 7.4), which involve (I) 'face-on' interaction, and (II) 'edge-on' interaction of the cyclopropane with the surface. The symmetry of the free cyclopropane molecule is D_{3h} while that of the 'face-on' sorption complex in zeolites would be C_{3v} and that of the 'edge-on' complex, C_{2v}. Table 7.4 shows the correlation of the symmetries of the normal modes of gaseous cyclopropane with those of the adsorption complexes of different symmetries. From the infrared spectra of the adsorbed species, the mode of interaction of cyclopropane can be determined, since the E' mode of the free molecule (Table 7.4) will also be an E mode in the complex with C_{3v} symmetry and split to A_1 and B_2 modes in the complex with C_{2v} symmetry. The modes are all formally infrared and Raman active. Two E' modes which are strong in the infrared spectrum of the gas phase are the ν_8 (CH) and $\nu_9(CH_2)$ bands which occur at 3024 and 1432cm^{-1}. Both of these bands can be observed in the infrared spectra of cyclopropane adsorbed onto zeolites.

Propene has C_s symmetry in both the gas and adsorbed phases, and hence all the normal modes are infrared active.

Table 7.2 Raman and infrared spectra of cyclopropane in the range 4000-1100

Assignment	Raman Liquid (cm^{-1})	Infrared Gas (cm^{-1})
$\nu_1 + \nu_{11}(E')$; $\nu_8 + \nu_{11}(E')$		3845(w)
$\nu_2 + \nu_5 + \nu_{10}(E')$		3580(w)
ν_6 CH (A_2'')		3103(vs)
ν_{12} CH (E'')	3080(m)	
ν_1 CH (A_1')	3029(s)	
ν_8 CH (E')		3024(vs)
$2\nu_2(A_1')$	3011(s)	
$4\nu_{14}(A_1' + 2E')$	2952(w)	
$2\nu_9(A_1' + E')$	2854(w)	
$\nu_3 + \nu_9(E')$		2631(w)
$\nu_5 + \nu_9(E')$; $\nu_2 + \nu_{10}(E')$		2493(w)
$\nu_2 + \nu_{11}(E')$		2330(w)
$\nu_9 + \nu_{14}(A_2'')$		2178(w)
$\nu_5 + \nu_{10}(E')$		2084(s)
$\nu_{10} + \nu_{11}(A_1' + E')$	1873(vw)	1888(s)
$\nu_7 + \nu_{14}(E')$		1779(w)
$\nu_4 + \nu_{14}(E')$		1739(m)
ν_2 CH_2 (A_1')	1504(w)	
$2\nu_{14}(A_1' + E')$	1454(m)	
ν_9 CH_2 (E')	1435(m)	1432(s)
ν_3 C_3 (A_1')	1189(vs)	

Table 7.3 Raman and infrared spectra of propene in the range 4000-1100

Assignment	Raman Liquid (cm^{-1})	Infrared Gas (cm^{-1})	Assignment	Raman Liquid (cm^{-1})	Infrared Gas (cm^{-1})
ν_1(A')	3087(w)	3082(m)	$2\nu_{18}$(A')		1976(vw)
$\nu_6 + \nu_8$(A')		3067(w)	$2\nu_{13}$(A')		1830(m)
ν_2(A')	3010(sb)	3012(m)	$\nu_{17} + \nu_{20}$(A')		1718(w)
ν_3(A')	2990(w)	2979(s)	ν_6(A')	1648(vs)	1647(s)
ν_{15}(A")	2956(vw)	2960(m)			1520(vw)
$2\nu_{16}$(A')		2942(s)	$\nu_{19} + \nu_{20}$(A')		1508(vw)
ν_4(A')	2924(vs)	2916(s)			1489(vw)
$2\nu_7$(A')	2890(m)	2884(m)	ν_{16}(A")		1472(m)
ν_5(A')	2857(w)	2852(m)	ν_7(A')	1448(w)	1448(s)
$2\nu_8$(A')	2823(w)		ν_8(A')	1415(m)	1416(w)
$2\nu_9$(A')	2795(vw)		ν_9(A')		1399(w)
$\nu_7 + \nu_{10}$(A')	2763(vw)		ν_{10}(A')	1297(vs)	1287(w)
$\nu_8 + \nu_{10}$(A')	2732(w)				1317(w)
$2\nu_{10}$(A')		2574(w)	ν_{11}(A')		1244(w)
$2\nu_{17}$(A')		2320(w)			1224(m)
$\nu_7 + \nu_{20}$(A')		2035(w)	ν_{17}(A")		1166(w)

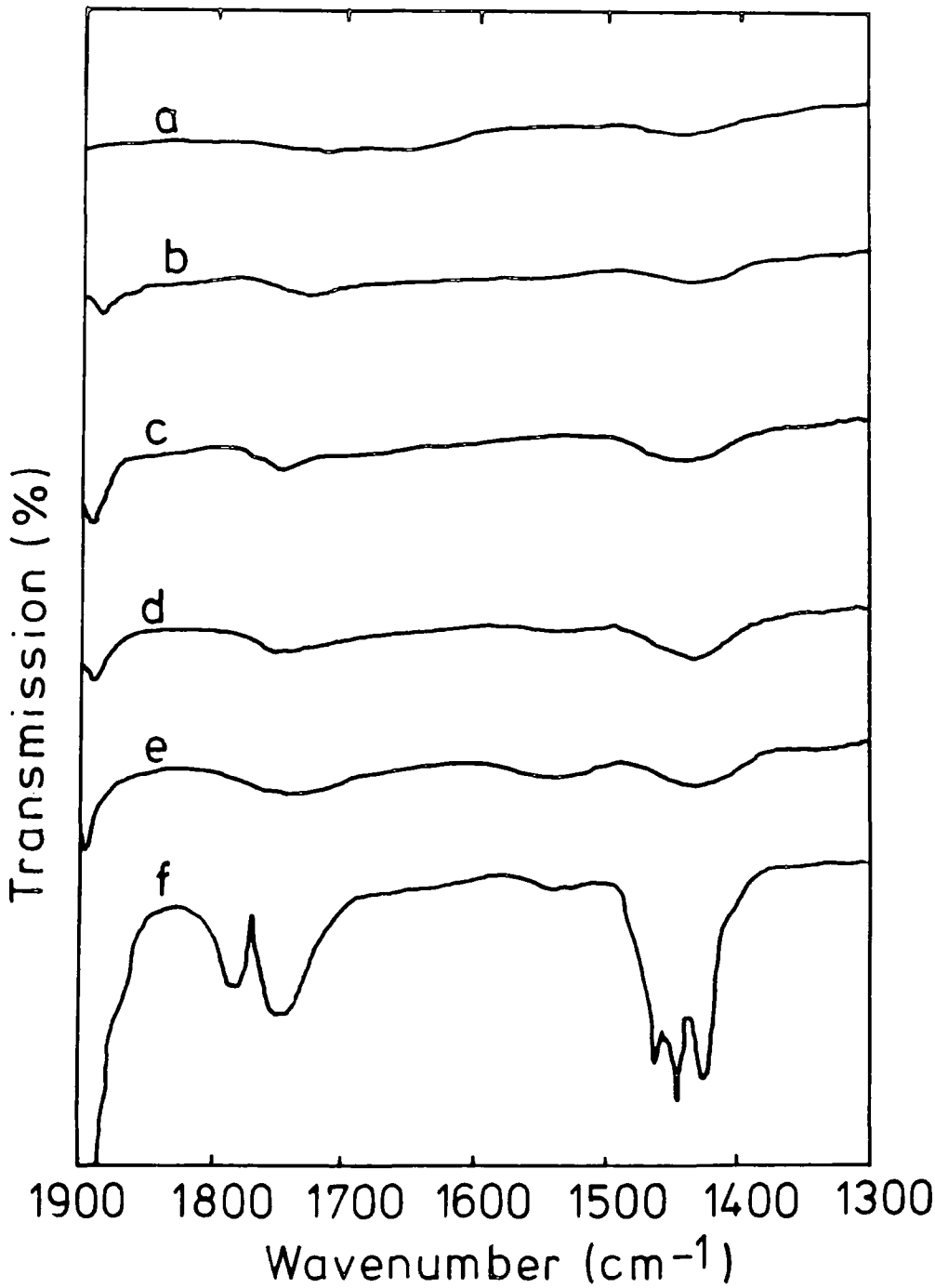

Figure 7.21. Spectra of cyclopropane at different pressures: (a) 5 torr, (b) 10 torr, (c) 30 torr, (d) 50 torr, (e) 100 torr and (f) 200 torr.

Table 7.4 Activities of the adsorbed cyclopropane compared with the free molecule

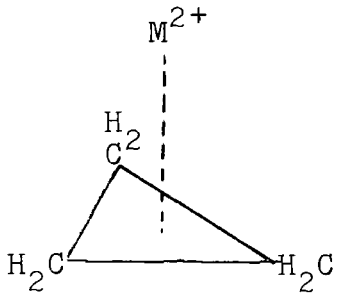

'Face-on' interaction

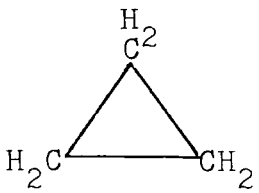

Free molecule

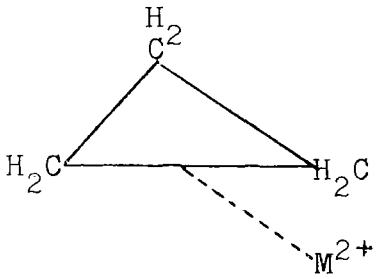

'Edge-on' interaction

	C_{3v}		D_{3h}		C_{2v}	
(IR,R)	A_1	——	A_1' (R)	——	A_1	(IR,R)
(IR,R)	A_1	——	A_2'' (R)	——	A_1	(IR,R)
(Inactive)	A_2	——	A_2' (Inactive)	——	B_2	(IR,R)
(Inactive)	A_2	——	A_1'' (Inactive)	——	A_2	(R)
(IR,R)	E	——	E' (IR,R)	⟨	A_1	(IR,R)
					B_2	(IR,R)
(IR,R)	E	——	E'' (IR,R)	⟨	A_2	(R)
					B_1	(IR,R)

$\Gamma_{VIB}(C_{3v}) = 6A_1 + 2A_2 + 8E$

$\Gamma_{VIB}(D_{3h}) = 3A_1' + A_2' + 4E' + A_1'' + 2A_2'' + 3E''$

$\Gamma_{VIB}(C_{2v}) = 9A_1 + 2A_2 + 8B_1 + 5B_2$

It will be shown later that the bands which we observe due to propene adsorbed onto the cations are shifted to lower frequencies compared with the gas phase.

(a) ZnNaA

The experiments using ZnNaA were conducted with samples subjected to different pretreatment conditions, exposed to the same pressure of cyclopropane (5 torr), and left in contact with the samples for 1 hour. For sample Zn(16,623), a range of different pressures (10,50 and 100 torr) of cyclopropane were used (see table 7.1).

Figures 7.22a, 7.23a, 7.24a and 7.25a show the spectra of the samples Zn(18,523), Zn(16,623), Zn(36,623) and Zn(38,723) at room temperature respectively. Spectra of the same samples were obtained immediately on exposure to 5 torr cyclopropane (Figures 7.22b-7.25b) and were left in contact with this pressure of cyclopropane for 1 hour (Figures 7.22c-7.25c).

In all of the samples except Zn(38,723), the isomerization of cyclopropane occurred spontaneously as can be seen by the appearance of the ν(C=C) band of propene at 1616cm^{-1}. For Zn(38,723),however, the isomerization of cyclopropane occurred more slowly although after 1 hour exposure the ν(C=C) band can be seen clearly (Figure 7.25c). Upon admitting 5 torr of cyclopropane to sample Zn(38,723), three new bands in the region 1900-1300cm^{-1} were observed, at 1880, 1462 and 1432cm^{-1}, which are due to adsorbed cyclopropane. By analogy with the spectra of the gas phase, we assign these bands as follows; 1880cm^{-1} to $\nu_{10} + \nu_{11}$ ($A_1' + E'$), 1462cm^{-1} to ν_2 (A_1') and 1432cm^{-1} to ν_9 (E') (Table 7.5). The ν_2 band is inactive in the infrared spectrum of the gas phase and the appearance of this band indicated the lowering of

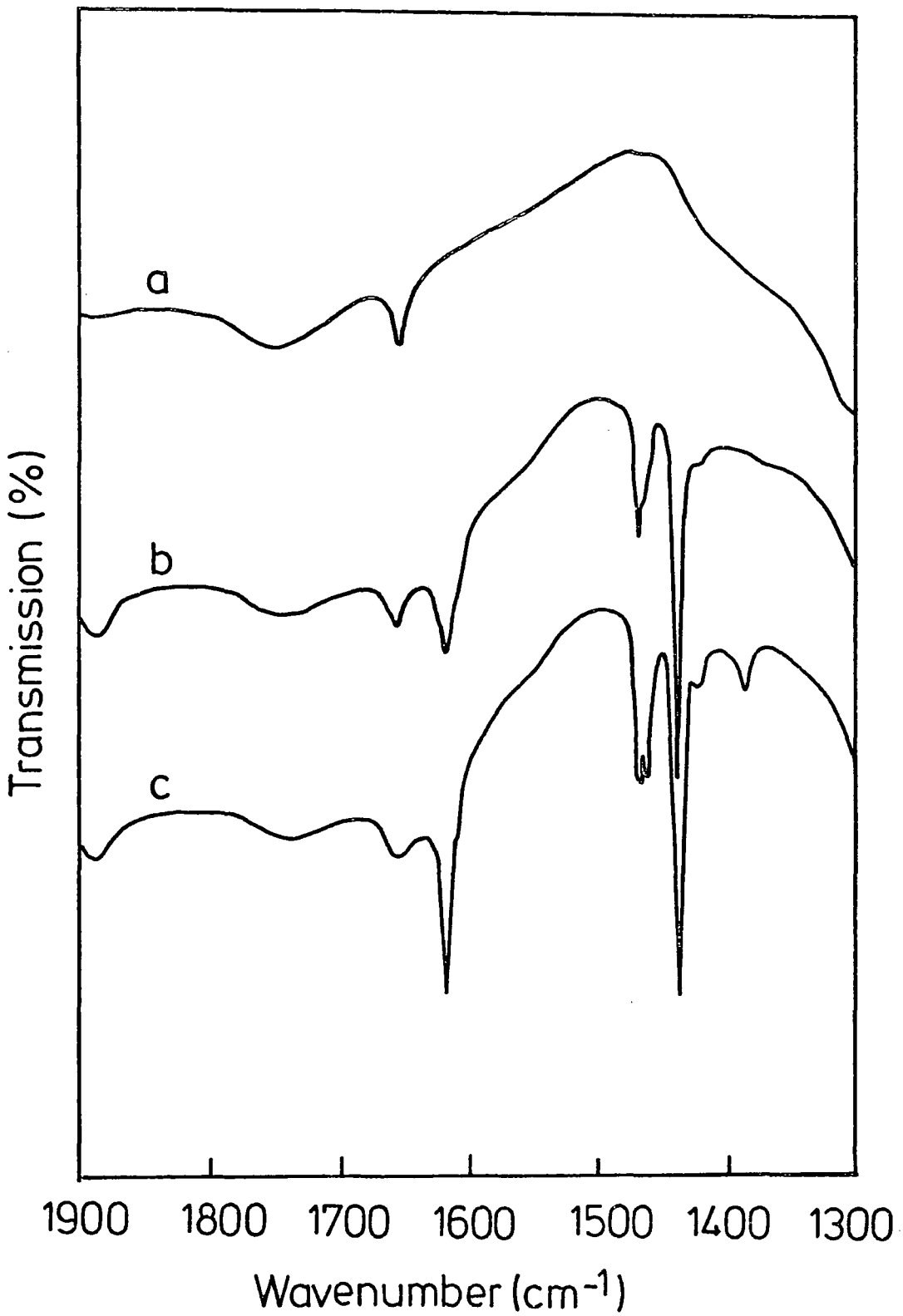

Figure 7.22. ZnNaA zeolite after heating at 523K for 18 hours:
(a) at ambient temperature
(b) sample (a) after admitting 5 torr cyclopropane
(c) sample (b) after 1 hour.

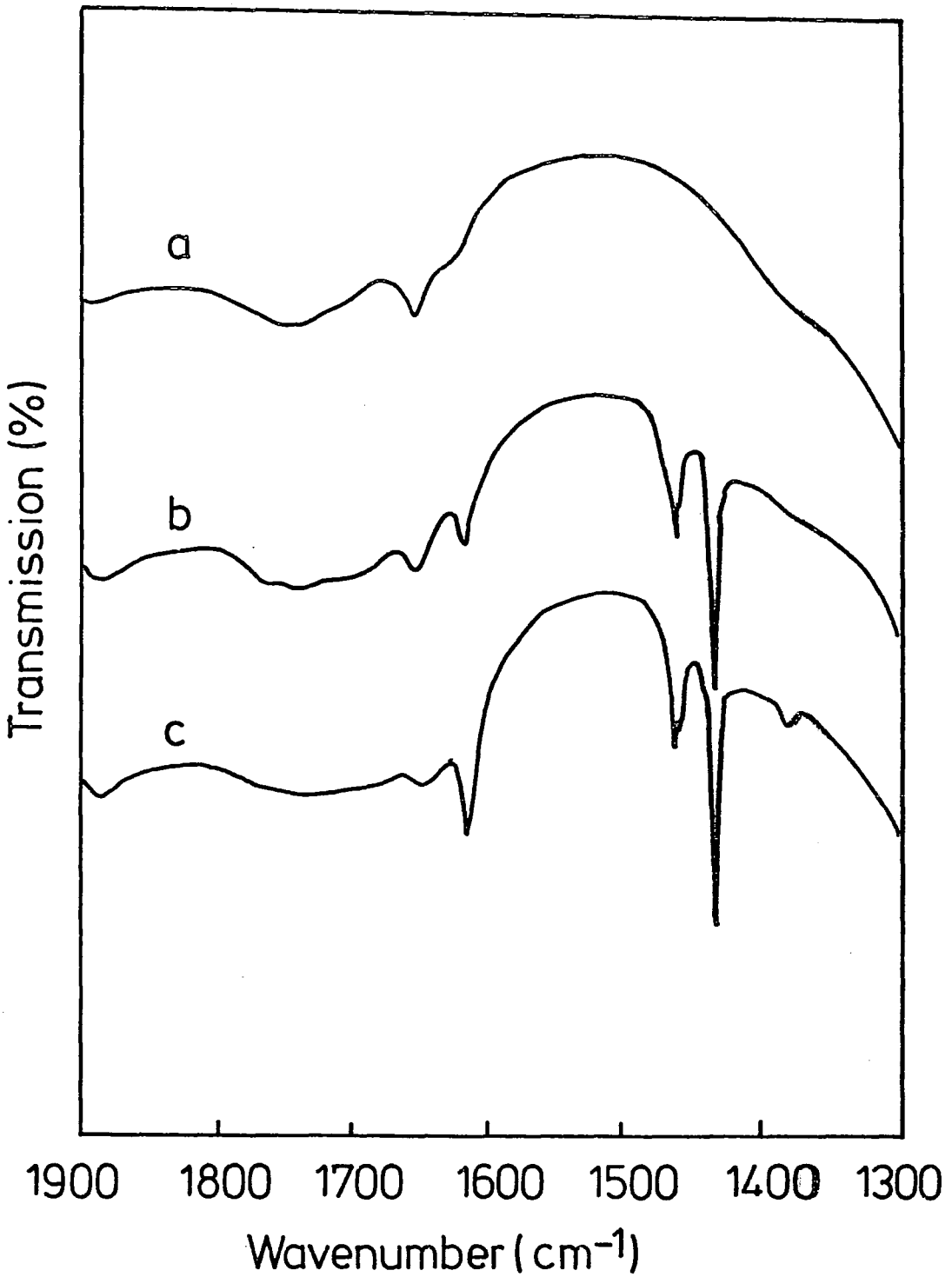

Figure 7.23. ZnNaA zeolite after heating at 623K for 16 hours:
(a) at ambient temperature
(b) sample (a) after admitting 5 torr cyclopropane
(c) sample (b) after 1 hour.

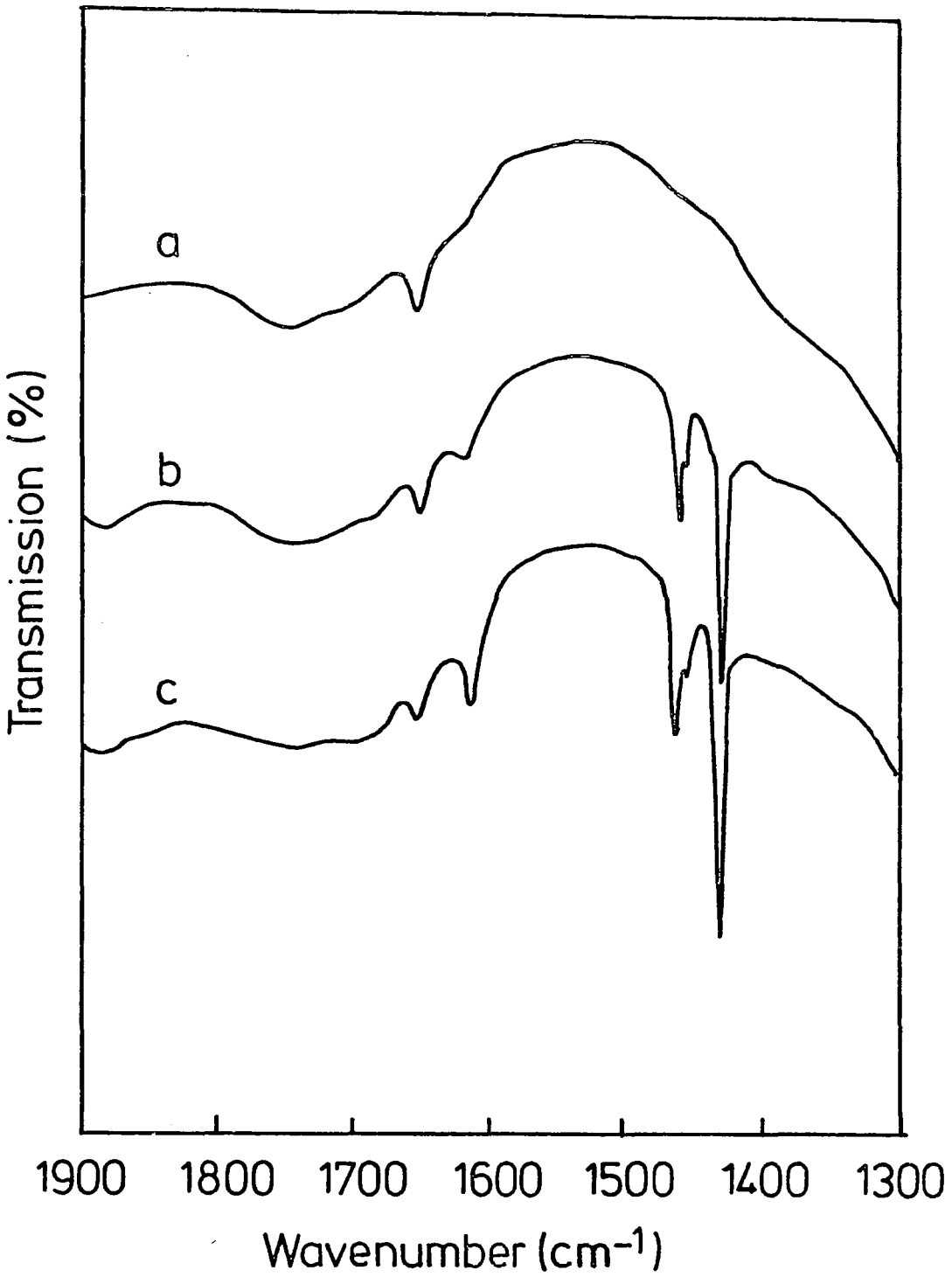

Figure 7.24. ZnNaA zeolite after heating at 623K for 36 hours:
(a) at ambient temperature
(b) sample (a) after admitting 5 torr cyclopropane
(c) sample (b) after 1 hour.

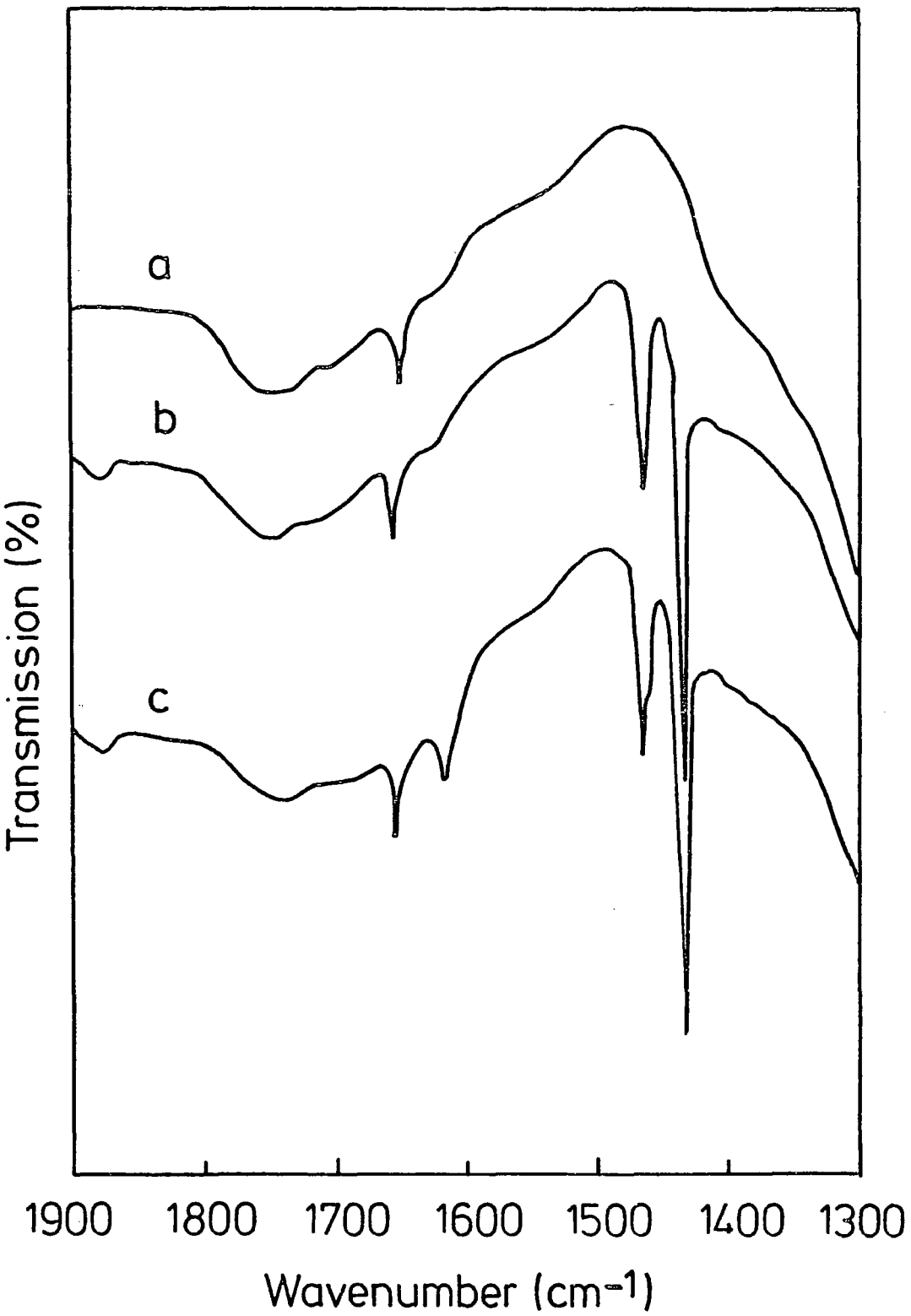

Figure 7.25. ZnNaA zeolite after heating at 723K for 38 hours:
(a) at ambient temperature
(b) sample (a) after admitting 5 torr cyclopropane
(c) sample (b) after 1 hour.

symmetry of the cyclopropane molecule in the adsorbed state compared with the free molecule. The assignment of the infrared spectrum of adsorbed cyclopropane is given in table 7.5.

From table 7.5 it can be seen that the $\nu_8(E')$ and the $\nu_9(E')$ bands at 3020 (Figure 7.26c) and 1432cm^{-1} (Figure 7.25b) respectively, are not split and because of this it is most probable that the mode of interaction of the sorbed cyclopropane must be that of a 'face-on' interaction with the cation (refer table 7.4). This finding is in agreement with the conclusion reached by Klier et al[28] from their u.v. reflectance spectra of cyclopropane adsorbed onto partially Ni(II) exchanged type A zeolites and Seff et al[36] in their single crystal x-ray work of cyclopropane adsorbed onto partially Co(II) and Mn(II) exchanged type A zeolites.

In samples Zn(18,523), Zn(16,623) and Zn(36,623), however, upon admitting 5 torr cyclopropane (Figures 7.22b, 7.23b and 7.24b), apart from the ν(C=C) band at 1616cm^{-1} due to adsorbed propene, other bands due to adsorbed propene are also observed at 1456, 1432, 1416 and 1380cm^{-1}. These bands are assigned by analogy with the assignments for the free molecule as shown in table 7.6. As we shall show later, the band at 1432cm^{-1} is due to both the adsorbed cyclopropane and propene.

In order to characterize the catalytic activity of the samples, the appearance and intensity of the ν(C=C) band of propene together with the number of bands due to adsorbed propene observed in the region 1900-1300cm^{-1} were considered. This consideration is justified in view of the data obtained immediately after cyclopropane adsorption at different pressures on Zn(16,623) (Figure 7.27). Note that each scan took 10 minutes, so that the final scan of the sample with 100 torr of

Table 7.5 Assignments of the infrared spectra of cyclopropane adsorbed onto ZnNaA (Zn(38,723)) and NiNaA (Ni(40,723)) in the range 4000-1300cm^{-1}

ZnNaA	ZnNaA.C_3H_6	NiNaA	NiNaA.C_3H_6	Assignment*
-	3100(vw)	-	-	$\upsilon_6(A_2'')$
-	3020(w)	-	-	$\upsilon_8(E')$
-	2100(vw)	-	-	$\upsilon_5 + \upsilon_{10}(E')$
-	1888(w)	-	-	$\upsilon_{10} + \upsilon_{11}(A_1' + E')$
1745(mb)	1745(mb)	-	-	zeolite framework
1700(wsh)	1700(wsh)	-	-	zeolite framework
1655(m)	1655(m)	1665(vs)	1665(vs)	$\upsilon_2(H_2O)$
1620(s)	1620(sh)	-	-	zeolite framework
-	1462(s)	-	1460(m)	υ_2 (A_1')
-	1432(vs)	-	1432(m)	$\upsilon_9(E')$

* According to free molecule.

Table 7.6 Bands observed which are due to propene in the region 1900-1300cm^{-1} for ZnNaA after various pretreatment conditions (cm^{-1})

Assignment* \ Samples	Gas phase	Zn(18,523)	Zn(16,623)	Zn(36,623)	Zn(38,723)
υ_6(A') C=C stretch	1647(s)	1616(vs)	1616(s)	1616(m)	1616(m)
υ_{16}(A") CH_3 antisymmetric deformation	1472(m)	1456(s)	1456(m)	1458(sh)	1458(sh)
υ_7(A') CH_3 antisymmetric deformation	1448(s)	1432(vs)	1432(vs)	1432(vs)	1432(vs)
υ_8(A') CH_2 deformation	1416(w)	1416(w)	-	-	-
υ_9(A') CH_3 symmetric deformation	1399(w)	1380(w)	1380(w)	-	-

* According to free molecule.

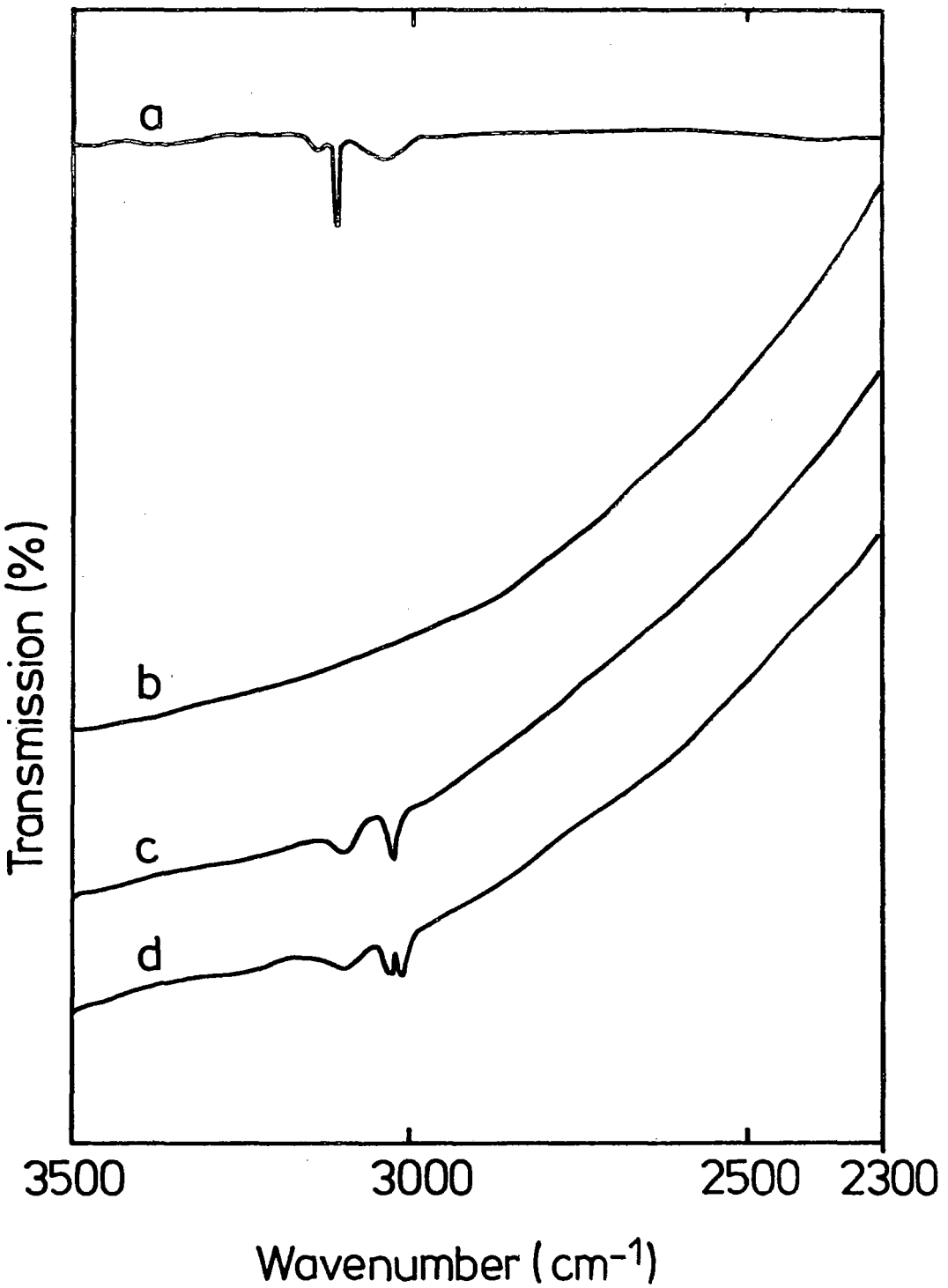

Figure 7.26. (a) Gas phase cyclopropane (5 torr)
(b) sample Zn(38,723) at ambient temperature
(c) sample (a) after admitting 5 torr cyclopropane
(d) sample (c) after 1 hour.

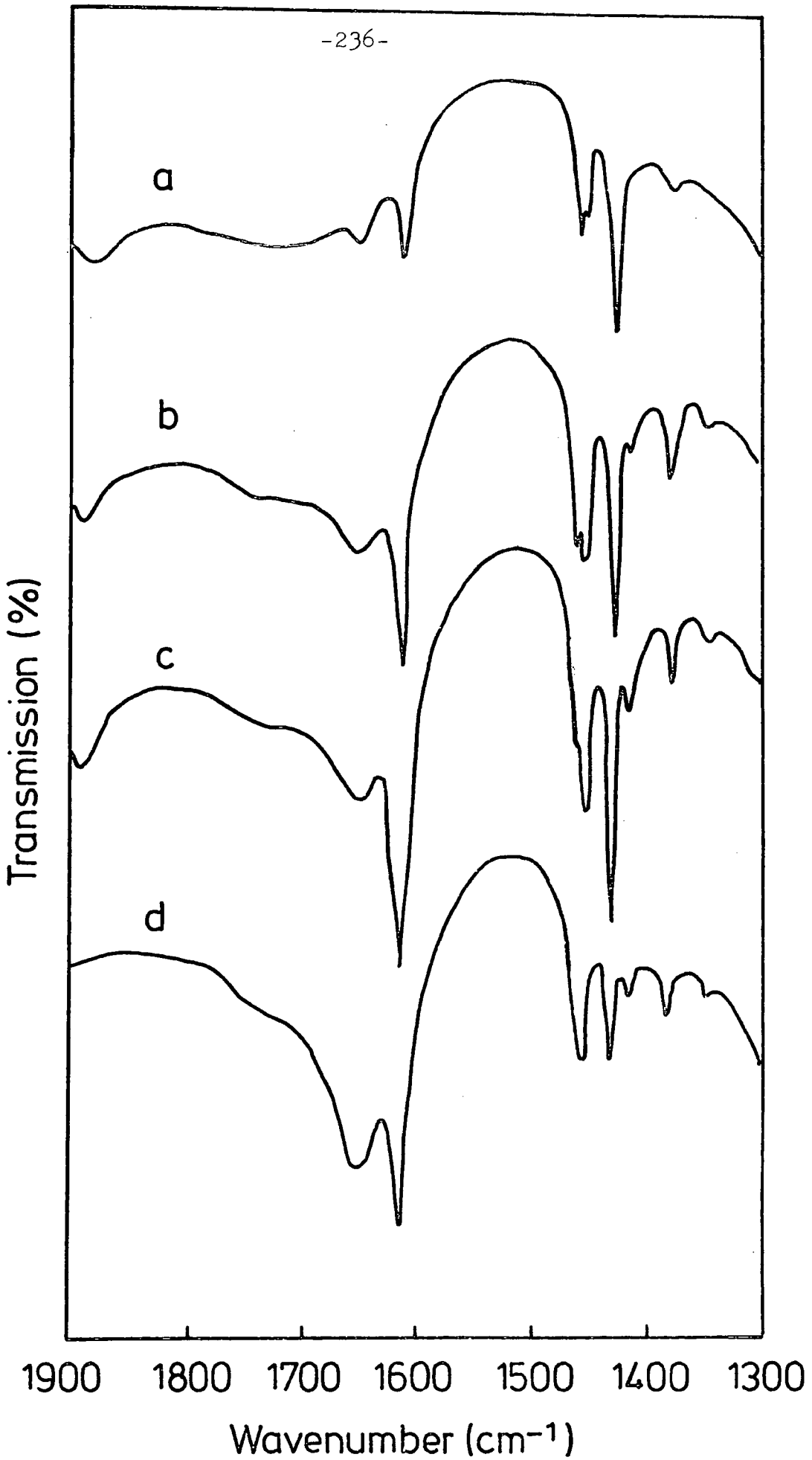

Figure 7.27. Sample Zn(16,623) after admitting: (a) 10 torr, (b) 50 torr and (c) 100 torr cyclopropane, (d) sample (c) after 5 minutes evacuation.

cyclopropane would mean that the sample was in contact with cyclopropane for approximately 1 hour (plus the time taken when admitting the gas into the system). More bands due to propene were observed as the pressure of cyclopropane increased. Increasing the pressure of cyclopropane to 100 torr (Figure 7.27c) cause the band at 1456cm^{-1} due to ν_{16}(A") of propene, which is a shoulder at first (Figure 7.27a) to become more intense and finally obscure the band at 1462cm^{-1} which is due to adsorbed cyclopropane.

On increasing the pressure of cyclopropane, the relative intensity of the 1462cm^{-1} band, which is due to adsorbed cyclopropane, remains constant while, all other bands at, at 1516, 1456, 1432, 1416 and 1380cm^{-1} which are due to adsorbed propene, increase in relative intensity (Figures 7.27a, b and c). Cyclopropane, therefore, must be adsorbed at a different site from propene. Propene is probably adsorbed onto the cations since the bands ν_6 (C=C stretch), ν_{16} (CH_3 antisymmetric deformation), and ν_7 (CH_3 antisymmetric deformation), are shifted to lower fequencies compare with the gas phase (Table 7.6). It is not impossible for cyclopropane and propene to be adsorbed at two different sites since more than one zinc(II) ions are found at two different locations (S2* and S2') after dehydration (Section II).

On evacuating the cell for 5 minutes at room temperature (Figures 7.27d, 7.28b and 7.29d) for samples Zn(5,16,623), Zn(5,38,723) and Zn(5,2,653), the band at 1462cm^{-1}, due to adsorbed cyclopropane, disappears while the band at 1432cm^{-1}, which is due to both adsorbed cyclopropane and propene, is much less intense. The bands observed in these samples, Zn(5,16,623)

Zn(5,38,723) and Zn(5,2,653) are due to propene only (Figures 7.27d 7.28b and 7.29d), suggesting that adsorbed cyclopropane can easily be removed by 5 minutes evacuation at room temperature. It was found that the bands due to propene could not be removed even in samples Zn(30,2,653) and Zn(30,38,723) as shown in figures 7.29e and 7.28c respectively.

After 30 minutes evacuation at room temperature, the sample Zn(2,653) was heated and the bands due to propene disappear on heating the sample to 473K. This shows that propene is more strongly adsorbed to the cations than cyclopropane. Liengme and Hall[14], in their infrared studies of propene adsorbed onto decationated X and Y zeolites, also found that the adsorbed propene could only be removed when the sample was heated in their case, to a temperature of 523K.

The catalytic activity of the samples may be assessed by the appearance of the υ(C=C) band of propene together with the number of bands due to adsorbed propene observed in the region 1900-1300cm^{-1}. Based on the above assumptions, the spectra of the samples Zn(18,523), Zn(16,623), Zn(36,623) and Zn(38,723) upon addition of 5 torr cyclopropane (Figures 7.22b-7.25b) and after allowing the sample to remain in contact with this pressure of cyclopropane for 1 hour (Figures 7.22c-7.25c) can be compared. It was found that the catalytic activities of the samples are in the order: Zn(18,523) > Zn(16,623) > Zn(36,623) > Zn(38,723). (Those bands due to propene formation for all four samples are given in Table 7.6). This work clearly shows that the rate of isomerization of cyclopropane to propene on ZnNaA is a function of pretreatment conditions and most probably that water plays an important role.

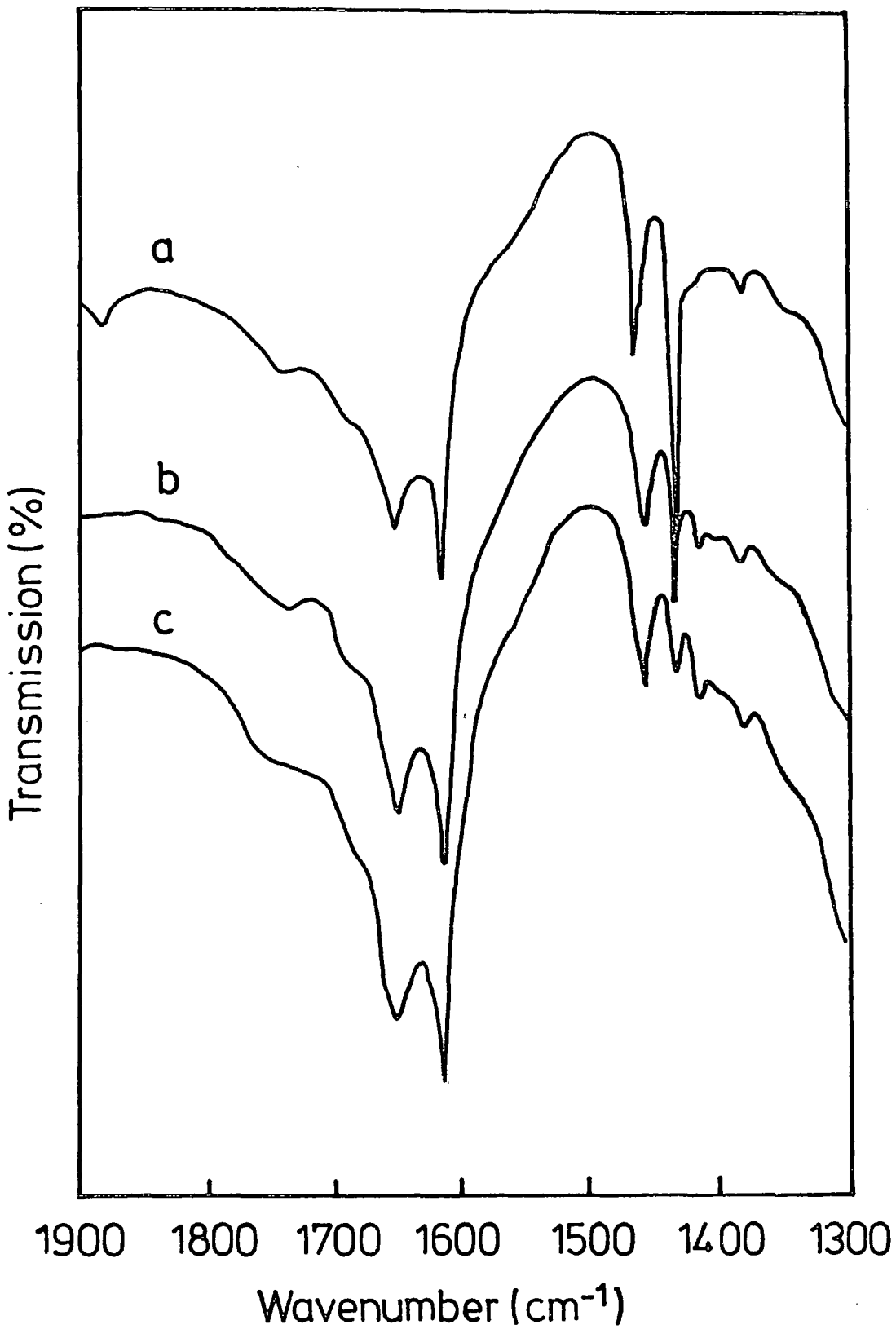

Figure 7.28. ZnNaA zeolite after heating at 723K for 38 hours:
(a) after admitting 10 torr cyclopropane
(b) sample (a) after evacuation for 5 minutes
(c) sample (b) after evacuation for a further 25 minutes.

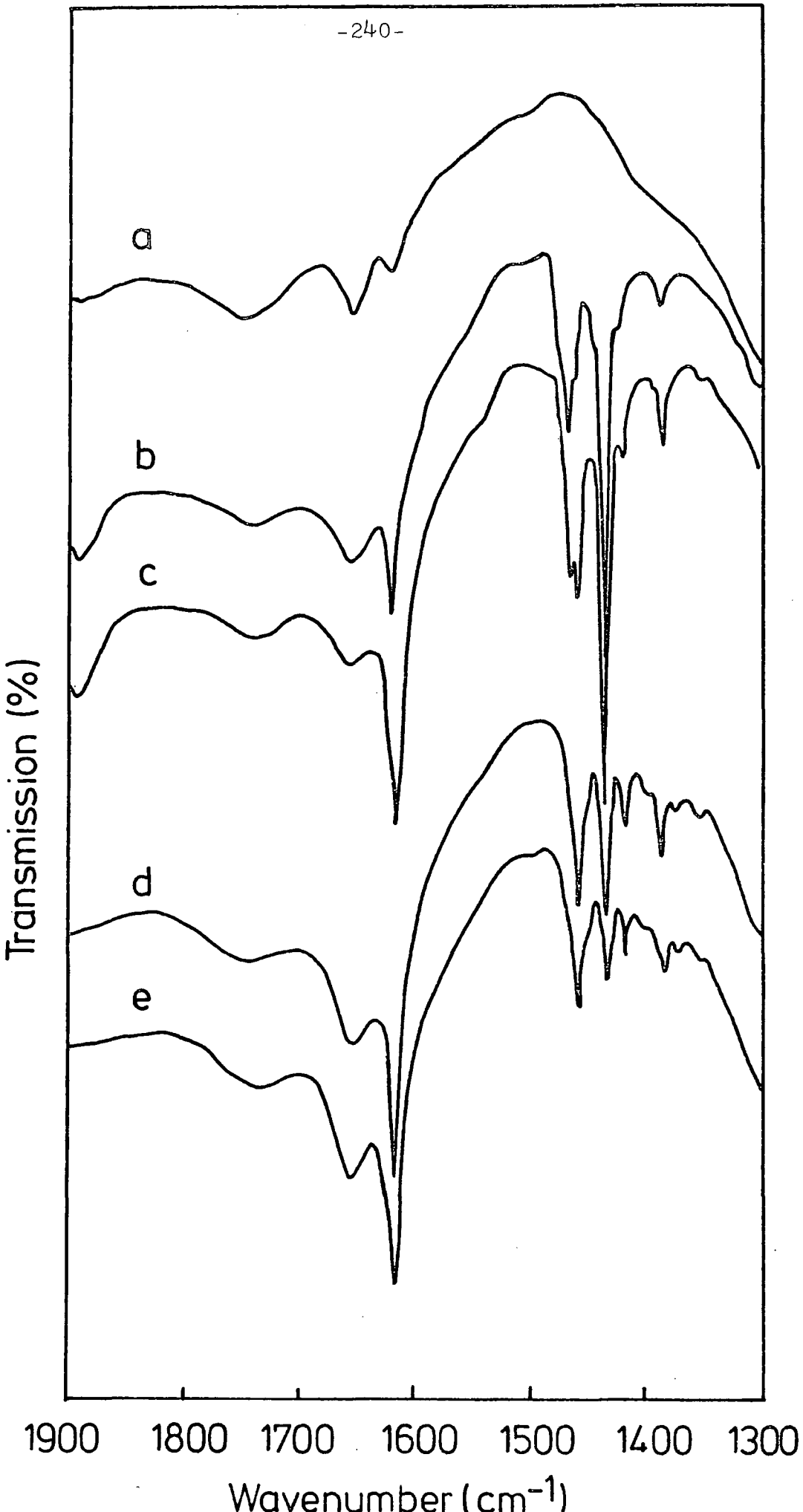

Figure 7.29. (a) sample Zn(2,653) at ambient temperature (b) sample (a) after admitting 10 torr and, (c) 30 torr C_3H_6 (d) sample (c) after evacuation for 5 mins., and (e) 30 mins.

The above indicates that the isomerization of cyclopropane must proceed via a non-classical carbonium ion. The mechanism given by George and Habgood[10] is compatible with the present finding, that is;

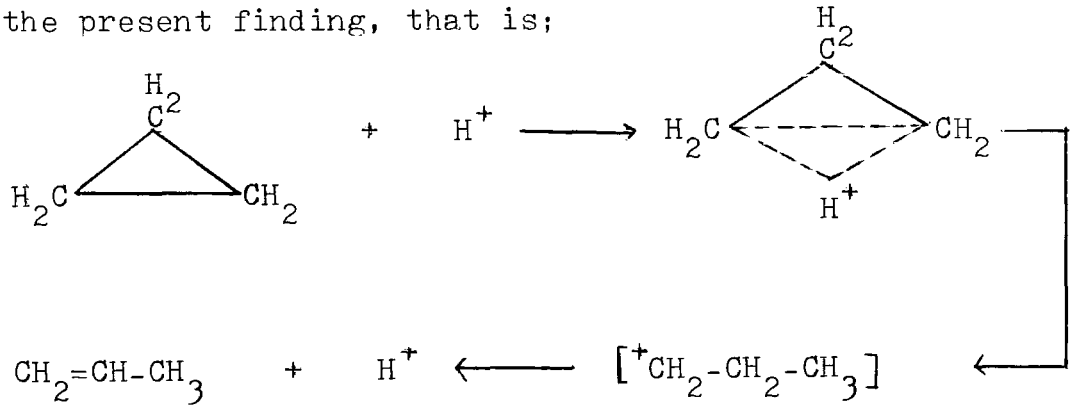

Based on the above equation, bands are expected which are due to c - $C_3H_7^+$ and the primary propyl ion.

The c - $C_3H_7^+$ ion has a C_{2v} symmetry. As we have explained earlier cyclopropane with C_{2v} symmetry causes the $\nu_8(E')$ and $\nu_9(E')$ bands in the gas phase (3024 and 1432cm^{-1}) to split to two modes (A_1 and B_2). In figures 7.30a, 7.31a, 7.32a and 7.26b are shown the spectra of samples Zn(18,523), Zn(16,623), Zn(36,623) and Zn(38,723) at room temperature in the region 3500-2300cm^{-1}, while in figures 7.30b-7.32b and 7.26c are shown the spectra of the same samples upon admitting 5 torr cyclopropane. The spectra after allowing the samples to remain in contact with 5 torr cyclopropane for 1 hour are shown in figures 7.30c-7.32c and 7.26d. The spectra of the samples in this region are rather poor since the signal-to-noise ratio is small. However, despite this, it is notable that in all of the data collected after leaving the samples to remain in contact with 5 torr cyclopropane for 1 hour (Figures 7.30-7.32c and 7.26d), the band at 3020cm^{-1} (ν_8,E') seems to be split to two bands of approximately equal intensity at 3020and 3010cm^{-1}. This is not found in the spectrum of the sample Zn(38,723) immediately

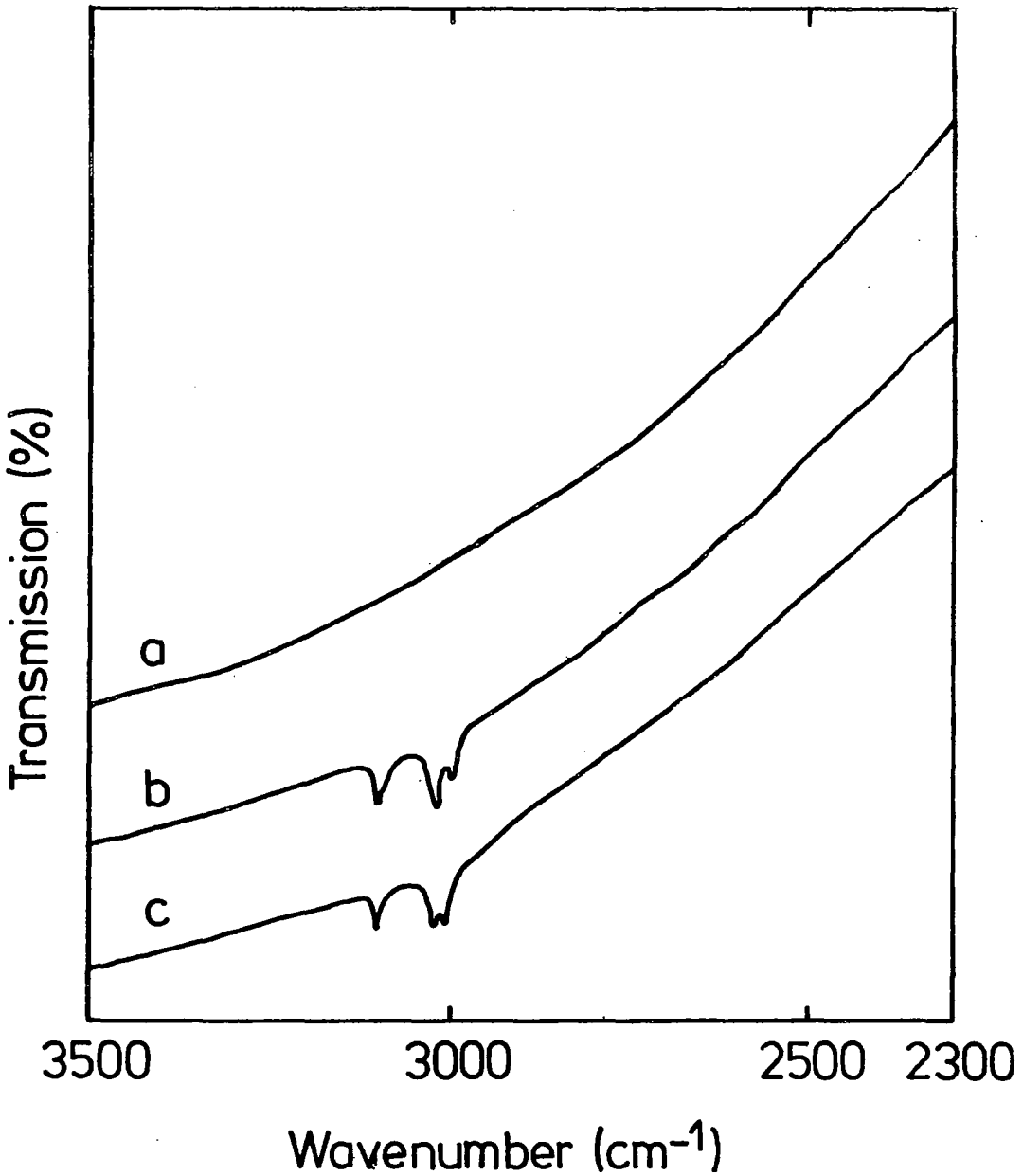

Figure 7.30. ZnNaA zeolite after heating at 523K for 18 hours:

(a) at ambient temperature

(b) sample (a) after admitting 5 torr cyclopropane

(c) sample (b) after 1 hour.

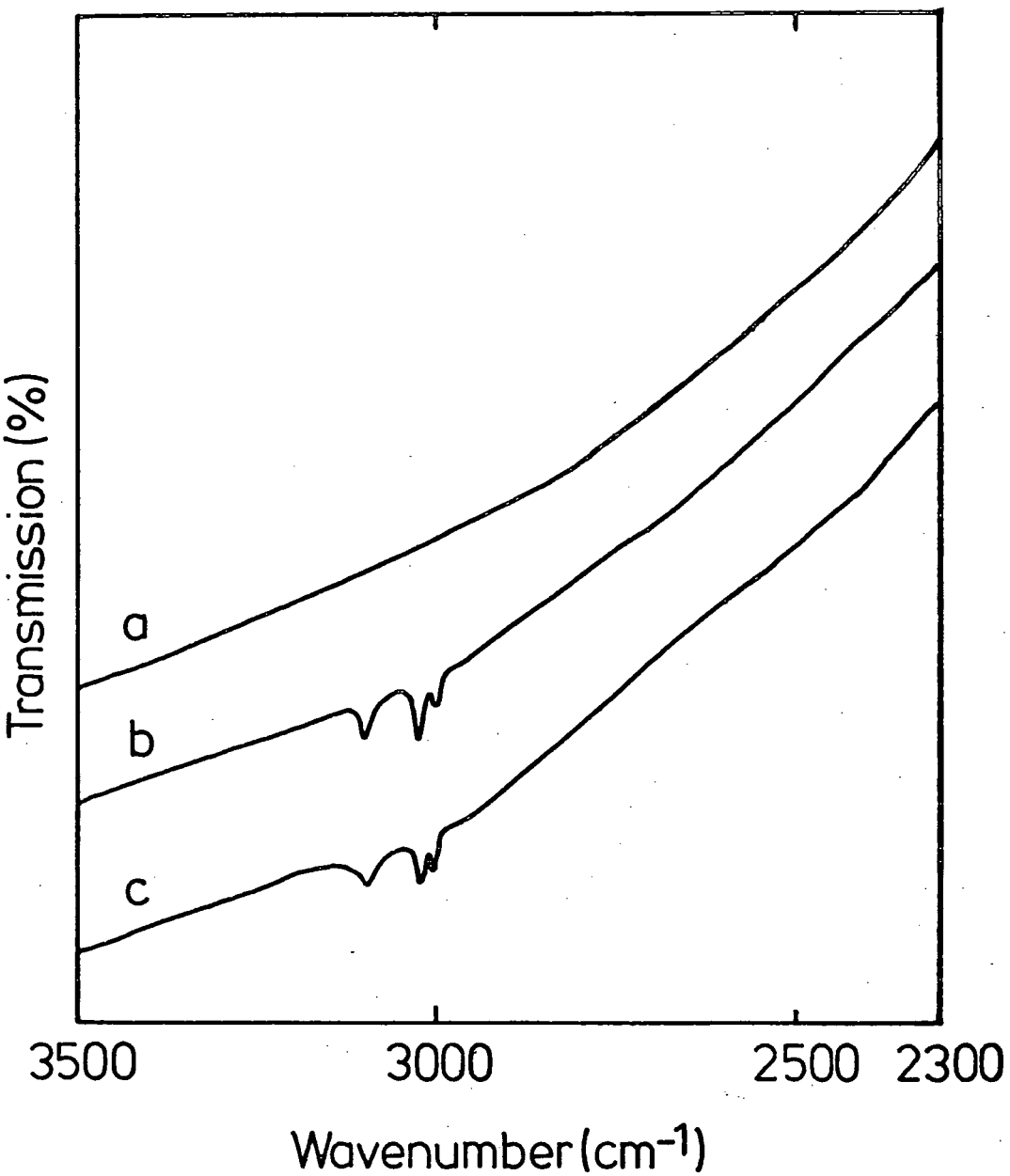

Figure 7.31. ZnNaA zeolite after heating at 623K for 16 hours:

(a) at ambient temperature

(b) sample (a) after admitting 5 torr cyclopropane

(c) sample (b) after 1 hour.

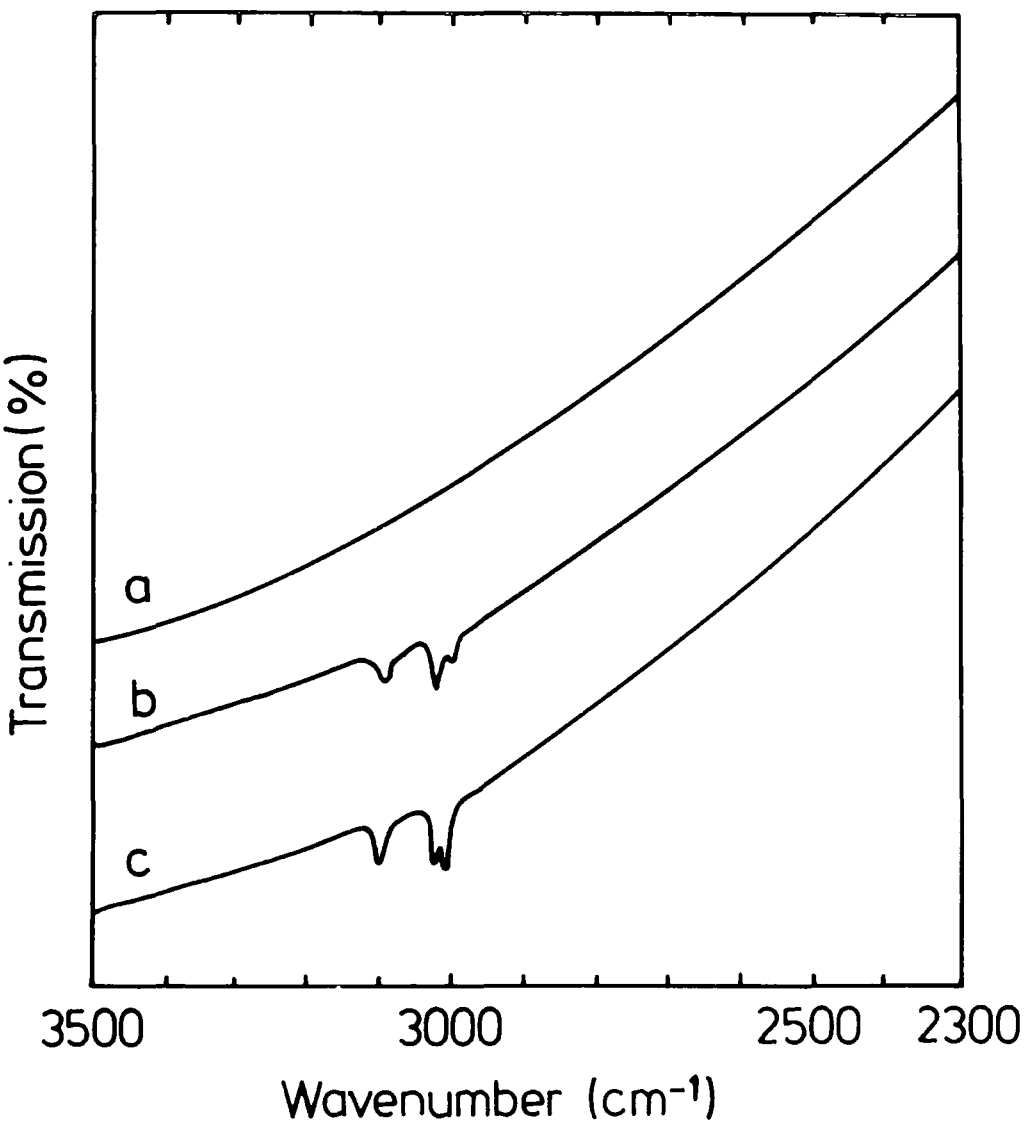

Figure 7.32. ZnNaA zeolite after heating at 623K for 36 hours:
(a) at ambient temperature
(b) sample (a) after admitting 5 torr cyclopropane
(c) sample (b) after 1 hour.

upon admitting 5 torr cyclopropane (Figure 7.26c) which suggested that the cyclopropane is adsorbed to the cations with a 'face-on' interaction. This band, however, is split (Figure 7.26d) after allowing the sample to remain in contact with cyclopropane (5 torr) for 1 hour. We, in view of the above data, suggest that the splitting of the $3020cm^{-1}$ band could be due to the formation of c - $C_3H_7^+$. This means that the $3020cm^{-1}$ is due to both cyclopropane and c-$C_3H_7^+$. The fact that we observe another band at $3010cm^{-1}$ suggest that the formation of c - $C_3H_7^+$ is a slow process. From the infrared spectra of a number of boron compounds[41,42], the stretching frequencies of the bridging hydrogen atoms are expected to be in the range $2220-1600cm^{-1}$. We could not, however, observe any band in this region which we could assign as due to the stretching frequencies of the bridging hydrogen atom. This could be because the hydrogen is just weakly bonded to the two carbon atoms.

The ring opening of this c - $C_3H_7^+$ accompanies the formation of the primary propyl ion. No band due to the primary propyl ion was observed perhaps because the formation of propene from the primary propyl ion is a fast reaction. No bands due to by-products are observed.

(b) NiNaA

Two differently prepared samples Ni(2,673) and Ni(40,723) were used. Water cannot be removed totally from these samples as shown in figures 7.33a and 7.35a. Thus, the interaction of cyclopropane with anhydrous NiNaA cannot be studied.

In figure 7.33a is shown the spectrum of Ni(40,723) upon addition of 5 torr of cyclopropane while in figures 7.35b and 7.35c are shown the spectra of Ni(2,673) after admitting

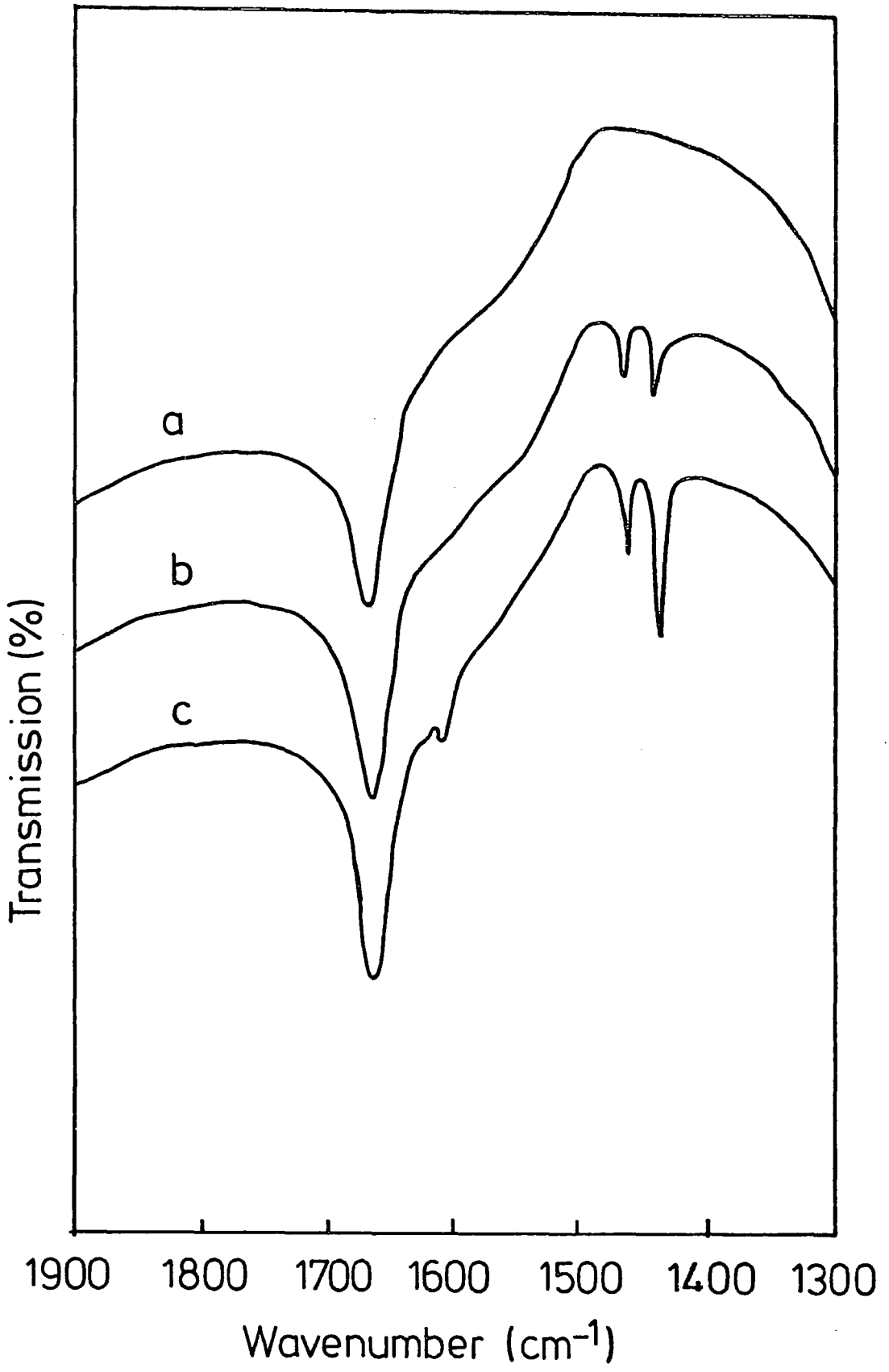

Figure 7.33. NiNaA zeolite after heating at 723K for 40 hours:
(a) at ambient temperature
(b) sample (a) after admitting 5 torr cyclopropane
(c) sample (b) after 1 hour.

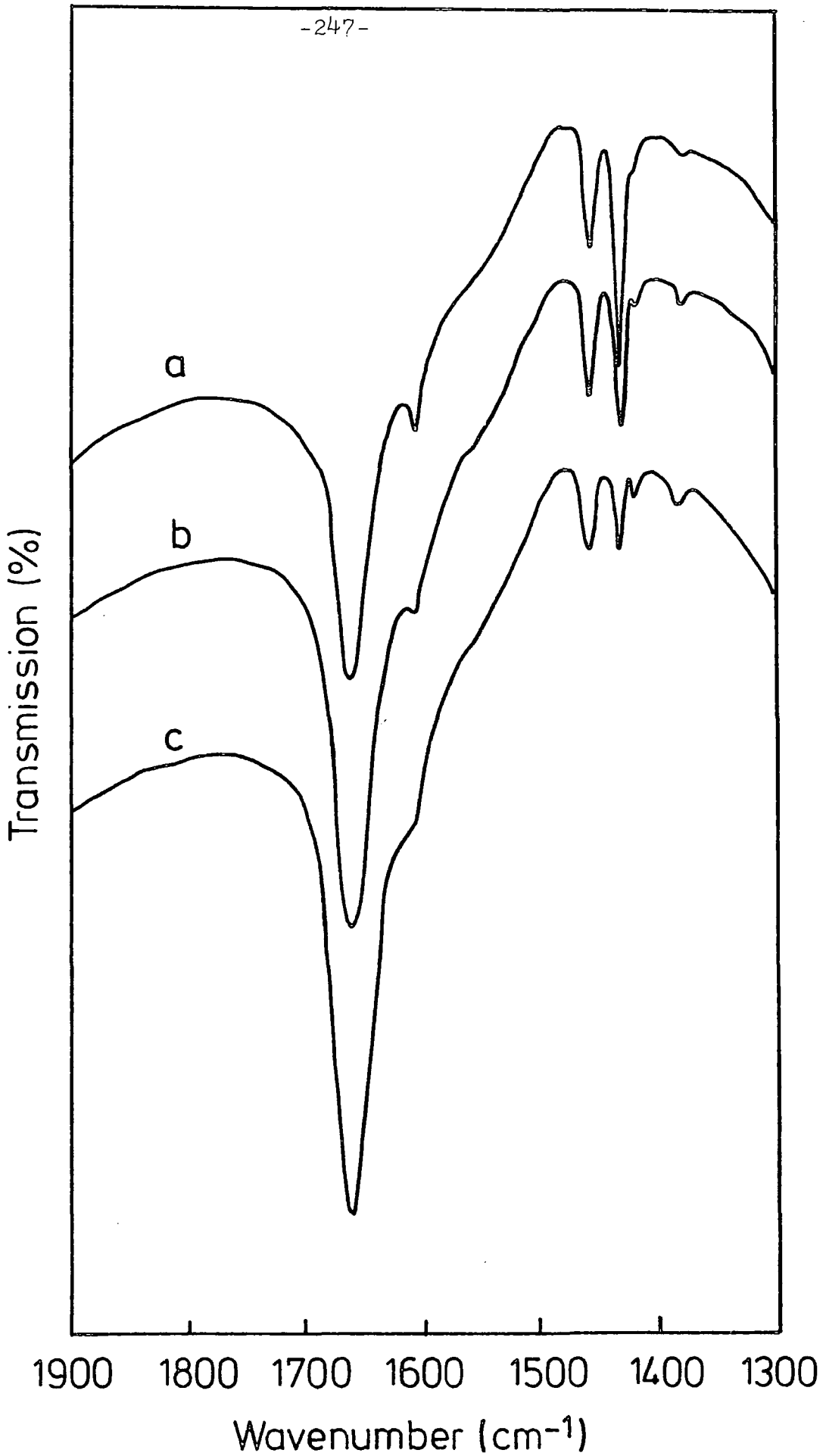

Figure 7.34. NiNaA zeolite after heating at 723K for 40 hours:
(a) after admitting 10 torr cyclopropane
(b) sample (a) after evacuation for 5 minutes
(c) sample (b) after evacuation for a further 25 minutes.

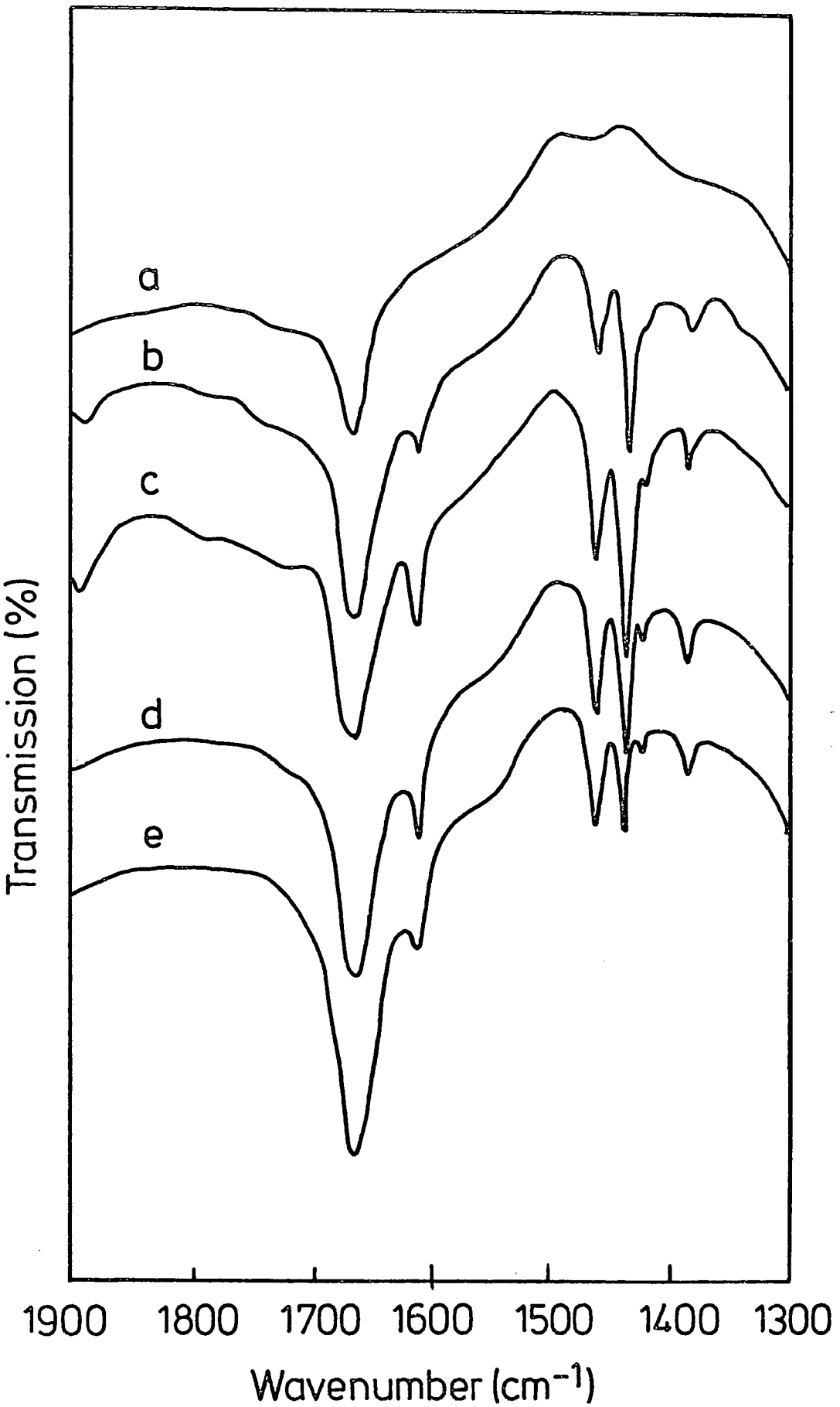

Figure 7.35. NiNaA zeolite after heating at 673K for 2 hours:
(a) at ambient temperature
(b) sample (a) after admitting 10 torr cyclopropane
(c) sample (a) after admitting 30 torr cyclopropane
(d) sample (c) after evacuation for 5 minutes
(e) sample (d) after evacuation for a further 25 minutes.

10 and 30 torr of cyclopropane respectively.

As with the ZnNaA samples the data is best interpreted using a model in which cyclopropane is adsorbed onto Ni(II) cations via a 'face-on' interaction. The assignment of the bands due to adsorbed cyclopropane (C_{3v} symmetry) is given in table 7.5.

For sample Ni(2 , 673), isomerization of cyclopropane occurred spontaneously while for Ni(40,723), isomerization occurred more slowly but bands due to adsorbed propene are observed after 1 hour contact (Figure 7.33c). On evacuating the cell for 5 minutes at room temperature, for samples Ni(5,2,673) and Ni(5,40,723) (Figures 7.34b and 7.35d), it was observed that the cyclopropane was desorbed. The desorption of cyclopropane was accompanied by the decrease in the intensity of the bands at 1460 and 1432cm^{-1} due to adsorbed cyclopropane, and only bands due to propene were then observed. The bands due to propene are not removed even in samples Ni(30,2,673) and Ni(30,40,723) (Figures 7.35e and 7.33c).

As in ZnNaA, propene is adsorbed more strongly on Ni(II) ions than the cyclopropane since propene could not be removed even after evacuating the cell for 1 hour at room temperature. Table 7.7 gives the assignment of propene adsorbed onto NiNaA.

(c) CuNaA

Cyclopropane is not adsorbed onto CuNaA even at pressure of 100 torr. The only bands observed in this spectrum are those of the gas phase (Figure 7.36b) and all of these bands disappear on evacuating the sample for 1 minute at room temperature.

Table 7.7 Assignment of the bands which are due to propene in samples Ni(2,673), Ni(40,723) and Cu(2,673) (cm^{-1})

Ni(2,673)	Ni(40,723)	Cu(2,673)	Propene(gas)	Assignment*
1608(m)	1608(m)	1665(s)	1647(s)	ν_6(A') C=C stretch
1456(s)	1460(s)	1472(m)	1472(m)	ν_{16}(A") CH_3 antisymmetric deformation
1432(vs)	1432(vs)	1444(s)	1448(s)	ν_7(A') CH_3 antisymmetric deformation
1418(vw)	1420(sh)	1425(vw)	1416(w)	ν_8(A') CH_2 deformation
1380(w)	1380(w)	1400(w)	1399(w)	ν_9(A') CH_3 symmetric deformation

* According to free molecule.

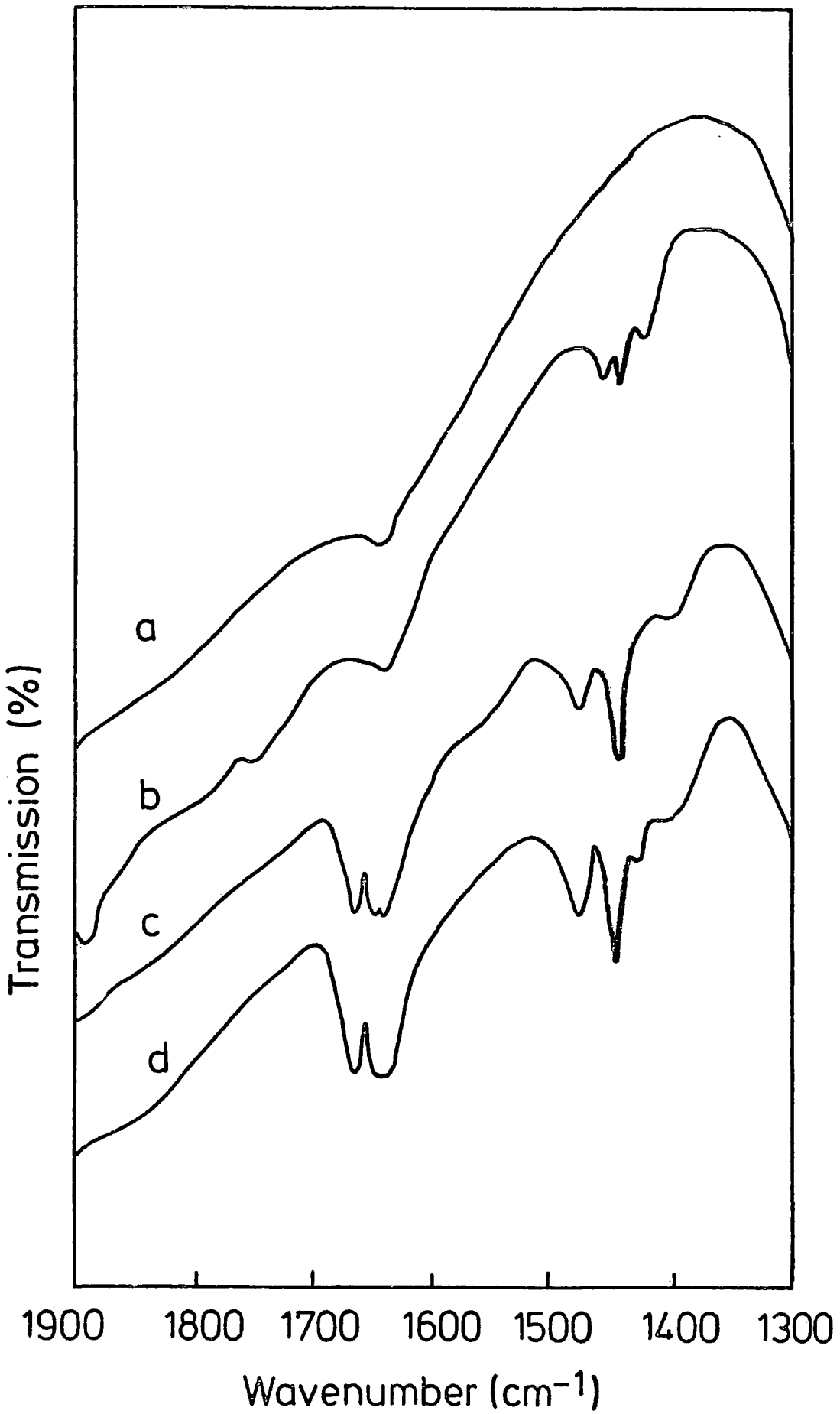

Figure 7.36. CuNaA zeolite after heating at 673K for 2 hours:
(a) at ambient temperature
(b) sample (a) after admitting 100 torr cyclopropane
(c) sample (b) at 473K
(d) sample (b) at 573K.

No bands due to adsorbed cyclopropane were observed upon adsorption of 5 torr of cyclopropane onto the Cu(2,673) sample. The pressure of cyclopropane was then increased and, at 100 torr, the sample was heated. Isomerization of cyclopropane occurred only after heating the sample to 473K (Figure 7.36c) and the bands in this spectrum which are due to propene are given in table 7.7. Three bands are observed in the region 1700-1600cm^{-1} at 1665, 1655 and 1635cm^{-1}. The band at 1665cm^{-1} is assigned to the ν(C=C) of propene while the 1655 and 1635cm^{-1} bands are assigned to the deformation modes of water at two different sites. These bands at 1655 and 1635cm^{-1} are assigned as above because they are comparable to the bands observed on dehydrating CuNaA (refer to part (a) of this section). On further heating the sample CuNaA with 100 torr of cyclopropane to 573K (Figure 7.36d), the 1635cm^{-1} band disappears. Again, this compares with the spectra observed on dehydrating CuNaA.

The bands due to propene (Table 7.7) occur either at the same or higher frequencies than the equivalent gas phase bands. This may indicate that the isomerization of cyclopropane over CuNaA occurs on the surface. Another proof was obtained recently[43], when in the study of the adsorption of propene onto CuNaA, it was found that propene was not adsorbed on the cations.

The observation that the cyclopropane is not adsorbed onto CuNaA and isomerization to propene only occurs at 473K on the surface of the zeolite can be explained either by:

(i) Cu ions in zeolite cavities are less reactive than either ions even though Cu is in between Ni and Zn in the 1st row transition metals in the periodic table. This is so perhaps, because of the presence of Cu^{+} in the CuNaA which have reduced polarizing power compared with Cu^{2+} ions. In terms of polarizing power (charge/ionic radius), Ni^{2+} is expected to be more reactive than Zn^{2+} and Cu^{+} but because, in our NiNaA samples, there is still so much water in the samples as was observed in the spectrum of Ni(40,723) (Figure 7.33a) at room temperature, the reactivity of Ni^{2+} was reduced. Hence, the observed reactivity order was ZnNaA > NiNaA > CuNaA.

(ii) As found in NaA, the largest molecule that can enter the pores of the zeolite is C_2H_2 (refer Chapter II) and only by exchanging the Na^{+} with divalent cations such as Mn^{2+}, Co^{2+}, Ni^{2+} and Zn^{2+} can larger molecules such as cyclopropane enter the pores of the zeolites. Perhaps, the size of the pores of CuNaA does not allow the cyclopropane molecule to enter the zeolite cavities. Here again, this is because of the presence of Cu^{+} in CuNaA. Therefore, the reaction took place on the surface of CuNaA.

VI Conclusion

Cyclopropane was found to absorb to the cations in ZnNaA and NiNaA via a 'face-on' interaction. The isomerization

of cyclopropane to propene takes place via a protonated cyclopropane intermediate (c - $C_3H_7^+$), which on ring opening gives popene probably via a propyl cation. Water was found to promote the isomerization of cyclopropane in sample ZnNaA.

The existence of the bands due cyclopropane and propene in the spectra of ZnNaA and NiNaA suggests that these two gases were adsorbed at two different sites. Since cyclopropane can be removed after 5 minutes evacuation at room temperature and propene was removed only after heating the sample to 473K, it was concluded that propene adsorbed to the cations more strongly than cyclopropane.

For CuNaA, however, no interaction between the cation and cyclopropane was observed at room temperature. Upon heating the sample with 100 torr of cyclopropane, isomerization occurred at 473K. It was suggested that isomerization due to c-C_3H_6 occurred at the external surface, and that propene was not adsorbed on the cations.

References

1. Roberts, R.M., J.Phy. Chem., 63, 1400 (1959)
2. Hall, W.K., Lutinski, F.E. and Gerberich, H.R. J. Catal., 3, 512 (1964).
3. Gerberich, H.R., Hightower, J.W. and Hall, W.K., J. Catal., 8, 39 (1967).
4. Hightower, J.W. and Hall, W.K., J. Am. Chem. Soc., 90, 851 (1968)
5. Hightower, J.W. and Hall, W.K., J. Phys Chem., 72, 4555 (1968)
6. Larson, J.G., Gerberich, H.R. and Hall, W.K., J. Am. Chem. Soc., 87, 1880 (1965).
7. Hall, W.K., Larson, J.G. and Gerberich, H.R., J. Am. Chem. Soc., 85, 3711 (1963).
8. Besset, D.W. and Habgood, H.W., J. Phys. Chem., 64, 769 (1960).
9. Bartley, B.H., Habgood, H.W. and George, Z.M., J. Phys. Chem., 72, 1689, (1968).
10. George, Z.M. and Habgood, H.W., J. Phys. Chem., 74, 1502 (1970).
11. Flockhardt, B.D., McLoughlin, L. and Pink, R.C., J. Chem. Soc. Chem. Comun., 818 (1970).
12. Tam, N.T., Cooney, R.P. and Curthoys, G., J.Catal, 44, 81 (1976).
13. Kiricsi, I., Hannus, I., Varga, K. and Fejes, P., J. Catal., 63, 501 (1980).
14. Liengme, B.V and Hall, W K., Trans. Faraday Soc., 62, 3229, (1966).
15. Forster, H. and Seebode, J., In press.
16. Pickert, P.E., Rabo, J.A., Dempsey, E. and Shomaker, V., Proc. 3rd Intern. Congr. Catalysis, Wiley, New York (1965)

17. Rabo, J.A , Angell, C.L , Kasai, P.H and Shomaker, V , Disc. Farraday Soc., 41, 328, (1966).

18. Gourisetti, B., Cosyns, J. and Leprince, P., Compt. Rend., 258, 4547 (1964).

19. Goursietti, B., Cosyns, J. and Leprince, P., Bull., Soc. Chim. France, 3, 1085 (1966).

20. Olah, G.A., Friedel-Crafts and Related Reactions, Wiley-Interscience, New York (1964).

21. Kim, Y. and Seff, K., J. Phys. Chem., 84, 2823 (1980).

22. McCusker, L.B. and Seff, K., J. Phys. Chem., 85, 405 (1981).

23. Raghavan, N.V. and Seff, K., J Phys. Chem., 80, 2133, (1976).

24. Riley, R.E. and Seff, K., Inorg. Chem., 14, 714 (1975).

25. Yanagida, R.Y., Vance, T.B Jr. and Seff, K., Inorg. Chem., 13, 723 (1974).

26. Riley, P.E. and Seff, K., Inorg. Chem., 13, 1355 (1974).

27. Firor, R.L. and Seff, K , J Phys. Chem., 82, 1650 (1978)

28. Klier, K. and Ralek, M., J. Phys. Chem. Solids, 29, 951 (1968).

29. Egerton, T.A. and Vickerman, J.C., J. Chem. Soc. Trans. Faraday I, 69, 39 (1973).

30. Kellerman, R. and Klier, K., Surface and Defect Properties of Solids, 4, 1 (1975).

31. Gal, I.J., Jankovic, O., Malcic, S., Radovanov, P. and Todorovic, M., Trans Faraday Soc., 67, 999 (1971).

32. Jablonski, J.M , Mulak, J. and Romanowski, W , J Catal., 47, 147 (1977).

33. Ichikawa, T. and Kevan, L., J. Am. Chem., Soc., 103, 5358 (1981).

34. Narayana, M. and Kevan, L., J. Chem. Phys., 75, 3269 (1981)

35. Lee, H.S. and Seff, K., J Phys. Chem., 85, 397 (1981)

36. Cruz, W.V., Leung, P.C.W. and Seff, K., J. Am. Chem. Soc.,

100, 6997 (1978).

37. Adams, D.M. and Lock, P.J., J. Chem. Soc. (A) 2801 (1971)

38. Nakamoto, K., Infrared and Raman Spectra of Inorganic and Coordination Compounds, Wiley-Interscience, New York (1978).

39. Herzberg, G., Infrared and Raman Spectra of Polyatomic Molecules, D. Van Nostrand Company, New York (1945).

40. Howard, J. and Braid, I.J., Personal Communication.

41. Bellamy, L.J., Gerrale, W., Lappert, M.F., and Williams, R.L., J. Chem. Soc., 2412 (1958).

42. Hrostowski, H.J. and Pimental, J.C., J Amer. Chem. Soc., 76, 998 (1954).

43. Howard, J. and Nichols, J.M., Personal Communication.

CHAPTER VIII

INFRARED STUDIES OF HYDROGEN SULFIDE ADSORBED ONTO A SERIES OF TRANSITION METAL EXCHANGED TYPE A ZEOLITES

I. Introduction

Hydrogen sulfide, a commonly occurring industrially generated atmospheric pollutant, has a noxious odour and is very toxic. Various adsorbents, including zeolites, have been used to remove hydrogen sulfide from flue gases, ecetera. In view of the importance of the removal of H_2S from gas streams a considerable quantitv of research is, and has been carried out on the adsorption of H_2S e.g. zeolites 4A and 5A are being used to remove H_2S from natural gas. It is therefore of interest to study the interaction of H_2S with a series of transition metal exchanged tvpe A zeolites.

In previous studies[2-6], H_2S was found to adsorb either molecularly or dissociatively onto a series of zeolites. In the latter case, H_2S was dissociated to SH^- and H^+ ions, resulting in the formation of hydroxyl groups (SH^- and H^+ ions being associated with the cations and framework oxygens, respectively). In the former case, however, H_2S was found either to be adsorbed on the cations[2] or to hydrogen bond to framework hydroxyls[7].

In several infrared spectroscopic studies of the adsorption of H_2S on various adsorbents[2,5,7-9], the formation of water was observed. There is, however, disagreement between the authors as to the reason for its formation. Some authors[2,5,7,9] considered it to be the result of oxidation by oxygen in the gas phase and others[8] proposed that the formation of water was due to the oxidation of H_2S by framework oxvgen ions.

In this chapter, we report infrared studies of the adsorption of H_2S on Cu^{2+}, Ni^{2+}, Zn^{2+}, Mn^{2+}, and Co^{2+} exchanged type A zeolites. Previous studies of H_2S adsorption onto zeolites will be discussed in section III. The structure of hydrated and dehydrated Cu(II), Ni(II) and Zn(II) exchanged type A zeolites have already been discussed in chapter VII, while that of Mn(II) and Co(II) will be discussed in the following section.

II. Structure of hydrated and dehydrated partially exchanged Mn(II) and Co(II) type A zeolites

(a) Hydrated partially exchanged Mn(II) type A zeolite

A single crystal analysis of hydrated $Mn_{4.5}Na_3A$ zeolite has been carried out by Seff et al[10,11]. The 4.5 Mn(II) ions were found at three-fold positions, slightly into the large cavity (S2*). These Mn(II) ions were found to be pentacoordinate in a trigonal-bipyramidal manner (Figure 8.4a). The axial ligands are two non-equivalent water molecules, $H_2O(1)$ and $H_2O(2)$ with Mn(II) .... OH_2 distances of 2.03(6) and 2.06(7)Å, respectively. The three equivalent equatorial framework O (3) atoms were 2.28(1)Å from Mn(II), affording the Mn(II) ions nearly regular trigonal bipyramidal coordination.

Stereoviews of the hydrated MnNaA are given in figures 8.1 and 8.2. The probable positions of 29.5 water molecules per unit cell have been determined and the 3 Na^+ ions could not be located with certainty.

(b) Dehydrated partially exchanged Mn(II) type A zeolite

In the dehydrated $Mn_{4.5}Na_3A$ studied by Seff et al[10,11], the sample was heated to 623K for 24 hours. A stereoview of the dehydrated MnNaA is shown in figure 8.3[10,11]. 4.5 Mn(II) and 3 Na^+ ions were located on three-fold axes close to the

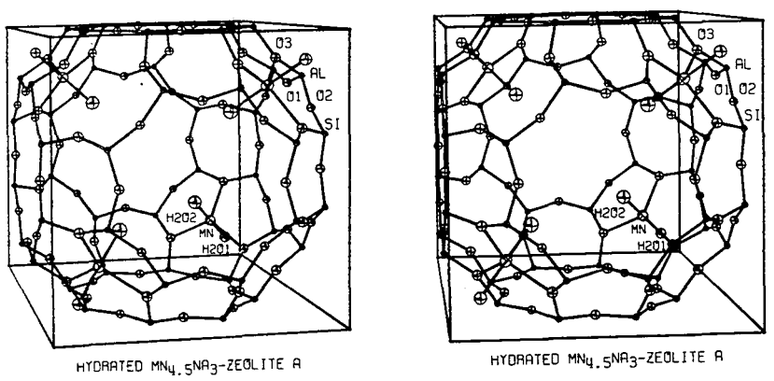

Figure 8.1. A stereoview of the hydrated MnNaA unit cell is shown. The trigonal-bipyramidal coordination about Mn(II) is indicated by solid lines. Only the water molecules which participate in coordination are included. Ellipsoids of 20% probability are used[11].

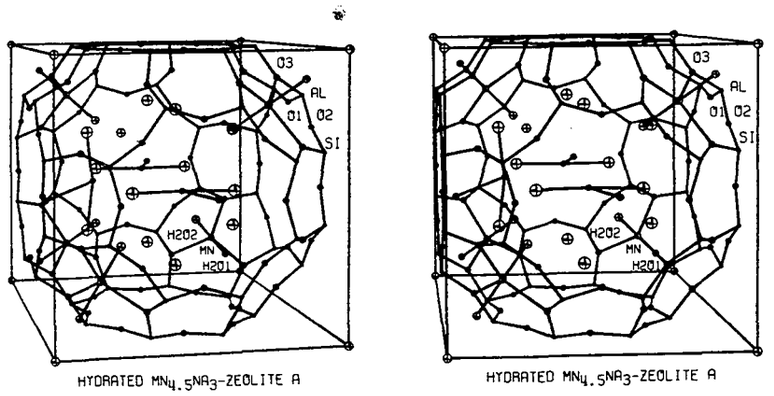

Figure 8.2. Stereoview of hydrated MnNaA including all cations and water molecules. Ellipsoids of 5% probability are used[11].

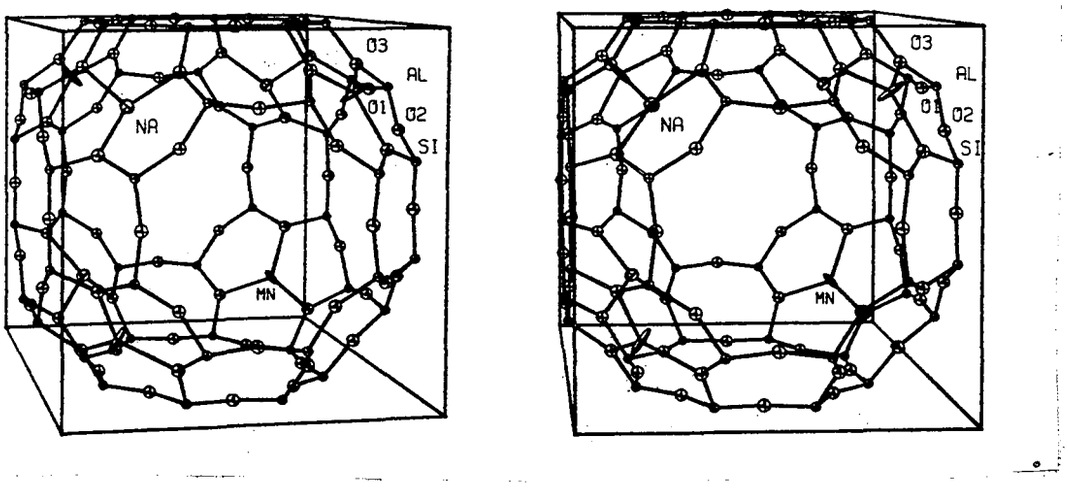

Figure 8.3. A stereoview of the dehydrated MnNaA unit cell. The trigonal approaches made by Mn(II) and Na^+ to framework oxygen atoms are indicated by solid lines. Ellipsoids of 20% probability are used[11].

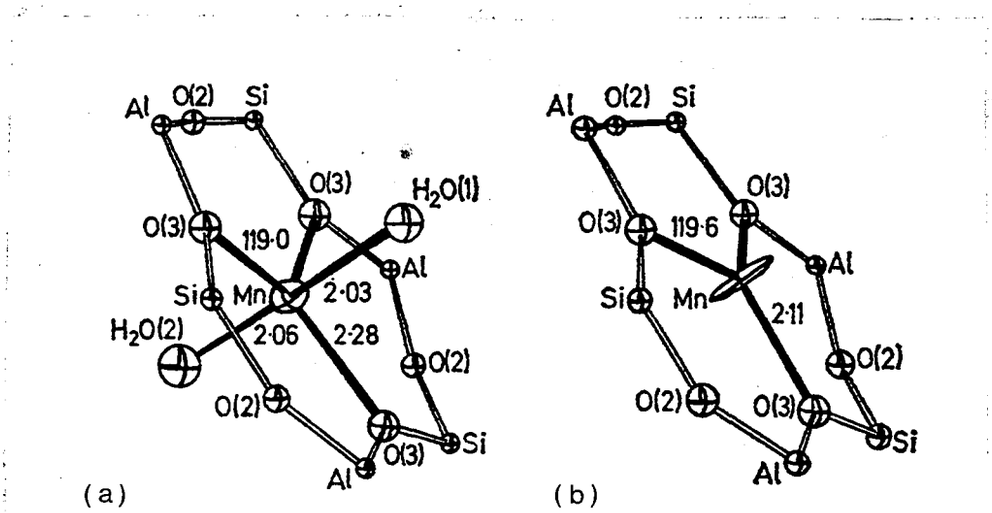

Figure 8.4. Equivalent Mn(II) occupied 6-ring windows of the hydrated MnNaA (a) and the dehydrated MnNaA (b) are shown. Ellipsoids of 20% probability are used[10.11].

plane of the 6-oxygen windows. The Mn(II) ions were recessed slightly into the sodalite cage (S2') while the Na^+ ions were recessed slightly into the large cavity (S2*). Both Mn(II) (Figure 8.4b) and Na^+ ions were trigonally coordinated to sets of three framework oxygens at 2.11(1) and 2.16(5)Å, respectively.

(c) Hydrated partially exchanged Co(II) type A zeolite

The structure of hydrated partially exchanged Co(II) type A zeolite (Co_4Na_4A) has been determined by Seff et al[12]. The four Co(II) ions were located at two distinct crystallographic sites. One Co(II) ion was located at the centre of the sodalite cage (SU) and the other three Co(II) ions were distributed about equivalent sites on unit cell threefold axes. The Co(II) ion at site SU was coordinated by a regular octahedron of water molecules (Figure 8.5) with a Co to H_2O distance of 2.11(3)Å.

The remaining Co(II) ions have unusual zeolitic cation coordination environments and apparently promote an extensive hydrolysis of the aluminosilicate framework, and consequently produce Bronsted acid sites. Accordingly, the authors[12] suggested that the weakening of the bonds between (Si,Al) atoms and the hydrolyzed framework oxygen atoms could be due to some ligands from the Co(II) coordination sphere (probably OH groups resulting from hydrolysis), approaching the positively charged (Si,Al) ions sufficiently close to form bridged Co - OH - (Si,Al). Three water molecules each dissociated to form protons and three Co - OH - (Si,Al) bridges to each Co(II) ion. Another water molecule, located well into the large cavity, is coordinated to each Co(II) ion at a fourth position (Figure 8.6).

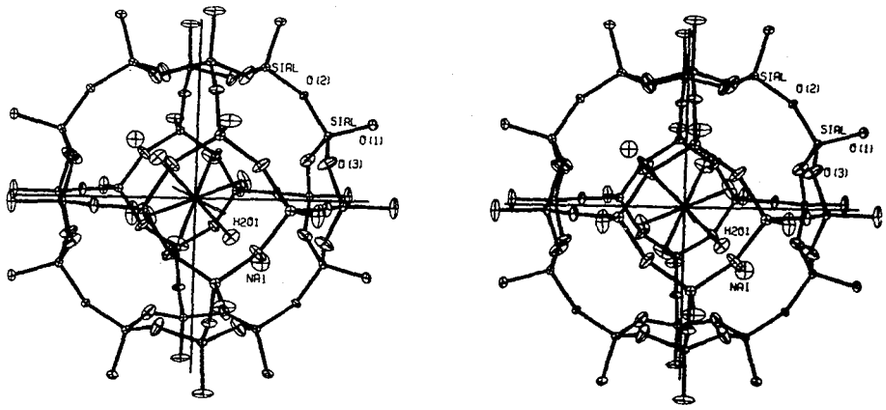

Figure 8.5. A stereoview of the octahedral coordination about the Co(1) ion in the small cage. Ellipsoids of 30% probability are used[12]. Co(1) refers to site SU in the text.

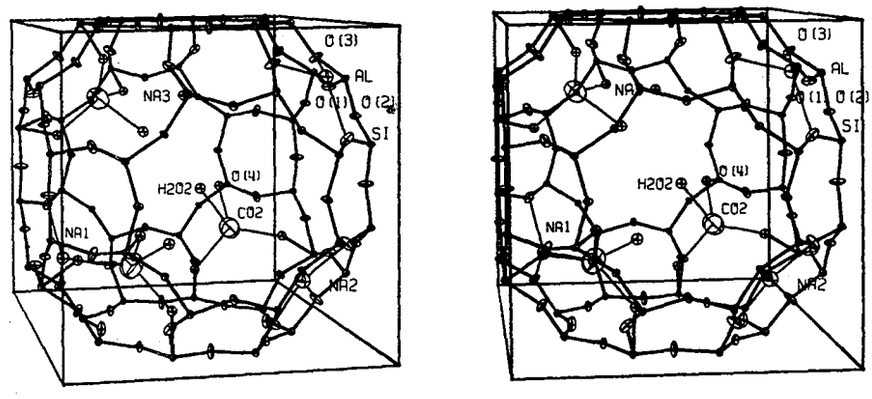

Figure 8.6. A stereoview of the unit cell. Heavy bonds indicate coordination about the cations. Ellipsoids of 20% probability are used[12]. Co(2), Na(1), Na(2) and Na(3) refer to sites S2*, S2', S2* and S3 in the text.

Two Na^+ ions were located near the 6-ring windows but recessed into the sodalite unit (S2'). A third Na^+ ion was located also near the 6-ring windows but protruded into the large cavity (S2*). The fourth and final Na^+ ion was found in the large cavity at a fourfold symmetry site (S3)

(d) Dehydrated partially exchanged Co(II) type A zeolite

In this case the Co_4Na_4A zeolite sample was heated at 623K for 48 hours[13,14]. The Co(II) ions, like the Mn(II) ions, were found to occupy threefold axis sites, near the 6-oxygen windows, but recessed by 0.16(4)Å into the sodalite cage (S2') (Figures 8.7 and 8.8). Each Co(II) ion is arranged trigonally in the 6-oxygen ring with a Co-O distance of 2.06(1)Å [13].

III. Relevant previous studies of H_2S adsorbed onto zeolites

Forster and Schuldt[2] studied the adsorption of H_2S on zeolites NaA and $Na_{4.4}Ca_{3.8}A$ using infrared spectroscopy. The zeolites were dehydrated at 725K for 15 hours before adsorption of H_2S. In the case of NaA, these authors found that the new band observed at 2500cm^{-1} shifted to higher wavenumbers with increasing coverage. For CaNaA, upon adsorption of H_2S, a band appeared at 2540cm^{-1} which remained unshifted over a wide range of coverage. The molecularly adsorbed H_2S in both samples could be removed easily by evacuation at room temperature.

An additional weak band near 2585cm^{-1} was observed for NaA zeolite which could be removed only after heating to above 475K. A weak absorption band in the OH region was also observed at the same time. The appearance of these bands indicate that the2585cm^{-1}band may be due to a firmly bound SH^- species.

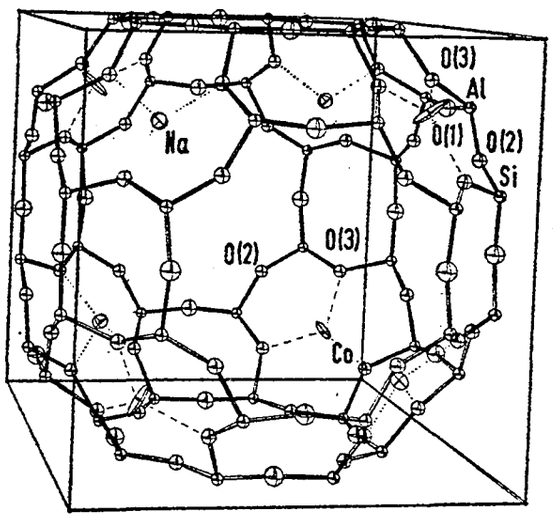

Figure 8.7. The unit cell of partially Co(II) exchanged fully dehydrated zeolite Type A. Ellipsoids of 20% probability are used[13]. The near trigonal planar coordination of the Co(II) ions is indicated by dashed lines. Sodium ion coordination is indicated by dotted lines.

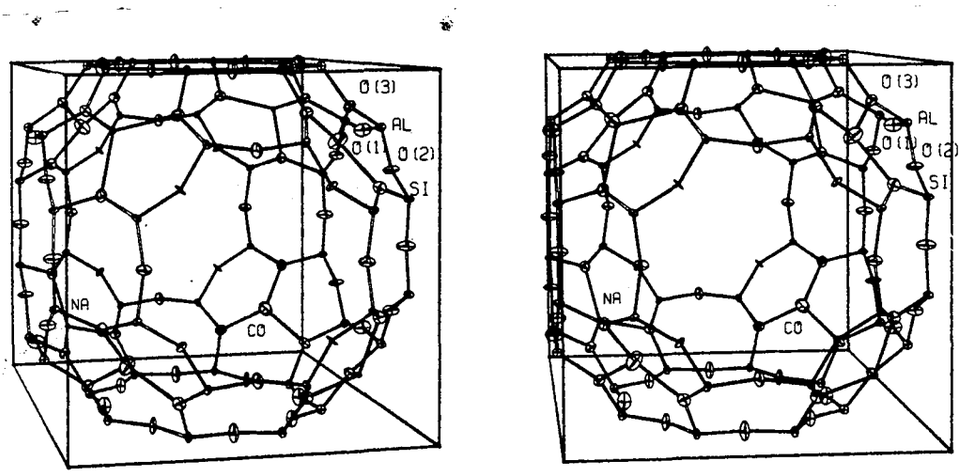

Figure 8.8. A stereoview of the dehydrated Co_4Na_4A zeolite. Ellipsoids of 20% probability are used[14].

Water formation during H_2S adsorption was also observed.

From their infrared data, the authors[2] concluded that in the zeolite NaA, H_2S was adsorbed at two different sites while in the zeolite CaNaA, all the H_2S occupied equivalent sorption sites and that no significant adsorbate-adsorbate interaction occurred. They assigned the observed absorption band at 2500cm^{-1} for NaA and 2540cm^{-1} for CaNaA to the ν_3 vibration (antisymmetric stretching of H_2S which occur at 2684cm^{-1} in the gas phase[17]). In common with most authors[3,7], they failed to observe the bending vibration ν_2 of adsorbed H_2S. Water formation was explained by the authors[2,9] as due to the reaction of adsorbed H_2S with molecular oxygen from the gas phase, a reaction which according to the authors is thermodynamically favoured.

Infrared investigations of H_2S adsorption on faujasite-type zeolites with systematically varied Si:Al ratios (1.05-3.24) have been carried out by Karge and Rasko[3]. The zeolite samples were degassed for 2 hours at 673K (or923K) before being allowed to cool to room temperature. H_2S at pressures 1,5,20,30 and 50 torr were then admitted to the cell.

Upon adsorption of H_2S (1 torr), the authors observed a band at 3650cm^{-1} in the OH region together with a band at 2560cm^{-1}. On zeolites for which the Si:Al ratio is up to 2.5, increasing the H_2S pressure caused a decrease in intensity of the OH band at 3650cm^{-1}, which developed during H_2S adsorption. Simultaneously in these zeolites, a broad absorption band at around 3400cm^{-1} developed. The 2560cm^{-1} band for NaX became asymmetric, broadened, and shifted to lower frequency, while the same band for NaY remained symmetric and occurred at an almost constant frequency.

The authors[3] suggested that the OH band at 3650cm^{-1}, which appeared after H_2S adsorption was due to proton attachment to

framework oxygens (the proton arising form the dissociation of H_2S). Interaction between this newly formed OH and H_2S was inferred from the decrease in intensity of the 3650cm^{-1} band and the parallel formation of the broad feature at 3400cm^{-1} at higher pressures. The band at 2560cm^{-1}, which appeared upon adsorption of 1 torr H_2S, was caused by a dissociative adsorption since OH was formed. Hence, this band was assigned to the stretching vibration of SH^- species.

The band broadening, frequency shift to lower wavenumber, and asymmetric shape of the 2560cm^{-1} band, in NaX, with increasing pressure was suggested by the authors to be a consequence of both chemisorption and physisorption of H_2S. On the other hand, the NaY samples showed broad bands at generally constant frequency, indicating that non-dissociative adsorption took place. Correspondingly, no OH was observed for the NaY samples. Both the dissociative and non-dissociative adsorption were reversible since the OH, SH^- and H_2S bands could be removed by evacuation.

NMR data for H_2S adsorption on faujasite-type zeolites was reported Lechert and Hennig[15,16]. Their assumption that H_2S may be adsorbed to some extent dissociatively (with formation of SH^- and OH^+), particularly in the case of NaX agrees with the conclusion reached by Karge and Rasko[3].

Deo et al[7], in their infrared studies of H_2S adsorbed onto NaY zeolite observed a band at 2575cm^{-1} due to the adsorbed species. Unlike Forster and Schuldt[2] and Karge and Rasko[3], they assigned this band to the stretching vibrations (ν_1 and ν_3) of H_2S and the first overtone of the bending vibration ($2\nu_2$). These bands occur at frequencies 2611(ν_1), 2684(ν_3) and 2422($2\nu_2$)cm^{-1}, respectively in the gas phase[17]. In agreement with other authors[2,3], Deo et al also did not

observe a band which could be assigned to ν_2 of H_2S (ν_2 occurs at 1290cm^{-1} in the gas phase[17]). Deo et al[7], in their infrared studies also observed the formation of water which they explained was due to the oxidation of H_2S with chemisorbed molecular oxygen.

In another experiment, Deo et al[7] absorbed H_2S onto a HY zeolite. Their results differ from those for NaY zeolite in that, no oxidation of H_2S took place and a broad band at 3200cm^{-1} was observed on the HY sample. This band was assigned to H_2S hydrogen bonded to surface hydroxyl.

H_2S adsorption onto NaA and Ni_xNaA (where $0.3 \leq x \leq 2.0$) were measured gravimetrically by Ezzamarty et al[4]. At room temperature the authors found that the adsorption capacity of the nickel form was slightly higher than for the sodium form. The difference in the adsorption capacity between Ni_xNaA and NaA increased with increasing adsorption temperature. Data for samples with various values of x, showed that, for a constant adsorption temperature (298K), the mass of residue after desorption (thought to be S or S^-) increases with nickel loading. It was concluded that since H_2S desorbed quantitatively from NaA at 623K, some chemical reaction had occurred between H_2S and Ni_xNaA. This indicates that some oxygen from the zeolite was extracted as water molecules according to the following:

$$H_2S + O^{2-} \longrightarrow H_2O + S^{2-}$$

IV Experimental

The ZnNaA, NiNaA and CuNaA samples used were from the same batches prepared as described in chapter VII. Mn and Co exchanged type A zeolites were prepared by ion exchanging NaA (Union Carbide Corporation) in 0.1M of $MnSO_4$ and $Co(NO_3)_2$

respectively at room temperature for 3 days. Both the $MnSO_4$ and $Co(NO_3)_2$ were obtained from BDH (Analar Grade). After the ion exchange, the samples were analysed and found to have the following compositions:

$Mn_{3.5}Na_{5.0}Al_{12}Si_{12}O_{48}$ and $Co_{4.0}Na_{4.0}Al_{12}Si_{12}O_{48}$.

The notations MnNaA and CoNaA will be used in the text to describe the above samples.

Hydrogen sulfide was obtained from BOC Special Gases and was purified by the freeze-pump-thaw technique before use. The purity of the gas was checked by mass and infrared spectroscopy.

Each of the samples used was dehydrated as follows: ZnNaA, 673K for 2 hours; NiNaA, 623K for 18 hours; CuNaA, 723K for 24 hours; MnNaA, 723K for 2 hours and CoNaA, 723K for 2 hours. Spectra of the samples at different temperatures during dehydration were measured. The dehydration of ZnNaA, NiNaA and CoNaA has already been dicussed in chapter VII.

In each case, after the dehydration process, the sample was allowed to cool to room temperature and the spectrum re-measured. H_2S at a pressure of 5 torr was admitted to the cell and the spectrum of the sample recorded. The pressure of H_2S was increased to 50 torr and the spectrum of the sample recorded once more before evacuating the cell for 5 minutes and a further 25 minutes. Following each evacuation, the spectrum of the sample was measured. In the case of ZnNaA, after evacuation overnight, the sample was heated and the spectra obtained at various temperatures.

V. Results and discussion

(a) Dehydration of MnNaA and CoNaA

Figures 8.9 to 8.11 show the spectra of MnNaA, NaA and CoNaA at various temperatures during dehydration. In the spectra

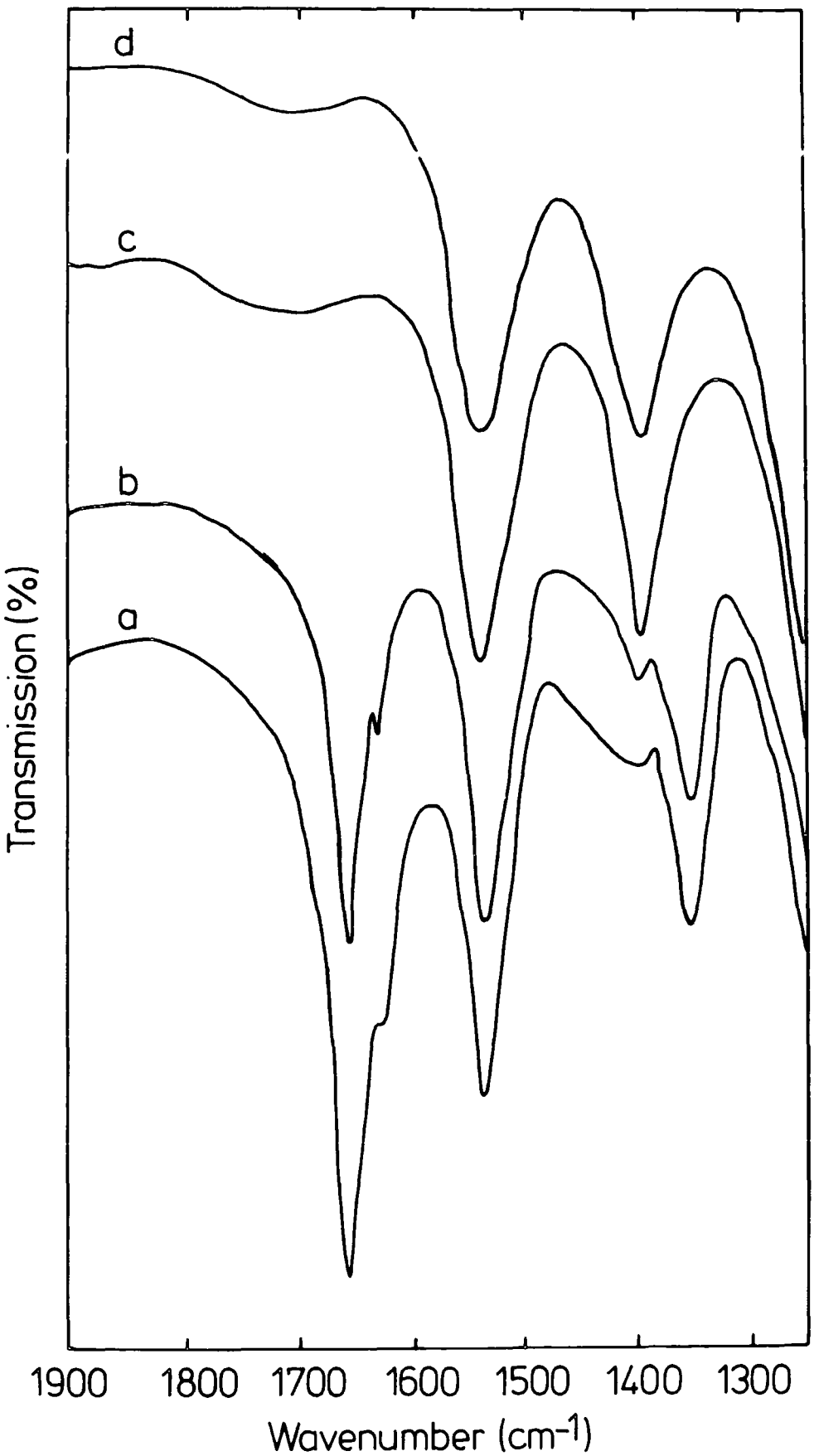

Figure 8.9. MnNaA zeolite at: (a) 293K,
(b) 503K, (c) 583K and (d) 723K.

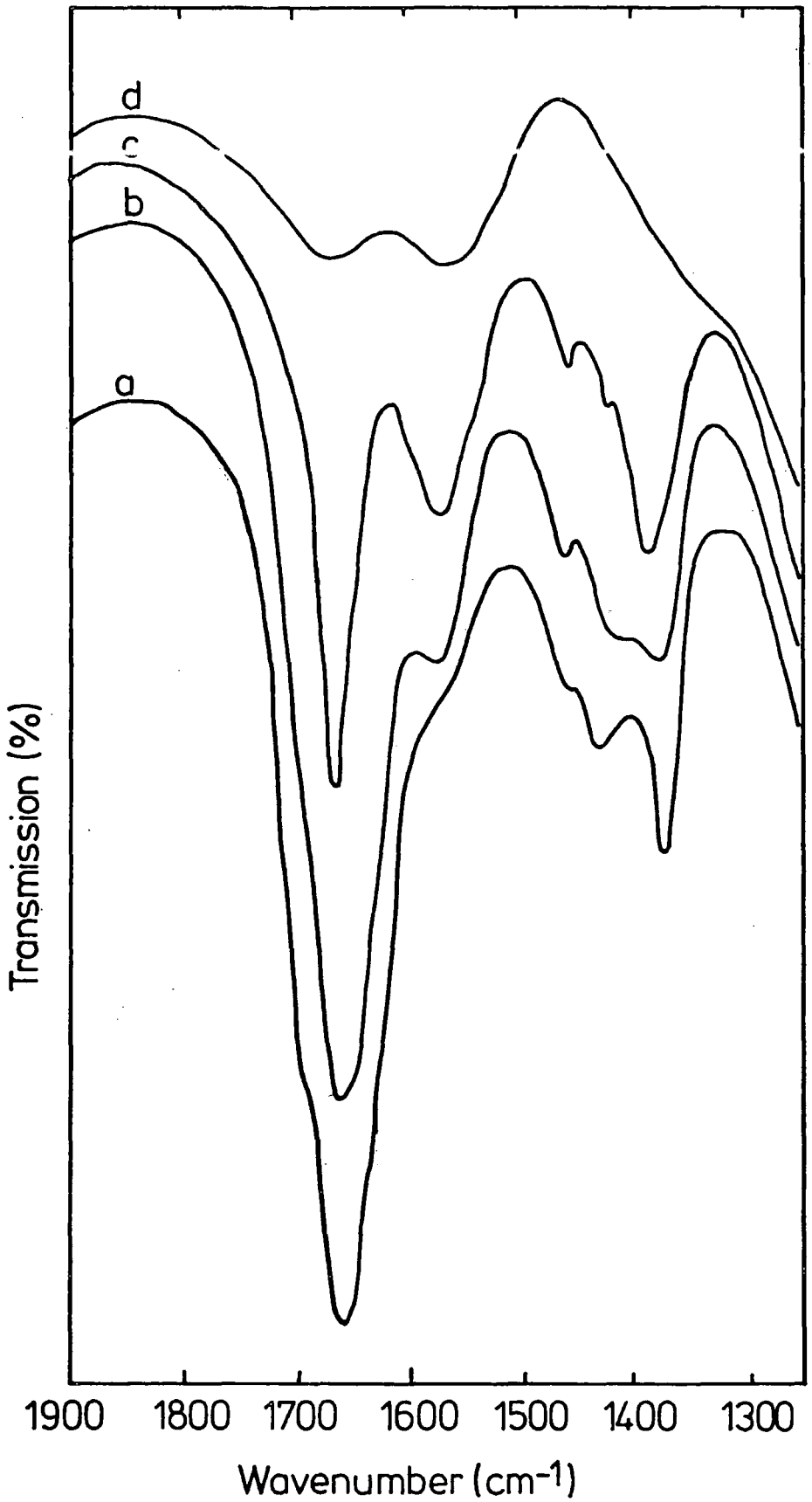

Figure 8.10. NaA zeolite at: (a) 293K, (b) 373K, (c) 473K and (d) 573K.

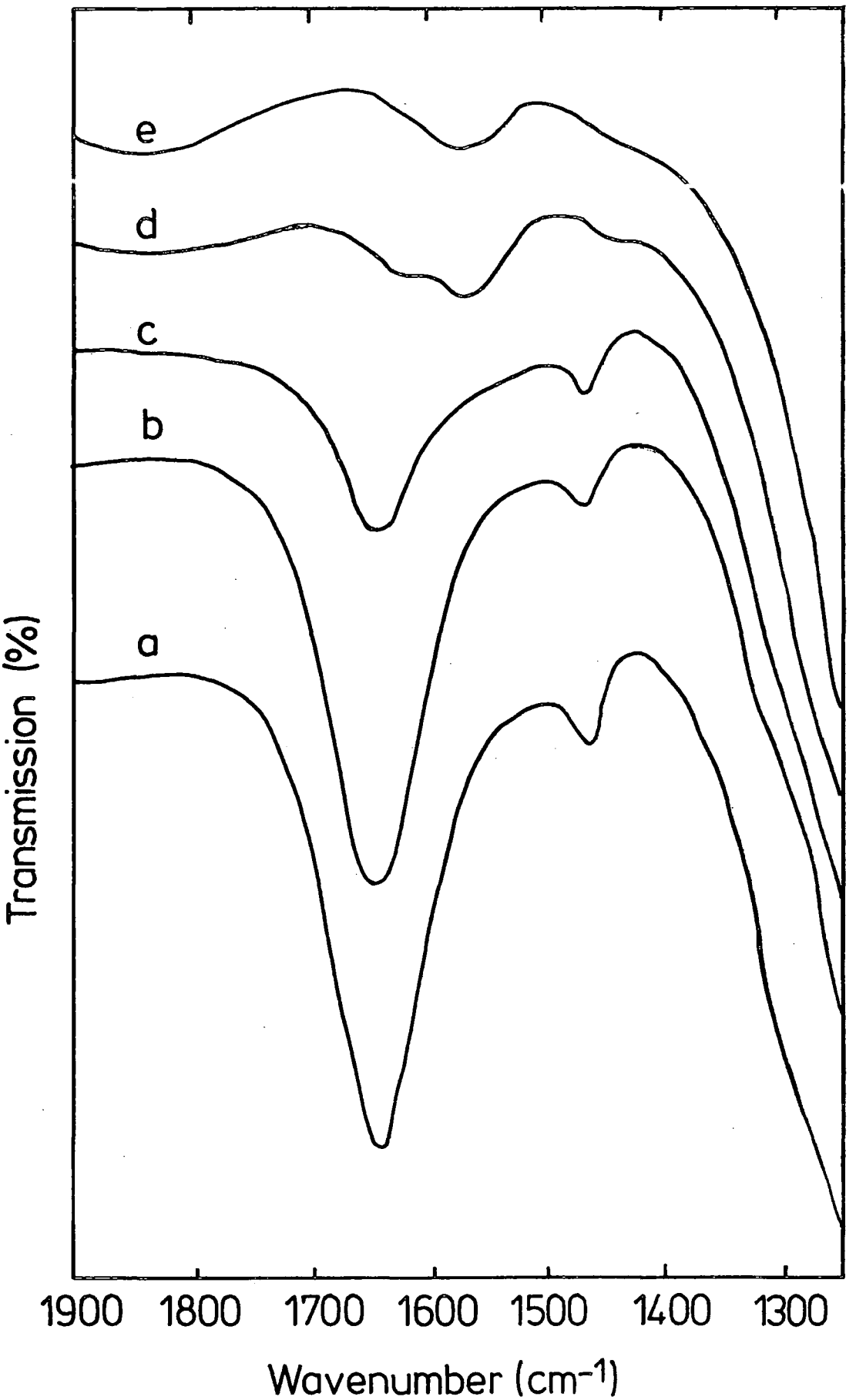

Figure 8.11. CoNaA zeolite at: (a) 293K, (b) 453K, (c) 553K, (d) 643K and (e) 723K.

of the samples at room temperature, we observed a strong sharp band at 1655cm^{-1} with a shoulder at 1625cm^{-1} (Figure 8.9a) for MnNaA; a strong broad band at 1675cm^{-1} with a weak shoulder at 1700cm^{-1} (Figure 8.10a) for NaA and a very broad band at ~ 1650cm^{-1} (Figure 8.11a) for CoNaA. All these bands are assigned to the deformation mode of water. As the samples were heated we observed that the bands, which we have assigned to the deformation mode, decrease in intensity and disappear at 583K for MnNaA (Figure 8.9c), 673K for NaA (Figure 8.10d) and 723K for CoNaA (Figure 8.11e). This indicates that most of the water has been removed from the zeolite cavities. It should be noted that, in the case of MnNaA part of the band at 1655cm^{-1} re-appears on allowing the sample to cool to room temperature (Figure 8.14a). We have explained in chapter VII (Section Va), that the re-appearance of this band could be due either to the nature of the zeolite itself, or more likely, from water being readsorbed from the surrounding of the cell.

In the spectrum of MnNaA at room temperature (Figure 8.9a), we also observed three bands at 1540(s), 1400(w) and 1355(s)cm^{-1}. The band at 1400cm^{-1} increases in intensity and also changes in shape on heating while the band at 1355cm^{-1} disappears in the spectra of the sample at 583 and 723K (Figures 8.9c and d) Comparing these spectra with the spectra of NaA at various temperatures (Figure 8.10), it can be seen that the bands in the region 1500-1300cm^{-1} disappear at 673K in the spectrum of NaA (Figure 8.10d). This indicates that the band at 1400cm^{-1} in the spectrum of MnNaA at 723K (Figure 8.9d) is a result of Mn^{2+} ion movement. In agreement with the single crystal x-ray analysis[10,11], the Mn^{2+} ions appear to move from one site (1355cm^{-1} band at room temperature and 503K) to another site (1400cm^{-1} band at 583 and 723K). From single crystal x-ray

analysis (Section II), the Mn(II) ions were found at sites S2* in the hydrated form, and at sites S2' in the dehydrated form (623K).

Unlike the 1355cm^{-1} band, which on dehydration moves to 1400cm^{-1}, the band at 1540cm^{-1} remains at the same position and with approximately unchanged intensity. This band could be due to a framework vibration related to both Na^+ and Mn^{2+} ions. In the spectrum of NaA at 673K (Figure 8.10d), a band is observed at 1575cm^{-1} but is not as intense as the 1540cm^{-1} band in the spectra of MnNaA (Figures 8.9a-d). Consequently, our assignment that the Mn^{2+} ions are located at two sites is at variance with the conclusion reached by Seff et al[10,11] in their x-ray analysis (Section II).

In the spectrum of CoNaA, a band is oberved at 1460cm^{-1} (Figure 8.11a) which disappears on heating (Figures 8.11d and e). It will be shown later (Figure 8.15a) that this band reappears on allowing the sample to cool to room temperature, indicating that it could be due to a framework vibration that is sensitive to temperature. At high temperatures (643 and 723K), a broad band appears at 1570cm^{-1} (Figures 8.11d and e) which was not observed in the spectrum of the sample at room temperature. The non-observation of this band at 293, 453 and 553K could be due to it being obscured by the broad water band at 1650cm^{-1}. By analogy with the spectra of NaA (Figure 8.10), the 1570cm^{-1} band could be due to a framework vibration related to Na^+ ions.

(b) Adsorption of H_2S

H_2S at pressures of 5 and 50 torr was admitted to ZnNaA, NiNaA, CuNaA, MnNaA and CoNaA zeolites. In the infrared spectrum of pure H_2S gas obtained at 445 torr, we observed two weak bands at 3800 and 1330cm^{-1}. It should be noted that at

5 and 50 torr (the pressures of H_2S used in the present experiments), no band was observed in the gas phase spectrum.

Figure 8.12a shows the spectrum of ZnNaA (293K) after heating to 673K for 2 hours, while figures 8.12b and c show the spectra of the same sample after admitting 5 and 50 torr of H_2S respectively.

Upon admitting 5 torr of H_2S, we observe the following bands in the infrared spectrum, 3500, 3100, 2560, and 1655cm^{-1}. Increasing the pressure of H_2S affects only the 1655cm^{-1} band which increases in intensity. The bands at 3500 and 1655cm^{-1} may be assigned to the stretching and bending modes of water. In agreement with Forster and Schuldt[2,9], the formation of water could be due to the oxidation of H_2S with molecular oxygen in the gas phase. This is so since the formation of water is dependent on the pressure of H_2S.

The 2560cm^{-1} band is very broad and asymmetric and because of this, we may assign this band to the stretching modes of both the SH^- species and H_2S. In tables 8.1 and 8.2 are given values of ν_3 (antisymmetric stretch of H_2S) and the $\nu(SH^-)$ in different environments. As can be seen, our assignment of the 2560cm^{-1} band to both adsorbed SH^- and H_2S, is within the range of $\nu(SH^-)$ given by Chi and Nixon[18] and Cade[19], and also in agreement with most authors in their assignments of the ν_3 mode of H_2S. Our assignment therefore indicates that there are two types of adsorption processes, the dissociative (H_2S dissociated to H^+ and SH^-; H^+ forms hydroxyl group with framework oxygen and SH^- is associated with the cations), and the non-dissociative.

Confirmation of the existence of both adsorption processes is obtained by the observation of a broad band at 3100cm^{-1} which is due to H_2S hydrogen bonded to the structural

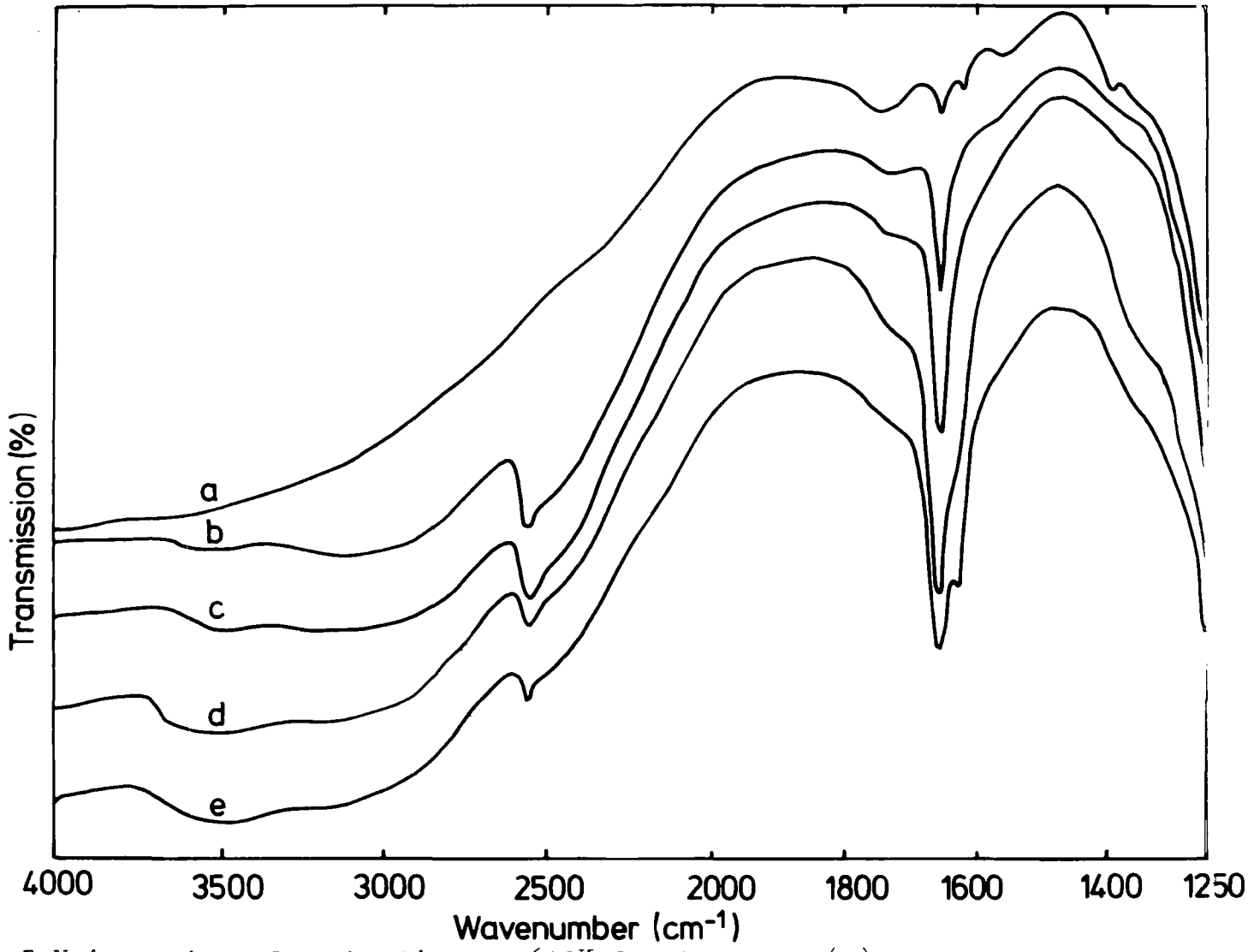

Figure 8.12. ZnNaA zeolite after heating at 673K for 2 hours: (a) at ambient temperature, (b) sample (a) after admitting 5 torr H_2S, (c) sample (a) after admitting 50 torr H_2S, (d) sample (c) after evacuation for 5 minutes and (e) sample (c) after evacuation for 30 minutes.

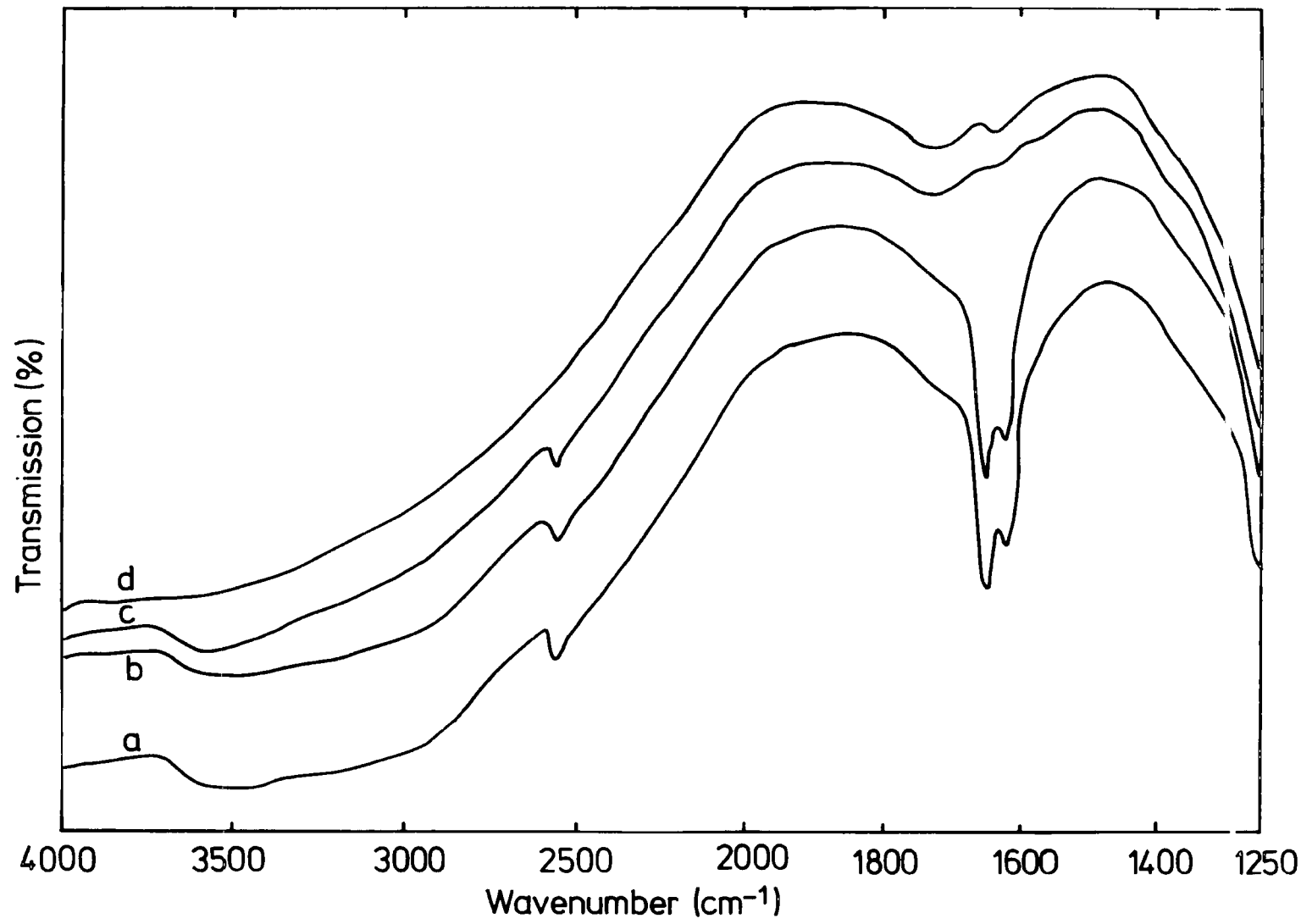

Figure 8.13. (a) sample 8.12(e) after evacuation for a further 1 night, (b) sample (a) at 383K, (c) sample (a) at 523K and (d) sample (a) at 623K.

Table 8.1 Infrared band of ν_3 (antisymmetric stretch of H_2S) in different environments

	ν_3, cm^{-1}	Ref.		ν_3, cm^{-1}	Ref.
Gas phase	2684	17	NaY	2575	7
Solid (66K)	2544	20	NaY	2560	3
Solid (112K)	2562	20	NaA	2480-2520	2
Kr matrix	2618	21	CaNaA	2540	2
N_2 matrix	2633	22	ZnNaA	2560	Our work
Alumina	2560	7	MnNaA	2560	
	2568	8	CoNaA	2550	

Table 8.2 Wavenumbers of SH^- anion band in different environments

	ν(SH), cm^{-1}
NaSH in nujol	2538
NaSH in NaBr	2569
Free SH^-	2545-2595

hydroxyl. As explained earlier, the hydroxyl groups originate from the dissociation of H_2S and subsequently bonding of the H^+ to framework oxygen. The assignment of the 3100cm^{-1} band to hydrogen bonded H_2S is in agreement with that of Deo et al[7], who also observed a broad band at 3200cm^{-1} for H_2S adsorbed on HY zeolite.

We could not observe the OH stretching vibration in the spectra of the sample upon admitting 5 and 50 torr H_2S because the intensity of this band is weak and is further reduced by hydrogen bonding to the H_2S.

The sample was evacuated for 5 minutes and a further 25 minutes at room temperature (Figures 8.12d and e). On evacuating the sample for 5 minutes, the 2560cm^{-1} band becomes weaker and the water band at 1655cm^{-1} developed a shoulder at 1625cm^{-1}. Their shoulder increases in intensity in the spectra of the sample after 30 minutes and overnight evacuation at room temperature (Figure 8.12e and 8.13a). As explained in chapter VII, during the dehydration of ZnNaA, the 1625cm^{-1} band is due to water at a site which is different from that associated with the 1655cm^{-1} band.

It seems probable, from the spectra of the sample evacuated for 30 minutes and then overnight, to conclude that one of the adsorbed species has been removed, because the 2560cm^{-1} band is now reduced in intensity and is less broad. However, we are not able to tell with cetainty, which of the adsorbed species is desorbed. The most likely one would be the SH^- anion since the broad band at around 3100cm^{-1}, which is due to hydrogen bonded H_2S, remains.

The sample was then heated and spectra obtained at the elevated temperatures (Figures 8.13b-d). The 2560cm^{-1} band could only be removed on heating the sample above 523K. Our observation that there are two types of

adsorption processes is in agreement with the work of Karge and Rasko[3], for H_2S adsorbed on NaX zeolite.

Since for NiNaA, we observed only a broad band at 4000-2300cm^{-1} and for CuNaA, no band was observed which could be assigned to the adsorbed species, the spectra of H_2S adsorbed on NiNaA and CuNaA will not be discussed further.

In figure 8.14a is shown the spectrum of MnNaA at room temperature after heating to 723K for 2 hours. Figures 8.14b and c show the spectra of the same sample after admitting 5 and 50 torr of H_2S respectively. In the spectrum of the sample before adsorption we observe a weak band at 3500cm^{-1} and a medium intensity band at 1655cm^{-1} which we have assigned to the stretching and bending modes of water. Two other bands, observed at 1540 and 1400cm^{-1}, have already been discussed (part (a)) as due to framework vibrations related to cation movements.

Upon adsorption of 5 and 50 torr of H_2S (Figures 8.14b and c), the bending mode of water at 1655cm^{-1} increases in intensity while the bands which are related to cation movements are shifted to 1565 and 1370cm^{-1}. We also observe two new bands at 3100(vb) and 2560(mb)cm^{-1}. Just as for ZnNaA + H_2S, we assign the broad and asymmetric band at 2560cm^{-1} to both the stretching vibrations of both SH^- and H_2S. Here again, this is an indication of the presence of both dissociative and non-dissociative adsorption. The existence of these two types of adsorption processes is confirmed by the observation of a broad band at 3100cm^{-1} which was assigned to hydrogen bonded H_2S. Confirmation that the SH^- is

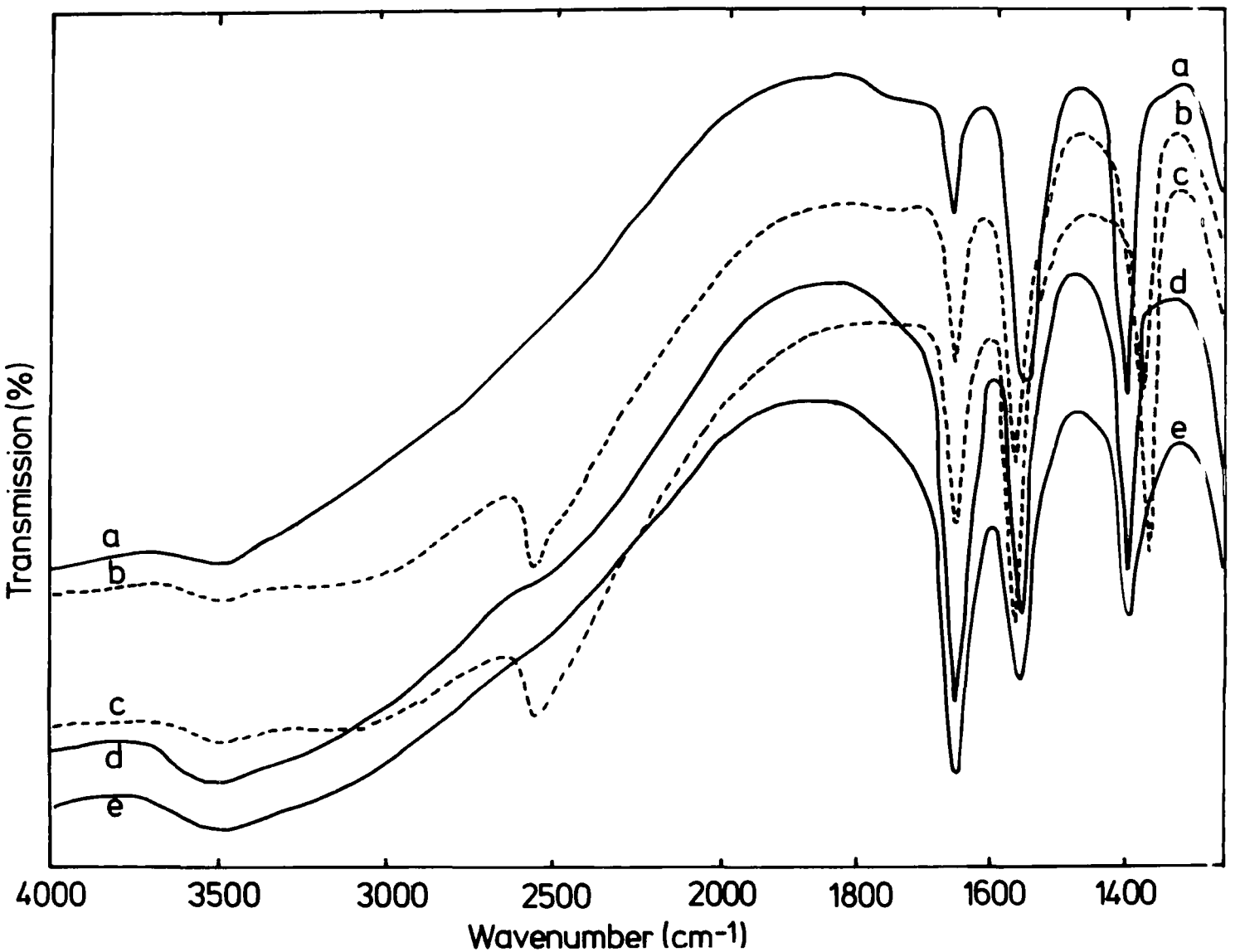

Figure 8.14. MnNaA zeolite after heating at 723K for 2 hours: (a) at ambient temperature, (b) sample (a) after admitting 5 torr H_2S, (c) sample (a) after admitting 50 torr H_2S, (d) sample (c) after evacuation for 5 minutes and (e) sample (c) after evacuation for 30 minutes.

associated with the cations is obtained in this particular zeolite (MnNaA), because the bands at 1540 and 1400cm^{-1}, which are associated with cation vibrations, are shifted to 1565 and 1370cm^{-1} upon adsorption of H_2S (Figures 8.14b and c).

Both the dissociatively and the non-dissociatively adsorbed species are weakly held since they are removed by 30 minutes evacuation at room temperature (Figure 8.14e). The bands at 1575 and 1370cm^{-1} returned to their original positions at 1540 and 1400cm^{-1} after the adsorbed species were removed. Clearly, this shows that our assignment of the 1540 and 1400cm^{-1} bands to the framework vibrations related to cation movement is correct.

In contrast with the adsorption of H_2S on ZnNaA and MnNaA, H_2S adsorbed onto CoNaA only gives a weak band at 2550 cm^{-1}. Figures 8.15a, b, and c show the spectra of CoNaA; at room temperature after heating to 723K for 2 hours and after admitting 5 and 50 torr of H_2S, respectively.

The 2550cm^{-1} band, because it is symmetric and in the absence of the observation of any band which can be assigned to hydrogen bonding, is deduced to be the result of non-dissociative adsorption. Hence, this band is assigned to ν_3, the antisymmetric stretching of H_2S. Just as the MnNaA system, H_2S was found to adsorb weakly in CoNaA since it can be removed by 30 minutes evacuation at room temperature (Figure 8.15e).

In accordance with our observations for H_2S adsorbed on ZnNaA and MnNaA, water formation was observed in the spectra of H_2S adsorbed onto CoNaA. This adds strength to our earlier conclusion for ZnNaA and MnNaA that the formation of water was due to the oxidation of H_2S with molecular oxygen present as impurities in the gas phase. In agreement with some

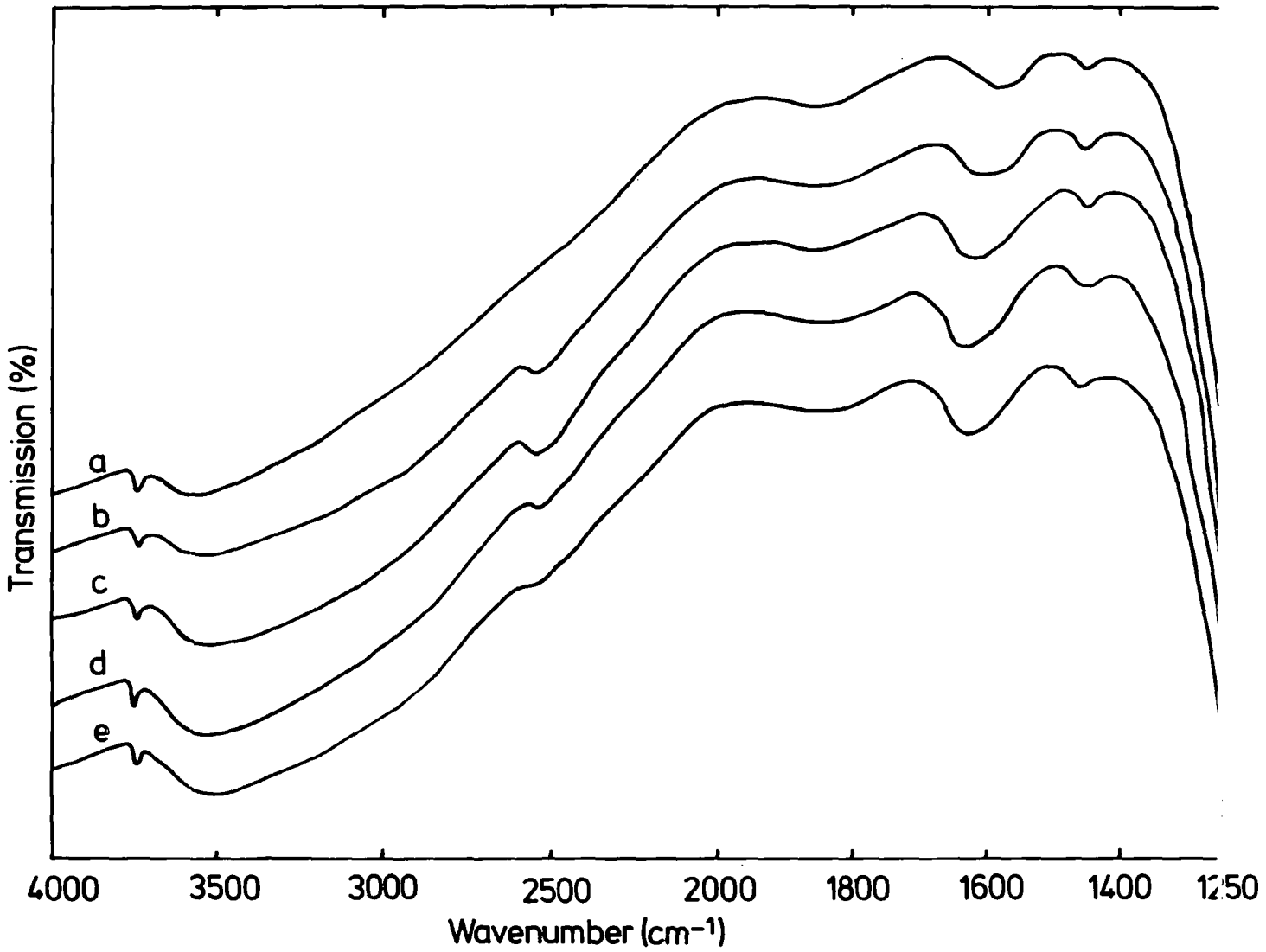

Figure 8.15. CoNaA zeolite after heating at 723K for 2 hours: (a) at ambient temperature, (b) sample (a) after admitting 5 torr H_2S, (c) sample (a) after admitting 50 torr H_2S, (d) sample (c) after evacuation for 5 minutes and (e) sample (c) after evacuation for 30 minutes.

authors[23,24], the oxidation of H_2S by air or oxygen over X-type and A-type zeolites occurs according to the following reaction:

$$H_2S + \tfrac{1}{2}O_2 \longrightarrow S + H_2O$$

VI Conclusion

Upon adsorption of H_2S onto ZnNaA and MnNaA, the infrared band observed at 2550cm^{-1} was found to be broad and asymmetric. It was concluded that this band was due to the products of both dissociative and non-dissociative adsorption of H_2S. The presence of both types of adsorbed species was confirmed by the appearance of a broad band at 3100cm^{-1} which was due to H_2S hydrogen bonded to the surface hydroxyl, which was formed by the attachment of the proton of the dissociatively adsorbed H_2S to framework oxygen. The non appearance of the OH band in the spectra of the samples upon adsorption of H_2S was explained as due to it being weak and the intensity was reduced further by hydrogen bonding.

Of the two types of adsorption processes on ZnNaA, one was found to be weakly held since it could be removed by evacuation at room temperature. The strongly adsorbed species, most probably the hydrogen bonded H_2S (the broad band at 3100cm^{-1} still remained), was only removed after the sample was heated to above 523K. In MnNaA, however, both types of adsorbed species were weakly held and could be removed easily by evacuation.

Our conclusion that there were two types of adsorption processes is in agreement with that reached by Karge and Rasko[3] for NaX zeolite.

For H_2S adsorbed onto CoNaA, we observed a weak symmetric band at 2550cm^{-1}. We assigned this to the υ_3, antisymmetric stretching mode of H_2S. Accordingly, no OH band or band which is due to hydrogen bonded H_2S was observed. H_2S was weakly

held in CoNaA sample because it could be removed by evacuation at room temperature.

In all cases (ZnNaA, MnNaA and CoNaA), we observed the formation of water. This finding is in agreement with most authors[2,3,7,8], in their study of H_2S adsorbed onto a range of zeolites.

References

1. Lee, H., Adv. Chem. Ser., 121, 311(1973)
2. Forster, H., and Schuldt, M., J. Colloid Interface Sci., 52, 380(1975).
3. Karge, H.G., and Rasko, J., J. Colloid Interface Sci., 64, 522(1978).
4. Ezzarmarty, A., Hemidy, J.F., and Cornet, D., Proc. Intern. Conf. Zeolites, 5, 424(1980).
5. Liu, C.L., Chuang, T.T., and Dalla Lane, I.G., J. Catal., 26, 474(1972).
6. Hosotbuso, T., Sugioka, M., and Aomura, K., Hokkaido Daigaku Kogakubu Kenkyu Hokoku, 102, 119(1981).
7. Deo, A.V., and Dalla Lane, I.G., Habgood, H.W., J. Catal., 21, 270(1971).
8. Slager, T.L., and Amberg, C.H., Can. J. Chem., 50, 3416 (1972).
9. Forster, H., and Schuldt, M., J. Catal., 40, 391(1975).
10. Yanagida, R.Y., Vance, T.B., and Seff, K., J. Chem. Soc. Chem. Comm., 382(1973).
11. Yanagida, R.Y., Vance, T.B., and Seff, K., Inorg Chem., 13, 723(1974).
12. Riley, P.E., and Seff, K., J. Phys. Chem., 79, 1594(1975).
13. Riley, P.E., and Seff, K., J. Chem. Soc. Chem. Comm., 1287(1972).
14. Riley, P.E., and Seff, K., Inorg. Chem., 13, 1355(1974).
15. Lechert, H., and Hennig, H.J., Proc. 3rd. Int. Conf. on Molecular Sieves, 319(1973).
16. Lechert, H., and Hennig, H.J., Z. Phys. Chem., 76, 319(1971).
17. Herzberg, G., Infrared and Raman Spectra of Polyatomic Molecules, Van Nostrand, London(1945).
18. Chi, C.K., and Nixon, E.R., J. Phys. Chem Solids, 33, 2101(1972).

19. Cade, P.E., J. Chem. Phys., 47, 2390(1969).

20. Reding, F.P., and Hornig, P.F., J. Chem. Phys., 27, 1024(1957).

21. Barnes, A.J., and Howells, J.D.R., J. Chem. Soc. Faraday Trans. II, 68, 729(1972).

22. Tursi, A.J. and Nixon, E.R., J. Chem. Phys., 53, 518(1970).

23. Kerr, G.T., and Johnson, G.C., J. Phys. Chem., 64, 381(1960).

24. Addison, W.E. and Walton, A.J., Chem. Soc. (London), 4741(1961).

SOME SUGGESTIONS FOR FUTURE WORK

We have shown that $Cu^{I}Y$ can be prepared from $Cu^{II}Y$ inside an infrared cell. This opens up the possibility of studying, at a molecular level, the influence of cation oxidation state on adsorbate-adsorbent interactions and on the catalytic properties of zeolites.

Further experiments on cyclopropane adsorption and isomerization, using methyl substituted and deuterated cyclopropanes etc. should yield additional insight into the isomerization and reaction mechanisms. Co-adsorption of other species (e.g. propene) should yield definitive information on the adsorption and active sites.

One of the major motivations behind all of my work was the wish ultimately to study reacting species. It is clear that high quality infrared data of adsorbates can be obtained on self supported zeolite discs but further work on dynamic systems would require additional apparatus. The major new items would be:

(1) A Fourier transform spectrophotometer. For species reacting rapidly the relatively long scan time of a dispersive instruments seriously influences the quality of information that can be obtained.

(2) The provision of flow controllers so that quantities of gases (vapours) could be admitted at a known and constant rate to the cell. This would enable us (if the cell was simultaneously evacuated at the appropriate rate) to study systems under steady state conditions.

In addition to some of the systems mentioned above I suggest that studies of the following would be appropriate at

the present time.

(A) A number of reports have shown that sulfur compounds such as H_2S and SO_2 promote the catalytic activity of zeolites. There are, however, few reports on the mechanism of the promoting action of these adsorbed sulfur compounds or of the interaction between the sulfur species and zeolites. With the new apparatus mentioned above, these experiments could be carried out and the mechanism studied in detail.

(B) In view of the current high level of interest on highly siliceous zeolites and their obviously fascinating properties, detailed infrared studies of species such as C_2H_4, CH_3OH, $(CH_3)_2O$ etc. within their frameworks is highly desirable. This work should be done over a range of temperatures (up to ~673K) since this is of relevance to their potential applications in $CO + H_2$ and methanol conversion.

Now that the appropriate experience has been gained, the next major phase of the research work should be directed at more technologically relevant systems and these should be studied as close as possible to the conditions of industrial usage.